Photon-number-resolving detectors and their applications in quantum technologies

a Ph.D. thesis

by

Josef Hloušek

Faculty of Science | Palacký University

Olomouc
2022

Abstract

In quantum optics, the main object of interest is the individual energy quanta of light, photons. Every modern quantum photonics experiment hinges on the ability to generate, detect, and manipulate the states of light at the single-photon level. One of the most essential questions is unveiling the nature of light from the perspective of its statistical properties. Photon statistics characterization relies on the capability to distinguish, detect, and count individual photons. As a consequence, the scientific community has devoted significant effort to accomplishing photon-number resolution by various detection approaches employing different physical phenomena. Nowadays, photon-number-resolving detectors represent the rapid advancement of the field of light detection with tremendous interdisciplinary application potential.

The aim of this dissertation is to design and experimentally develop an ultra-precise detection technique for measuring the photon statistics of an unknown optical signal and its statistical correlations. Developed measurement workflow free of systematic errors consists of a reconfigurable photon-number-resolving detector, custom electronic circuitry, and a novel data processing algorithm. The result opens new paths for optical technologies by providing access to the photon-number information without the necessity of full detector tomography. It also aims to directly evaluate key quantities such as correlation functions and nonclassicality metrics rather than full tomography of the photon statistics.

Furthermore, the Thesis presents the application of the precise measurement of photon statistics to characterize the physical processes that generate the optical signal, modify the statistical properties of quantum states of light, and characterize single-photon detectors. It was possible to successfully detect chaotic, classical, nonclassical, non-Gaussian, and negative-Wigner-function light. Modifying the statistical properties of light was achieved by subtracting individual photons from the thermal states of light. The thesis also presents methods of conditional and deterministic preparation of classical states of light out of thermal equilibrium, which can be employed as useful sources for future experiments in the field of quantum thermodynamics. Finally, a method for certifying two highly non-classical properties of quantum detectors - quantum non-Gaussianity and negativity of the Wigner function - is presented. In this approach, the role of measurement and state is reversed with respect to the standard certification of the quantum non-Gaussian character of quantum states.

Keywords: Photon; statistics of light; counting statistics; single-photon detector; photon-number-resolving detector; photon subtraction; quantum non-Gaussianity.

Declaration

This Ph.D. Thesis "Photon number resolving detectors and their applications in quantum optics" is an original work of its author. The Thesis has been written to fulfill the Ph.D. program Optics and Optoelectronics graduation requirements. The Thesis was written under the guidance of supervisor prof. Mgr. Radim Filip, Ph.D. and co-superviser RNDr. Miroslav Ježek, Ph.D.. All sources are properly cited under References. The Thesis is based on scientific works published in collaboration with other co-authors. The contribution of the author is outlined in the Author contributions. This Thesis uses only the resources cited in the Bibliography section. Palacký University has the rights to archive, publish and distribute the Thesis according to its internal regulations and the Czech law. This Thesis may be freely distributed in an unchanged form.

Title:	Photon-number-resolving detectors and their applications in quantum optics
Author:	Mgr. Josef Hloušek
ORCID:	0000-0003-2923-3492
ResearcherID:	D-2890-2018
Supervisor:	prof. Mgr. Radim Filip, PhD.
Co-supervisor:	RNDr. Miroslav Ježek, PhD.
Ph.D. programme:	Optics and Optoelectronics
Institution:	Department of Optics, Faculty of Science, Palacký University
Year:	2022
Pages:	122

Detektory počtu fotonů a jejich aplikace v kvantových technologiích

disertační práce

Josef Hloušek

Přírodovědecká fakulta
Univerzita Palackého

Olomouc
2022

Anotace

Hlavním objektem zájmu v kvantové optice jsou jednotlivá energetická kvanta elektromagnetického záření, fotony. Moderní kvantová fotonika stojí na experimentálních technikách generace, detekce a manipulace se stavy světla na úrovni jednotlivých fotonů. Jednou z nejvýznamnějších charakterizačních metod je zkoumání světla z hlediska jeho statistických vlastností. Měření fotonové statistiky libovolného stavu světla se opírá o schopnost rozlišovat mezi jednotlivými fotony a určovat jejich počet. Vědecká komunita věnovala mnoho úsilí, aby dosáhla rozlišení počtu fotonů pomocí rozličných detekčních přístupů. Detektory s rozlišením počtu fotonů posouvají hranice v oblasti pokročilé detekce světla a se svým velkým mezioborovým aplikačním potenciálem se staly technologickou špičkou.

Cílem disertační práce je návrh a experimentální realizace ultrapřesné detekční techniky měření statistiky počtu fotonů neznámého optického signálu a jeho korelačních vlastností. Vyvinutá detekční technika je nezkreslená systematickými chybami, což je revoluční vlastnost, jíž nedosahují ani kryogenické detektory na bázi supravodivého přechodu. Detekční technika byla ověřena experimentálně pro desítky různých statistik světla včetně neklasických zdrojů a výpočetně pro desetitisíce numericky simulovaných optických signálů. Metoda je škálovatelná a nevyžaduje náročnou charakterizaci detektoru nebo korekce nedokonalostí detektoru, což řeší dlouhodobě existující problém detekce statistiky světla nezávislé na detekčním zařízení.

Precizní měření statistiky počtu fotonů se v předložené práci využívá k charakterizaci typu procesu generace světla, k cílené modifikace statistických vlastností kvantových stavů světla a k charakterizaci jednofotonových detektorů. Podařilo se úspěšně kvantifikovat světelné zdroje chaotického, klasického, neklasického a negaussovského světla. Modifikace statistických vlastností světla bylo docíleno subtrakcí jednotlivých fotonů z termálních stavů světla. Práce uvádí metody podmíněné a deterministické přípravy klasických stavů světla mimo termodynamickou rovnováhu za účelem demonstrace kvantových termodynamických jevů. Dále je prezentována metoda certifikace dvou vysoce neklasických vlastností jednofotonových detektorů - kvantové negaussovosti a negativity Wignerovi funkce. V diskutovaném přístupu je role měření a stavu obrácená s ohledem na běžné testování negaussovského charakteru kvantových stavů.

Klíčová slova: foton, statistické vlastnosti světla, detekční statistika, jednofotonový detektor, jednofotonový detektor s částečným rozlišením počtu fotonů, subtrakce fotonů, kvantová negaussovost

Čestné prohlášení

Tato disertační práce "Detektory počtu fotonů a jejich aplikace v kvantových technologiích" je originálním a samostatným dílem svého autora. Práce byla napsána tak, aby splňovala standardní požadavky pro úspěšné absolvování doktorského studijního programu Optika a optoelektronika. Práce byla sepsána pod odborným vedením školitele prof. Mgr. Radima Filipa, Ph.D. a konzultanta RNDr. Miroslava Ježka, PhD. Použité zdroje jsou řádně uvedené v sekci References. Práce je založena na publikacích vzniklých ve spolupráci s dalšími spoluautory. Přínos autora je deklarován v sekci Author contributions. Práci je možné volně šířit v nezměněné podobě. Univerzita Palackého má právo uchovávat, zveřejňovat a šířit práci dle svých vnitřních předpisů a českého práva.

Název:	Detektory počtu fotonů a jejich aplikace v kvantových technologiích
Autor:	Mgr. Josef Hloušek
ORCID:	0000-0003-2923-3492
ResearcherID:	D-2890-2018
Školitel:	prof. Mgr. Radim Filip, PhD.
Konzultant:	RNDr. Miroslav Ježek, PhD.
Studijní obor:	Optika a optoelektronika
Instituce:	Katedra optiky, Přírodovědecká fakulta, Univerzita Palackého
Year:	2022
Pages:	122

Acknowledgements

I would like to express my gratitude towards people who have supported me all through the research and writing process. First, I would like to express my special thanks to Miroslav Ježek for his enthusiastic encouragement, invaluable mentoring, inspiring discussions, ideas, and for his leadership in the Quantum Optics Lab. I am also grateful for his guidance, beneficial consultations and constant support during my studies. He directly helped me throughout the journey, from searching a topic up till submitting the dissertation. I also want to thank my supervisor Radim Filip for his support, guidance, patience, help, scientific discussions, which improves my theoretical background, and for our common projects. He continuously motivated me and conveyed an enthusiasm towards my research. I am thankful to the whole QOLO team for their help and for maintaining a friendly and open atmosphere; with special thanks to Ivo Straka and Martina Nováková (Miková) for their unceasing assistance and support. I would also like to thank other members of Department of Optics for various support and their collaboration. I would like to acknowledge my colleagues from Institute for Theoretical Physics, University of Stuttgart for their collaboration. Special thanks go to Tobias Denzler. I thank all the collaborators I have not yet named with special thanks to Vojtěch Švarc and Michal Dudka, who shared their experimental know-how with me. I also thank our administrative team for making everything work.

I am especially grateful to all my friends I met at the department, namely Jaromír Běhal, Jan Bílek, Robert Stárek, Dominik Koutný, and Martin Paúr, for their pleasant company, friendly attitude and creative environment. In addition, a very special thanks goes to my family for their continuous support, endless patience, love, and care. Last but not least, my warmest thanks belong to my charming wife Dagmar and lovely daughter for their unconditional support and motivation throughout the dissertation.

Thank you

Pepa

List of publications

The following page contains lists of selected articles covering the results presented in this Thesis.

First-author publications

A1 J. Hloušek, M. Ježek, and R. Filip, 'Work and information from thermal states after subtraction of energy quanta', Sci. Rep. **7** (2017).

A2 J. Hloušek, M. Dudka, I. Straka, and M. Ježek, 'Accurate detection of arbitrary photon statistics', Phys. Rev. Lett. **123** (2019).

A3 J. Hloušek, M. Ježek, and J. Fiurášek, 'Direct experimental certification of quantum non-Gaussian character and wigner function negativity of single-photon detectors', Phys. Rev. Lett. **126** (2021).

Other co-author publications

C1 I. Straka, L. Lachman, J. Hloušek, M. Miková, M. Mičuda, M. Ježek, and R. Filip, 'Quantum non-gaussian multi-photon light', Npj Quantum Inf. **4** (2018).

C2 J. Mika, L. Podhora, L. Lachman, P. Obšil, J. Hloušek, R. F. M. Ježek, and L. Slodička, 'Generation of ideal thermal light in warm atomic vapor', New J. Phys. **20** (2018).

Articles in preparation

P1 J. Hloušek, J. Grygar, M. Dudka, and M. Ježek, 'High-resolution multi-channel coincidence counting system for large-scale photonic quantum technology', in preparation (2022).

P2 J. Hloušek, T. Denzler, V. Švarc, M. Ježek, E. Lutz, and R. Filip, 'Experimental quantum photonic Maxwell's demon', Submitted (2022).

Author contributions

The projects presented in this Thesis are the product of the close scientific colaboration. Here I give a detailed account of my speciffic involvements and contributions to each presented project and also appropriate credit to co-authors is ascribed.

[A1] J. Hloušek, M. Ježek, and R. Filip, *'Work and information from thermal states after subtraction of energy quanta'*, Scientific Reports **7**, 13046 (2017).
I constructed experimental setup, performed measurements and numerical simulations, and analyzed data. Miroslav Ježek helped supervise the project. Radim Filip suggested the theoretical idea, performed calculations, and supervised the project. All authors participated in writing the manuscript.

[C1] I. Straka, L. Lachman, J. Hloušek, M. Miková, M. Ježek, and R. Filip, *'Quantum non-Gaussian multiphoton light'*, Nature Partner Journals Quantum Information **4**, 4 (2018).
Lukáš Lachman and Radim Filip are responsible for the theoretical part. Ivo Straka constructed the source, performed the measurement, and process the data. I constructed the PNRD and helped with the alignment and setting the detector. All authors provided critical feedback and helped shape the research, analysis and manuscript.

[C2] J. Mika, L. Podhora, L. Lachmann, P. Obšil, J. Hloušek, M. Ježek, R. Filip, and L. Slodička, *'Generation of ideal thermal light in warm atomic vapor'*, New Journal of Physics **20**, 093002 (2018).
Jaromír Mika measured and proccesed the data. Lukáš Podhora built the experimental setup. The theoretical analysis was performed by Lukáš Lachman and Radim Filip. Petr Obšil prepared the pumping laser. I and Miroslav Ježek analyzed data, retrieved photon statistics and characterized the quality of observed Bose–Einstein statistics by evaluation of the Shannon entropy and relative entropy. Radim Filip and Lukáš Slodička initiated and coordinated project. All authors contributed to the manuscript preparation.

[A2] J. Hloušek, M. Dudka, I. Straka, and M. Ježek, *'Accurate detection of arbitrary photon statistics'*, Physical Review Letters **123**, 153604 (2019).
I worked out almost all of the technical details, and performed the numerical calculations for the suggested measurement workflow. I also built the experimental setup and performed the measurements and data analysis. Miroslav Ježek initiated and coordinated the project and supervised the experiment. Ivo Straka construct the a down-conversion source and participated in data analysis. I prepared the manuscript and all authors were involved in creating and revising the manuscript. All authors contributed to the discussion of the results.

[A3] J. Hloušek, M. Ježek, and Jaromír Fiurášek, *'Direct experimental certification of quantum non-Gaussian character and Wigner function negativity of single-photon detectors'*, Physical Review Letters **126**, 043601 (2021).
Jaromír Fiurášek initiated and coordinated the project. He was the lead investigator, responsible for all major areas of concept formation. I built the experimental setup for the direct certification of non-classical features of quantum detectors and performed the measurement and data analysis. Miroslav Ježek supervised the experiment and participated in analysis and interpretation of data. I and Miroslav Fiurášek provided the theoretical analysis and simulations of the detector response to explore the non-Gaussian character and Wigner function negativity of SPAD. Jaromír Fiurášek prepared the manuscript and all authors were involved in creating and revising the manuscript. All authors contributed to the discussion of the results.

[P1] J. Hloušek, M. Dudka, J. Grygar, and M. Ježek, *'High-resolution multi-channel coincidence counting system for large-scale photonic quantum technology'*.
I built the experimental setup for the multi-coincidence measurement and performed the measurement and data analysis. Michal Dudka designed and built presented high-resolution multi-channel

coincidence counting system (CCU). Jan Grygar and Michal Dudka analyzed the performance and capabilities of the CCU, and developed the software library. Miroslav Ježek initiated and coordinated the project. I wrote the manuscript with input from all authors.

[P2] J. Hloušek, T. Denzler, V. Švarc, M. Ježek, Eric Lutz, and R. Filip, *'Experimental Quantum Photonic Maxwell Demon'*.
Radim Filip conceived the idea and were in charge of overall direction and planning. Eric Lutz coordinated and supervised the theoretical statements of quantum thermodynamics. Tobias Denzler performed the analytic thermodynamical calculations and helped carry out the simulations. Vojtěch Švarc built a fully tunable and switchable coupler and assisted with the data collection. I built experimental setup, measured and analyzed the data. Miroslav Ježek helped carry out the experiment and contributed to the interpretation of the results. All authors contributed to the manuscript preparation.

Funding

The research presented in this Thesis was primarily supported by the Czech Science Foundation under the projects 17-26143S and 21-18545S. We have also received national funding from the MEYS and the funding from European Union's Horizon 2020 (2014-2020) research and innovation framework program under grant agreement No 731473 (project 8C18002). Project HYPER-U-P-S has received funding from the QuantERA ERA-NET Cofund in Quantum Technologies implemented within the European Union's Horizon 2020 Programme. Finally, Palacky University supported presented research by IGA projects: IGA-PrF-2016-009, IGA-PrF-2017-008, IGA-PrF-2018-010, IGA-PrF-2019-010, and IGA-PrF-2020-009.

Contents

Preface

My interest in optics goes back to my high school years. In the early stage of my bachelor's studies, I have joined the research group Quantum Optics Lab Olomouc, especially the photonic sources & detectors team. Under the co-supervision of Miroslav Ježek, I have actively participated in research projects of the lab. I started working on experimental research in the field of detection of single photons, photon-number-resolving techniques, and characterization of sources of light at the single-photon level. Our scientific efforts resulted in the development of an efficient workflow for photon-number detection of arbitrary optical signals with unprecedented accuracy (fidelity > 0.999) and a dynamic range of photon-number resolution up to 50. We also developed a method for direct verification of the highly nonclassical features of optical quantum measurements, such as quantum non-Gaussianity and the negativity of the Wigner function. Simultaneously, this experimental direction has been supported by my collaborations in quantum optics theory with supervisor Radim Filip and Jaromír Fiurášek.

This Thesis comprehensively presents mostly experimental outcomes based on the results achieved during my post-graduate studies at the Department of Optics, Faculty of Science, Palacký University, Olomouc. All of the results presented henceforth was conducted in the Quantum Optics Lab Olomouc. The presented Thesis is based on five published publications denoted in List of publications under [A1–A3, C1, C2]. The Thesis also uses other results achieved in ongoing projects whose manuscripts [P1, P2] are in preparation at the time of writing.

To bring the reader closer to the contribution of the presented experimental work, I aim to give a review of the experimental implementations and applications of single-photon detection and resolving the number of photons. I believe this Thesis will be of broad interest primarily to scientists working in the fields of quantum foundations, quantum information processing and quantum communication. Presented detection workflow can also be directly translated to other experimental platforms like emerging biomedical imaging and particle-tracking techniques. Moreover, the community dealing with a conditioned modification in photon statistics to achieve the required properties of measured light should appreciate the contribution of the presented results.

Olomouc
December 2022

Josef Hloušek
hlousek@optics.upol.cz
@PepaHlousek

Chapter 1

Introduction

In recent decades, a large part of the quantum optics community has focused on developing and characterizing single-photon light sources and detectors. It has been almost 90 years since the demonstration of the devices exhibiting single-photon sensitivity [1–3]. This major breakthrough initiated a multitude of new developments and technical improvements in single-photon technologies [B1–B5, 4–12]. Specifically, it includes quantum photonics technologies for single-photon generation [13–25], manipulation [26–36], and detection [37–74]. Appropriate detection techniques are necessary to determine the quality of the methods for generating quantum states of light. The generation of single photons goes hand in hand with their accurate detection, and technological progress in one of these disciplines will inevitably contribute to innovation in the other.

In general, single-photon detector (SPD) approaches are based on a proportional conversion of absorbed photons to current or voltage pulses, which are amplified and measured. These well-defined detector output signals "clicks" are collected and processed by electronic counting devices whose functionality solely depends on the used application. The growth of the optical network complexity in photon-consuming applications, such as multi-photon boson sampling [75–79], high-dimensional entanglement [80–85], and multi-photon qubits quantum information processing [86–88], motivates the research for detection technology improvements to process a high number of photons in the explored signal. Nowadays, highly efficient low-noise single-photon detectors are still merging as important devices for realizing many photonic applications [33, 89–101], both classical and quantum. However, studying and exploiting quantum properties of light rely on precise measurement and manipulation of light at the single-photon level. One of the critical requirements allowing this research area is the capability to detect and count individual photons. Of particular interest are the advanced detection techniques that make possible to distinguish the exact number of photons arriving at the detector. As indicated, the growing demand in modern quantum physics experiments for this type of information about the statistical properties of light drives the current effort to improve these advanced detection technologies.

Conventional single-photon detection concepts are primarily sensitive to the presence of light without any information about the number of input photons [B2, B4, B5, 5, 6, 8–12, 102]. Nevertheless, even these detection devices can be employed in a temporal or spatial configuration to obtain photon-number resolution [50, 64, 103–109]. In addition, the development of a new class of detectors based on superconducting materials has demonstrated inherent sensitivity to individual numbers of photons [B2, 38, B6]. These devices significantly outperform all existing single-photon detectors in detection efficiency and timing jitter. Advanced photon-number-resolving detectors (PNRDs) found their broadwise applicability in modern optical experiments benefits from the counting individual photons of the optical signal. The knowledge of photon-number statistics allows for

exploring the statistical properties of an unknown state of light required for the complete classification of optical sources. Photon-number resolution is a pivotal problem of quantum technology, impacting quantum metrology [110, 111], information processing [86–88, 112], and imaging [113]. The measurement of the statistical properties of light is a condition of secure communication [114] and quantum simulation. Furthermore, novel super-resolving emitter counting techniques will incorporate quantum statistics and correlations into classical super-resolving imaging. The recent progress in integrated photonics transforms SPDs and PNRDs into feasible technology for integrated quantum photonic systems [21, 22, 52, 58, 59, 62, 63, 65, 69, 71, 112, 115–120]

1.1 Outline

This Thesis covers most of the experiments and results of scientific research, which were realized during my Ph.D. study. My research is primarily focused on the precise measurement and conditional and deterministic modulation of quantum statistics of light using a photon-number resolving detector. Additionally, this type of detection device is employed in a novel direct experimental certification of the non-Gaussianity of the quantum optical detectors, namely single-photon avalanche diodes.The Thesis has in total five chapters organized as follows.

First, I start with the key goals and objectives of the presented research (Section 1.2), its challenges, further improvements, and its applicability in modern quantum experiments. Special emphasis is given to provide adequate information about the study area for the readers to analyze and evaluate proposed research in the context of the state-of-the-art methods in the field of photonic detection techniques and requisite complex signal processing (Section 1.3). I give details about basic properties and measurement metrics that are generally accepted for the characterization of the quantum state. Notably, key insights into different aspects of modern approaches of photon-number-resolving detectors are reviewed.

In Chapter 2 I give a brief account of experimental methods that are used in disertation. The key theoretical and experimental terminology is introduced and explained. The subject of Section 2.1 is the statistical properties of light, namely: definition in Fock basis and phase space, and how it can be obtained. Section 2.2 introduces several parameters associated with photon statistics which are commonly used to characterize quantum states of light. Furthemore, the various techniques to generate different quantum states of light are described (Section 2.3). Section 2.4 reviews one of today's most used single-photon detectors in optical laboratories: single-photon avalanche diode. In Section 2.5, the spatial multiplexed detection technique is fully discussed. In addition, the methods to reconstruct the photon statistics from the measured click statistics such as direct inversion and maximum-likelihood strategies are analyzed (Section 2.6).

In Chapter 3, an accurate detection technique is proposed that can distinguish between number of photons to achieve photon statistics and statistical correlations of the unknown state of light. Section 3.2 provides the description of the experimental implementation of the developed detection method based on a complex detector capable of partial photon-number resolution composed of several multiplexed single-photon avalanche photodiodes. Section 3.3 treats the problem of the electronic signal processing. Section 3.4 focuses on numerical simulations of the photon statistics retrieval processes in order to compare several algorithms in terms of accuracy and convergence speed. Experimental demonstration of the detection approach to access photon statistics is presented in Section 3.5. Various light sources were used to test the response of the detector: stabilized laser, quasi-thermal light, and heralded single-photon source based on spontaneous parametric down conversion. Finally, I discuss the future challenges of technological development and photon-statistics retrieval required to bring the presented PNRD configuration even further (Section 3.6).

Chapter 4 extends the arbitrary photon statistics detection concept to modify the statistical properties of light. Single-shot photon counting is used for conditional subtraction of the exact number of photons from the pseudo-thermal light to increase the mean photon number of the output state of light (Section 4.2). Furthermore, it is shown that these out-of-equilibrium states of light are useful for many applications in quantum information and thermodynamics. In Section 4.3 I discuss results of a custom-built source of arbitrary super-Poissonian statistics based on l-photon subtraction and active feedforward control and swapping. This experimental approach allows for deterministic generation of light states with super-Poissonian statistics created by mixing thermal state with the l-photon subtracted thermal state. Subsequently, the thermodynamics analysis of a quantum bosonic Maxwell's demon is presented.

Chapter 5 introduces a novel method to experimentally certify the quantum non-Gaussian character (Section 5.2) and Wigner-function negativity (Section 5.3) of the quantum photonic detectors. The presented technique builds on previous works focused on certification of quantum non-Gaussian character of quantum states and extends it to the detectors. Regularization of the detector POVM elements is done by using noiseless attenuation, which can be experimentally implemented by specific probe states: a vacuum state and two thermal states with different mean photon numbers.

Finally, the main results of the Thesis are reviewed in Chapter 6. I summarize our particular results and findings (Section 6.1). In Section 6.2 I also give the overview of problems and possible extensions of the developed methods.

1.2 Goals of the Thesis

The quantum properties of light are determined by its statistical properties. The knowledge of photon statistics can facilitate many applications not only in photonic quantum technology [86–88, 112] but also in quantum imaging [113], quantum metrology [110, 111], and many other fields. However, accurate detection of arbitrary photon statistics is still challenging mainly due to finite dynamic range of existing photon-number-resolving detectors. The chief goal of this Thesis is to advance scalable detection method of ultra weak photonic signals and remove some drawbacks of current analyzers of quantum statistics to achieve unprecedented accuracy of photon-number resolution without the necessity of detector tomography. We dealt with experimental development and characterization of a measurement workflow free of systematic errors consisting of a complex reconfigurable partial photon-number-resolving detector, custom electronic circuitry, and novel data processing algorithm.

Particularly, we have developed a complex single-photon detector capable of photon-number resolution with a fully tunable number of input channels, optimized efficiency, and time response. Presented detector is based on multiplexing of binary single-photon detectors. The tunability of the developed detector enables us to easily change the number of constituent single-photon detectors. Optical signal under test can be analyzed by one detector, two detectors (Hanbury-Brown and Twiss measurement), three detectors, and so on. This reconfigurability is useful for direct tests of nonclassical features of various physical systems, as it was later demonstrated.

The large number of output channels represents a challenge to subsequent data processing. Coincidence counters need to register single-detection events in all the output channels as well as all the possible coincidence events between the channels. The real-time processing of coincidence events becomes essential in the large-scale modern quantum photonics experiments, where the total number of events is too large to be stored and post-processed. Taking these requirements into account, we developed an ultra-fast multi-channel coincidence system with ten picosecond jitter allowing sub-nanosecond coincidence windows and dead time smaller than recovery time

of the used single-photon detectors. The coincidence unit was designed for counting coincidence events from singles to 16-fold coincidences with the full channel-number resolution.

Employing the advanced quantum reconstruction algorithms we have compensated for imperfections of detection process to estimate the photon statistics from the measured counting distribution. In addition, the photon statistics retrieval method has to cope with incomplete data which is the a typical problem of the channel-limited photon counting measurement. We have solved the inverse task of photon statistics retrieval by developing efficient algorithm based on the maximization-expectation method weakly-regularized by maximum-entropy principle which significantly improved the precision of the photon statistics measurement proposed so far. It breaks the finite-multiplexing limit and achieves unprecedented accuracy of photon-number resolution demonstrated for various photonic signals, including highly non-classical states, which surpasses even bleeding-edge cryogenic detectors.

Afterwards, employing a developed detector we have performed the measurement of quantum statistics of light from various sources. We also aim for direct evaluation of key statistical quantities, such as moments, Fano factor, entropy, $g^2(\tau)$ and other correlation parameters. Additionally, the non-classicality of multi-photon states of light was discerned. Experimental data confirmed the numerical simulations and quantified the developed method as a plausible characterization of the statistical properties of unknown states of light.

Furthermore, the developed detector enabled the realization of projects investigating conditional and deterministic modification of quantum statistics of light. Knowledge of the statistical properties of light allowed us to prepare states of light with super-Poissonian statistics. First, the conditional subtraction of l single photons from the thermal states of light results in a l-photon subtracted thermal states exhibiting super-Poissonian statistics with a l-times larger mean photon number than of the original thermal state. However, the photon correlation decreases closer to Poissonian light, and the mean photon number grows faster than its standard deviation. We performed this experiment to simulate thermodynamic processes, namely the dissipation of the energy of a quantum oscillator into a cold reservoir to produce energy that can be used to do work or transfer information. Afterwards, we used experimental experience with the generation of out-of-equilibrium states to design and implement a more advanced method to deterministically modify the statistical properties of light. By exploiting this technique, a complex triggering, controlling, and fast optical switching between states of light employing the novel fast photonic switch based on Mach-Zehnder interferometer, we have experimentally generated and characterized deterministic out-of-equilibrium states. As a result, other thermodynamic simulations were performed to analyze bosonic Maxwell's demon in the quantum regime.

The final goal of the work was to develop a new characterization method for photonic detectors. The presented approach requires only three probe states without any need for complex tomographic data processing. Accurate detection of photon statistics has application potential in the precise preparation of these probe states of the light, namely vacuum state and two thermal states with different mean photon numbers. Our efficient scheme allows the direct certification of quantum non-Gaussianity [121] or Wigner function negativity [122] of the optical quantum detector while avoiding all potential complications of quantum detector tomography. The results shown that this detector benchmarking technique can lead to further insight on the capabilities and limitations of quantum detectors.

In the future, our results could pave the way for precise verification and benchmarking of various photonic sources, a key requirement for their applications in diverse fields. It includes the characterization of statistics of single-photon and entangled sources with imminent applications in quantum communications. Future development of the presented detector will tackle the problem of super-resolution and counting of emitters with different brightness, blurred due to diffraction, and buried in excess noise. Also, the developed detection workflow allows for a single shot measure-

ment, as required for conditional state preparation [123], linear-optics quantum computing [124], quantum repeaters [125] and etc.

1.3 Contemporary state of research

In this part of the Thesis, I provide a brief overview and an assessment of the contemporary state of research in photon-number-resolving detection and related fields. I aim to present the most current research questions, problems, and perspectives that has not been explored yet. outlook on the previously conducted researches related to the main theme of this dissertation to help readers Also, it is addressed here why the proposed research is crucial in the context of modern quantum photonics and technology.

Characterization of quantum states of light
The detection method used for the quantum state characterization essentially affects how we describe these photonic states of light. In other words, wave-particle dualism also manifests itself in the task of detecting the properties of light in terms of its intensity. Generally, there currently exist two quantum detection approaches: optical homodyne detection and photon counting at single-photon level.

Continuous-variable (CV) homodyne tomography method is based on continuous quantum variables, the quadrature amplitudes of the electromagnetic field [126–132]. The method of optical homodyne tomography allows to measure phase sensitive properties of light and is suited to full tomographic reconstruction [B1]. Quadrature operators in a phase space representation are closely related to the wave nature of light. Optical homodyne detection uses interference between the investigated state and an intense reference laser beam (called local oscillator) at a balanced beam splitter. There were intensive research to develop methods to fully, or partially, reconstruct density matrix of the quantum state [132, B7]. Naive linear reconstruction methods usually fail as they lead to a rapid increase of noise. This can be resolved by using more advanced and robust statistical reconstruction methods such as the maximum-likelihood estimation method [133–137]. Nevertheless, the noise in the data still needs to be small (i.e. the number of measurements large) to obtain sufficient statistics and good reconstruction. It raises the question, what is the efficient tomographically complete set of measurements. Quantum homodyne tomography of an optical state is also the competing technique for determining the photon-number distributions (diagonal elements of the density matrix) but there are several disadvantages that one should be aware of. The implementation of homodyne detection needs the appropriate mode matching of the signal with a suitable local oscillator. Local oscillator mode has to overlap spatially and spectrally with the signal. Any imperfections in mode mismatch translate into losses that prevent accurate estimation of the overall detection efficiency.

Alternatively, instead of full tomographic characterization of the optical state under test, only a statistical characteristics, such as moments, Fano factor, entropy, $g^{(2)}$ and other correlation parameters can be extracted from measurements of photon statistics [A2, 138–150]. The discreteness of the allowed energies (due to particle nature of light) is reflected in this photon counting measurements [B1, B4, B8]. To cope with the quantum state characterization at the single-photon level, photon-number-resolving detection techniques are required to reveal information about the photon statistics of investigated light. Photon statistics measurement by photon counting is less demanding than full quantum homodyne tomography but still seriously limited in its dynamic range. As with all quantum detectors, photon-number-resolving detectors yield a finite-sized data, which bear a non-trivial relation to the input photon statistics. Retrieving the photon statistics from the raw data output of such detectors represents an open problem. To be more precise, the question is how

far we can improve the photon statistics retrieval accuracy given by the limited dynamic range, noise performance, crosstalk effect, and non-unity efficiency of the photon-number-resolving detector. The extreme difficulty here lies in improving the dynamical range and solving the ill-posed photon-statistics retrieval problem [B7, B9, 151].

Additionally, one can combine the advantages of the coherent detection scheme and photon-number-resolving detectors in a hybrid photodetection scheme [152–156]. Interferometric scheme of homodyne-like detectors can be extended by using SPDs or PNRDs instead of conventional photodiodes. This detection configuration allows getting more information about the unknown input state, which conditions the realization of new states or operations. The interferometric part yields phase-sensitive information, and PNRDs classify the statistical properties of photons to assess the quantumness of the output signals. This type of hybrid detection scheme paves the way to the implementation of continuous-variable communication schemes.

Single-photon detectors

This Subsection is written for the purpose of providing an insight into the background of single-photon detection technology. I describe briefly the major issues of the single-photon detectors. A detailed review can be found in the following references: Enss [B2], Silberhorn [5], Eisaman et al. [8], Natarajan et al. [9], Migdall et al. [B4], Chunnilall et al. [10], Hadfield [B5], Osellame et al. [11], and Zwiller et al. [12].

In general, single-photon detector is a device capable of registering the presence of photons. With the increase in interest in single-photon technologies, SPDs have become crucial for many applications which benefit from single-photon sensitivity. Continuous improvement of their performances rapidly expands the range of applications in various branches of industry, applied research, material science, and many other fields based on technologies capable of measuring ultra-weak optical signals. With the advent of ultra-sensitive detectors and quantum-enhanced metrology, we tend to perform measurements at the ultimate sensitivity levels dictated by the laws of physics [94, 95]. The goal is to reach the quantum advantage to improve the sensitivity of a measurement beyond the shot-noise limit, or to relax the requirements of the measurement, such as the minimum required detection efficiency. Optical transmittance measurement assisted by correlated photons and single-photon detectors can serve as a prominent example of a quantum-enhanced measurement scheme [97, 100, 157]. Single-photon detectors allow deeper insights into the quantum light sources characterization [C1, 158], non-classical light manipulation [159, 160], and modification of the statistical properties of light [28, 30, 161, 162]. As enabling the mass-manufactured devices, they are the most commonly used to read out the quantum information in quantum communication, computing, simulation, and cryptography [33, 89, 92, 99, 101, 163–167]. Using these devices, large-scale quantum photonics experiments such as Boson sampling [77, 78] were realized to demonstrate a advantage of quantum computing over the conventional supercomputers. Single-photon detectors have also found broad range of applications in biological and medical diagnostic procedures such as diffuse optical tomography [91], positron emission tomography [168], DNA sequencing [169–172], bioluminescence characterization [173], single-molecule detection and spectroscopy [90, 174–178], fluorescence microscopy and life-time measurement [96, 146, 179–181], and imaging and particle-tracking techniques [182–184]. Another single-photon detector starved applications are fiber-link characterization employing optical time-domain reflectometry (OTDR) [93, 105, 185–188], and the interaction of light with materials analysis [98, 189]. The preceding list of single-photon detector applications serves only as an example of their ultra-wide use. Many other applications can be found in the recommended literature listed above.

Detecting a light signal at the single-photon level is a difficult task. These days, a host of photodetector technologies built on various device structures, materials, and non-trivial physical phenomena have been realized to achieve single-photon sensitivity. These devices very often work

in the critical mode of operation; a single photon is able to induce macroscopic changes in the state of an electrical circuit, which are further amplified to be easily measurable. Specifically, a single-photon detector outputs an electronic pulse when a single or more photons are detected. A complex electronic circuitry is incorporated into each single-photon detector to register the electrical response corresponding to the optical detection. The number of the output electronic events in a given time duration (typically per second) is termed the detection rate; it is given in units of counts/s, or simply Hz.

Unfortunately, SPDs suffer from multiple undesirable features [B4, 5, 7] such as saturation effects and noise that complicate their electrical output. The measurement precision at the single-photon level is severely affected by the nonlinearity of the employed photonic detectors [190, 191]. The reason is that the other systematic errors need to be eliminated to reach the quantum regime, while the single-photon detectors themselves maintain strong inherent nonlinearity. Specifically, sometimes the detector outputs a pulse even when no photon is detected due to various noise contributions (i.e. dark counts [42, 192]) or as a result of previous detection (afterpulses [193–199] or twilight pulses [200–202]). Furthermore, the detector occasionally fails to detect photons because it is not ready to do so after the previous detection event, such as during recovery time, latching [9] etc. One can observe a complex interplay of detector-specific phenomena, such as dark counts, dead time, recovery transition, multi-photon response, and latching. These detection imperfections cause highly nontrivial nonlinear behaviour that is much stronger compared to classical photodiodes used for a high-intensity light. Notably, they are specific to a particular single-photon detector due to their different operational principles and prevent us from reaching the ultimate precision of quantum-enhanced measurements. Thus, characterization of single-photon detectors has become an important task in order to compare and select detector with the best parameters for specific applications. With this goal in mind, it is of paramount importance to improve our knowledge of single-photon detector behaviour and performance parameters. A perfect single-photon detector should meet several requirements such as high detection efficiency, the largest possible detection bandwidth, low noise, large dynamic range, and linear response. There exist significant interplay between detection efficiency, dark counts, operating temperature, etc. In most applications, however, only one or two parameters is critical and others are often compromised.

In the following, I give an brief overview of the single-photon detectors. The discovery of the photoelectric effect initiated the invention of the first single-photon detector, photomultiplier tube (PMT) [1]. This device was first used to detect single photons approximately 90 years ago. Nowadays, the efficiency of PMTs is rather small, typically in the range of 10% to 50%, and therefore unsuitable for modern quantum experiments. Currently, single-photon avalanche diode (SPAD) is probably the most used photodetectors optimized for single-photon detection that works at room temperature or slightly below. The sensitivity to single photons is based on a negative biased p-n junction above the breakdown voltage where electron-hole pair can trigger an avalanche multiplication process of free charge carriers (Figure 1.1(a)). The photon-count conversion process is controlled by an electronic circuit that performs the following operations: (1) detects the leading edge of the avalanche current corresponding to the avalanche breakdown, (2) generates and standards an output electric pulse, (3) lowers the applied bias voltage to the breakdown voltage, thus starting the avalanche quenching process, and (4) restores the photodiode voltage to the operating value at which the photodiode is capable of further detection. Avalanche photodiode (APD) operating in this so called Geiger mode [102], discriminates only between „zero photons“ and „one photon or more“ without further photon-number resolution. Their robustness, compactness, and relatively high quantum efficiency in the near infrared region has led to massive use in a plethora of applications. As of today, SPADs keep proving their prominent role in quantum photonics experiments especially when polarization insensitivity or a wide active area of the detector is required. Another example of practical applications of SPADs are experimental setups that do not

allow the use of a cryostat. I give a detailed review of the SPAD fundamentals and of the relevant characteristics of its operation in Section 2.4.

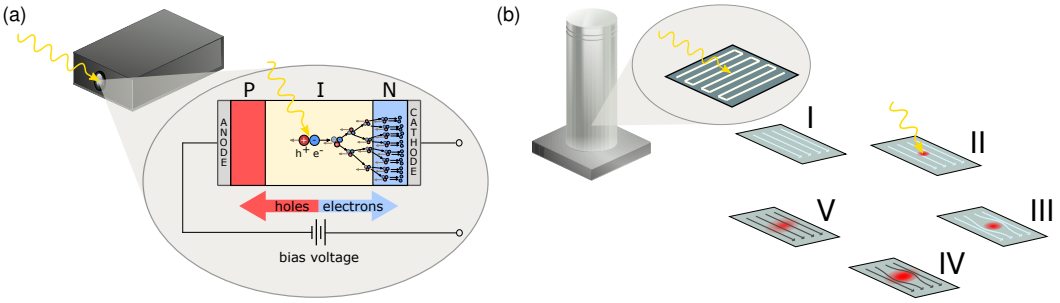

Figure 1.1: Single-photon detection: (a) single-photon avalanche photodiode, and (b) superconducting nanowires single-photon detector.

Since the first demonstration of single-photon detection with superconductors [41], intensive research to effort technical improvements in superconducting-based technology has started [44, 55, 69, 203–206]. Current state-of-the-art technological platform for single-photon detection based on superconducting materials combines a high efficiency, low timing jitter, relatively short recovery time, and negligible dark counts. However, these types of materials need to be cooled down to cryogenic temperature [B2, B5, B6]. Here is a list of superconducting devices: superconducting quantum interference device (SQUID) [207], hot electron bolometer, transition edge sensor (TES) [B6], and superconducting nanowire single-photon detector (SNSPD) [12]. Here I focus mainly on the SNSPD and TES as an established technology with remarkable performance up to date. TES, in addition to single-photon sensitivity, provides a photon-number resolution, hence they are described in more detail in the following Subsection *Photon-number-resolving detectors*. Detailed information about other cryogenic detectors can be found in the references mentioned above.

SNSPDs usually have a nanowire/nanostrip structure with a nanoscale active area and operates significantly below room temperature, typically in the range of 1 - 4 K. When a photon is absorbed by the current-biased SNSPD, a local resistive domain can be observed, resulting in a voltage pulse, which indicates a detection event. The absorption of a photon in a superconducting nanowire produces a growing hotspot self-heated by Joule heating (Figure 1.1(b)). Thus, the recovery circuit returns the optimal current to the nanowire and cool down the system. However, the operation of SNSPD suffers from the latching behaviour. It means that the detector is not able to detect incident photons because the cooling process of the hotspots (created by previous photon absorption) becomes slower than the electrical response of readout and recovery circuits. Even if we set the electrical response time longer enough to avoid this latching effect, detector recovery speed is still limited by the thermal response of the superconducting materials itself. SNSPDs reach quantum efficiency above 95% [208, 209], low dark counts (0.01 Hz) [66], and timing jitter down to 2.6 ps. It is important to stress that these properties have never been achieved in the same device due to limits of detector subtleties and technological trade-offs [9, 55]. The prevalent designs of SNSPD are based on the nanowires yielding the efficiency depending on the polarization of light, which limits their applications in polarization-based experiments. However, a SNSPD development driven by applications requirements resulted in the demonstration of the polarization independent detection devices employing various different approaches [47, 54, 57, 67, 210–212].

Furthermore, several types of single-photon detectors, including SPADs, SNSPDs, and TESs, have been successfully integrated into waveguides [52, 58, 65, 69, 71, 116–120, 213–215] and cavities [59, 62] with the aim to increase the detection probability. These successful integration processes

also initiated the integration of modern quantum photonic technologies to build fully integrated quantum systems where generation, manipulation, and detection are all included on the same chip. Integrated quantum photonic circuits have emerged as a compact and scalable platform for modern complex quantum information science technologies and applications [112] such as quantum key distribution, random number generator, quantum information processing, multi-photon interference, boson sampling, and quantum walks. However, despite partial successes in integrating SNSPD with quantum circuits [116, 117] or photon sources [21, 22] so far, integration of all components in one chip has not yet been realized. Further pioneering investigations in the field of integrated quantum photonics have to be done to overcome all remaining challenges.

To conclude, the indisputable advantage of SPADs is that the detection process is immune to magnetic fields, insensitive to polarization of the light, and operates without cryogens. SNSPDs as low-temperature single-photon detectors with leading performances such as high efficiency, low noise, and excellent timing resolution set new benchmarks in the field of single-photon detection. TESs are also powerful single-photon detectors with high efficiency and low dark counts. In addition, they are energy-resolving detectors of single photons with, unfortunately, limited dynamic range.

Photon-number-resolving detectors

A photon-number-resolving detector, in general, is defined as a detector that can determine the number of photons in an input optical signal. In other words, it is a photon detector combining single-photon sensitivity with a linear response – its electronic output is proportional to the photon number. Four aspects are typically discussed in connection with these detectors; namely, the resolution of individual photons, the dynamic range given by the maximum detectable photon number, overall efficiency, and the detector speed given by the maximum repetition frequency. In the following, let me introduce the most promising photon-number-resolving approaches up to date and review the operating principles and the latest advances in the performance of various methods and PNRD configurations. In particular, the trade-offs and limits of these devices are compared and discussed.

A range of important quantum photonics experiments exploits the unique capabilities of PNRD. Photon-number resolution brings detection to the next level and enables fundamental advances in almost every light-detection application. Obviously, efficient detection with the full photon resolution dramatically reduces errors in a host of research fields focusing on quantum measurements. PNRD architectures cope with the incoming photon-number statistics measurement and characterization of quantum states [143, 145, 147–150, 216–222]. They can determine whether a state of light is classical or non-classical [118, 143, 145, 147, 223–226]. PNRDs also found their applications in particle physics to detect Cherenkov photons [227] or positrons [228]. Furthermore, the precise knowledge of the statistical properties of light is required to prepare the conditional states of light whose quality of preparation significantly depends on the ability to resolve the photon number. Specifically, PNRDs give rise to the development of optical sources of single-photon [23, 24] and clusters of N single-photon states or multi-photon Fock states [20, 25, 229–234], non-Gaussian quantum states [123, 235], and NOON states [236, 237]. PNRDs are needed in the fields of the quantum communication, quantum computing, and quantum information processing [33, 88, 124, 238–243]. PNRDs have also demonstrated their application potential in quantum metrology [94, 110], sub-wavelength interferometry [244], and the ultimate phase estimation [245–247]. Applications of the PNRDs have been extended to modern sensing and imaging technology [248] applicable in biomedical and biophotonics research [106, 113, 146, 249, 250]. Another potential application of PNRDs was recently highlighted in improvements of the signal-to-noise-ratio in laser-based radar (LIDAR) systems [251, 252] by thresholding the photon number instead of directly detecting intensity.

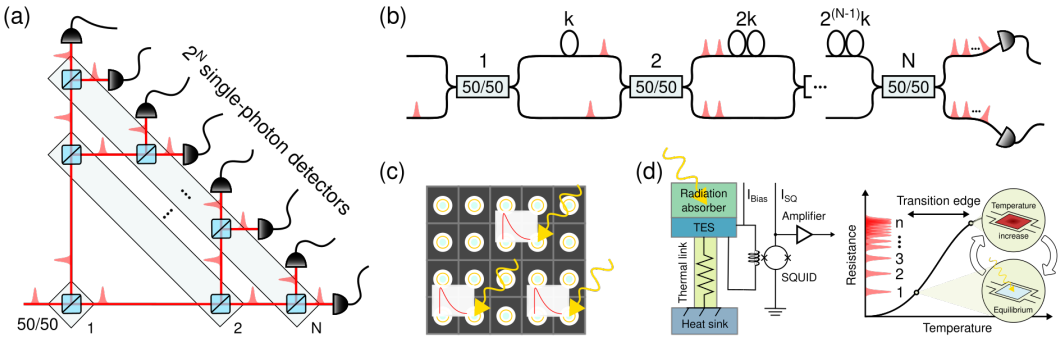

Figure 1.2: Photon-number-resolving detectors: (a) spatially-multiplexed optical network, (b) time-multiplexed optical network, (c) multi-pixel detector, and (d) transition edge sensor.

To this date, many various technological approaches to reach the photon-number resolution have been designed and experimentally verified (Figure 1.2). These approaches can be divided into two categories: inherent photon-number-resolution [B5, B6] and multiplexing/multipixeling detection scheme [5, 8, 10, 12]. The former, single-photon detectors with inherent photon-number resolution, intrinsically produce an electronic output proportional to the number of absorbed photons. Such inherent energy/quanta resolution was obtained for a family of cryogenic devices, namely visible-light photon counters (VLPC) and TES [B5, B6].

One of the first realizations of a photon-number-resolving detector was the visible-light photon counter. VLCPs are semiconductor-based photon-number-resolving detectors offering high detection efficiency (over the 90% at maximum) from visible wavelengths up to 1 μm [253]. These detectors operate at the temperature around 6 K. In principle, VLPC outputs a voltage pulse which is proportional to the number of simultaneously absorbed photons. However, as the number of photons increases, the distinguishability between the corresponding voltage pulses decreases dramatically. As of today, the photon-number detection with the resolution of up to 5 photons was performed [142, 204, 254]. The main disadvantages of VLPC are rather high dark counts of tens of kHz at maximum, quite large dead time of 100 ns, and a low max count rate of approximately 100 kHz.

Another type of single-photon detectors with photon-number-resolving capability whose operation relies on low-temperature superconducting materials is TES (Figure 1.2(d)). These versatile energy resolving detectors of single photons are highly sensitive microcalorimeters operating near thermal equilibrium [38]. The operating temperature is below 1 K (typically 100 - 400 mK) that places significantly higher demands on the experimental techniques and sophisticated laboratory equipment. However, low operation temperatures imply low thermal noise reflecting in the negligible dark counts. The absorption of an incident photon heats the superconducting transition causing a change in resistance to draw a current processed by fast SQUID read-out electronics [53, 60, B6, 255–258]. Transition-edge sensors report the highest detection efficiencies close to 100% (>98% at 850 nm and >95% at 1550 nm). Nevertheless, these detectors possess a slow response with the typical recovery time on the order of a few microseconds, limiting the maximum rate below 1 MHz. They also have a finite energy resolution limit due to crosstalk between detected photon numbers. TES typically resolves up to 10 or 20 photons, depending on the wavelength. The latest work pre-published on arXiv even extends the resolving capability of the TES detector to a maximum of 37 photons [74].

Additionally, contrary to general belief, conventional APDs are partially capable of detecting the number of photons by precise measuring of the very weak avalanches at the early stage of

their development [48, 259, 260]. In this sub-saturated mode, the single-photon avalanche diode is gated by subnanosecond excess bias voltage pulses. To resolve the incident number of photons, the avalanche current has to be measured shortly after the onset of avalanche build-up and before it saturates in the device. A special self-differencing electronic circuits [261] eliminating the capacitive response of the APD allows the detection of these unsaturated avalanches, for which the output voltage scales proportionally with the number of absorbed photons. This type of detection device is able to resolve avalanches up to four photons so far. Also, the first evidence of multi-photon resolution using a conventional one-pixel superconducting nanowire single-photon detector was presented [68]. This is made possible by the photon-number-dependent resistance of the nanowire during an optical wavepacket detection event. As a result, the generated electronic signals have different rise times, which can be measured by low-noise read-out circuit. This method indicates the photon-number resolution of up to four photons so far. Thus, both mentioned photon counting methods are significantly limited by their low dynamic range.

As an alternative to the mentioned devices inherently resolving the photon numbers, multiplexing or multipixeling of binary detectors transforms these ordinary single-photon detectors into PNR detector architectures. Generally, the indivisibility of single photons allows splitting the optical signal among a number of on/off detectors forming an optical multiplexing network [103]. There is a long history of the photon-number-resolving detectors using spatial [A2, 50, 64, 105–108, 262, 263] and time-multiplexed [45, 64, 104, 109, 264–267] networks probabilistically splitting the initial light into multiple number of output modes measured by binary detectors. In a similar manner, individual single-photon detectors can be arranged in an array to create a multi-pixel active area of the new detector with photon-number resolution [105–108, 113, 262, 263, 268–272].

Spatial multiplexing is typically formed by beam splitter cascade to divide the optical field into many spatial modes (Figure 1.2(a)). Such spatially distinguished photons are detected by regular single-photon detectors conveniently integrated into the multiplexed detector [A2, 64, 144, 218, 273]. There is a considerable interest in modeling a response of spatial multiplexing detection scheme [23, 103, 268, 274, 275]. These types of PNR detectors can be employed in applications where time response is crucial. The overall dead time of this architecture is given by the largest of all dead times of the employed individual detectors. However, the total jitter will scale with the number of detection channels M as $\tau_{\text{tot}} = \sqrt{M}\tau$, where τ is the jitter of a single constituent detector. These PNRDs also suffer from dynamic range-versus-scalability compromise.

Another PNRD multiplexing approach is based on measuring temporal modes instead of spatial modes (Figure 1.2(b)). Particularly, an efficient loop-based architecture was experimentally demonstrated [45, 104, 109, 264–267, 276–278]. Though being economical in respect to the number of on-off detectors employed, the extreme difficulty with loop-based approaches lies in reaching a large number of output detection channels in a short period of time, which translates to the requirements of low loss and high extinction ratio of the multiplexed network and, at the same time, high efficiency and short recovery time of the single-photon detectors employed. Decreasing the losses and balancing temporal multiplexers require a great deal of optimization [267] or even active signal switching [279]. Recently, temporal multiplexing with a binary switch was demonstrated to overcome saturation limitation, and extend the sensitivity of single-photon binary detectors [109].

The last alternative is to divide the active area of the detector into many pixels (Figure 1.2(c)). Many schemes of multi-pixel photon counters (MPPC) [105–108, 113, 262, 263, 269–272, 280, 281] have been reported. Recently, integrated superconducting nanowire single-photon detectors arranged into arrays were developed [63, 69, 115]. This method makes it possible to design a detector with a large number of detection channels in a small footprint. On the other hand, multi-pixel PNRDs typically suffer from strong coupling between different pixels (crosstalk effects) [282–284], which demands an extensive characterization of the detector [285] and advanced numerical post processing to correct for the imperfections [270, 281]. Also, the multi-pixel detectors offer very lim-

ited reconfigurability and complicate channel balancing. Still, a 24-pixel photon-number-resolving detector based on superconducting nanowires was developed and tested with coherent states [63].

Unfortunately, an ideal unlimited photon-number resolution is practically impossible due to finite photon number sensitivity, non-unity detection efficiency, and noise performance of the generally accepted interpretation of photon-number-resolving detection techniques. As the number of photons increases, the inherent ability of employing materials to distinguish between the photons decreases. Alternatively, the finite number of channels, pixels, or loops of the detector limits the achievable dynamic range of photons. Among the approaches proposed so far to photon-number-resolving detection, TES and VLPC benefit with the inherent capability to discriminate photon number observing near-unity detection efficiency. Compared to SPAD and SNSPD, TESs exhibit relatively poor timing performance; a timing jitter in order of ns and a recovery time typically several hundreds of ns. In addition, VLCPs are not sensitive at telecommunication wavelengths. Still, conventional SNSPDs and APDs in sub-saturated mode provide multi-photon detection but very limited resolution and dynamic range. On the other hand, spatially and time-multiplexed optical networks promise a wider dynamic range with almost no crosstalk between detection channels. Time multiplexing of single-photon detectors is easily scalable but suffers from effects of fiber dispersion and losses. Or, as is the case with TESs, approaches based on time-multiplexing are plagued by long dead times [109], complicating their use in telecommunications. Implementing multi-pixel photon counters, where several APDs or SNSPDs referred to as pixels are embedded into a single chip, is limited by high dark counts and crosstalk probability. The array of SNSPDs offers a high detection efficiency. However, the effect of crosstalk between pixels is unique to these detectors and must be taken into consideration. Recently, inherent photon-number-resolving TES detectors were spatially multiplexed into a system capable of resolving higher tens of photons in the presence of not inconsiderable crosstalk [20, 60, 74]. To conclude, it is impossible to highlight only one of the mentioned photon-number-resolving approaches proposed so far, as neither offers sufficient PNR detection quality.

Multi-photon coincidence data acquisition and processing

A coincidence counting unit (CCU) is a device that can count the coincidences of two or more electrical inputs. The increasing complexity of the recent scientific experiments challenges developing efficient multi-channel coincidence counting systems with high-level functionality. The information about successful detection events gives rise to a histogram of all possible n-fold coincidences or can be directly employed as a trigger signal for implementing the real-time feed-forward control to change the performance of the system or measurement configuration. Also, CCU performance parameters such as a high number of channels, high counting rate, channel-number resolution, and on-the-fly analysis of multiple photon coincidences are in demand.

Precise coincidence counting systems are useful tools widely employed in engineering and science applications requiring detecting a huge number of photons (or other particles) and processing the detected signals. Historically, the development of coincidence counting techniques was a necessary ingredient for a massive boom of discoveries in particle physics [286]. One of the latest works using coincidence counting electronics is the LHCb experiment at CERN standing behind the discovery of a new class of particles - a type of four-quark particle [287]. These counting devices found their application in biochemistry and molecular biology in the field of biomedical imaging and particle-tracking techniques [96, 250, 288–290]. Modern quantum photonics is advancing a new trend of experiments with the increasing number of components and complexity [75, 76, 79, 84]. These large-scale photonics systems hinge on the ability to generate, control, and analyze the multi-photon quantum states [81, 82, 84, 291] frequently used in quantum applications such as quantum communications [292, 293], quantum computation and simulations [294]. Particularly, complex coincidence processing has become an integral part of verifying unknown optical states

detected by photon-number-resolving detectors based on multiplexing [A2, 103, 274]. Verified statistical properties of light are routinely applied to quantify the non-classicality of light [C1, 225, 295–297]. Alternatively, information about the number of photons could be used in the implementations of feed-forward control to change the performance of the system or measurement configuration. The single-run output of the CCU can be used for direct modification of the statistical properties of the initial light in a way of multi-photon subtraction [35, 298].

Conventional approaches to coincidence evaluation are 1. time to amplitude converter (TAC) together with a single or multi-channel analyzer, 2. time to digital converter (TDC) followed by postprocessing, and 3. logic overlap coincidence systems realized with discrete components or using a field-programmable gate array (FPGA). TAC and TDC both typically offer tens of picosecond resolution. TACs are not easily scaled up for multi-coincidence systems and possess a considerable dead time limiting rate throughput to tens of thousand events per second [299, 300]. TDC based solutions stream time tags to a computer for further processing. Therefore a large amount of data is processed offline. Alternatively, TDCs are combined with an FPGA for the subsequent processing [301]. Pulse overlap coincidence systems use fast logic gates and multiplexers to capture detection events and detect coincidences [300]. Coincidence counting and histogramming could be programmed into a microcontroller (MCU) [302] or an FPGA [303]. Functional blocks such as internal delay lines, coincidence counter, and processor could be implemented in the same FPGA chip [304–307]. Lately, multi-channel TDC based coincidence counter architecture in the same FPGA chip while providing real-time operation was introduced [308].

States of light generated by the controlled photon addition and subtraction

The ability to control physical systems at the quantum level is essential for quantum applications. The conditional addition and subtraction of single or multiple photons from the light field represent experimental techniques widely used for modification of statistical properties of quantum states of light. Designing and realizing the schemes of adding or subtracting a higher number of photons in the laboratory have been challenging tasks to the researchers. Different measures have been applied to quantify the effect of subtraction procedures [309–311]. Detailed discussion of these experimental techniques is presented in [B3].

The excitation of classical states by a single photon was formulated in the early 1990s [312]. A beam splitter (BS), one of the most commonly used optical components for a optical experiments, proved to be a suitable experimental device for approximating the creation and annihilation operator. Employing BS with transmittance close to unity allows preparing conditional output states by mixing the signal modes while measuring photons in one of the output channels. Conditional output measurement makes these unique quantum state preparation techniques probabilistic with a typical low success rate. Additionally, the ability to resolve photon number plays a key role in the scenario of multiple photons subtraction/addition. In general, the conventional addition and subtraction operations are not just a matter of photons. In recent years, single-phonon – a quantum of vibrational mechanical energy [313] or a quantum of sound energy [314, 315] – addition and subtraction was experimentally demonstrated.

The addition and subtraction procedures [B3, 26, 28, 30, 32, 161, 316–318] have shown strong promise in preparing various quantum states: photon subtracted thermal states [29, 31, 162, 298, 319], photon added thermal states [29, 319–322], and photon added coherent states [27]. Additionally, these procedures transform a classical to a non-classical states [27, 323, 324]. The photon subtraction can also be employed in entanglement distillation [325–327]. They have been used for quantum filtering [328], noiseless amplification [329–331], quantum cloning [332], enhanced interferometry [333], etc. Shaping the statistics of light and using non-classical optical signals as measurement probes allow for increasing the precision of length measurements [111, 334].

Chapter 2

Methods and tools

In Chapter 2, I briefly summarize all the main theoretical formalism and experimental methods used in the Thesis. I focus on defining research methodology based on the previous books [B1–B5, B7–B19] and review articles [5, 8, 10, 11, 112, 311, 335].

First, I discuss light in a sense of photons as quanta of the electromagnetic field and their statistical properties. I give an overlook of the quantum states and their photon statistics that occurred in the Thesis. The quantum states of light are commonly identified and characterized by several parameters related to the statistical properties. The most significant ones are defined below. Following, I discuss the methods of carrying out research work that explains the techniques used for the generation of various quantum states of light such as pseudo-thermal light, multi-photon subtracted states of light, and multi-photon states of light. Furthermore, the applicability, functionality, and parameters of a single-photon avalanche photodiode are discussed. These single-photon detectors served as a building block of a spatial multiplexed photon-number resolving detector. I performed analytical modeling of a balanced spatial multiport to fully describe the transformation of the incident light. Finally, I make a special effort to explain the photon statistics retrieval methods using different reconstruction algorithms.

2.1 Statistical properties of light

The quantum theory of light via quantization of Maxwell's equations implies the existence of elementary excitations of the electromagnetic field - photons. A photon represents the smallest energy quantum that an electromagnetic field (at a given frequency) can exchange with its surroundings. The energy of the photon is defined as $E = \hbar\omega$, where $\hbar$ is the reduced Planck constant and ω represents frequency. These particles behaves like independent oscillators and thus quantized electromagnetic field is described by a Hamiltonian

$$\hat{H}_k = \sum_k \hbar\omega_k \left(\hat{n}_k + \frac{1}{2}\right), \tag{2.1}$$

where $\hat{n}_k$ stands for the operator of number of photons in a mode k. To simplify the notation, let us discuss a light occupying a single mode with average energy

$$\langle n|\hat{H}|n\rangle = \hbar\omega\left(n + \frac{1}{2}\right). \tag{2.2}$$

The states $|n\rangle$ are called Fock states. The Fock state basis is a convenient description of light frequently used when a statistical features of light are measured. The energy $\hbar\omega/2$ is associated with the vacuum state $|0\rangle$ (there is no photon present: $n = 0$). The creation $\hat{a}^\dagger$ and annihilation $\hat{a}$ operators change the number of photons in the Fock state basis

$$\hat{a}|n\rangle = \sqrt{n}|n-1\rangle \quad \text{and} \quad \hat{a}^\dagger|n\rangle = \sqrt{n+1}|n+1\rangle, \tag{2.3}$$

where $\sqrt{n}$ and $\sqrt{n+1}$ are proportionality factors coming from the symmetric indistinguishable nature of bosons. Creation and annihilation operators obey the commutation relation for a bosonic system $\left[\hat{a}_i, \hat{a}_j^\dagger\right] = \delta_{i,j}$, $\left[\hat{a}_i, \hat{a}_j\right] = \left[\hat{a}_i^\dagger, \hat{a}_j^\dagger\right] = 0$, where $\delta_{i,j}$ is a Kronecker delta. Fock states form the orthonormal basis $\langle n|m\rangle = \delta_{n,m}$. They are also eigenstates of the number operator $\hat{n}|n\rangle = \hat{a}^\dagger\hat{a}|n\rangle = n|n\rangle$, where n is an integer non-negative number indicating the number of photons. Any Fock state $|n\rangle$ can be obtained by application of the creation operator to the vacuum $|0\rangle$,

$$|n\rangle = \frac{1}{\sqrt{n!}}\hat{a}^{\dagger n}|0\rangle. \tag{2.4}$$

A generic quantum state of light is fully represented by its density matrix

$$\hat{\rho} = \sum_{i,j} P_{i,j}|\psi_i\rangle\langle\psi_j|, \tag{2.5}$$

where $P_{i,j} = \langle\psi_i|\rho|\psi_j\rangle$ and states $|\psi_{i,j}\rangle = \sum_n \langle n|\psi_{i,j}\rangle|n\rangle$. For a continuous basis, like position eigenbasis, the summation turns into an integration. The density matrix in the Fock basis can be written as

$$\hat{\rho}_{n,m} = \sum_{n,m} P_{n,m}|n\rangle\langle m|. \tag{2.6}$$

In this Fock state representation, the diagonal elements $P_{n,m}$ indicate the probability of registering just n photons when measuring the state (2.6)

$$P_{n,n} = \langle n|\hat{\rho}|n\rangle = \mathrm{Tr}[\hat{\rho}|n\rangle\langle n|] = p_n, \tag{2.7}$$

obeying $\mathrm{Tr}[\hat{\rho}_{n,n}] = \sum_n p_n = 1$. The Wigner function is a frequently employed tool for a description of the quantum states of light [126, 145, 221, 336, 337]. Operators of coordinate $\hat{x}$ and momentum $\hat{p}$ are defined using annihilation and creation operators $\hat{x} = \sqrt{\frac{\hbar}{2\omega}}\left(\hat{a} + \hat{a}^\dagger\right)$ and $\hat{p} = \imath\sqrt{\frac{\hbar\omega}{2}}\left(\hat{a}^\dagger - \hat{a}\right)$, satisfying the commutation relation $[\hat{x}, \hat{p}] = \mathrm{i}\hbar$. The Wigner function of the conjugate variables is a quasi-probability function introduced by Wigner in 1932 [338],

$$W(x,p) = \frac{1}{\pi\hbar}\int dx' e^{\imath 2x'p}\left\langle x - x'|\rho|x + x'\right\rangle. \tag{2.8}$$

Alternatively, Wigner function can be written in terms of density matrix $\hat{\rho}$

$$W_{\hat{\rho}}(x,p) = \frac{1}{\pi\hbar}\int dx' e^{\imath 2x'p}\rho_{mn}\left\langle x - x'|m\right\rangle\left\langle n|x + x'\right\rangle = \sum_m\sum_n \rho_{mn}W_{mn}(x,p). \tag{2.9}$$

For the diagonal elements $W_{mn}(x,p) = W_n(x,p) = \frac{1}{\pi\hbar}\int_{-\infty}^{\infty}\mathrm{d}y\,\psi_n(x-y)\psi_n^*(x+y)\mathrm{e}^{2iyp}$, where $\psi_n(x)$ is a wave function of the n-th Fock state. The Wigner function can also be achieved directly by measuring the mean value of parity operator $\langle P\rangle = \sum_n(-1)^n p_n$ since $W(0,0) = \langle P\rangle/\pi$.

2.2 Characterization of statistical properties of light

The various techniques for determining the statistical properties of light are discussed in Section 1.3. The statistical distribution of the number of photons p_n provides fundamental information on the intrinsic statistical nature of photons in any light source. Specifically, the first and second central moments are often examined,

$$\langle n\rangle = \mathrm{Tr}[\hat{a}^\dagger \hat{a}\hat{\rho}] = \sum_{n=0}^{\infty} n p_n \quad \text{and} \quad \left\langle (\Delta n)^2 \right\rangle = \sum_{n=0}^{\infty} \left(n - \langle n\rangle\right)^2 p_n. \tag{2.10}$$

The relation between the first and second moments of photon statistic distribution defines what kind of light field it is. In general, three different types of photon statistics can be obtained:

$$\begin{aligned} &\text{Poissonian:} && \langle (\Delta n)^2\rangle = \langle n\rangle, \\ &\text{sub-Poissonian:} && \langle (\Delta n)^2\rangle < \langle n\rangle, \\ &\text{super-Poissonian:} && \langle (\Delta n)^2\rangle > \langle n\rangle. \end{aligned} \tag{2.11}$$

The features crucial for fundamental research as well as many photonic applications are non-classicality and a deviation from Poisson statistics. Thus, parameters revealing the property of the state of light related to its statistics is often verified, like the Fano factor, the Mandel parameter, the binomial parameter, and second order Glauber correlation function. These characteristics depend on the first two moments of photon statistics, particularly the mean photon number $\langle n\rangle$ and the second moment $\langle n^2\rangle$, but behave differently in the presence of losses.

The Fano factor [339], defined as the variance-to-mean ratio of photon number,

$$\text{Fano} = \frac{\langle (\Delta n)^2\rangle}{\langle n\rangle}, \tag{2.12}$$

is viewed as a noise-to-signal ratio and serves as convenient noise-indicator of a non-classical field [340]. Following the above remarks, for Fano < 1, the light has photon number noise smaller than coherent light and is referred to as sub-Poissonian. Coherent light with Poissonian distribution exhibits Fano $= 1$. Whereas for Fano > 1, the light is called super-Poissonian. Specifically, for thermal light Fano $= \langle n\rangle + 1$ scales linearly with $\langle n\rangle$ and approaches unity only for very small mean photon numbers $\langle n\rangle$. In a similar manner, the Mandel parameter is defined as a ratio of the first and the second moments of photon distribution [138],

$$Q_{\mathrm{M}} = \frac{\langle (\Delta n)^2\rangle - \langle n\rangle}{\langle n\rangle} = \text{Fano} - 1. \tag{2.13}$$

This parameter is frequently used for experimental characterization of the departure of the photon statistics from Poissonian distribution [138, 341]. Poissonian distribution with the mean photon number $\langle n\rangle = \langle (\Delta n)^2\rangle$ reaches the Mandel parameter $Q_{\mathrm{M}} = 0$. Chaotic thermal light with super-Poissonian statistics reveals photon bunching and the Mandel parameter $Q_{\mathrm{M}} = \langle n\rangle$. Specifically, $Q_{\mathrm{M}} = 0$ define a boundary between classical and quantum fields [139, 341]. A specific issue that needs to be addressed is that Q_{M} cannot be measured directly due to the inability to register the true number of photons in an initial light. Thus, the Mandel parameter can be negative even if the optical field is completely classical. These false non-classicality certifications are caused due to the effects of noise and losses. In particular, losses annihilate some photons, and thus the photon statistics for a small number of counts are affected [274].

The difficulties associated with the difference of the measured click statistic from the photon statistics can be partially eliminated by redefining the mentioned parameter [342]. The counting distribution c_{m} of M on-off detector mechanism, namely the first and the second moment of this probability distribution of the coincidence events, defines the binomial parameter as:

$$Q_{\mathrm{b}} = \frac{\langle (\Delta c)^2 \rangle}{\frac{\langle c \rangle}{M}\left(1 + \frac{\langle c \rangle}{M}\right)} - 1, \tag{2.14}$$

where $\langle c \rangle = \sum_{i=0}^{M} i c_i$, and $\langle (\Delta c)^2 \rangle = \sum_{i=0}^{M} (i - \langle c \rangle)^2 c_i$. The Q_{b} should converge to Q_{M} for $M \to \infty$. Negative values of the binomial parameter $Q_{\mathrm{b}} < 0$ serve as a witness of the non-classical character of the initial state of light [342], and non-negative values $Q_{\mathrm{b}} \geq 0$ for classical states.

Another quantity depending on the first two moments of photon statistics is the normalized second-order intensity correlation function $g^{(2)}(0)$, routinely applied to quantify the photon correlations of light [295, 296]. The undeniable advantage is that this parameter does not change with loss. This non-classicality character quantification is based on examining correlations aspects of intensity fluctuations. Normalized second-order intensity correlation function for stationary light is defined as

$$g^{(2)}(\tau) = \frac{\left\langle \hat{a}^{\dagger}(t)\, \hat{a}^{\dagger}(t+\tau)\, \hat{a}(t+\tau)\, \hat{a}(t) \right\rangle}{\left\langle \hat{a}^{\dagger}(t)\, \hat{a}(t) \right\rangle^2}. \tag{2.15}$$

We will discus special case of $\tau = 0$. Than we can write $g^{(2)}$ in terms of the number operator as

$$g^{(2)}(0) = \frac{\langle \hat{n}(t)\,(\hat{n}(t) - 1) \rangle}{\langle \hat{n}(t) \rangle^2}. \tag{2.16}$$

Focusing on photon statistics p_n, the second order Glauber correlation function can be rewritten as

$$g^{(2)}(0) = \frac{\mathrm{Tr}\left[\hat{\rho}\hat{n}\,(\hat{n} - 1)\right]}{\left(\mathrm{Tr}\left[\hat{\rho}\hat{n}\right]\right)^2} = \frac{\sum_{n=0}^{\infty} n\,(n-1)\, p_n}{\left(\sum_{n=0}^{\infty} n p_n\right)^2} = \frac{\langle n\,(n-1) \rangle}{\langle n \rangle^2} = \frac{Q_{\mathrm{M}}}{\langle n \rangle} + 1. \tag{2.17}$$

The light sources exhibit bunching $g^{(2)}(0) > g^{(2)}(\tau \neq 0)$ or antibunching $g^{(2)}(0) < g^{(2)}(\tau \neq 0)$. The source with Poissonian statistics has $g^{(2)}(\tau) = 1$. One can determine the type of photon statistics based on the value of $g^{(2)}(\tau)$ for $\tau = 0$:

$$\begin{aligned} &\text{Poissonian}: && g^{(2)}(0) = 1 \\ &\text{sub-Poissonian}: && g^{(2)}(0) < 1 \\ &\text{super-Poissonian}: && g^{(2)}(0) > 1. \end{aligned} \tag{2.18}$$

The super-Poissonian statistics is inherent in both classical and non-classical states of light. However, only the non-classical states can exhibit sub-Poissonian statistics.

Since $g^{(2)}(0)$, defined using the first and second moments of photon statistics (2.17), cannot be directly measured, anticorrelation α parameter measurements are performed for a single-photon-level radiation sources using the Hanbury-Brown-Twiss (HBT) setup (Fig. 2.1(b)):

$$\alpha = \frac{P_{12}}{P_1 P_2} \simeq \frac{2p_2}{p_1^2} \simeq g^{(2)}(0), \tag{2.19}$$

where P_{12} is the probability that both detectors 1 and 2 click, P_1 is the probability that detector 1 clicks, and P_2 is the click probability of detector 2. The probabilities p_1, p_2 stand for observing the

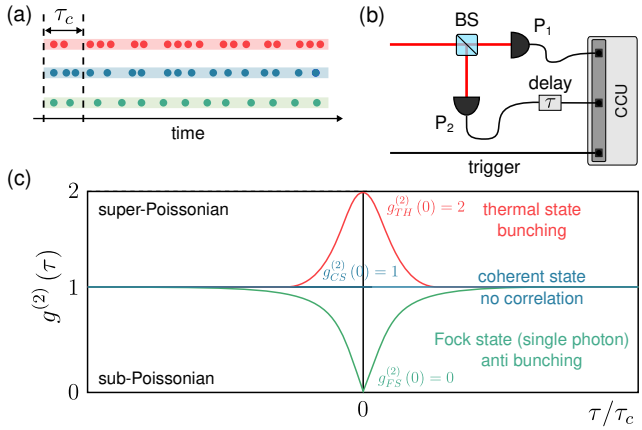

Figure 2.1: (a) Photon bunching (red), random distribution (blue), and photon antibunching (green), (b) a Hanbury Brown-Twiss arrangement for two-photon coincidence counting, and (c) the normalized second-order intensity correlation function: thermal state (red), coherent state (blue), and Fock state (green).

single photon and two photon. For single-photon signals with a low detection rate ($\langle n \rangle \ll 1$ with $p_1 \gg p_2 \gg p_{n\gg 2}$), the approximation works, and the value of the HBT measurement agrees well with $g^{(2)}(0)$ parameter [343]. Unfortunately, for states with non-negligible multiphoton content, the HBT fails to produce the correct value of $g^{(2)}$ [344].

2.3 Generation of quantum states of light

In this section, I give a brief overview of the quantum states of light such as coherent state, thermal state, multi-photon subtracted thermal states, and multi-photon states of light. From an experimental point of view, the corresponding light generation techniques are also discussed. Additionally, a list of applications of these states of light is given.

2.3.1 Coherent light

Coherent light is generated by optical sources of constant optical power (mean photon flux), but the distribution of photons at the time of their registration by the detector is completely uncorrelated (Figure 2.1(a)). In other words coherent state $|\alpha\rangle$ is defined as a coherent superposition of pure states. Such light is generated via a coherent process of stimulated emission in a highly-saturable laser. The phase reference can be obtained by splitting such intensive light at a beam splitter as it preserves the Poissonian statistics. The expansion of coherent state in the Fock basis is

$$|\alpha\rangle = e^{-\frac{1}{2}|\alpha|^2} \sum_n \frac{\alpha^n}{\sqrt{n!}} |n\rangle \,. \tag{2.20}$$

Photon statistics of coherent state reads

$$p_n^{\mathrm{CS}} = |\langle n|\alpha\rangle|^2 = \frac{\langle n\rangle^n}{n!} e^{-\langle n\rangle}. \tag{2.21}$$

Since the Poissonian statistics exhibits the variance equal to the mean photon number $\langle (\Delta n)^2 \rangle = \langle n \rangle$, coherent states have Fano $= 1$, the Mandel parameter $Q_{\mathrm{M}} = 0$, and $g^{(2)}(0) = 1$ proving no

photon correlations. For large $\langle n \rangle$, the maximum probability of n photons in a mode corresponds to the mean photon number $\langle n \rangle$, and Poissonian statistics approaches the Gaussian distribution with photon number standard deviation $\sqrt{\langle n \rangle}$.

Coherent states produced by a laser are used as information carriers in optical communications and quantum key distribution protocols. Non-orthogonality of coherent states guarantees that they cannot, in general, be discriminated without error. It represents an advantage for quantum key distribution [345–347]. Coherent states can be used for crosstalk calibration method [284]. In addition, employing photon addition, the single-photon-added coherent light states were generated to analyze the evolution of the quantum-to-classical transition [27, 321, 323].

2.3.2 Pseudo-thermal light

Thermal light is an incoherent mixture of different photon number states $|n\rangle$. The thermal equilibrium condition states that the probability distribution of energy E_n in one mode follows the Boltzmann distribution. Thermal state as a mixed state can be written as sum over all possible number states

$$\hat{\rho}_{\mathrm{th}} = \sum_n \frac{e^{-\beta E_n}}{Z_0} |n\rangle \langle n| , \tag{2.22}$$

where $\beta = 1/(k_B T)$, $Z_0 = 1 + \bar{n}$ denotes the partition function, $\bar{n} = 1/(e^{\beta\hbar\omega} - 1)$ is the mean thermal photon number, $E_n = \hbar\omega n$ is energy of n photons, and ω is the optical frequency. Thermal light exhibits the photon statistics with Bose-Einstein distribution

$$p_n^{\mathrm{th}} = \frac{1}{\langle n \rangle + 1} \left(\frac{\langle n \rangle}{\langle n \rangle + 1} \right)^n . \tag{2.23}$$

As might be expected, the probability of the number of photons decreases geometrically as the number of photons increases. Thus, the variance $\langle (\Delta n)^2 \rangle = \langle n \rangle + \langle n \rangle^2$ is larger than the mean photon number $\langle n \rangle$ for Poissonian statistics of independent photons. Due to this fact, thermal light obeys the super-Poissonian probability distribution of the photon number. The photon statistics moments yield Fano $= \langle n \rangle + 1$, $Q_{\mathrm{M}} = \langle n \rangle$, and $g^{(2)}(0) = 2$.

Thermal states of light can be directly applied in a broad range of applications including diagnostics of quantum states [148, 216, 219], enhancement of nonlinear effects like optical harmonic generation [108, 348, 349] and two-photon fluorescence [350], quantum imaging [351–353], quantum enhanced interferometry [244, 333], generation of nonclassicality [320–322], tests of robustness of quantum communication protocols and quantum key distribution [354], and ghost imaging [355–360]. Ideal thermal light statistics is also required for proof-of-principle tests of quantum thermodynamics [A1, 361]. However, it is the actual spectral bandwidth which represents a crucial parameter for potential improvement of waste majority of applications of thermal light.

The real thermal light sources exhibit very short coherence times and low photon number per mode. Therefore, pseudo-thermal sources are commonly used in optical experiments to obtain single-mode thermal statistics with larger photon number and sufficient coherence time. In general, there exists two ways how to obtain thermal light: direct modulation of light intensity or thermal emission. One of the most widely used methods to generate pseudo-thermal light is the scattering the coherent light by a moving diffuser, see Figure 2.2. The scattered amplitude of the electric field is Gaussian distributed and the distribution of the intensity obeys negative exponential statistics, the same as a real thermal light source. As a diffuser, the ground glass is frequently used [362–365]. A laser beam is focused on the surface of the ground glass by a lens. Passing the light through a rotating diffuser introduces complex and randomly scattered light. A single-mode optical fiber is

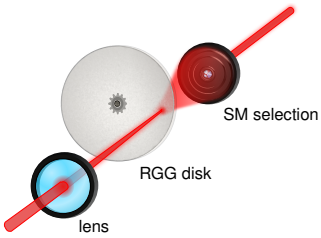

Figure 2.2: The experimental arrangement for producing pseudo-thermal light: focus lens; rotating ground glass (RGG) as a diffuser; single-mode (SM) selection. Bose-Einstein photon number distribution is realized by intensity modulation via scattering the coherent light by a moving diffuser - rotating ground glass. The generated pseudo-thermal light is collected by a single-mode optical fiber to select a single spatial mode.

used to collect the scattered light and select a single spatial mode. At the output we obtain a clean spatial mode with random amplitude and phase yielding narrower linewidth than natural thermal light. The coherence time can be adjusted by varying the angular velocity of the disk and is limited to a few Mhz range [366]. A suitable alternative to ground glass was found to be a disordered lattice [296, 367].

Further, another methods of random switching of intensity levels was developed, using a digital micromirror device [368], a programmable acousto-optic modulator [369–371], and an integrated electro-optical Mach-Zehnder modulator driven by an arbitrary signal generator [372]. The major benefit of these fully programmable modulators is that they allow to produce any classical light statistics. One can also directly modulate the laser pumping current [373] or couple the laser light into an optical multimode fiber [374]. Alternatively, thermal states can be observed directly from the thermal emission. However, it is quite challenging to reach an ideal thermal state. Almost ideal thermal light can be generated by amplified spontaneous emission [375], dye molecules in a microcavity [376, 377] and atomic ensembles [C2]. Unfortunately, these methods are more demanding on laboratory equipment and experimental skills.

2.3.3 Multi-photon subtracted thermal states of light

The controlled photon subtraction and addition are experimental techniques frequently used in optical state preparation (see Section 1.3). These light modification procedures have drawn much attention because of the needs of modern quantum applications. The conditional output states after application of photon subtraction or addition read

$$\hat{\rho}_{\mathrm{sub}} = \frac{\hat{a}\hat{\rho}_{\mathrm{IN}}\hat{a}^{\dagger}}{\mathrm{Tr}[\hat{\rho}_{\mathrm{IN}}\hat{a}^{\dagger}\hat{a}]} \quad \text{and} \quad \hat{\rho}_{\mathrm{add}} = \frac{\hat{a}^{\dagger}\hat{\rho}_{\mathrm{IN}}\hat{a}}{\mathrm{Tr}[\hat{\rho}_{\mathrm{IN}}\hat{a}\hat{a}^{\dagger}]}. \tag{2.24}$$

In the following, the emphasis is primarily on the photon subtraction. It is important to stress that the behaviour of the mean number of quanta of the state subjected to the subtraction process depends on the initial state statistics. The mean energy increases (decreases) when a photon is subtracted from a super-Poissonian (sub-Poissonian) state [B3, 30, 318]. The subtraction does not influence a state only governed by Poissonian statistics; coherent state is eigenstate of the annihilation operator.

As already pointed out in Goals of the Thesis 1.2, I am interested in the multi-photon subtraction employed to modify the statistical properties of the initial light, namely single-mode thermal state.

The density matrix of the multi-photon subtracted single-mode thermal state is defined as

$$\hat{\rho}_{\mathrm{th}}^{l} = \frac{\hat{a}^{l}\hat{\rho}_{\mathrm{th}}\hat{a}^{\dagger l}}{\mathrm{Tr}[\hat{\rho}_{\mathrm{th}}\hat{a}^{\dagger l}\hat{a}^{l}]} = \sum_{n=0}^{\infty} \frac{(n+l)!}{n!l!} \frac{n_{\mathrm{th}}^{n}}{(1+n_{\mathrm{th}})^{l+n+1}} |n\rangle\langle n|, \tag{2.25}$$

where l is the number of subtracted photons and n_{th} stands for mean photon number of the input thermal state. The photon statistics of these states is given by the Mandel-Rice distribution

$$p_{n}^{l} = \frac{\frac{(n+l)!}{n!l!}\left(\frac{n_{\mathrm{th}}}{1+n_{\mathrm{th}}}\right)^{n}}{(1+n_{\mathrm{th}})^{l+1}}. \tag{2.26}$$

Additionally, these unique states of light follows normalized i-th order intensity correlation function

$$g_{l}^{(i)}(0) = \frac{\langle \hat{a}^{\dagger i}\hat{a}^{i}\rangle}{\langle \hat{a}^{\dagger}\hat{a}\rangle^{i}} = \frac{(l+i)!}{l!\,(l+1)^{i}}. \tag{2.27}$$

In general, with increasing number of subtractions l, the mean photon number of the conditioned output state is l-times larger than of the original thermal state and the resulting photon statistics converges to the Poisson distribution. The transition follows a similar path in $\langle n\rangle$ vs $g^{(2)}$ and $\langle n\rangle$ vs Q diagrams as multi-mode thermal light, however, the multi-photon subtracted thermal states are single-mode states.

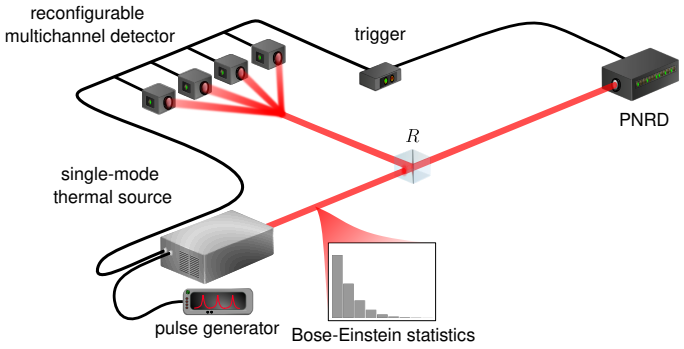

Figure 2.3: Multi-photon subtracted single-mode thermal states of light generation. Experimental realization of the subtraction of l photons from a thermal state consists of pseudo-thermal state preparation, beam splitter with reflectivity R, reconfigurable multichannel detector for counting reflected photons, and photon-number-resolving detector (PNRD) for output state analysis.

The subtraction can be successfully performed even under imperfect conditions and by using inefficient photodetectors with $\eta < 1$. Experimental realization of the photon subtraction employing low-reflectivity beam splitter is shown in Figure 2.3. Reflected port is detected by multichannel detector to distinguish number of subtracted photons. The probability of detecting l photons with multichannel detector employing M single-photon detectors follows

$$p_{l} = \binom{M}{l} \sum_{j=0}^{l} \binom{l}{j} (-1)^{l-j} \frac{1}{1+\eta R n_{\mathrm{th}}\left(1-\frac{j}{M}\right)}. \tag{2.28}$$

Taking into account the reflectivity R of the beam splitter and detection efficiency η, the density

matrix of the output state after the l photons are successfully detected reads

$$\hat{\rho}_{\mathrm{th}}^{l} = \sum_{n=0}^{\infty} \frac{1}{p_l} \binom{M}{l} \sum_{j=0}^{l} \binom{l}{j} (-1)^{l-j} \frac{1}{n_{\mathrm{th}}(1-R)} \frac{1}{\lambda_j^{n+1}} |n\rangle\langle n|, \tag{2.29}$$

where $\lambda_j = 1+1/n_{\mathrm{th}}(1-R)+\eta R/(1-R)(1-j/M)$. For the low reflectivity close to zero, equation (2.29) approaches the density matrix of ideal photon subtraction (2.25).

Multi-photon subtraction processes continuous in time were first analyzed to conditionally manipulate the statistics and also increase the energy of thermal light [378, 379].The series of multi-photon subtraction experiments with thermal light also demonstrated a conditional instantaneous increase of mean energy by a subtraction of quanta from single-mode thermal state [28, 161, 162]. Recently, we realize two experiments with thermal states after subtraction of l-photons, see Chapter 4.

2.3.4 Multi-photon states of light

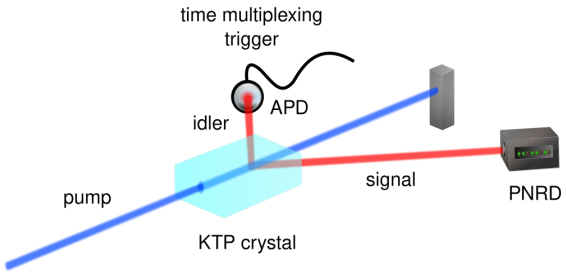

Figure 2.4: The generation of single-emitter clusters: heralded SPDC using time-multiplexing trigger.

Over the past few years, generation of the higher Fock states of light $|n\rangle$ with a constant number of n photons [20, 25, 230–233, 380] became of foundational interest with significant practical impact in quantum technology. It is still experimentally challenging to generate arbitrary multi-photon Fock states $|n\rangle$. Fortunately, multi-photon states of light can be prepared as a cluster of N identical single-photon emitters in separate modes $|1\rangle^{\otimes N}$. The generation of statistics with controllable multi-photon content from a well-established photon source based on multiple high-quality single photons triggered to suppress random noise is depicted in Figure 2.4. The continuous-wave spontaneous parametric down-conversion (SPDC) is employed to generate sequences of N_{p} heralded single photons that were collectively measured on a multichannel detector. Correlated pairs of photons generated in parametric down-conversion process are well known and commonly used as a probabilistic source of very high-quality heralded single-photon states. Instead of conventional heralding with a single-photon detector, we use an optical time-multiplexing setting that exploits a parametric down-conversion source for an multi-photon state generation up to nine heralded photons. This kind of optical source simulates incoherent mixing of signals from a cluster of N_{p} identical single-photon emitters in a separate modes,

$$\hat{\rho}_{N_{\mathrm{p}}} = \sum_{n=0}^{\infty} \binom{N_{\mathrm{p}}}{n} \xi^{N_{\mathrm{p}}-n} (1-\xi)^{n} |n\rangle\langle n|, \tag{2.30}$$

where ξ represent collection and detection loss. The photon statistics is than

$$p_n^{N_\mathrm{p}} = \binom{N_\mathrm{p}}{n} \xi^{N_\mathrm{p}-n} (1-\xi)^n \tag{2.31}$$

with the first and second moment

$$\langle n \rangle = (1-\xi)\, N_\mathrm{p} \quad \text{and} \quad \langle (\Delta n)^2 \rangle = (1-\xi)\, \xi N_\mathrm{p}. \tag{2.32}$$

As indicated in formula (2.31), sub-Poissonian photon statistics is very sensitive to optical losses and inefficient detection. These exotic states yield Fano $= \xi$ and $Q_\mathrm{M} = \xi - 1$. In contrast, ideal Fock states have no uncertainty in intensity $\langle (\Delta n)^2 \rangle = 0$ with Fano $= 0$ and $Q_\mathrm{M} = -1$. However, loss independent second order Glauber correlation function is identical for both, $g^{(2)}(0) = 1 - \frac{1}{N_\mathrm{p}}$, and proves nonclassicality for any N_p if the statistical error is small enough.

Nonclassical sources made for quantum technology have properties that cannot be duplicated using classical sources, but they are difficult to demonstrate experimentally, especially with inefficient detectors. Nonclassical states of light are of fundamental importance in quantum optics, optical quantum communication, quantum information processing, and quantum metrology. The nonclassical states of optical fields are commonly defined as those whose Glauber-Sudarshan representation [381, 382] does not satisfy properties of an ordinary probability distribution. An important subclass of nonclassical states is represented by states with negative Wigner function [27, 159, 336, 383–385]. Recently, another interesting sub-class of nonclassical states has been proposed, termed quantum non-Gaussian states [121]. These states cannot be expressed as a convex mixture of Gaussian states. Preparation of quantum non-Gaussian states thus requires nonlinear interaction or detection beyond the class of Gaussian operations that comprise interference in passive linear optical interferometers, quadrature squeezing, and homodyne detection. While every state with negative Wigner function is a quantum non-Gaussian state, the class of quantum non-Gaussian states is strictly larger and contains also states with positive Wigner function. During recent years, the quantum non-Gaussian states have been the subject of intensive research [C1, 158, 160, 304, 337, 386–401]. Several criteria and witnesses for detection of quantum non-Gaussian states have been established [304, 337, 386–392], and the quantum non-Gaussian character of various sources of nonclassical light has been demonstrated experimentally [C1, 158, 160, 393–396]. The most common way to generate a quantum non-Gaussian state of light is to first generate a suitable multimode nonclassical Gaussian state, perform measurements with single-photon detectors on some of its modes and condition on photon detection [27, 159, 383–385, 393, 394, 396, 402].

2.4 Single-photon avalanche photodiode

Here, I review the fundamental principles of a single-photon avalanche photodiode and its applicability in a host of branches of industry, applied research, scientific applications and material science. Nevertheless, the topic of SPADs has been discussed in more detail in the following review articles and books [B4, 5, 6, 8, 10, 11, 102].

While not achieving as remarkable performance as SNSPDs or TESs, today SPADs still offer a valid alternative. As compact mass-manufactured commercial devices, SPADs are the most commonly used detectors providing the best practical solution for single-photon detection, especially for their room temperature operation with good performance and low price. One can find them in every photonics laboratory. These detectors have been widely used and studied since the late 1950s [403]. SPADs can be used either individually for single-photon detection or multi-pixeled

or multiplexed into an array to offer new ways to measure the statistical properties of light. Currently, integrated SPADs represent a promising technology in future room-temperature chip-based quantum photonic applications [65, 119].

Single-photon avalanche diodes are enabling technology frequently used for photon detection in the field of quantum optics [B4, 10]. This class of single-photon detectors is a very important tool for the characterization of quantum light sources [14, 159, 160] or modification of statistical properties of light by photon subtraction and addition [A1, B3, 27, 28, 30, 161, 322, 323]. They are employed in optical quantum communication technologies [404], quantum random number generator [101, 163, 166, 167], and quantum cryptography [89, 92, 165]. They found their applications in metrology [110, 111] and optical time domain reflectometry (OTDR) [93, 185–187, 405]. Their ability to detect low light signal has led to massive use in biomedical science like a fluorescence microscopy in a process of mapping and counting single molecules [90, 173, 175, 176, 406]. Consequently, thanks to their broadwise applicability, characterization of SPADs have become an important task in order to compare and select detector with the best parameters for the specific application.

2.4.1 Principle of operation

A proportional conversion of photons to electrons must inevitably involve a mechanism that amplifies the energy retrieved from the absorption of photons to the macroscopic level. To reach a sufficient gain, SPAD operates in a bistable regime (also termed the Geiger mode [102]). Geiger mode is the most commonly used regime achieved by a reverse bias higher than the breakdown voltage. In general, there are two modes of operation depending on the desired application. The first is a free-running mode, where the SPAD is biased above the breakdown voltage to effectively detect randomly incoming photons [61]. The second mode is designed to detect photons in well-defined time windows. In this mode, termed a gated mode [72, 83, 407–417], SPAD is usually reverse biased below its breakdown voltage for a given duration in each gating cycle, see Figure 2.5.

The incoming photon is converted to a free carrier of electric charge, which is amplified by the avalanche process to produce a macroscopic electric pulse. Photo-excitation of an electron-hole pair (carrier) triggers carrier multiplication. A cascade of impact ionization events results in a macroscopic current between the APD electrodes that can be easily detected by an electronic circuitry and converted to the output signal of the detector. The current continues to flow until the self-sustaining avalanche is quenched to exit critical mode and prevent the diode from being destroyed. The detector is not able to respond to the incident photons until the quenching process is completed and the reverse bias is restored to its original value. The quenching could be done passively or actively. Different classes of quenching circuits such as passive quenching [42, 413, 418] and active quenching [61, 419–425] were realized so far. Among ordinary quenching techniques, a hybrid quenching combines the above-mentioned quenching and resetting circuits to benefit from the advantages of selected ones [416, 426]. The avalanche-quenching and restoring circuits [42] dramatically affect the performance of the detector. Generally, employing the passive-quenching process the detector recovery is substantially extended, typically 1 μs, which limits the maximum frequency of detection events. Alternatively, active quenching benefits from excellent performance such as very high dynamic range and short quenching time. On the other hand, if the recovery time is too short, the effect of afterpulsing increases. The passive quenching with an active reset circuit [427, 428] was designed to reduce afterpulsing for SPADs. There are many other quenching and restoring approaches, for example, the gated quenching circuits can be employed to reduce dark counts; active restoring employing transistor achieves shorter reset time, etc. Additionally, it is important to stress that the integration of the quenching circuit directly with the detector was successfully done [429]. This fact has contributed significantly to the future use of

this detection technology in modern photonic systems.

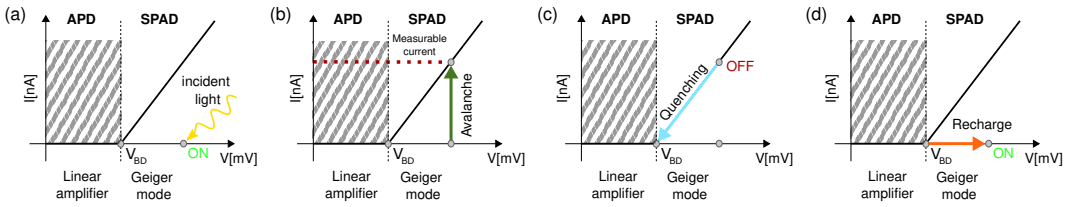

Figure 2.5: Single-photon avalanche diodes principle of operation: (a) photon absorption, (b) generated electron-hole pair triggers avalanche to create measurable current, (c) quenching reduces bias voltage to prevent destroying photodiode, and (d) resetting bias voltage to prepared photodiode for next photon absorption.

2.4.2 Parameters

Unfortunately, in practice, the response of single-photon detectors can exhibit intriguing nonlinear effects that affect the measurement precision at the single-photon level. Their single-photon sensitivity is more or less limited by saturation effects and noise performance. One can observe a complex interplay of detector-specific phenomena, such as dark counts, dead time, recovery transition, multiphoton response, and latching. Specifically, SPADs suffer from noise production due to thermal generation of the charge carriers, recovery time losses due to the recharge process of the quenching system and afterpulsing effect due to the trapped charge carriers created during the avalanche process [102]. These effects cause highly nontrivial nonlinear behavior that is much stronger compared to classical photodiodes.

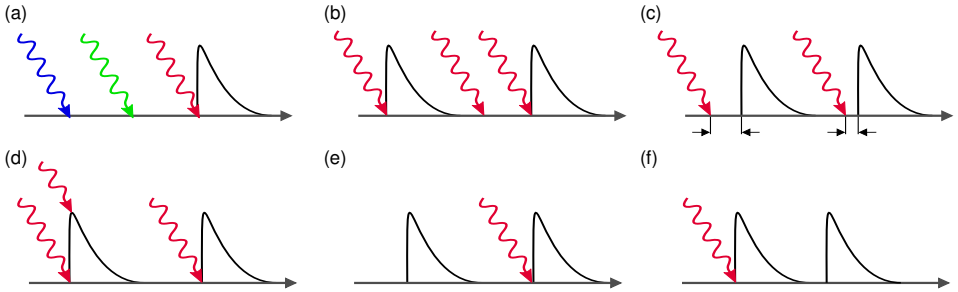

Figure 2.6: Different detection phenomena related to single-photon avalanche diodes: (a) spectral response, (b) detection efficiency, (c) jitter, (d) dead time, (e) dark counts, and (f) afterpulses.

The material from which the detector is made determines its *spectral response*. It means that the detector is sensitive only over the limited operating wavelengths (Figure 2.6(a)). Additionally, a successful detection could only be produced by absorption of an incident photon in its active area. However, it is not guaranteed that these photons cause the generation of an electron-hole-pair initiating an avalanche (Figure 2.6(b)). As indicated, *detection efficiency* is defined as the ratio of the number of photons resulting in a detection signal to the number of photons incident on the detector [200, 275]. Ideally, the conversion time of the input optical signal to the output electrical pulse should be constant. This time interval between the photon absorption and the output electric pulse generation is termed as *timing jitter* (Figure 2.6(c)). It is evidence of the random nature of the physical mechanisms involved in the operation of the detection device. Technically, this parameter

is defined as the full-width half-maximum (FWHM) of the detector time response function. SPADs exhibit timing jitter typically on the order of hundreds of picoseconds. Interestingly, timing jitter is a function of detection rate.

Each detection event is followed by the time interval during which an avalanche is extinguished (Figure 2.6(d)). During this time, the detector fails to detect photons because it is not ready to do so after the previous detection event, appearing to be turned off. This time interval called *dead time* is fully adjustable by the configuration of the electronic circuitry and is very often artificially extended to avoid unwanted effects. The dead time is considered to be the main saturation parameter limiting the maximum detection rate of the detector (Figure 2.7). Today's commercial SPADs guarantee a dead time on the order of tens to hundreds of nanoseconds. Furthemore, the time required for the recovery process to reach full photon detection capability with maximum detection efficiency is called *reset time*. We define the *recovery time* as the sum of the dead time and the reset time.

The real SPAD registers false detection events even when no optical signal is incident on its active area (Figure 2.6(e)). This effect is caused by random movements of the electric charge carriers in the semiconductor material of the detector (spontaneous thermal excitation or tunneling effect) [42, 192, 430, 431]. Such a spurious signal is referred to as *dark counts* and plays a similar role to the dark current in classical photodiodes. Dark counts obey Poissonian statistics [430, 431] and are indistinguishable from photon detection events. Typical values for commercially used SPADs are tens to thousands of dark counts per second. In a similar manner, *afterpulsing* behaviour introduces a positive feedback immediately after detection or even during the recovery process of the detector (Figure 2.6(f)) [193, 194, 198, 199]. As each avalanche pulse passes through the acceleration region of a semiconductor device, some charge carriers could be trapped in the imperfections in the crystal lattice. These carriers remain trapped for some time. After this time, they are subsequently released due to thermal excitation. If this happens during the recovery process, it can cause the generation of another avalanche strongly correlated with the previous one during which the charge carriers were trapped. This phenomenon can cause an increase in false counts and inhibit high frequency operation of SPADs. It depends on several parameters such as temperature, the total charge that flows through the device, and trap density of the used material. Also, the recovery process affects this phenomenon [427]. Alternatively, *twilight pulsing* are triggered by photons incident during the reset time [200–202]. The probability of twilight pulses occurrence is proportional to the number of these photons. These parasitic detection events occur immediately after the recovery time.

As single-photon detectors become a widespread technology, also characterization techniques come to the fore. As of today, the various performance parameters of the single-photon detectors have been studied [42, 192–194, 200, 202, 275, 427, 432–436]. Accurate characterization of parameters of single-photon detectors involves experimental skills in a number of competing techniques. Common investigation of saturation effects requires time-domain measurement using high resolution measuring devices and a sub-nanosecond pulsed laser source with controllable repetition rate [198, 199, 437–439]. There also exist several measurement techniques to obtain the noise performance analysis [201, 440].

2.4.3 SPAD response model

Let us summarize the fundamentals of single-photon avalanche photodiodes and basic principles of detection imperfections. SPAD outputs an electronic pulse when one or more photons are detected [B4, 10]. The detection events (also termed counts or clicks) possess a statistical distribution given by the detected state and the detector's response. The detection rate R^{det} is then a nonlinear function of the incident rate R. Sometimes the detector outputs a pulse even when no photon is detected due to various background contributions (dark counts - R_{D}) or as a result of a previous detection (SPAD afterpulses - $\langle n_{\mathrm{AP}} \rangle$). Furthermore, the detector occasionally fails to detect photons

because it is not ready to do so after the previous detection event, such as during dead time.

Theoretical models of the SPAD response function

There is a great number of results in modelling the response of SPAD with the ultimate goal of including all the relevant factors [201, 202, 434–436, 439, 440]. Their accuracy has been limited so far and many counter-examples exist for which the measured SPAD response differs significantly from the theoretical model. Consequently, determining the nonlinearity of the SPAD response and finding the optimum detection rate to access the minimum achievable deviation from the ideal linear behavior represents a significant challenge.

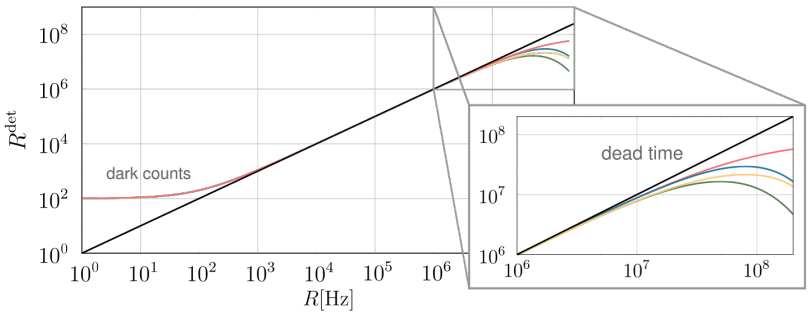

Figure 2.7: The detection rate R^{det} as a function of the incident rate R. Shown are different dead time models: the NP model (red), the P model (blue), the NP-P model (green), and the P-NP model (yellow). Black solid line represents response of the linear detector. Shown is an example case of an actively quenched SPAD: $R_{\mathrm{D}} = 100$ Hz, and $\tau = 25$ ns.

The effect of dead time in Geiger-mode SPADs is akin to Geiger-Müller (GM) counters [B10, B13, 432, 441, 442, B20, 443–446]. Two basic types of idealized models for dead time have been defined [B13, 441, B20]. Namely, it is the paralyzable dead time τ_{P} model

$$R_{\mathrm{P}}^{\mathrm{det}}(R) = (R + R_{\mathrm{D}}) \exp(-(R + R_{\mathrm{D}})\,\tau_{\mathrm{P}}), \tag{2.33}$$

and the non-paralyzable dead time τ_{NP} model

$$R_{\mathrm{NP}}^{\mathrm{det}}(R) = \frac{R + R_{\mathrm{D}}}{1 + (R + R_{\mathrm{D}})\,\tau_{\mathrm{NP}}}. \tag{2.34}$$

For the non-paralyzable case, each registered detection is followed by dead time, during which no further events are registered. In the paralyzable case, dead time follows every detection, even those that occur within a previous dead time and are not otherwise recorded. This case covers the fact that secondary detections in GM tubes still require quenching, but are not registered due to low voltage output. In the case of GM counters, single-parameter dead-time models are just an approximation. Hybrid models were proposed by combining paralyzable and non-paralyzable dead times: the NP-P model [447], and the P-NP model [445, 448]. Figure 2.7 shows the effect of the dark counts and dead time to the detection rate R^{det}. Actively quenched SPADs exhibit afterpulsing and twilight pulsing that affect the mean detection rate [202]. Both effects can be evaluated numerically, or – if we neglect the temporal distribution of afterpulses – an approximate rate formula can be used [202],

$$R_{\mathrm{AP}}^{\mathrm{det}}(R) = \left[\left(\frac{1}{R + R_{\mathrm{D}}} - \alpha\right) \mathrm{e}^{-\langle n_{\mathrm{AP}}\rangle} + \tau_{\mathrm{NP}}\right]^{-1}. \tag{2.35}$$

The new parameters are the mean number of afterpulses per detection $\langle n_{\mathrm{AP}}\rangle$, and the twilight-pulse proportionality constant α. As one would expect, when both of these parameters are zero, the formula (2.35) is reduced to the basic non-paralyzable model (2.34).

Positive-operator valued measure

In quantum physics, characterizing an unknown detector consists of determining its positive-operator-valued measure operators (POVM). To obtain the corresponding POVM, detector tomography based on probing with precisely calibrated signals was suggested [190, 449–456]. However, if the tomography does not include memory effects, the results can be compromised [457]. In general, POVM gives the probability of any measurement outcome for arbitrary input state. Given an input state $\hat{\rho}$, the probability c_m of obtaining detection outcome m is given by formula $\mathrm{Tr}[\hat{\Pi}_m\hat{\rho}]$, where $\hat{\Pi}_m$ is the detector POVM. The POVM satisfies the positivity and semi-definiteness $\hat{\Pi}_m \geq 0$, and $\sum_m \hat{\Pi}_m = \mathbb{1}$. In general, a detector with no phase dependence will be described by POVM elements diagonal in the Fock basis. POVM elements of the SPAD as a binary detector is given by $\hat{\Pi}_0 = |0\rangle\langle 0|$ and $\hat{\Pi}_1 = \mathbb{1} - |0\rangle\langle 0|$, a more realistic detector with efficiency η

$$\hat{\Pi}_0 = \sum_{n=0}^{\infty} (1-\eta)^n \, |n\rangle\langle n| \quad \text{and} \quad \hat{\Pi}_1 = \sum_{n=0}^{\infty} [1-(1-\eta)^n] |n\rangle\langle n|. \tag{2.36}$$

Eventually, taking into account the probability of dark counts R_{D}, we can rewrite $\hat{\Pi}_1$:

$$\hat{\Pi}_{\mathrm{SPAD}} = \sum_{n=0}^{\infty} [1-(1-R_{\mathrm{D}})(1-\eta)^n] \, |n\rangle\langle n|. \tag{2.37}$$

Neglecting other saturation effects and noise performance, formula (2.37) is frequently used to characterize or predict the single-photon avalanche detector response.

2.5 Spatial multiplexed detector

Single-photon detectors can be used as a basic building block in a spatially multiplexed configuration. Photon-number resolution is obtained by transforming the incident light into an uniform spatial distributions detected by independent detectors. The POVM elements of ideal phase-insensitive photon-number-resolving detector are the projectors on the Fock states $\hat{\Pi}_m = |m\rangle\langle m|$. Unfortunately, photon-number-resolution is limited due to non-idealities such as the finite number of detection channels, noise performance, and non-unity detection efficiency. Consequently, the POVM elements should be defined as $\hat{\Pi}_m = \sum_{n=0}^{\infty} C_{mn}|n\rangle\langle n|$, where $C_{mn} = \langle n|\hat{\Pi}_m|n\rangle$ stands for conditional probability to obtain m clicks given an impinging Fock state $|n\rangle$.

Here I define analytical model fully characterizing the response of spatial multiplexed detector. Specifically, we analyze a detector where the input signal is evenly split among M output ports each terminating with a binary on-off detector that distinguishes the presence and absence of photons with detection efficiency η and can generate a dark count with probability R_{D}. In practice, each of the single-photon detectors will have slightly different detection efficiency η_j. This can be compensated for by perfect balancing of the individual detection channels such that in each channel the product of the corresponding transmittance of the multiplexing optical network and the quantum detection efficiency of the detector will become a constant. Each incoming photon thus reaches one of the M output channels with the same probability and is detected in each channel with the same total detection efficiency η. The efficiency η can be inferred from an independent measurements, and is assumed to be constant during the PNRD operation. We associate a POVM element $\hat{\Pi}_m$ to

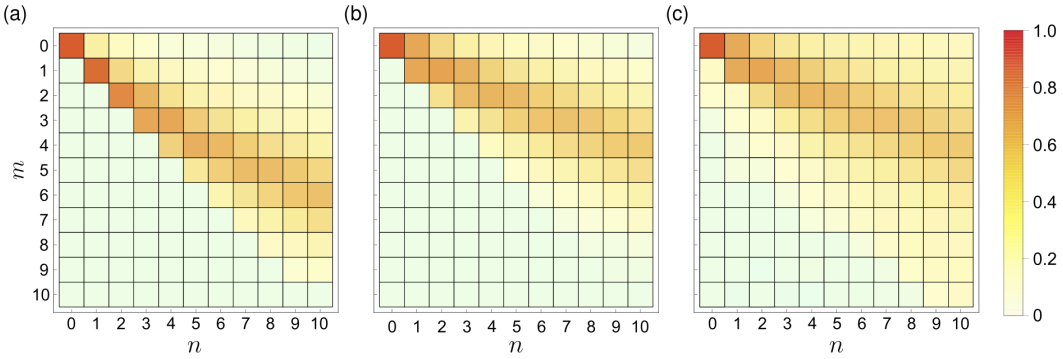

Figure 2.8: The conditional matrix: (a) $\eta = 100\%$, $R_D = 0$, (b) $\eta = 50\%$, $R_D = 0$, and (c) $\eta = 50\%$, $R_D = 1.44\times10^{-6}$.

the event when exactly m out of the M detectors click, irrespective of which set of the detectors clicked. The probability of observation of such m detected simultaneous clicks conditioned by n incident photons, $C_{mn} = 0$ for $m > n$ [103, 264, 274] can be expressed as:

$$C_{mn} = \binom{M}{m} \sum_{j=0}^{m} (-1)^j \binom{m}{j} (1 - R_D)^{M-(m-j)} \left[(1-\eta) + \frac{(m-j)\,\eta}{M} \right]^n . \tag{2.38}$$

In Figure 2.8 the presented conditional probabilities are visualized for several different values.

Consequently, the conditional matrix (2.38) is used for photon statistics retrieval for all the sources characterized, without the need for a tomographic characterization of the detector [285, 449, 450, 453, 454, 458, 459]. Specifically, the click statistics c_m is determined by the photon statistics p_n,

$$c_m = \mathrm{Tr}[\hat{\Pi}_m \hat{\rho}] = \sum_{n=0}^{\infty} C_{mn}\, p_n. \tag{2.39}$$

The formulation (2.39) is valid for any input state of light. The photon statistics retrieval methods are treated in more detail in the following Section (2.6).

2.6 Photon statistics retrieval methods

Finding the photon statistics p_n, $n = 1 \ldots \infty$, that satisfies the system of equations (2.39) for a particular *measured* click statistics d_m, $m = 0 \ldots M$, represents a core problem of photon statistics measurement. This inverse problem is ill-posed because 1. it is obviously underdetermined, 2. the theoretical click probabilities c_m are not available in real measurement as we acquire relative frequencies d_m instead, which sample the true probabilities (sampling noise), and 3. for PNRDs that are not free of systematic errors, other imperfection can be present like imbalance, crosstalk, and temporal correlations. The PNRD reported here is almost free of these technical imperfections. The first two issues, however, remain for any PNRD detector, and the photon statistics retrieval has to take them into account. Fortunately, we have additional information facilitating the retrieval, i.e. the photon number probabilities are non-negative and normalized. The elements of photon statistics are also typically non negligible only within a finite range of photon numbers. Indeed, the classical states of light possess a decaying tail, and nonclassical states such as single-photon states are actually defined on a finite support. There are many techniques for photon statistics retrieval, direct inversion and maximum-likelihood approach being probably the most frequently employed.

In what follows we present the basic ideas of these techniques and present a novel method based on an iteration technique known as expectation-maximization algorithm weakly regularized by maximum-entropy principle.

2.6.1 Direct inversion

The retrieval technique based on the direct inversion of the system of linear equations (2.39) requires setting a cut-off – the maximum photon number $n_{\max}$, typically equal to the number of PNRD ports. The truncated problem possesses a single solution

$$\tilde{p}_n = \sum_{m=0}^{M} (C^{-1})_{nm}\, d_m, \tag{2.40}$$

the non-negativity of which is not guaranteed, hence not representing a physically sound photon statistics. Here C^{-1} represents the inverse matrix to the conditional matrix C. The solution (2.40) often reaches negative values and artificial oscillations. These adverse effects are particularly noticeable in the practical case of non-unity efficiency $\eta < 1$ with the limited number M of output ports and the mean photon number of the incident light comparable or higher than M. The non-negativity constraint can be incorporated using linear programming, for instance, which reduces the volume of the p_n domain by the factor of $2^{n_{\max}}$. Also, the cut-off can be increased to $n_{\max} > M$ rendering the problem underdetermined. The solution of such a pseudoinverse [B11, B16] often diverges or, at least, amplifies a sampling noise. Various regularization methods are used to make these issues less pronounced [B9, 151, 460, 461]. Despite all the mentioned issues the direct inverse methods are frequently used due to their speed and widespread implementation in many numerical libraries and computing systems.

2.6.2 Maximum likelihood estimation

Another technique to achieve the inversion of the conditional probability matrix is well known maximum-likelihood (ML) principle and the expectation-maximization (EM) algorithm, which provides a robust method for finding a solution (ML estimate) [462, 463]. The likelihood of measuring the particular data distribution $\{d_m\}$ given the input photon statistics $\{p_n\}$ and measurement device C is given by the multinomial distribution, proportional to

$$\prod_{m=0}^{M} c_m^{d_m} = \prod_{m=1}^{M} \left(\sum_{n=0}^{n_{\max}} C_{mn} p_n \right)^{d_m}, \tag{2.41}$$

which is a convex functional defined on a convex set of $\{p_n\}$ distributions. The maximization of the likelihood functional yields a single global maximum in the case of $n_{\max} \leq M$ or a single plateau of maxima in the case of underdetermined problems. A logarithm of the likelihood is often used instead, which does not change the convexity feature. Also, the normalization $\sum p_n = 1$ condition is incorporated with the help of a Lagrange multiplier D,

$$L\left[\{p_n\}\right] = \sum_{m=0}^{M} d_m \ln c_m - D\left(\sum_{n=0}^{n_{\max}} p_n - 1 \right). \tag{2.42}$$

The zero variation is a necessary condition for an extreme of the likelihood functional,

$$\delta L = L\left[\{p_n + \delta p_n\}\right] - L\left[\{p_n\}\right] = \sum_{m=0}^{M} \frac{d_m}{c_m} \sum_{n=0}^{n_{\max}} C_{mn}\delta p_n - D \sum_{n=0}^{n_{\max}} \delta p_n = \sum_{n=0}^{n_{\max}} \left(\sum_{m=0}^{M} \frac{d_m}{c_m} C_{mn} - D \right) \delta p_n = 0 \tag{2.43}$$

for each $\{\delta p_n\}$, which is equivalent to

$$\sum_{m=0}^{M} \frac{d_m}{c_m} C_{mn} - D = 0, \tag{2.44}$$

except at the boundary of the domain where $p_n = 0$. To include this boundary condition, the extremal equation is formulated as

$$\sum_{m=0}^{M} \frac{d_m}{c_m} C_{mn} p_n = D p_n. \tag{2.45}$$

A summation over n yields

$$D = \sum_{m=0}^{M} \frac{d_m}{c_m} \sum_{n=0}^{n_{\max}} C_{mn} p_n = \sum_{m=0}^{M} d_m = 1, \tag{2.46}$$

where the constraint $\sum p_n = 1$ and the normalization of the click data have been applied. The functional (2.42) can be maximized over $n_{\max}+1$ variables using downhill simplex method or other standard numerical methods [464, 465]. To keep the non-negativity constraint, the variables p_n can be parametrized as R_n^2, the downside of which is even more complicated structure of the log-likelihood function. This approach is straightforward but numerically demanding as the dimension of the problem increases. Alternatively, an iterative solution of the extremal equation (2.45), which is a form of the EM algorithm, can be carried out as was suggested by Banaszek for the first time [216, 266, 466],

$$\Pi_n^{(k)} p_n^{(k)} = p_n^{(k+1)}, \qquad \Pi_n^{(k)} = \sum_{m=0}^{M} \frac{d_m}{\left(\sum_j C_{mj} p_j^{(k)}\right)} C_{mn}. \tag{2.47}$$

The iteration process is started with an initial positive statistics, typically chosen as the uniform distribution, $p_n^{(0)} = 1/(n_{\max}+1)$. Then the kernel $\Pi_n^{(0)}$ of the map (2.47) is evaluated for the initial iteration step, and the first iteration $\{p_n^{(1)}\}$ is obtained by the application of the kernel on the initial statistics. The normalization $p_n^{(1)} / \sum p_n^{(1)}$ has to be performed if the data $\{d_m\}$ are not properly normalized. The iteration process is repeated until the distance between $(k+1)$-th and k-th iteration is smaller than some given value,

$$\sqrt{\sum_n \left(p_n^{(k+1)} - p_n^{(k)} \right)^2} < \epsilon. \tag{2.48}$$

Throughout this work the value $\epsilon = 10^{-12}$ is used for all the performed photon statistics retrievals. When sufficient mathematical conditions are fulfilled, the procedure converges to the fixed point of the map (2.45), i.e. to the maximum-likelihood estimate of photon statistics [462, 463].

2.6.3 Expectation-maximization-entropy algorithm

For underdetermined problems, when $n_{\max} > M$, the EM algorithm converges to a particular solution depending on the initial distribution $\{p_n^{(0)}\}$. All the possible solutions reache the same value of the likelihood (given the data d_n) and cannot be distinguished by ML principle itself. In such cases, the common strategy is to allow for some kind of regularization or damping to select the most "simple" solution from the plateau of all ML solutions or, in other words, to prevent overfitting of the data. Entropy characterizes the solution complexity and its maximization reflects minimum prior information. Entropy maximization is frequently used for regularization of inverse problems in various applications like image reconstruction, seismology, and electromagnetic theory [B12, B14], and also in machine learning and quantum state estimation [467, 468]. Adopting this idea, we have applied entropy maximization to EM algorithm to obtain the most-likely estimate of photon statistics with the largest entropy. The resulting strategy not only offers improved fidelity of the retrieved statistics but also makes the iteration process faster. The derivation of the expectation-maximization-entropy (EME) algorithm is analogous to derivation (2.42)-(2.47) but the regularized functional E is used instead of simple log-likelihood,

$$E\left[\{p_n\}\right] = \sum_{m=0}^{M} d_m \ln c_m + \lambda \sum_{n=0}^{n_{\max}} p_n \ln p_n - D\left(\sum_{n=0}^{n_{\max}} p_n - 1\right). \tag{2.49}$$

Parameter λ scales the entropy regularization relative to the likelihood maximization. Performing variation of the log-likelihood-entropy functional E, eliminating the Lagrange multiplier D, and rewriting the extremal equation in the iterative form lead us to the EME algorithm

$$\begin{gathered} \Pi_n^{(k)} p_n^{(k)} - \lambda\left(\ln p_n^{(k)} - S^{(k)}\right) p_n^{(k)} = p_n^{(k+1)}, \qquad \Pi_n^{(k)} = \sum_{m=0}^{M} \frac{d_m}{\left(\sum_j C_{mj} p_j^{(k)}\right)} C_{mn}, \\ S^{(k)} = \sum_{n=0}^{n_{\max}} p_n^{(k)} \ln p_n^{(k)}. \end{gathered} \tag{2.50}$$

The initial iteration is chosen to contain no prior information about the statistics, $p_n^{(0)} = 1/(n_{\max} + 1)$, and the process is terminated based on the distance (2.48). An implementation of this algorithm in Python is presented in Ref. [469]. We have performed hundreds of photon statistics retrievals using measured data and thousands retrievals based on Monte Carlo simulated data with not a single failure of the EME algorithm convergence. We have also verified that the retrieved photon statistics does not depend on the initial iteration.

Chapter 3

Accurate detection of arbitrary photon statistics

Chapter 3 introduces the working principle of the detection-device-independent method for the photon statistics estimation of any initial photonic state. Photon number resolution is obtained by splitting an incident light field consisting of many photons in a balanced multiport optical network and measured with multiple single-photon detectors, so called multiplexing scheme. The technical realization of the developed detector is described in Section 3.2. A multichannel detector with M-independent electronic output signals from single-photon detectors requires adequate complex processing of these outputs. For this purpose, we have designed and built analog and digital homemade coincidence counting systems (Section 3.3). To reconstruct the photon statistics from the multiple coincidences measurement, we apply an expectation-maximization-entropy algorithm based on entropy regularization of the maximum-likelihood estimation (see Subsection 2.6.3). First, we did an extensive numerical analysis of the the retrieval algorithms. Numerically simulated click statistics of various light sources served as input datasets to certificate the speed and accuracy of the few reconstruction methods (Section 3.4). Afterwards, series of optical measurements were done to prove the photon-number-resolving capability of the presented detector. We achieved unprecedentedly accurate measurement of various photon-number distributions going beyond the number of detection channels, where the error is contributed primarily by the sources themselves. High-fidelity photon statistics reconstruction is verified for different sources of light including laser (Subsection 3.5.1), single- and few-mode thermal sources (Subsection 3.5.2), and a set of several single-photon emitters (Subsection 3.5.3). Finally, I discuss the achieved results, future improvements of the presented detection technique.

Chapter 3 is based on the following publications:
[A2] J. Hloušek, M. Dudka, I. Straka, and M. Ježek, '*Accurate detection of arbitrary photon statistics*', Physical Review Letters **123**, 153604 (2019).
[P1] J. Hloušek, M. Dudka, J. Grygar, and M. Ježek, '*High-resolution multi-channel coincidence counting system for large-scale photonic quantum technology*', in preparation.
[C1] I. Straka, L. Lachman, J. Hloušek, M. Miková, M. Ježek, and R. Filip, '*Quantum non-Gaussian multiphoton light*', NPJ Quantum Information **4**, 4 (2018).
[C2] J. Mika, L. Podhora, L. Lachmann, P. Obšil, J. Hloušek, M. Ježek, R. Filip, and L. Slodička, '*Generation of ideal thermal light in warm atomic vapor*', New Journal of Physics **20**, 093002 (2018).

3.1 Introduction

The one of the key tasks of quantum optics is to study the statistical properties of light. Optical signals are composed of individual energy excitations – photons. The probability distribution of the number of photons in an optical mode carries a great deal of information about physical processes that generate or transform the optical signal. Along with modal structure and coherence, the photon statistics provides full description of light. The statistical properties of the photon steam affect the properties of the resulted optical signal and its interaction with the environment. Generation of light statistics has been of paramount importance for understanding various phenomena in statistical and quantum optics since the presentation of pioneering experiments by Hanbury Brown and Twiss in 1956 [470, 471].

The very first attempt of direct photon statistics detection was performed in 1982 [140]. Since then, many photon statistics measurements have been made employing various experimental techniques such as optical homodyne detection [127, 472], on/off photodetectors [141, 148, 216–218, 274], silicon photomultiplier [219], and transition edge sensor [147, 220]. Alternatively, homodyne detection provides full information about quantum state of light, including phase information [132]. Unfortunately, the homodyning requires a proper (frequency adjusted) local oscillator, which is not accessible in many applications and for many sources like solid-state emitters, biomedical samples, and generally all multi-mode sources. In general, photon statistics measurement is less demanding than full quantum tomography but still represents a significant challenge due to limitations in finite dynamic range of detectors. Also, the non-unity overall detection efficiency, additional losses, or false detections dramatically invalidate true photon counting. This inability of the measuring devices to distinguish individual photons leads to a record of so-called click statistics, which indicates the photon statistics of the input state but does not directly match it. Fortunately, photon statistics can be reconstructed from the click statistics [A2, 141, 143, 144, 217].

Precise characterization of photon statistics is a crucial requirement for many applications in the field of photonic quantum technology [473] such as quantum metrology [110, 111], nonclassical light preparation [C1, 20], quantum secure communication [474], and photonic quantum simulations [361, 475]. It is essential in quantum communications, namely in quantum cryptography, where the security of the transmission is guaranteed only if the carrier signal of proper statistics is used. In addition, statistics of light plays a vital role in optical communications as it affects the sensitivity of optical receivers. Measurement of statistical properties and non-classical features of light also represents enabling technology for many emerging biomedical imaging and particle-tracking techniques [96, 250, 290]. Statistical correlations are routinely applied to quantify the non-classicality of light [295, 296]. Photon statistics measurement represents a special case of the network-assisted tomography with a vast number of practical applications. Photon statistics provides fundamental information on the nature of optical field and hence to discriminate between light sources in the classical or non-classical domain, and provides crucial information on the applicability of optical source such as single-photon sources [13, 220, 476], photon pair sources [14, 17, 477], cavity QED [15, 18], and lasers [19, 478]. Single-photon emitter counting and localizing are at the heart of modern super-resolution microscopy. Current non-destructive emitter counting methods are focused on correlation measurements in simple detection networks and comparison with an ideal noise-free model [96, 290].

3.2 Experimental implementation of the multiport optical network

This section provides detailed information about the multiport optical network reconfiguring the number of detection channels, and possible future extensions.

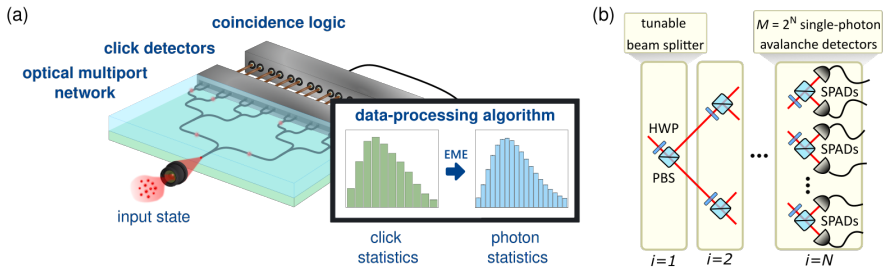

Figure 3.1: (a) The reported measurement workflow of arbitrary photon statistics detection using integrated quantum photonic elements. Ilustrated are: photon-number resolving detector based on spatial multiplexing scheme; high efficiency single-photon detectors; ultra-fast multichannel coincidence counting unit, and scheme of photon statistics retrieval. (b) Experimental setup of the PNRD based on a discrete optical network with full reconfigurability and continuous tunability of splitting ratios using half-wave plate (HWP) and polarizing beam splitter (PBS).

The reported photon-number-resolving detector is based on spatial multiplexing of the input photonic signal by a reconfigurable optical network as depicted in Figure 3.9. The multiport network consists of cascaded tunable beam splitters composed of a half-wave plate and a polarizing beam splitter. This high-performance reconfigurability architecture allows for accurate balancing of the output ports or, if needed, changing their number so there is no need to physically add or remove detectors. The whole network works as a 1-to-M splitter balanced with the absolute error below 0.3%. Specifically, it allows setting the configuration to Hanbury-Brown and Twiss measurement [470, 471]. Coupling between M different ports (crosstalk) is impossible, as the individual ports are completely spatially separated from each other into independent detectors. In this Thesis, the demand for laboratory equipment, especially single-photon detectors, limits the maximal number of detection channels to ten. Each of the ten channels is coupled to a multimode fiber and brought to a single-photon avalanche photodiode (SPAD, Excelitas) with system efficiency ranging from 60 to 70% at 810 nm, 200-300 ps timing jitter, and 20-30 ns dead time. The dead time of the presented photon-number-resolving detector is given solely by a dead time of the single constituent detector. The total jitter scales with the number of detection channels M as $\tau_{\text{tot}} = \sqrt{M}\tau$. In the worst case scenario, the total jitter ranges from 630 to 950 ps, approximately. Furthermore, differences in SPAD efficiencies and other optical imperfections or imbalances of the PNRD can be arbitrarily compensated by adjusting the splitting ratios of the optical network. The splitting ratios are set so that the detection rate in each channel is the same. As a result, the overall transmittance of each channel is the same (the product of the optical transmittance of the particular port and the efficiency of the SPAD sitting in that port). The PNRD then becomes a balanced detection multiplex with a global efficiency η that is a combination of all constituent losses. This means that all systematic errors are eliminated either by design or by a sufficiently precise adjustment, independently of constituent detectors employed. The total detection efficiency of 50(1)% is determined based on measured transmittance of the network and SPAD efficiencies specified by the manufacturer. For independent verification of the efficiency an absolute method using correlated photons can be used

[200, 275]. The non-unity system efficiency is caused by a sequence of five half wave plates and polarizing beam splitters with the total transmittance of 0.97^5, two lenses and two fiber couplings with the transmittance of 0.88, and the efficiency of SPAD detectors ranging from 0.6 to 0.7 with average value of 0.65. Hence, $0.97^5 \times 0.88 \times 0.65 = 0.49$. The efficiency can be improved by employing low-loss optics (especially polarizing beam splitters), anti-reflection coated fibers (transmittance 99%), and super-conducting nanowire single-photon detectors (system efficiency 90%). The improved efficiency can reach $0.985^5 \times 0.96 \times 0.9 = 0.8$. Based on the performed numerical simulations we expect that the resulting retrieved photon statistics will be nearly identical to the ones retrieved using the current version of the PNRD detector. The high-efficiency detector would find its application mainly in the case of low number of measurement runs and as heralding detector for a preparation of highly-nonclassical quantum states.

The use of independent detectors and well-balanced coincidence circuitry removes completely any crosstalk between the histogram channels yielding the perfect energy quanta resolution up to number of the channels used. Furthermore, the effects of dark counts and afterpulses are virtually eliminated by operating the detector in pulse regime with the repetition rate below approx. 5 MHz [199, 439]. The period between individual measurement runs can be ultimately decreased to be only slightly longer than the recovery time of the constituent single-photon detectors, as far as afterpulses are negligible or fast decaying like in the case of superconducting nanowire single-photon detectors [195–197]. It is important to stress here that the PNRD operates in real time and yields a result for every single input pulse with a latency (input-output delay) lower than 30 ns including the response of the SPADs, which allows its application also as a communication receiver, quantum discrimination device, or for a feedback operation. The period between individual measurement runs can be ultimately decreased to be only slightly longer than the recovery time of the constituent single-photon detectors, provided that afterpulsing is low enough.

3.3 A custom coincidence counting system

In order to process the output electronic pulses from a complex optical network of single-photon detectors, we designed and developed a custom coincidence logic. We have tested two implementations of the coincidence circuit, analog and digital ones.For repeated measurement runs, a simple summation of synchronized electronic pulses from single-photon detectors allows obtaining a histogram of coincidence events which is a sufficient outcome for the application of the photon statistics retrieval approach. However, in many modern photonic experiments, more complex processing of multichannel electronic outputs is required. Therefore, we built a coincidence system that can distinguish n-fold coincidences with the full detection channel number resolution.

3.3.1 Analog coincidence circuit

The analog solution employs commercial electronic modules, namely 300 MHz discriminators (Phillips Scientific NIM MODEL 708), delay lines (Phillips Scientific NIM MODEL 792), and an array of 250 MHz linear fan-in/out units (Phillips Scientific NIM MODEL 740). The propagation delay is approximately 10 ns (excluding coaxial patch cords) and the coincidence window should be larger than 20 ns because of few-nanosecond rise and fall times and time jitter. The bandwidth can be further increased utilizing a passive RF summation circuitry (Mini Circuits ZC16PD-252-S+) instead of the active fan-in units. We verified this option and reached the propagation delay below 5 ns, coincidence window 10 ns, and sub-ns jitter given mainly by the discriminator. The number of channels of the PNRD can be increased to several dozens while keeping the same analog electronic

signal processing technique. Potential disbalance in the summation circuitry can be corrected by careful adjusting the amplitude of the individual electronic pulses produced by the discriminator.

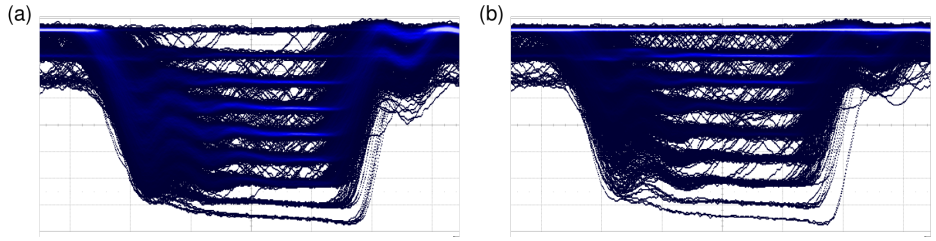

Figure 3.2: Active summation of detector output signals using fan-in units. Output signals are digitized with oscilloscope. Shown are: (a) coherent state, and (b) thermal state.

After the analog summation, the output signal is digitized with 20 GSa/s by a 1.5 GHz oscilloscope operating in a memory-segmentation regime (Teledyne LeCroy). Each of the thresholded voltage levels (eleven in our case) corresponds to the particular number of multi-coincidences. Figures 3.2 and 3.3 show energy quanta resolution for active and passive summation of optical network outputs. As a result, passive RF summation using a 16-channel power splitter/combiner proved to

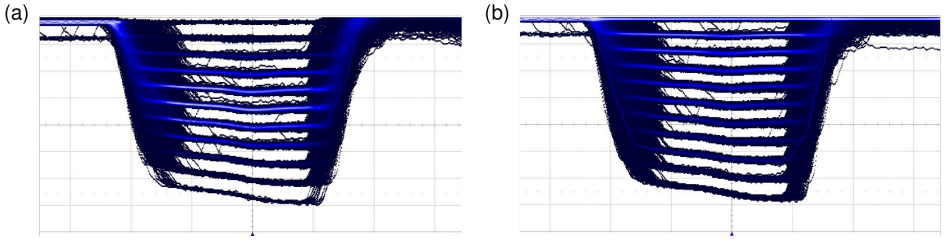

Figure 3.3: Passive RF summation of detector output signals. Output signals are digitized with oscilloscope. Shown are: (a) coherent state, and (b) thermal state.

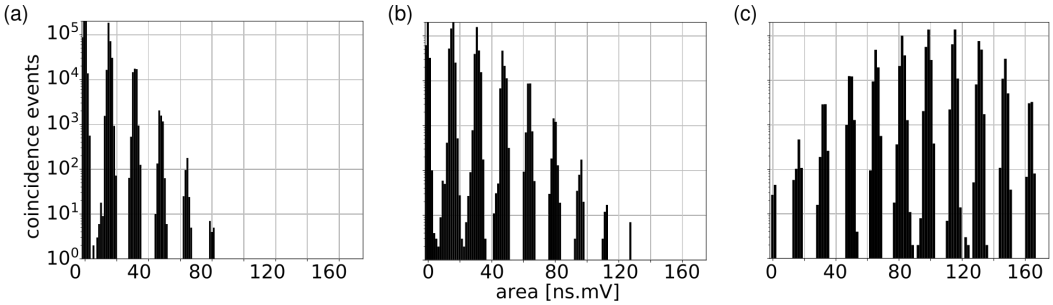

Figure 3.4: Pulse-height spectrum of the analog output of the reported PNRD for coherent states of various mean photon number $\langle n \rangle = 1$ (a), 5 (b), and 20 (c).

be the ideal choice for the near-ideal resolution of individual voltages. The pulse-height spectrum of the resuled analog output of the multiport network is shown in Figure 3.4. The spectra are plotted in log-scale to emphasize the perfect energy resolution and the absence of any crosstalk effects or background noise.

3.3.2 Digital coincidence circuit

Alternatively, a fully digital coincidence device can be employed. We developed an ultra-fast electronic multi-channel coincidence unit based on a custom emitter-coupled logic (ECL) circuit for counting detection events from singles to 16-fold coincidences with the full channel-number resolution. The device performs a real-time classification of all possible detection events in a 2^{16}-element histogram with the rate of up to 3 million events per second. The full histogram contains more information than required for click statistics and is further reduced to just 17 elements – no detection, singles, two-photon events,... 16-photon events. Alternatively, our coincidence counting unit (CCU) architecture allows advanced event triggering for the maximum input frequency of up to 800 Mhz. This trigger mode can be employed in complex photonic systems, e.g. for driving a feed-forward loop or active subtracting photons. The CCU is operable in the sub-100 ps coincidence windows regime with less than 10 ps overall jitter; applicable in quantum photonic experiments employing low-timing jitter photonic sources and single-photon detectors (< 30 ps).

Device design and operation

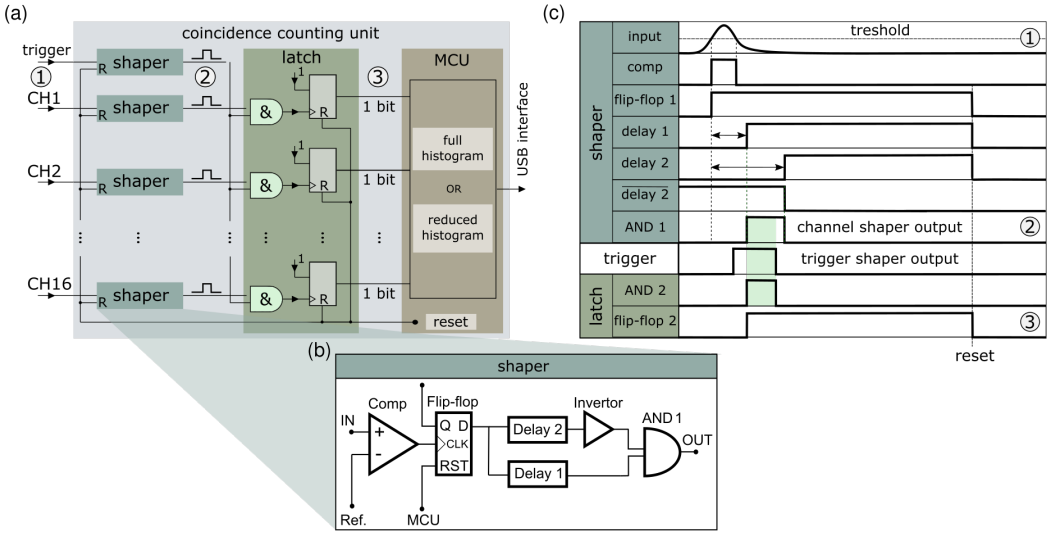

Figure 3.5: A functional flow block diagram of the coincidence counting system: (a) the main building blocks: the pulse reshaping process, coincidence counting and storing, (b) a block diagram of a shaper, and (c) the operation principle of the signal processing.

Developed ultra-fast electronic multi-channel coincidence unit is based on ECL circuitry consisting of fast comparators, delay lines, and basic gates with fast transition times. The Figure 3.5(a) shows an overview of the CCU architecture. The coincidence counting system consists of three main parts: input signal shaper, latch, and data processing. The device accepts 16 data inputs and a single gate input and yields the complete histogram of 2^{16} multi-coincidences of the inputs concerning the gate signal. Each input channel contains a shaping circuit to detect an input signal edge and provides the output ECL pulse of a given width and delay. Shaper is a crucial circuit building block comprised of a fast comparator, multiple delay lines, and basic gates (see Figure 3.5(b)). For a detailed description of the pulse shaping and processing, see the Figure 3.5(c)). Input electrical signal is processed by the fast comparator (an adjustable threshold from 1 V to 4 V) to convert it from the original waveform to a start pulse triggering the first flip-flop circuit. The flip-flop is used

to store state information and enable the creation of a time window independent of the input signal. The flip-flop output is split into two signals and modified by parallel delay lines and invertors. The time window is defined as an output of AND gate that implements the logical conjunction of these delayed signals. The first/second delay line sets the rising/falling edge of the time window. The width of the time window is given as the time difference between these two propagation delays. The time windows of individual channels can be tuned independently. A system of parallel delay lines automatically compensates for the finer input pulse time alignment. After signal shaping, the signal and trigger pulse are processed by the latch. The latch composed of 16-input AND gates and the flip-flop circuits counts all possible coincidences between the rising edge of one exclusive signal (trigger) and 16 rising edges of the signal time windows and stores information about successful coincidence events and single-channel pulses. The AND gates generate an output pulse only when incoming pulses and triggers are received simultaneously. Data from the latch is transferred in the form of bits.

The information about successful coincidence events can be directly employed as a trigger signal for implementing the real-time feed-forward control to change the performance of the system or measurement configuration. The maximum input frequency of advanced event triggering is up to 800 Mhz. In principle, this gating mode is limited only by the maximum operating frequency of delay lines.

Alternatively, this data type could give rise to a histogram of detection events. In this paper, the MCU is used for configuration, monitoring, and data processing and storing in the memory. The CCU has a USB interface (the RTC+CTS protocol) for communication and data readout with a 10^6 baud rate.The presented CCU architecture allows us to define the coincidence operational condition and operate in two specific work regimes depending on the complexity of the measurement. One can store complete information about all possible coincidence events ($2^{16} = 65536$ kinds of coincidence events in total), called the ”full histogram” regime, or throw away information about the number of channels and count only specific coincidences of the same order. For our concrete technical solution, the maximum processing rate is about 3M events per second for the reduced histogram and 2M events for the full histogram. This difference between maximum operating rates is caused by more complex data processing.

Furthermore, the CCU is also operable in a self-calibrating regime. The system of the two parallel delay lines in each counting channel primarily allows precisely setting the coincidence channels parameters. Additionally, a fine-time resolution delay line step guarantees efficient measurement of produced coincidence window.

Coincidence unit performance

To characterize the performance and capabilities of the presented device, we have chosen these figures of merit: (1) the minimum and maximum coincidence window length, (2) timing granularity, (3) jitter, (4) higher-order coincidence failure probability, and (5) the maximum detection rate. Employed high-speed ECL components with fast transition times such as comparators, D flip-flops, precision programmable delay lines, and differential AND gates guarantee short propagation delay below 5 ns. We could not examine the jitter of the CCU directly, because all time discrepances are under the resolution of our 1.5 GHz oscilloscope. However, it can be stated that the overall jitter of the presented CCU architecture is less than 10 ps.

The complete coincidence window characterization is performed by CCU itself. The fine-time resolution of the delay-lines system allows us to scan individual coincidence windows. Each delay line has 1024 discrete steps with a different propagation delay dependent on the temperature. The average discrete delay-line step is 9(1) ps. We analyzed the coincidence window’s width and rising and falling edges. The whole measurement is based on changing the mutual position of the trigger and channel pulse. As a result, we got the number of coincidence events as a function of time

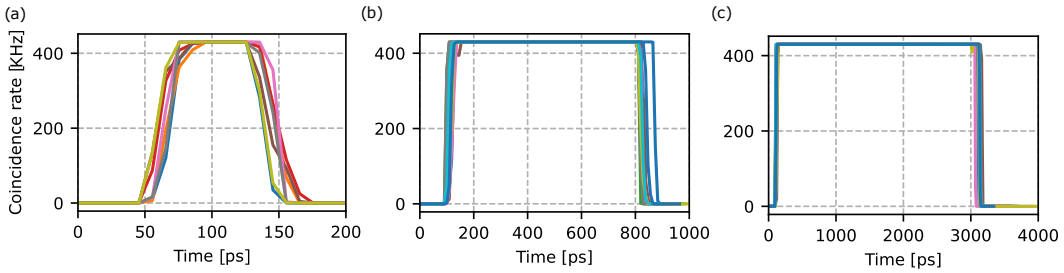

Figure 3.6: Full scan of the coincidence window of (a) sub−100 ps (b) 700 ps and (c) 3 ns width.

delay. The minimum and maximum width of the coincidence window are sub-100 ps and 20 ns, respectively. The main limitation of the maximum coincidence window width is a fixed range of delays from 2.2 up to 14.8 ns for the used configuration. The results show that the coincidence windows are well defined in time, and they are almost perfectly rectangular with sharp edges with a value typically around 18(5) ps for all channels (see Figure 3.6 and 3.7(a)).

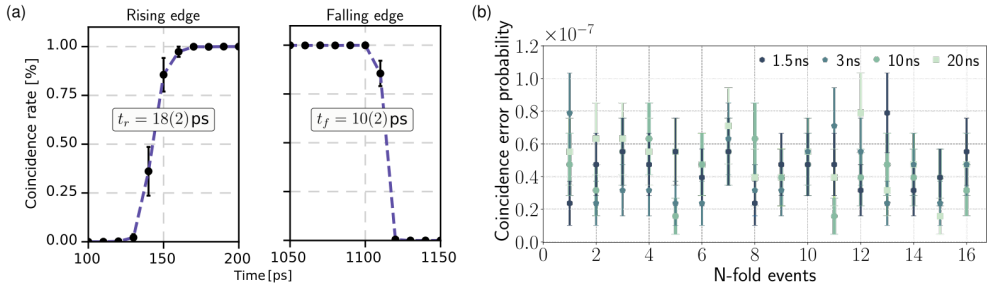

Figure 3.7: (a) The typical achieved width of the rising and falling edge (10 – 90%) of the coincidence windows (Shown is the coincidence window whose width is 1 ns). (b) Analysis of the coincidence error probability of the individual *n*-fold coincidences for several different widths of the coincidence windows: 1.5 ns, 3.0 ns, 10 ns, and 20 ns. Presented values are calculated as the average over the 250 measurement runs. The error bars represent one standard deviation.

Presented CCU meets the conditions of a high-resolution coincidence system with the same probability of occurring for all orders of coincidence events, see main text. We have analyzed the precision of counting coincidences for several configurations of coincidence window width from 1.5 up to 20 ns. A homemade multi-channel pulse generator with a repetition rate from 0.2 to 10 MHz was used as an input electrical signal. The signal is generated by a relaxation oscillator whose output is delayed by an RC low pass network and fast inverter with Schmitt trigger inputs (74ACT14T). This generator was developed to simulate the typical output signals from SPADs. The jitter of the individual channels is less than 10 ps instead of the typical 250 ps SPAD jitter. To evaluate the counting error of the number of coincidence events, the detection channels were turned off one by one. The figure 3.7(b) shows the analysis of counting coincidences precision for several configurations of coincidence window width from 1.5 up to 20 ns. All coincidence errors across all tested coincidence windows are lower than 1×10^{-7}. It means that all coincidences have the same probability, which indicates ultra-low losses of events during electrical signal processing. These negligible detection losses are initiated by resetting the latches, most probably caused by back reflections via imperfect impedance matching.

3.3.3 Discussion

With better programmability, readout speed, and the ability to read multi-coincidence events with full channel resolution, we have come to prefer the digital version of the coincident unit. The architecture of the CCU based on fast positive ECL circuits benefits from high-resolution coincidence counting. The CCU provides a fine-tunable coincidence window within a range of sub-100 ps – 20 ns with 10 ps resolution and 10 ps overall jitter. These allow recording ultra-low overlap between the input pulses and the gate signal down to a few dozen picoseconds, guaranteeing almost no losses of coincidence events across all coincidence orders. The overall coincidence error probability is below 10^{-9} percent. The presented CCU design can be easily scaled up to a few dozen input channels and can be considered as a practical counting device for multiple-output applications.

Ref.	[479]	[308]	[307]	[306]	[305]	[304]	CCU
Number of channels	20	8	32	8	48	8	16
Measurable coinc. folds	20	8	8	8	6	8	16
Max. input frequency [MHz]	400	40	80	50	76	163	800
Min. coinc. window [ns]	0.46	–	0.39	10	0.3	0.47	<0.1
Max. coinc. window [ns]	10	–	–	70	1.9	13.22	20

Table 3.1: Performance parameters comparison of proposed coincidence counting device and different coincidence counter approaches.

In Table 3.1, the performance summarization of the various CCU approaches is shown. Despite a large number of FPGA-based CCU channels, a relatively small number of these channels is employed in coincidence counting mode. Nevertheless, the device in Ref. [479] can detect up to twentyfold coincidences. Coincidence counting devices typically provide a minimum coincidence window in the sub-nanosecond range. Another critical parameter is the maximum input frequency ranging from several dozen to a few hundred MHz. Comparing these CCU approaches, the developed CCU offers high n-fold coincidences counting (n > 8), the shortest well-defined sub–100 ps coincidence windows with 10 ps overall jitter, and the highest maximum input frequency of 800 MHz.

The functionality of the presented device can be further extended and some of the characteristics can be improved. Coincidence counting and histogramming are programmed into an MCU (STM32F429), limiting the data processing sequence. Employing FPGA instead of MCU promises improvement in the speed of large datasets processing by order of magnitude. Additionally, FPGA can bypass the frequency limitation of CMOS to PECL Translator (800 MHz) and be directly employed to reset all components at the CMOS level to increase the maximum input frequency up to 1.5 GHz. If necessary, the range of the coincidence window width can be easily increased by modifying the distribution process of the trigger signal and the delay line system. It is also possible to increase the number of input channels and go beyond 16. Further advancing the coincidence counting and processing to a mesoscopic scale opens the way to ground-breaking applications in quantum communications, simulations, and boson sampling machines.

3.4 Numerical analysis of photon statistics retrival

We performed a numerical analysis comparing EME to other photon statistics retrieval methods. We numerically simulated click statistics (using $M = 10$ and $\eta = 0.5$) of several known initial states

and then applied direct inversion (Section 2.6.1), EM algorithm (Section 2.6.2) and EME algorithm (Section 2.6.3). To quantify the match between the real and estimated photon statistics, we used total variation distance and fidelity. Furthemore, we focused on the reconstruction accuracy and convergence speed of individual photon statistics retrieval methods.

3.4.1 Expectation-maximization-entropy algorithm

Here we present an expectation-maximization-entropy method, based on an expectation-maximization iterative algorithm weakly regularized by a maximum-entropy principle. The initial zeroth iteration is uniform; $p_n^{(0)} = 1/(n_{\max}+1)$ for sufficiently large $n_{\max} \gg \langle n \rangle$. Each subsequent iteration is

$$p_n^{(k+1)} = \Pi_n^{(k)} p_n^{(k)} - \lambda \left(\ln p_n^{(k)} - S^{(k)} \right) p_n^{(k)}, \tag{3.1}$$

$$\Pi_n^{(k)} = \sum_{m=0}^{M} \frac{c_m}{\left(\sum_j C_{mj} p_j^{(k)} \right)} C_{mn}, \quad S^{(k)} = \sum_{n=0}^{n_{\max}} p_n^{(k)} \ln p_n^{(k)}. \tag{3.2}$$

Here the superscript (k) denotes k-th iteration. Each iteration is evaluated for $n = 1, \ldots, n_{\max}$. The $\Pi_n^{(k)}$ is a function of the measured click statistics c_m and the efficiency η determined by a separate measurement. The click statistics c_m is determined by the photon statistics $c_m = \sum_n C_{mn} p_n$ [103, 264, 274], where C_{mn} gives the probability of m channels clicking upon the arrival of n photons (see Section 2.5), and $S^{(k)}$ is a negative von Neumann entropy. The parameter λ scales the entropy regularization relative to the likelihood maximization. The process is stopped when two subsequent iterations are practically identical. The retrieved statistics does not change for different initial iterations. The derivation of the algorithm is given in Section 2.6.3.

3.4.2 Reconstruction accuracy

The direct inversion method proved to be unsatisfactory, because non-negativity of the result is not guaranteed and therefore, some results do not represent a valid photon statistics. Those that do, exhibit the distance 2×10^{-2}, which is close to the results of the EM method. The EM algorithm guarantees positive-semidefinite results with average fidelity $\overline{F} = 0.997$. The total variation distances are similar to those obtained by direct inversion. An average distance 3×10^{-2} is reached for all tested sources. Finally, the presented EME method gives the best match while always maintaining non-negativity. The average fidelity $\overline{F} = 0.9996$ and average distance is 4×10^{-3}. Particularly, the total variation distance of this method is smaller by an order of magnitude across all states. The EME therefore significantly improves the results for all kinds of simulated statistics (Figure 3.8).

In Figure 3.9, we show by numerical simulation that the results of the EME algorithm approach the respective theoretical expectations as more data is acquired. This means that despite a limited number of channels $M = 10$, the chief source of error is the statistical/sampling error. We also verified that Δ stays the same if both the mean number of photons and the number of channels are doubled. Therefore, EME scales well to high photon numbers considering limited experimental resources. In addition, we analyzed the effect of the probability distribution of the zeroth iteration on the retrieved statistics for several different initial states of light. Achieved results show that the retrieved photon statistics does not change for different zeroth iterations. To conclude, the EME algorithm proves to be a robust photon statistics estimator.

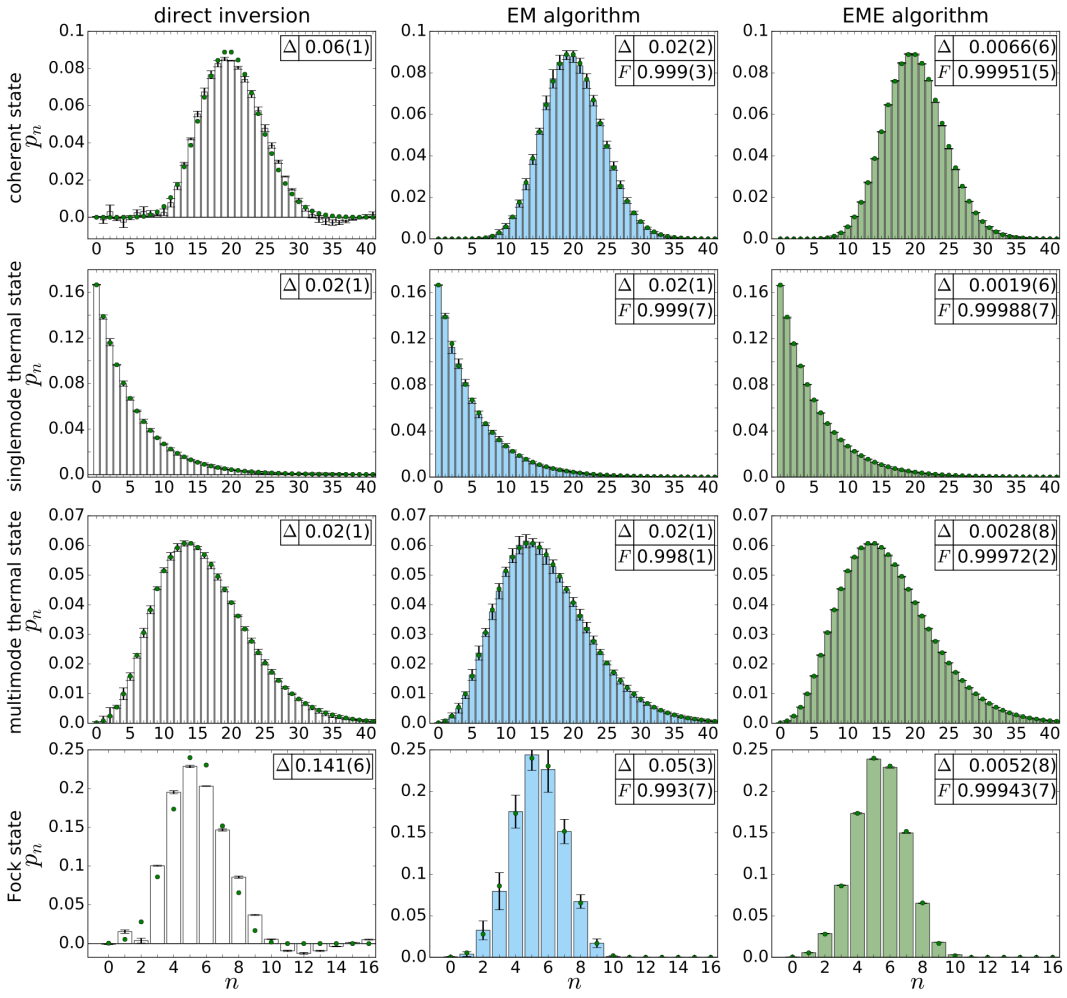

Figure 3.8: Photon statistics retrieval of various different states of light from numerically simulated click statistics. Each column shows a different retrieval method: direct inversion (Moore-Penrose pseudoinverse), EM algorithm, and EME algorithm, from left to right. The same amount of data (number of measurement runs) is used for each retrieval method to facilitate the comparison. The green points represent the corresponding true photon statistics.

3.4.3 Convergence speed

EME and EM exhibit significantly different convergence behaviour with respect to the iteration cut-off distance ϵ. For both methods, the inter-step distance decreases with the number of steps. For EM, the total variation distance to the expected photon statistics is non-monotone and eventually starts to rise. The result is that for low ϵ the retrieved photon statistics reveals considerable artifacts. EME does not show this issue. We demonstrate this effect on measured data for a Poissonian signal, see Figure 3.10. For both methods, the reconstructed photon statistics yield the same click statistics on the PNRD, but the ill-posed nature of the problem results in overfitting in the case of EM. For EME, the weak regularization eliminates this issue. We observed that this behaviour is stronger for smaller data sets. It may seem that using a certain optimal value of ϵ would solve the issue.

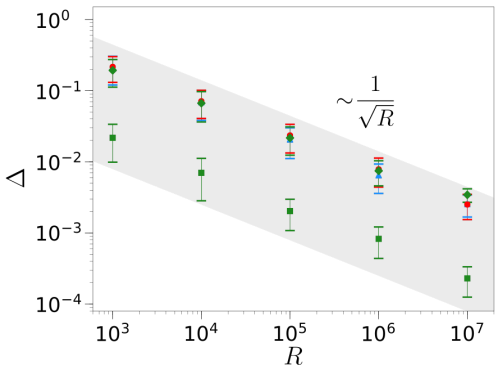

Figure 3.9: A numerical analysis of EME total variation distance Δ. With more measurement runs R, the statistical error in the data is lower and the EME result approaches the true photon statistics despite the limited number of channels $M = 10$. Here shown for various photon-number distributions and a single value of $\lambda = 10^{-3}$. Shown are: coherent state with $\langle n \rangle = 10$ (blue triangle up), thermal state with $\langle n \rangle = 5$ (red circle), N_p-photon cluster with $N_p = 1$ (green square), and $N_p = 9$ (green rhombus). The gray area illustrates the observed scaling ($0.25/\sqrt{R}$ to $14/\sqrt{R}$.)

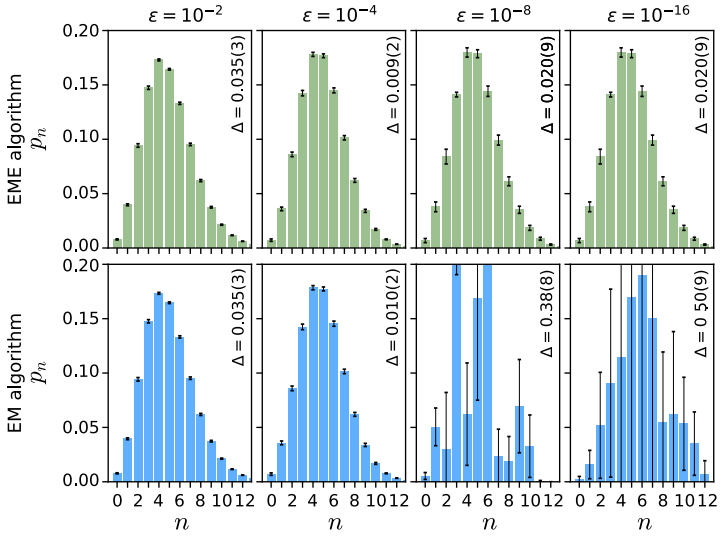

Figure 3.10: Poisson statistics $\langle n \rangle = 4.95$ reconstructed by EME (top row) and EM (bottom row) as a function of the iteration cut-off distance ϵ. All distributions are obtained from the same collection of 10 data sets, each containing 10^5 measurement runs. Inset numbers (top right) denote total variation distances to the ideal Poisson distribution.

Unfortunately, the optimal value depends on the photon statistics. When measuring an unknown distribution, the value of ϵ cannot be set beforehand, because no expected distribution is available.

The convergence speed analysis of the retrieval methods with respect to the measured data is shown in Figure 3.11. We compare the convergence of EM and EME in the case of a coherent state, a thermal state, a two photon-subtracted thermal state and a single-photon emitter. Figure 3.11 shows that EME converges faster by orders of magnitude than EM. Only for a single-photon emitter, both methods are on par (the green lines overlap). While EM usually requires at least 10^5 iterations, EME can do with less than 10^4.

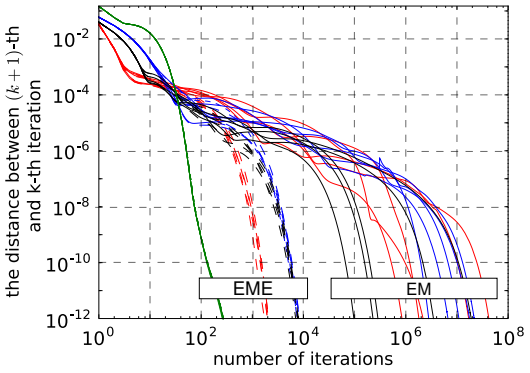

Figure 3.11: Photon statistics retrieval convergence demonstration of selected states: coherent state (blue), thermal state (red), 2-photon subtracted thermal state (black), and single-photon emitter (green). Shown are results for EM iterative process (full lines) based on Eq. (2.47) and for EME algorithm (dashed lines) based on Eq. (2.50). For each state five runs of individual retrievals were done.

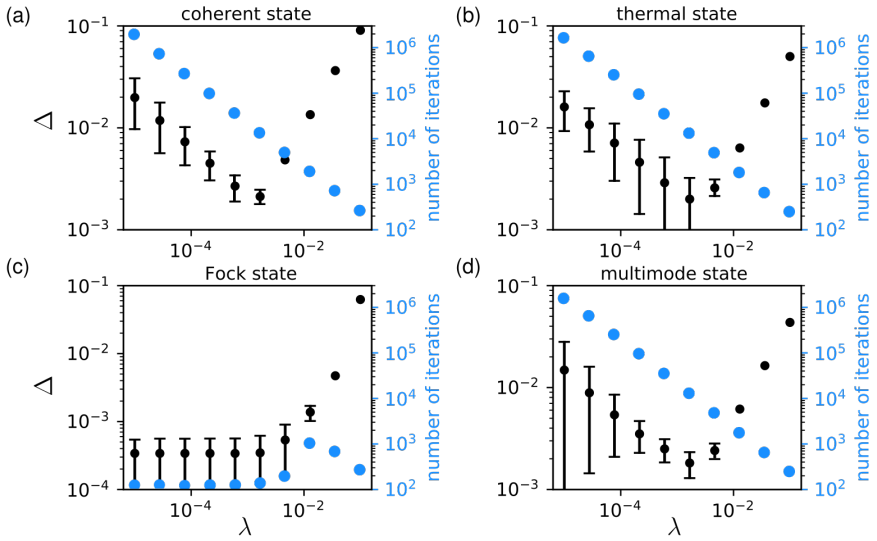

Figure 3.12: Accuracy and speed of photon statistics retrieval using EME algorithm versus the strength of entropy regularization characterized by the parameter λ. The total variation distance Δ characterizing the accuracy (black) and the number of EME iterations required (blue) are plotted for four different photon statistics. Shown are: (a) coherent state with $\langle n \rangle = 5$, (b) thermal state with $\langle n \rangle = 2$, (c) single-photon emitter ($N_p = 1$), and (d) multi-mode thermal states with $M_{th} = 2$. The data are simulated numerically (from true photon statistics) using Monte Carlo approach. For each value of λ the statistics retrieval is performed several times for different data sets to evaluate the repeatability, which is represented by error bars of Δ.

3.4.4 The strength of entropy regularization

Furthermore, we have performed a detailed analysis of accuracy and convergence speed as a functions of the regularization parameter λ for various photon statistics including strongly non-classical sub-Poissonian states. In case of small values of λ the EME approaches the common EM algorithm and the accuracy and repeatability of the solution decrease. For large λ the entropy regularization prevails and the solution is less likely to reproduce the data - the accuracy drops. Numerical simula-

tions revealed the dependence of the reconstruction method accuracy on the entropy regularization parameter (see Figure 3.12). There does not exist the parameter λ that is optimal regardless of the incident state of light and its mean photon number. The optimal value of the regularization parameter λ depends on the number of runs/data sets (R) and scales approximately as $\lambda \sim \frac{1}{\sqrt{R}}$. In our experiment, we typically work at the level of $R \approx 10^6$. Thus, $\lambda = 10^{-3}$ was found to be the best possible strength of entropy regularization to keep the total variation distance satisfyingly small for all the performed photon statistics retrievals (for all tested sources).

3.5 Application to quantum state measurement

In our experimental demonstration of photon statistics detection approach, we used a balanced configuration of the detector described in Section 2.5, and Section 3.2. We analyzed optical states such as coherent states, single-mode thermal states, multi-mode thermal states, and non-classical multiphoton states. First, the employed optical sources of various states of light are discussed in technical details. Subsequently, we processed the raw data from the multi-channel coincidence measurement to directly characterize the nature of initial states of light [342, 480]. Furthermore, we employed EME algorithm (see Section 2.6.3) to retrieve the photon statistics from the measured click statistics. We focus mainly on the discrepancy between the measured and the corresponding ideal photon statistics for dozens of measured photonic sources, characterized by the fidelity $F = \mathrm{Tr}[\sqrt{p_n \cdot p_n^{\mathrm{ideal}}}]^2$ and the total variation distance $\Delta = \sum_n |p_n - p_n^{\mathrm{ideal}}|/2$, both ranging from 0 to 1. Higher fidelity does not necessarily correspond to a stronger non-classical feature so other characteristics should also be evaluated [481]. Very often only a limited number of characteristics are evaluated and utilized to witness a particular feature of the source under the test. For each retrieved photon statistics we computed $\langle n \rangle$, $g^{(2)}$, Q_M, and *Fano*. We have varied the mean number of photons, the number of modes, and the number of superimposed photons. We also identified non-classicality of the multi-photon states of light by certifying the Wigner function. More details of these preferred quantities are given in Section 2.2.

3.5.1 Coherent state

As an initial coherent nanosecond pulsed light, we developed sub-ns-pulsed laser diode with variable repetition rates between 50 kHz to 2 Mhz. We employed a technique of gain-switching, frequently used for generating short optical pulses in a laser by modulating the laser gain via the electrical pulse pumping. We have reached $< 1\%$ pulse-to-pulse stability and similar long-term stability of the mean power by employing custom low-noise low-jitter pulse generator, laser diode selection, its thermal stabilization, and optimization of driving pulse duration and shape. The laser diode in constant current mode with the central wavelength of 810 nm is a temperature-stabilized and biased below the threshold current by a well-stabilized DC current. Periodical modulation of the laser gain is realized by mixing the ultra-short pumping pulses with the injection DC current at the bias tee. The applied pump power causes the generation of the optical pulse whenever the injection current rises above the threshold level. As an electrical pump home-made sub-nanosecond electronic pulse generator with an adjustable pulse width in the range of 0.5 ns to 5 ns was used. The peak amplitude of the electronic pulse was set to 4 V. The developed generator has two outputs, one of which serves as a trigger. The time delay between the trigger and pump signal can be set up to 224 ns to compensate for the different transit time of the optical part of the experiment. The mean optical power was modified by applying different levels of neutral density filters.

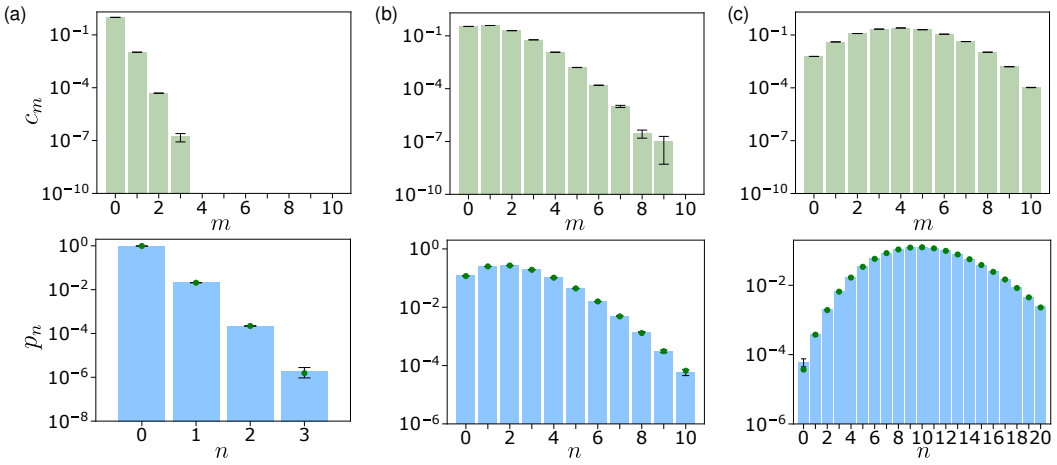

Figure 3.13: Experimental results of detection of photon statistics. Shown are the measured click statistics (green bars), retrieved (blue bars), and the corresponding theoretical photon statistics (green dots) of coherent state for several mean photon numbers $\langle n \rangle$: (a) $\langle n \rangle = 0.02119(3)$, (b) $\langle n \rangle = 2.144(3)$, and (c) $\langle n \rangle = 10.21(1)$. All distributions are plotted on a logarithmic scale.

The resulting coherent pulses measured by the PNRD detector display virtually perfect Poissonian statistics (see Figure 3.13). Retrieved photon statistics reaches fidelities $F > 0.9997$ (Figure 3.14(a)) and total variation distances $\Delta < 10^{-2}$ (Figure 3.14(b)) for all measured coherent states. Evidence of ideal Poisson statistics is also provided by the values of the evaluated parameters associated with the statistical properties of light. Figure 3.15(a) shows classical behaviour of Q_b parameter, as expected for coherent state ($Q_\mathrm{b} = 0$). The binomial parameter of the measured click statistics reaches low values close to zero, even negative ones caused mainly by fluctuations of the laser source. The Mandel parameter as a function of mean photon number of initial state is shown in Figure 3.15(b). We measured coherent states with Poissonian statistics with Mandel parameter Q_M ranging from -1×10^{-3} to 0.012 and the mean photon number exceeding $\langle n \rangle = 19.84(2)$. Achieved results show that the Mandel parameter is more sensitive to the mean number of photons of the incident radiation. As the mean number of photons approaches the number of detection channels, the value of the Mandel parameter deteriorates, moving away from the ideal value for Poisson light ($Q_\mathrm{M} = 0$). As one might expect, the correlation function reaches $g^{(2)}(0) = 1$ (Figure 3.15(c)) and Fano factor $Fano = 1$ (Figure 3.15(d)).

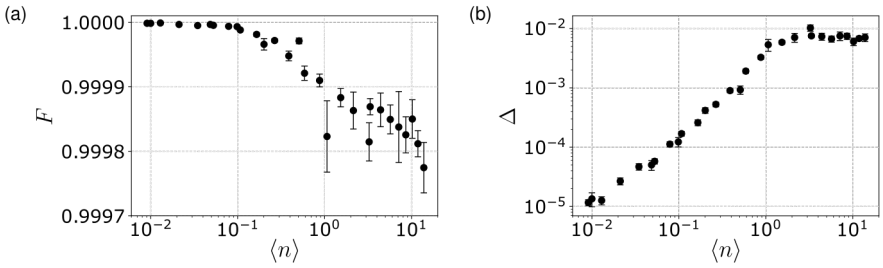

Figure 3.14: The discrepancy between the measured and the corresponding ideal photon statistics of coherent states characterized by (a) fidelity F, and (b) the total variation distance Δ.

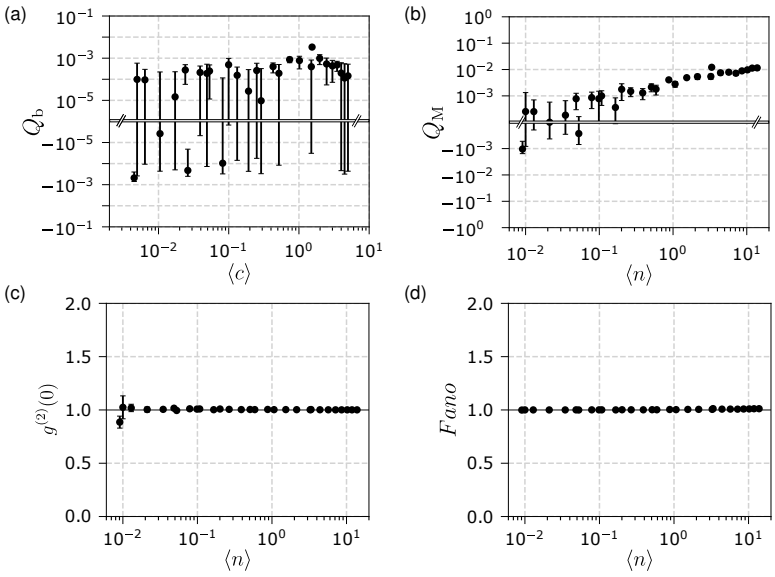

Figure 3.15: Characteristics of measured photon statistics of coherent states: (a) the binomial parameter, (b) the Mandel parameter, (c) $g^2(0)$ function, and (d) Fano factor. Solid curves represent theoretical models.

3.5.2 Thermal state

Pseudo-thermal light

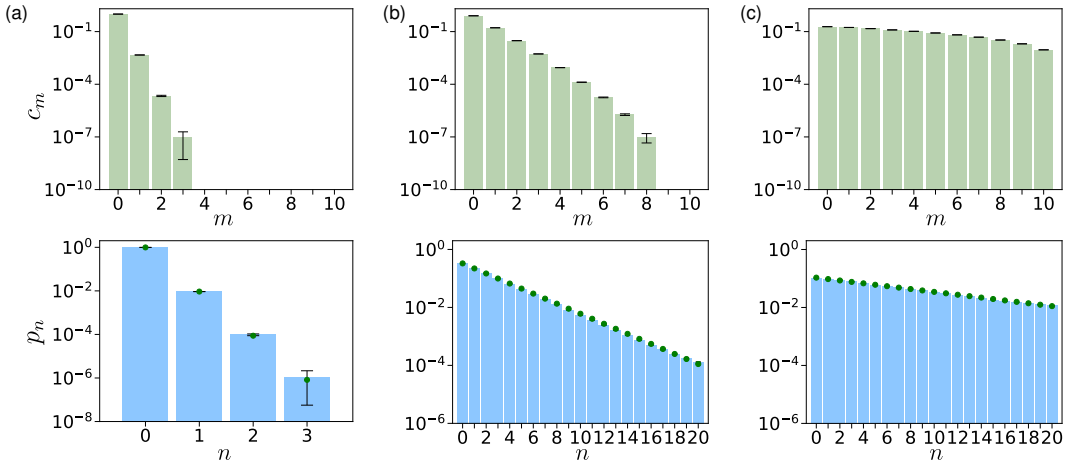

Figure 3.16: Experimental results of detection of photon statistics. Shown are the measured click statistics (green bars), retrieved (blue bars), and the corresponding theoretical photon statistics (green dots) of thermal state for several mean photon numbers $\langle n \rangle$: (a) $\langle n \rangle$ = 0.00949(5), (b) $\langle n \rangle$ = 1.993(1), and (c) $\langle n \rangle$ = 8.41(3). All distributions are plotted on a logarithmic scale.

Thermal states are generated by temporal intensity modulation of the initial coherent light by rotating diffuser with a random spatial distribution of speckles [362–365]. As a diffuser we employed 1500 grit N-BK7 ground glass disk (Thorlabs DG 20-1500-H2). The disk is attached to a

miniature DC motor with operating range from 3 up to 6 V (Multicomp MM28). The rotating speed of the disk at a constant current of 1 A (3 V) is 8000 rounds per minute, as given in the manufacturer's datasheet. The coherent pulsed light is focused on the diffuser surface by a high-precision aspheric lens with a focal length of 18.4 mm and numerical aperture of 0.15 (Thorlabs C280TM-B). We have measured the corresponding photon statistics to be nearly ideal Bose-Einstein distribution. In the initial stage of our experiment, we observed a discrepancy between measured photon statistics of RGG modulated light and the ideal Bose-Einstein statistics. It appeared later that the error was caused by a small inhomogeneity of the RGG disk. More consistent results can be attained using a direct programmable modulation of light intensity, which allows for preparation of near-ideal thermal state and also an arbitrary photon statistics, see Section 2.3.2.

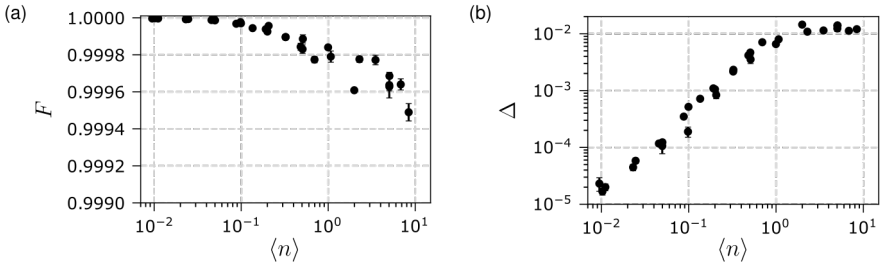

Figure 3.17: The discrepancy between the measured and the corresponding ideal photon statistics of thermal states characterized by (a) fidelity F, and (b) the total variation distance Δ.

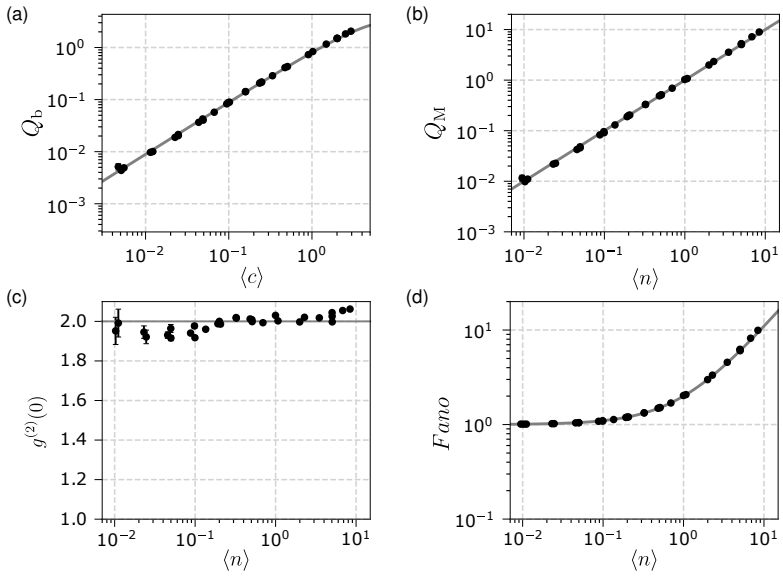

Figure 3.18: Characteristics of measured photon statistics of thermal light: (a) the binomial parameter, (b) the Mandel parameter, (c) $g^2(0)$ function, and (d) Fano factor. Solid curves represent theoretical models.

Figure 3.16 shows retrieved photon statistics of thermal states for several different mean photon numbers. Photon statistics are plotted on a logarithmic scale to better present a high accuracy of the retrieval process. The retrieved photon statistics reach $F > 0.9994$ and $\Delta < 1.5 \times 10^{-2}$ for all measured thermal states (Figure 3.17). Measured thermal states cover values of mean number of

clicks $\langle c \rangle$ up to 2.944(2) corresponding to $\langle n \rangle = 8.41(1)$. Just like ideal thermal light, generated pseudo-thermal light exhibits $Q_{\mathrm{b}} = (M-1)/(M/\langle n \rangle + 2)$ (Figure 3.18(a)), where M is the number of detectors, $Q_{\mathrm{M}} = \langle n \rangle$ (Figure 3.18(b)), $g^{(2)}(0) = 2$ (Figure 3.18(c)), and $Fano = \langle n \rangle + 1$ (Figure 3.18(d)).

Multi-mode pseudo-thermal light

Multi-mode thermal states were generated by selecting M_{th} thermal modes with the same overall mean photon number $\langle n \rangle = n_{M_{\mathrm{th}}} M_{\mathrm{th}} = n_{\mathrm{th}}$ but different temporal modulation. We have altered the effective number M_{th} of thermal modes by changing the size of the speckles collected via single-mode fiber. This was achieved by changing the diameter of the laser spot on the RGG disk and the distance between the disk and the fiber tip. The resulting Mandel-Rice statistics changes from Bose-Einstein to Poisson distribution with increasing number of modes (see Figure 3.21(c)). The multi-mode thermal state shows the largest discrepancy between the measured photon statistics and the corresponding ideal one, which is caused by its relatively complicated preparation. The intensity of the initial coherent state, its focusing on the RGG, and the fiber coupling are changed to simultaneously reach the required mean photon number and the variance compatible with the Mandel-Rice statistics, basically verifying $g^{(2)} = \frac{2M_{th}+1}{M_{th}} - 1$, where M_{th} is number of modes. Also, the used RGG has to be checked first for its roughness homogeneity by producing the ideal chaotic light with the Bose-Einstein photon statistics. If the RGG allows generating a super-chaotic statistics for any combination of the mentioned hardware parameters, it cannot be straightforwardly used to produce a proper transition from Bose-Einstein to Poisson statistics via the multi-mode Mandel-Rice statistics.

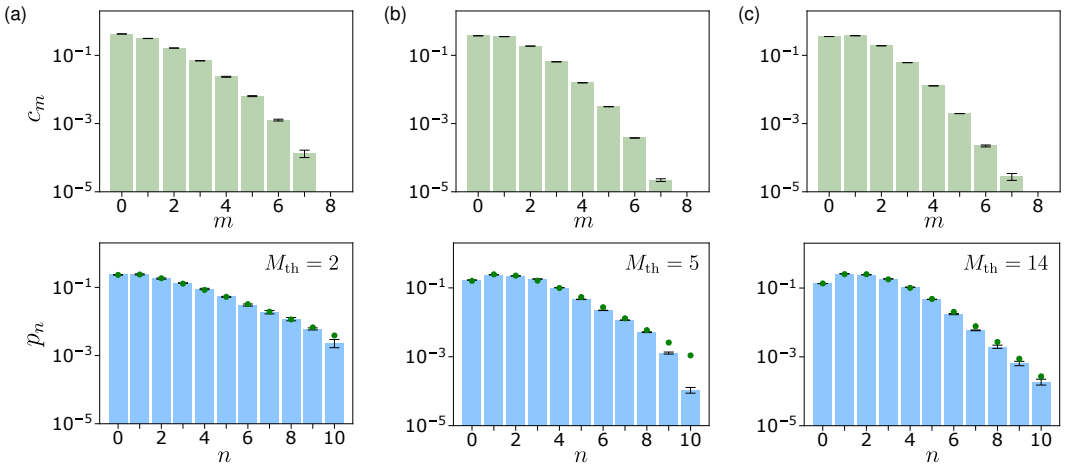

Figure 3.19: Experimental results of detection of photon statistics. Shown are the measured click statistics (green bars), retrieved (blue bars), and the corresponding theoretical photon statistics (green dots) of multi-mode thermal state for several number of modes M_{th}: (a) $M_{\mathrm{th}} = 1.95(3)$, (b) $M_{\mathrm{th}} = 5.19(2)$, and (c) $M_{\mathrm{th}} = 13.9(2)$. All distributions are plotted on a logarithmic scale.

The retrieved photon statistics of the prepared multi-mode thermal states with number of modes up to 14 are depicted in Figure 3.19. Due to the difficulty in preparing these states of light, the fidelity and total variation distance are the worst of all the measurements made, as shown in Figure 3.20. We experimentally demonstrated multi-mode thermal states from 1 up to 14 modes, specifically $M_{\mathrm{th}} = 1.95(3), 5.19(2)$, and $13.9(2)$. For the multi-mode thermal light, the variance converges to the mean photon number with increasing number of modes $\langle (\Delta n)^2 \rangle = \langle n \rangle + \frac{\langle n \rangle^2}{M_{\mathrm{th}}}$. Keeping

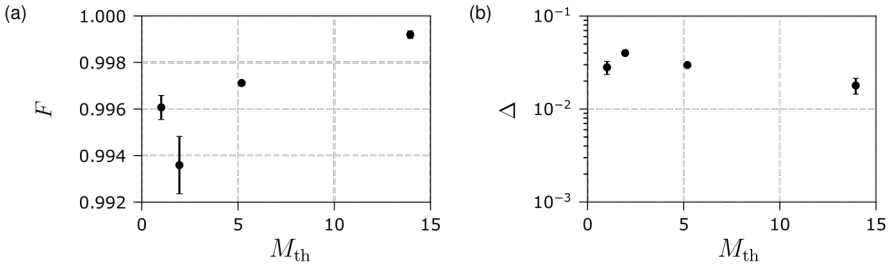

Figure 3.20: The discrepancy between the measured and the corresponding ideal photon statistics of multi-mode pseudo-thermal light characterized by (a) fidelity F, and (b) the total variation distance Δ.

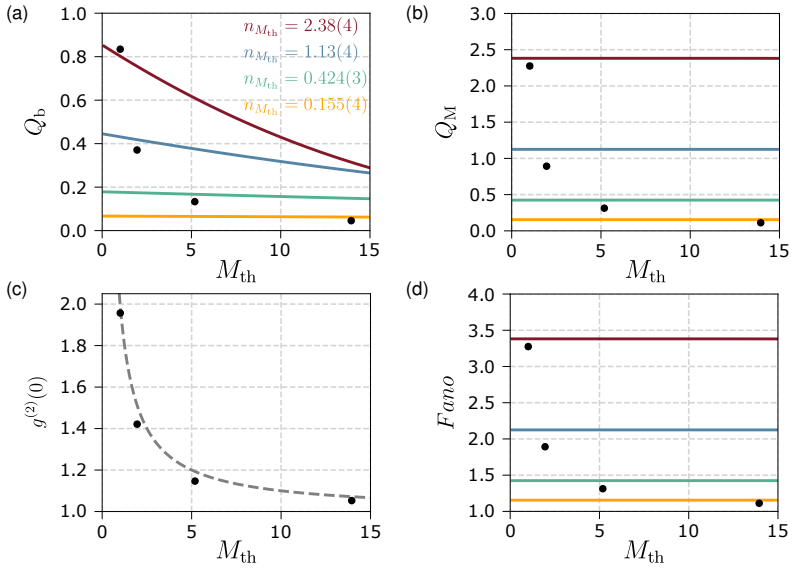

Figure 3.21: Characteristics of measured photon statistics of multi-mode pseudo-thermal light: (a) the binomial parameter, (b) the Mandel parameter, (c) $g^2(0)$ function, and (d) Fano factor. Solid curves represent theoretical models. Color coding stays for different mean photon number $n_{M_{\mathrm{th}}}$: 2.38(4) (red), 1.13(4) (blue), 0.424(3) (green), and 0.155(4) (yellow).

the overall mean photon number the same for all states, the mean photon number of initial modes are $n_{M_{\mathrm{th}}} = 2.38(4), 1.13(4), 0.424(3)$, and $0.155(4)$. For prepared multi-mode thermal states, we obtained the binomial parameter Q_{b} ranging from 0.046(2) to 0.83(2). The measured values of the Mandel parameter follows theoretical prediction $Q_{\mathrm{M}} = n_{M_{\mathrm{th}}}$ (Figure 3.21(b)). Also, the Fano factor depends on the number of modes and yields the $Fano = n_{M_{\mathrm{th}}} + 1$ (Figure 3.21(d)). In a similar manner, the second order correlation function decreases with increasing number of modes M_{th}, $g^{(2)}(0) = \frac{2M_{th}+1}{M_{th}} - 1$ (Figure 3.21(c)).

Ideal thermal light generated in warm atomic vapor

Here we introduce the experimental generation of light close-to-ideal thermal statistical properties by a natural physical mechanism. The thermal light state is prepared using a spontaneous Raman emission in a warm atomic vapor. The experimental realization employs ^{87}Rb energy level scheme. Ensemble of warm ^{87}Rb atoms are excited by frequency stabilized laser diode. The combin-

ation of a Glan–Thompson polarizer, Fabry–Pérot resonator and single-mode fiber is used to collect the emission. For more detailed information see Mika et al. [C2]. Within the chosen temporal mode width of 648 ps it would be practically negligible to observe four-coincidence events even on the measurement time scales of days. This allows us to employ only a three-detector scheme. The photon number probability distribution is estimated from the measured rates of singles, two-fold and three-fold coincidences using EME algorithm without any detection efficiency corrections.

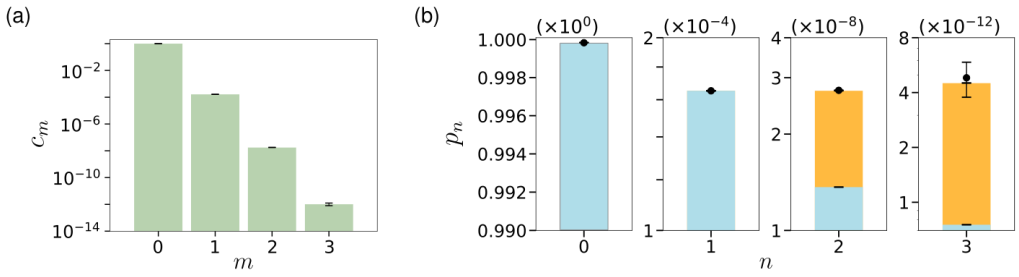

Figure 3.22: Experimental results of (a) measured click statistics and (b) retrieved photon statistics. The estimated photon statistics (black points) with the yellow and blue bars corresponding to the theoretical photon number distributions for ideal thermal and coherent light fields with the same mean photon number. Error bars correspond to estimated single standard deviations, which are for the first three bars ($n = 0, 1, 2$) smaller than the data point.

The estimated photon statistics corresponds to the ideal single-mode thermal light within statistical measurement errors (see Figure 3.22), which certifies the unambiguous preparation of the ideal thermal light statistics. To illustrate the significance of an ideal thermal statistics generation at such a low mean photon number of $\langle n \rangle = 1.64(1) \times 10^{-4}$, we compared our results with the ideal coherent state with same mean photon number (Figure 3.22(b)). The accuracy of the retrieval process is demonstrated by $F = 0.9999999999998(1)$ and $\Delta = 9(5) \times 10^{-11}$. We also evaluated several parameters related to the photon statistics, see Table 3.2. The presented data are in a good agreement with the theoretically expected values. To characterize the quality of observed Bose–Einstein stat-

	Q_b	Q_M	$g^2(0)$	S
data	$1.089(4) \times 10^{-4}$	$1.64(1) \times 10^{-4}$	2.00(1)	$1.81175(4) \times 10^{-3}$
model	1.101×10^{-4}	1.64×10^{-4}	2.00	1.81175×10^{-3}

Table 3.2: Characteristics of measured photon statistics. Shown are: binomial parameter, Mandel parameter, $g^2(0)$, and Shannon entropy. The uncertainties of the evaluated parameters have been estimated using the Monte Carlo routine from the uncertainties of the measured numbers of photon clicks. The results suggests the almost ideal thermal light generation.

istics, we employ the fundamental definition of the thermal light: it is light with maximum Shannon entropy $S = -\sum_{n=0}^{\infty} p_n \log p_n$, see Table 3.2. The actual distance between the ideal Bose–Einstein distribution and the measured one can be quantified by evaluation of the relative entropy. The relative Shannon entropy (Kullback-Leibler divergence) between the measured statistics and the reference probabilistic distribution is defined as $S(p_n|p_n^{ref}) = \sum_{n=0}^{\infty} p_n \ln p_n - \sum_{n=0}^{\infty} p_n \ln p_n^{ref}$. The evaluated relative Shannon entropies for the measured statistics with respect to ideal thermal and coherent state with the same mean photon numbers are $S(p_n|p_n^{th}) = 2(2) \times 10^{-14}$ and $S(p_n|p_n^{coh}) = 516(1) \times 10^{-11}$. Our results certify the relative thermodynamical closeness of the generated state to the ideal thermal state compared to a coherent state with the same energy.

3.5.3 Multi-photon states of light

Furthermore, we generate multi-photon states by mixing N_p single-photon states incoherently, using the process of continuous-wave spontaneous parametric down-conversion in a PPKTP crystal and time multiplexing. We took N_p successive time windows, when a single photon was heralded, and joined them into a single temporal detection mode. The resulting photon statistics measured for these highly-nonclassical multi-photon states corresponds extremely well with the ideal attenuated N_p-photon states up to $N_p = 9$. The measured mean photon number is lower than the number of superimposed photons due to non-unity efficiency of the source, $\eta_{\text{source}} = 55\%$, which is contributed the efficiency of the heralding detector (65%), single-mode-fiber collection efficiency (90%), and spectral filter transmission and other inefficiencies (94%).

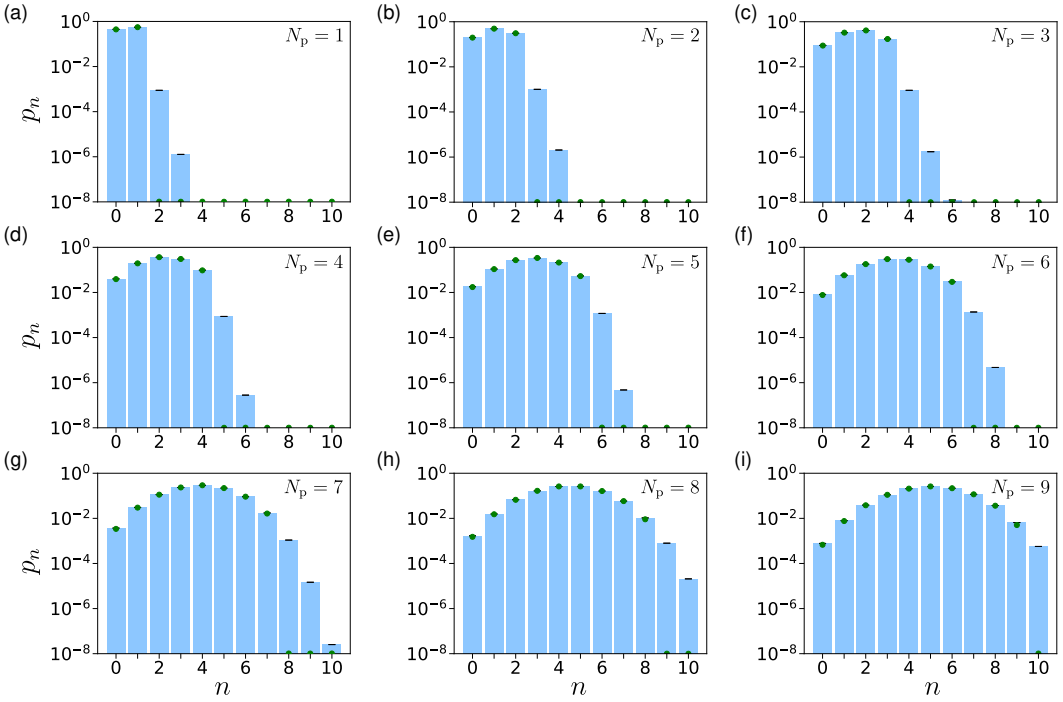

Figure 3.23: Experimental results of detection of photon statistics. Shown are the retrieved (blue bars) and corresponding theoretical photon statistics (green dots) of N_p-photon clusters: (a) $N_p = 1$, (b) $N_p = 2$, (c) $N_p = 3$, (d) $N_p = 4$, (e) $N_p = 5$, (f) $N_p = 6$, (g) $N_p = 7$, (h) $N_p = 8$, (i) $N_p = 9$.

We have performed approximately 3×10^5 measurement runs to build a click statistics for classical photon states. The measurement uncertainty has been evaluated by repeating the full acquisition ten times. For non-classical multi-photon states, we have performed the single acquisition with 10^{11} measurement runs and use Monte Carlo simulation for uncertainty evaluation. Monte Carlo method has also been used to quantify the statistical errors of retrieved photon statistics (Figure 3.23), fidelities(Figure 3.24(a)), and other parameters of interest (Figure 3.25).

One might conclude from the N_p–$g^{(2)}$ diagram shown in Figure 3.25 that non-classicality of the multi-photon state is reduced with the increasing number of photons superimposed. Photon statistics of these states are very close to a binomial distribution for all N_p and so they are strongly non-classical and non-Gaussian, as displayed by the Mandel Q_M parameter (Figure 3.25) or other advanced criteria [C1, 158, 229]. The normalized second-order correlation is completely loss in-

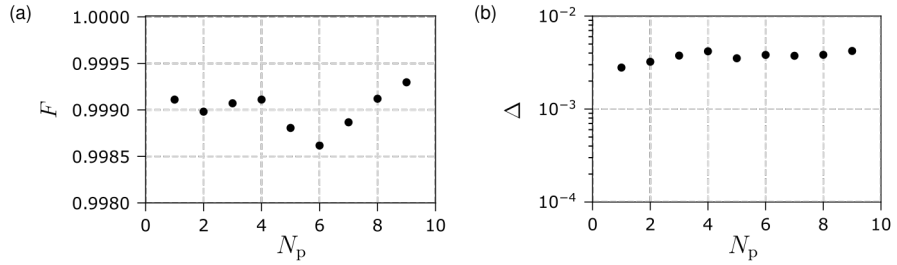

Figure 3.24: The discrepancy between the measured and the corresponding ideal photon statistics characterized by (a) fidelity F, and (b) the total variation distance Δ.

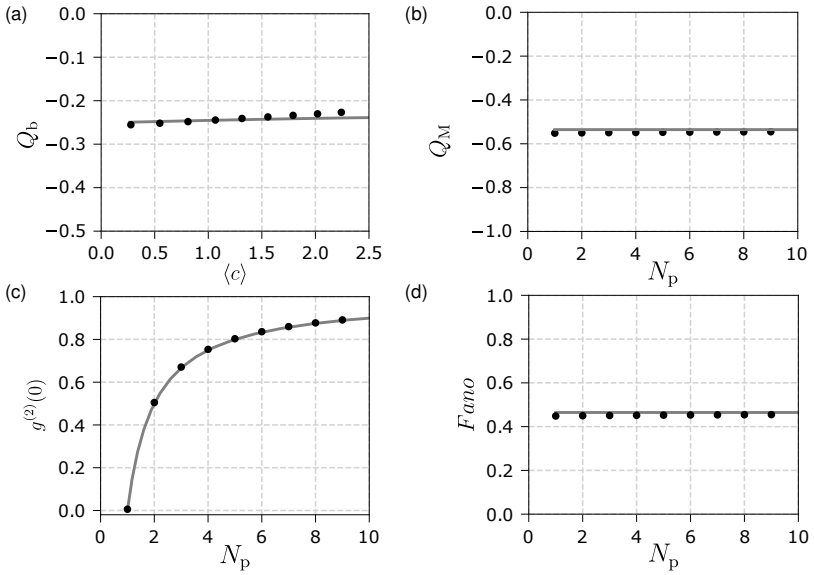

Figure 3.25: Characteristics of measured photon statistics: (a) the binomial parameter, (b) the Mandel parameter, (c) $g^2(0)$ function, and (d) Fano factor. Solid lines represent theoretical model (Equation (2.31)).

dependent while the Mandel Q_M parameter changes with the applied losses. As an example, the multi-photon states emitted by clusters of single-photon emitters would ideally display $Q_M = -1$, however, the real sources with limited collection efficiency show the value closer to zero. In our case of the emission emulated by merging of several heralded photons from parametric down-conversion process, the measured value $Q_M = -0.548(2)$ is given by the heralding efficiency of the source.

The retrieved photon statistics allows evaluating the Wigner function (see Section 2.1). In Figure 3.26 the Wigner function $W(x, 0)$ of single-photon state is depicted. To certify nonclassical character of this states, we also evaluated the value of the Wigner function in the region of $x = 0$, $p = 0$. We obtained the negative reaching $W_{N_p}(0, 0) = -0.033682(1)$. Having the full photon statistics retrieved, we can also apply quantum non-Gaussian tests based on state properties in phase space [304, 337, 390, 391]. We proved quantum non-Gaussian character of the measured multi-photon states up to nine photons [C1] applying recently devised click-based quantum non-Gaussianity criteria [389].

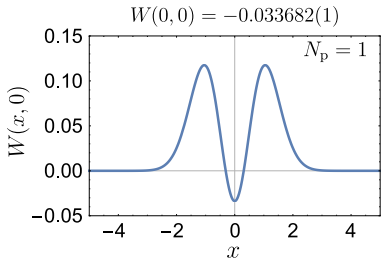

Figure 3.26: Wigner function $W(x,0)$ calculated from the retrieved photon statistics of $N_\mathrm{p} = 1$.

3.5.4 Summary of experimental results

To demonstrate the accuracy and wide applicability of the PNRD, we plotted $g^{(2)}$ parameter computed from the measured photon statistics and from the corresponding ideal statistics for 75 various optical signals (Figure 3.27(a)). Mean numbers of photons cover values up to 30 and faithful autocorrelation measurements range from $g^{(2)} = 6 \times 10^{-3}$ to 2. We demonstrate a similar characterization utilizing the Mandel Q_M parameter (Figure 3.27(b)). We can see the exceptionally accurate experimental characterization of the deviation from Poissonian statistics with the Mandel Q_M parameter ranging from -0.55 to 9 and the mean photon number exceeding 29.6(2). Furthermore, we show all the mentioned moments, non-classicality parameters, and Wigner-function-negativity characteristics for five selected photonic signals, see Table 3.3.

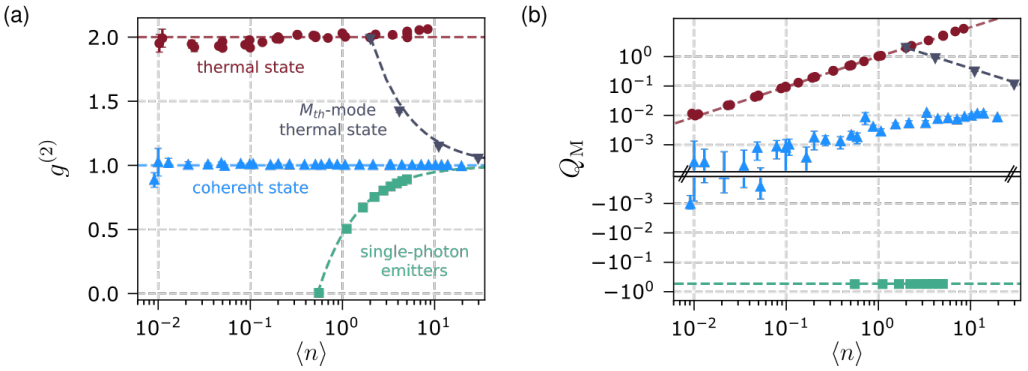

Figure 3.27: Characteristics of measured photon statistics for selected states. (a) The autocorrelation $g^{(2)}$ evaluated from the measured photon statistics (solid marker) and the corresponding ideal statistics (empty marker) of various optical signals with mean photon number $\langle n \rangle$. Shown are: coherent states with $g^{(2)} = 1$ (blue triangle up), thermal states (also termed chaotic light) with $g^{(2)} = 2$ (red circle), and M_th-mode thermal states with $M_\mathrm{th} = 1.01(1), 1.95(3), 5.19(2), 13.9(2)$ (violet triangle down). The cases of $M_\mathrm{th} = 1.01(1)$ coincide with thermal state. Furthermore, the emission from a cluster of N_p single-photon emitters is shown for $N_p = 1 \ldots 9$ with $g^{(2)} = 1 - 1/N_p$ (green square). (b) The Mandel Q_M parameter evaluated from the measured photon statistics of the same optical signals with the same marker/color coding. Coherent states are compatible with Poisson statistics $Q_\mathrm{M} = 0$, thermal states show super-Poissonian statistics with $Q_\mathrm{M} = \langle n \rangle$, multi-mode thermal states converges to Poisson distribution with increased number of modes. Highly nonclassical N_p-photon states reach $Q_\mathrm{M} = -0.55$ given by the limited efficiency of the single-photon source employed for their generation. The error bars are typically smaller than the symbol size.

Let me briefly summarize individual photon statistics measurements which were done. The

coherent state was prepared by using a gain-switched laser diode at 810 nm. The initial coherent pulses measured by the PNRD show almost perfect Poissonian statistics with $\overline{g}^{(2)} = 1.001(4)$ up to $\langle n \rangle = 19.56(2)$ with average fidelity $\overline{F} = 0.9997(1)$ and total variation distance $\overline{\Delta} = 3.1(3) \times 10^{-3}$. The thermal state was generated by temporal intensity modulation of the initial coherent light by a rotating ground glass. The scattered light is collected using a single-mode optical fiber. We measured almost ideal Bose-Einstein photon statistics depicted in Figure 3.16 with $\overline{g}^{(2)} = 2.00(1)$ up to $\langle n \rangle = 8.41(1)$, $\langle \Delta n^2 \rangle = 83.5(3)$ with $\overline{F} = 0.9998(1)$ and $\overline{\Delta} = 5.1(2) \times 10^{-3}$. We also analyzed light close-to-ideal thermal statistical properties generated in warm vapor. This quantum states, with smallest mean photon number we have measured so far $\langle n \rangle = 1.64(1) \times 10^{-4}$, achieved the best fidelity $F = 0.9999999999998(1)$ and total variation distance $\Delta = 9(5) \times 10^{-11}$. Additionally, we varied the number of the collected thermal modes, which yielded a signal governed by Mandel-Rice statistics, going from Bose-Einstein to Poisson distribution as the number of modes increased. We have managed to prepare and subsequently characterize thermal states with the number of modes from 1 up to 14. Furthermore, we generated multi-photon states by mixing incoherently several single-photon states from spontaneous parametric down-conversion using time multiplexing. N_p successive time windows, where a single photon was heralded, were merged into a single temporal detection mode. This source emulates the collective emission from identical independent single emitters [C1, 96, 250]. The resulting photon statistics measured for these highly nonclassical multi-photon states corresponds extremely well to the ideal attenuated N_p-photon states: for $N_p = 1$ and 9 with $\overline{F} = 0.9990(2)$ and $\overline{\Delta} = 3.7(4) \times 10^{-3}$. Also the $g^{(2)}$ parameter computed from the measured photon statistics perfectly agrees with the theoretical model $1 - 1/N_p$, see Figure 3.27(a).

	coherent		thermal		single photon		9-photon cluster	
	data	model	data	model	data	model	data	model
$\langle n \rangle$	4.95(2)	4.95	4.93(4)	4.93	0.554675(2)	0.55	5.00786(2)	4.95
$\langle (\Delta n)^2 \rangle$	4.99(5)	4.95	29.4(5)	29.24	0.2487836(3)	0.2475	2.27821(7)	2.2275
$g^{(2)}$	1.002(3)	1.0	2.01(1)	2.00	0.0057627(9)	0	0.891156(3)	0.8889
Q	0.01(1)	0.0	4.97(7)	4.93	-0.551478(2)	-0.55	-0.54507(1)	-0.55
$\langle P \rangle$	-0.003(8)	5×10^{-22}	0.089(7)	0.092	-0.105814(4)	-0.1	-	-
$W(0,0)$	-0.001(3)	2×10^{-22}	0.028(2)	0.029	-0.033682(1)	-0.03184	-	-

Table 3.3: Characteristics of measured photon statistics for selected states: coherent state, thermal state, 1-photon state, and 9-photon mixture. Standard deviations are evaluated by repeating ten times the whole process of the PNRD measurement, photon statistics retrieval, and characteristics evaluation. The amount of data acquired for single-emitter clusters were several orders of magnitude larger that for other states, which yields the corresponding error bars much smaller.

We utilize fidelity and total variation distance to compare the measured distribution with the ideal one. The worst and the best fidelities $F = 0.992$ and 0.9999 are reached across all the tested sources with average fidelity being $\overline{F} = 0.9996(3)$. The average distance is $\overline{\Delta} = 4.0(1) \times 10^{-3}$ for all the tested sources. For detailed data and comparison to plain EM, see Table 3.4. For a further detailed discussion of analysis of photon statistics retrieval methods, see Section 3.4. The errors of EME are caused by slight imbalances of splitting ratios in the PNRD, variations in PNRD efficiency η, and imperfections of the tested sources, which renders the actual accuracy of the PNRD even higher. Particularly, accurate preparation and characterization of thermal and super-chaotic states are highly nontrivial tasks subject to further research [C2, 108, 296].

	coherent		thermal		single photon		9-photon cluster	
	EM	EME	EM	EME	EM	EME	EM	EME
F	0.6(1)	0.9984(9)	0.69(2)	0.9978(5)	0.99394(2)	0.99912(1)	0.5467(2)	0.99930(2)
Δ	0.50(9)	0.002(9)	0.35(1)	0.033(3)	0.07424(1)	0.00088(1)	0.1752(5)	0.00407(1)

Table 3.4: The comparison of EM and EME results for the measured data. Coherent state $\langle n \rangle = 4.95(2)$, thermal state $\langle n \rangle = 4.93(4)$, single photon state $N_p = 1$, and 9-photon cluster $N_p = 9$. Both fidelity F and total variation distance Δ are shown. Standard deviations are evaluated by repeating the measurement and data processing ten times. The large distances observed for EM stem from overfitting the ill-posed problem. This is discussed in Section 3.4.

3.5.5 Discussion

A prominent feature of our detection of the photon statistics approach is its unprecedented accuracy. The detector measures photon statistics up to 30 photons with an average fidelity of 0.9993(3). We successfully detected dozens of various photonic sources ranging from highly non-classical quantum states of light to chaotic optical signals: chaotic, classical, nonclassical, non-Gaussian, and negative-Wigner-function light, such as photon-number states containing a single photon or a cluster of single photons. The results were obtained from raw data with no other processing than EME, and without any demanding detector characterization. Despite uncorrected systematic errors and significant variability of the input signal, our approach shows superior fidelity across the board with typical values exceeding 99.9% for mean photon numbers up to 29.6(2) and the $g^{(2)}$ parameter reaching down to a fraction of a percent. A specific issue that needs to be addressed is that the presented measurements have been performed with PNRD detector not optimized for detection efficiency. The overall system efficiency is estimated to be 49(1)%. The efficiency parameter η incorporated in photon statistics retrieval is chosen to be 0.5 to assure that the efficiency of the PNRD model is the same or higher than of the actual PNRD detector used. The same value of the efficiency is used throughout this Thesis for all the performed photon statistics retrievals (for all tested sources).

3.6 Summary and outlook

To conclude, we have reported a fully reconfigurable near-ideal photon-number-resolving detection scheme with custom electronic processing and EME photon statistics retrieval method. The PNRD design is free of systematic errors such as the channel crosstalk and temporal correlations, which are either negligible or can be arbitrarily decreased by the user. We have demonstrated exceptional accuracy of detected photon statistics that goes beyond the conventional limit of the number of PNRD channels. The presented approach to process data from photon-number-resolving detectors based on optical networks significantly improved the precision of the photon statistics measurement. It breaks the finite-multiplexing limit and achieves unprecedented accuracy of photon-number resolution demonstrated for various photonic signals, including highly non-classical states, which surpasses even bleeding-edge cryogenic detectors. The result opens new paths for optical technologies by providing access to the photon-number information without the necessity of detector tomography. There are, however, open questions regarding the scalability of the approach.

We introduced two different techniques to count and store the multi-coincidence events, a typical output from the complex multi-channel detection scheme. Developed digital coincidence unit based on ECL circuitry is high-performace counting device recording histograms of coincidence events with full channel resolution. However, used MCU limits the data processing sequence to

400 ns, approximately. In the future, using FPGA instead of MCU promisses improvement in the speed of processing of a large datasets by order of magnitude to tens of picoseconds.

Though having been demonstrated with common single-photon avalanche diodes, the reported measurement workflow is independent of the detection technology and can accommodate any on-off detectors. Furthermore, the multi-channel scheme allows for straightforward on-chip integration. Therefore, further improvements in speed, efficiency and compactness can be expected using superconducting single-photon detectors [49, 63, 69] coupled with waveguide technology [115, 118, 120, 197]. The discrete optical network employed in the reported PNRD features full reconfigurability and continuous tunability of splitting ratios, but extends over dozens square decimeters and limits the overall efficiency of the PNRD. There are other ways of producing multiple beams of uniform intensity: diffraction gratings (diffractive beam splitter) [482, 483], multiple-beam plate splitters [484], and $M \times M$ fiber splitters and fan-outs. These solutions possess limited efficiency and no tunability and reconfigurability. On-chip integration offers a significant reduction in size [118], however, the limited transmittance of a waveguide network and input/output coupling losses represent an issue. The tunability can be reached using interferometer networks with adjustable phase shifters [80, 451, 485, 486].

Building on the achieved results, we will work on future improvements to the used photon statistics retrieval method. The precision of the photon statistics retrieval can be further increased by optimizing over multiple parameters, such as the strength of regularization parameter λ, or iteration cut-off. Eventually, Δ becomes limited by machine precision and computation time. To further improve reconstruction accuracy and convergence speed, the analysis of the complex interaction of these parameters will be the subject of further research. Alternatively, the machine learning methods can cope with randomness of the detector and incomplete data, and bring a significant degree of robustness against perturbations and noise. Several metrology tasks mentioned so far have been boosted by methods of machine learning. Artificial neural networks were exploited for quantum state tomography by approximating the state wavefunction by a restricted Boltzmann machine [487–489] and for correcting systematic experimental errors during the reconstruction [490]. Classification and feature extraction from experimental data can also benefit from machine learning techniques, e.g. deep neural networks for entanglement witnessing [491] and an adaptive linear element neuron for identification of light sources based on their statistics [492].

Chapter 4

Controlled modification of statistical properties of light

The Chapter 4 presents the controlled modification of the statistical properties of light employing the developed photon statistics detection technique (Chapter 3). The knowledge of the exact number of photons in an incident light enables complex triggering and more efficient multi-photon subtraction and addition, which are essential techniques for manipulating states of light (Section 1.3, and Subsection 2.3.3). First, a conditional subtraction of multiple photons from the single-mode thermal state of light using a beam splitter with high transmission is proposed and experimentally demonstrated (Section 4.2). Later, achieved results give rise to the development of a scheme for the deterministic preparation of states with super-Poissonian statistics (Section 4.3). We conceived the idea of the multiport photonic SWAP gate involving classical feedforward swapping of the input modes. Multiport optical switchable coupler based on Mach-Zehnder interferometer [34] served for a fast swapping between high-fidelity single-mode thermal state and l-photon subtracted thermal states whenever a successful subtraction occurs. To demonstrate its high functionality, numerical predictions for many modes and subtractions were performed. In the first step, we experimentally verified one mode scenario with single-photon subtraction. These two advanced light manipulation approaches are qualified as a useful source for generating these out-of-equilibrium states employed in experiments with many applications in quantum information and thermodynamics [31, 162, 298, 318, 361, 493, 494]. Here, we experimentally demonstrated the relevance of multi-photon subtracted thermal states to perform work and carry information (Subsection 4.2.3). Additionally, states with super-Poissonian statistics can serve for successful information-to-energy conversion (Subsection 4.3.3).

Chapter 4 is based on the following publications:
[A1] J. Hloušek, M. Ježek, and R. Filip, '*Work and information from thermal states after subtraction of energy quanta*', Scientific Reports **7**, 13046 (2017).
[P2] J. Hloušek, T. Denzler, V. Švarc, M. Ježek, Eric Lutz, and R. Filip, '*Experimental Quantum Photonic Maxwell Demon*', Submitted (2022).

4.1 Introduction

Modern quantum applications frequently rely on controlling physical systems by conditionally adding or subtracting photons. These experimental techniques have been extensively applied to preparing unique photon added/subtracted quantum states [29, 31, 162, 298, 319–322], distilling entangled quantum states [325–327], transforming classical states to non-classical ones [27, 323], etc. Here, we mainly focus on the photon subtraction procedure employed in the generation process of the quantum states of light out of thermal equilibrium. This procedure applied to classical states has been used for quantum filtering [328], state preparation [31], noiseless amplification [329], quantum cloning [332], enhanced interferometry [495, 496] and recently, also to illustrate Maxwell demon in quantum thermodynamics [361, 497].

In quantum optics, such photodetection processes continuous in time were first discovered to conditionally manipulate the statistics and also increase the energy of thermal light [378, 379, 498, 499]. A weak dissipation of thermal energy of light to cold reservoir modes allows us to conditionally subtract individual quanta of that thermal energy by measuring the reservoir modes by quantum detectors. The subtraction procedure uses a basic dissipation mechanism with no other energy supply and can be successfully performed even under imperfect conditions and by using inefficient photodetectors. Over two decades, the continuous-time nonclassical state manipulations were extensively experimentally developed in cavity quantum electrodynamics [500, 501]. During the same period, the series of multi-photon subtraction experiments with thermal light also demonstrated a conditional instantaneous increase of mean energy by subtraction of quanta from single-mode thermal state [28, 161, 162]. Also, different measures have been applied to quantify the effect of these subtraction procedures [298, 309–311].

Quantum optics has proven to be a suitable experimental platform for proof-of-principle tests of many quantum physics processes, heavily stimulating other experimental platforms and advancing novel quantum technologies. Matter and radiation out of thermal equilibrium with an environment are significant resources of modern physics, information science, and technology. Thermal state of a cooled system is not in thermal equilibrium with its environment and can be used to perform work [B21] and carry information [502]. Preparation of the cooled state requires only a connection to a cold external reservoir where a large part of energy dissipates and, simultaneously, entropy gradually decreases. Similarly, by thermal heating from an external stochastic hot reservoir, we can enlarge mean energy, but also the entropy. A high-energy out-of-equilibrium state can also be prepared by external deterministic force [B17] applied to a thermal state. Such coherent driving renders the entropy lower than of the initial thermal state. It is the best classical way for the preparation of states capable of transmitting more information [502] and producing more work [503–508]. Alternatively, mechanisms that do not require either external heating or driving allow us to test non-equilibrium quantum thermodynamics merging with information theory [509, 510], also at currently unexplored experimental platforms.

In addition, energy may be extracted from information by an external controller in a Maxwell demon setting. The experimental realizations of such information-to-energy conversion in a quantum photonic setup made of two thermal light beams were performed [361, 497]. Feedforward operation related to successful subtraction on one mode leads to a difference in average energy between these two modes. This imbalance can be used to charge the capacitor by employing photodiodes [361]. In contrast, the work [497] discusses the implementation of a photonics Maxwell demon acting on thermal states with low mean photon number. These papers demonstrate the great potential of photonic experiments in proof-of-principle tests of thermodynamic concepts.

4.2 Thermal states after subtraction of energy quanta

Here, we propose and experimentally demonstrate an advanced approach, conditionally preparing more efficient multi-photon subtracted single-mode thermal states only by a weak dissipation, an inefficient quantum measurement of the dissipated thermal energy, and subsequent triggering of that states. We verify that the instantaneous subtraction of a number of quanta (photons) from a thermal state produces out-of-equilibrium states of light with increased average energy. Still, simultaneously it keeps the Fano factor constant [339]. It means that average energy increases hand-in-hand with its variance. Photons-subtracted thermal states represent a paramount example of out-of-equilibrium states that can be obtained without an external coherent deterministic drive or an additional thermal source of energy. These states can be employed as a useful source for various future experiments in currently joining fields of information theory and nonequilibrium quantum thermodynamics. We predict and demonstrate that such out-of-equilibrium states can provide work and carry information larger than what is available by any dissipative cooling mechanism.

To experimentally produce and analyze the out-of-equilibrium state, we follow a stream of optical experiments [28, 31, 161, 162, 328, 329, 332, 496]. The experimental scheme of photon subtraction is described in Section 2.3.3. To fully describe the performed l-photon subtraction, a detailed model has been developed Eq.(2.29). It takes into account actual experimental properties of the set-up: the beam-splitter reflectivity R, the number M of on-off detectors at the reflected port, and their detection efficiency. In the limit of $R \to 0$, the full numerical model is equivalent to an application of l-th power of annihilation operator to the input thermal state, which produces the ideal statistics Eq.(2.25). The numerical model has been used to evaluate all the parameters discussed.

4.2.1 Experimental setup

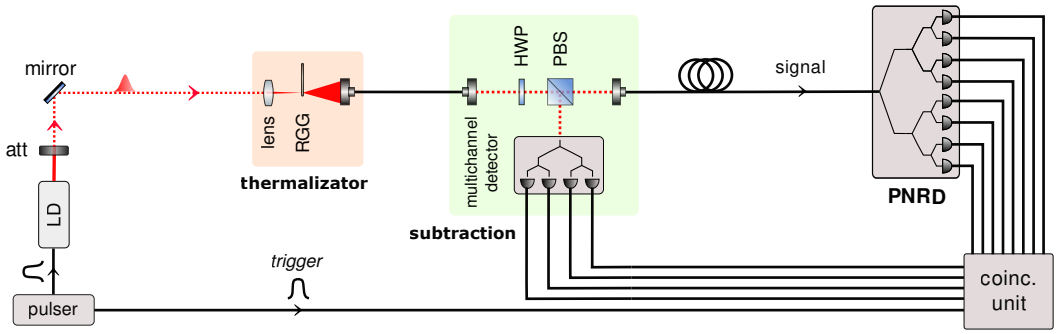

Figure 4.1: Preparation and characterization of l-photon subtracted single-mode thermal states. The subtraction of l-photon from the thermal state is implemented using a beam splitter with a tunable reflectivity R. The reflected port is detected by a multichannel detector formed by M on-off detectors. Coincidence detection events, when all the M detectors fire, trigger the output and verification stage consisting of a photon-number-resolving detector.

In our experiment (Figure 4.1), a single-mode thermal state with Bose-Einstein statistics determined only by the mean number n_{th} of energy quanta was generated employing a nanosecond pulsed laser diode (805 nm) in a gain switching regime with a repetition rate of 4 MHz modulated by RGG technique described in detail in Section 2.3.2. The Glauber second-order correlation function of the

generated pseudo-thermal state was evaluated, $g^2(0) = 2.00(3)$, to verify the high quality of the preparation stage.

Multi-photon subtraction is implemented by splitting the thermal state at a beam splitter, composed of a half-wave plate, followed by a polarizing beam splitter, with a reflectivity $R = 5\%$. In the first port, the reflected photons were detected via a reconfigurable multi-channel detector with M commercial on-off single-photon detectors. The maximum number of detectors was set to $M = 4$. To measure click statistics of the transmitted pulses, we used a photon-number-resolving detector (Section 3.2). For this concrete measurement, PNRD was modified to a balanced eight-channel port with eight single-photon avalanche photodiodes. When a reconfigurable multi-channel detector detects a (multi)coincidence in the reflected port, the heralded optical signal in the transmitted port is analyzed by the PNRD. The resulting coincidence statistics was acquired by the PNRD under the condition that exactly l detection events occurred at the reflected port. We have applied EME method (Section 2.6.3) to reconstruct resulting photon statistics from the multi-coincidence measurement.

The coincidence rates increase with increasing mean photon number of the initial thermal state. However, it is crucial to set the mean photon number low enough to measure a coincidence statistics of l-photon subtracted thermal state within the range of the PNRD. Mean photon number n_{th} of the l-photon subtracted thermal state increases with l by factor $(l+1)n_{\mathrm{th}}$. Taking into account the number of channels of the PNRD and its efficiency, we can safely set $n_{\mathrm{th}} = 2.05(1)$ for the maximum number of subtracted photons $l \leq 3$. At the same time, the selected mean photon number is high enough to keep the measurement time reasonably short.

4.2.2 Results

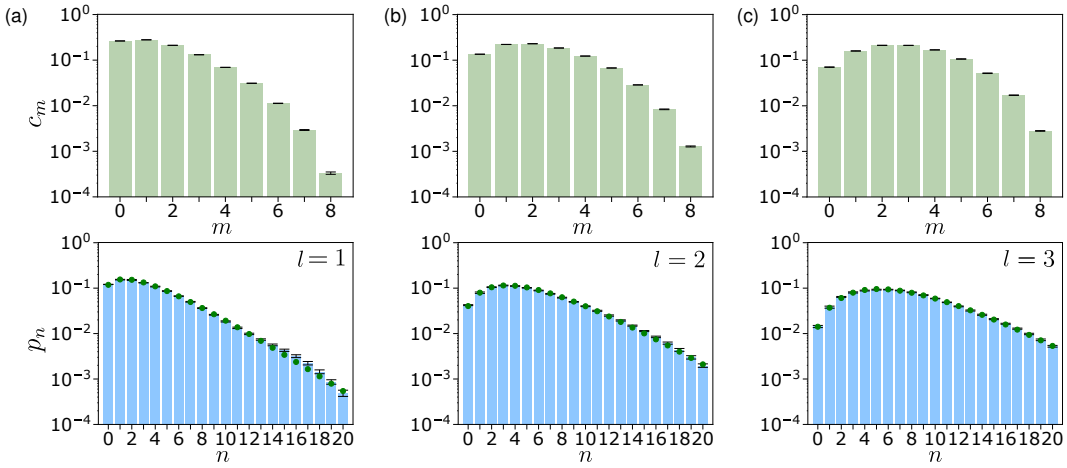

Figure 4.2: Experimental results of detection of photon statistics. Shown are the measured click statistics (green bars), retrieved (blue bars), and the corresponding theoretical photon statistics (green dots) of l-photon subtracted state for several numbers of subtracted photons l: (a) $l = 1$, (b) $l = 2$, and (c) $l = 3$. All distributions are plotted on a logarithmic scale.

In our present experiment, we have certified several essential parameters of the prepared l-photon subtracted thermal light governed by the statistics Eq.(2.29) to assess its performance. Figure 4.2 shows measured click statistics and retrieved photon statistics of l-photon subtracted states for several number of subtracted photons l: (a) $l = 1$, (b) $l = 2$, and (c) $l = 3$. The similarity of the

experimentally reconstructed photon number distribution with a theoretical distribution is quantified by fidelity and total variation distance (Figure 4.3). All photon number distributions exceed $F > 0.996$ and $\Delta > 10^{-2}$. In a similar manner, we evaluate the binomial parameter Q_b and the Mandel parameter Q_M (Figure 4.4). As we might expect, all measured states exhibit super-Poissonian statistics with $Q_\mathrm{b} > 0$ and $Q_\mathrm{M} > 0$.

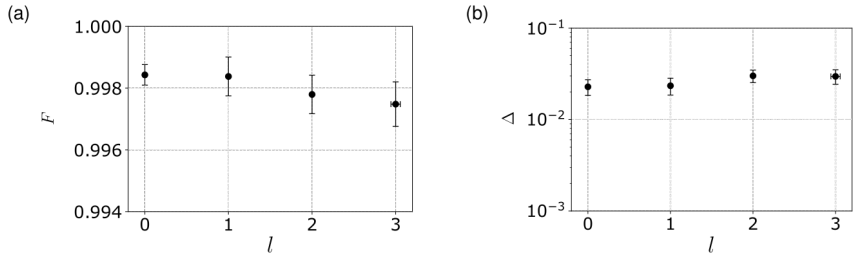

Figure 4.3: The discrepancy between the measured and the corresponding ideal photon statistics characterized by (a) fidelity F, and (b) the total variation distance Δ.

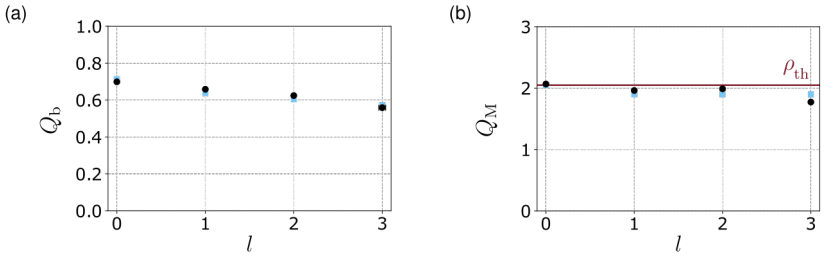

Figure 4.4: Characteristics of measured click and photon statistics: (a) the binomial parameter and (b) the Mandel parameter. Blue squares stand for theoretical model 2.29. Red line corresponds to input thermal state ρ_th with the mean photon number $n_\mathrm{th} = 2.05(1)$.

As has been already discussed (Section 2.3.3), the photon statistics of l-photon subtracted single mode thermal states yields a linearly increasing mean number of quanta, $\langle n\rangle = (l+1)n_\mathrm{th}$, where l in a number of conditional detection events. The monotonous increase is shown in Figure 4.5(a) for $n_\mathrm{th} = 2.05(1)$ set in our measurement. The second-order correlation function $g^2(0) = \frac{\langle a^{\dagger 2}a^2\rangle}{\langle a^\dagger a\rangle^2} = 1+\frac{1}{1+l}$ for Eq.(2.25) converges to unity, irrespectively to n_th. It is depicted in Figure 4.5(b). However, Fano factor $Fano = \langle(\Delta n)^2\rangle/\langle n\rangle = 1+n_\mathrm{th}$ is independent on l and it approaches unity only for very small $n_\mathrm{th} \ll 1$. To reach higher $\langle n\rangle$, l needs to be higher too, which is increasingly more challenging. Let us note that these results correspond to an instantaneous limit $p_l t \to 0$ of the continuous photodetection process, where p_l is the success probability of l-photon subtraction [379]. For $n_\mathrm{th} = 2.05(1)$, we experimentally demonstrate in Figure 4.5(c) that the conditional multi-photon subtracted thermal states indeed remain super-Poissonian. However, $g^{(2)}(0)$ is substantially reduced below 2, which holds for thermal light. Figures. 4.5(a,b,c) also show that the measured statistics and derived characteristics agree very well with the theoretical model.

Invariance of the Fano factor $Fano = 1+n_\mathrm{th}$ means that the variance $\langle(\Delta n)^2\rangle$ increases simultaneously with the increase of $\langle n\rangle$. However, $\langle(\Delta n)^2\rangle$ does not grow fast enough to render the state (2.25) useless. For example, mean-to-standard-deviation ratio $\mathrm{MDR} = \langle n\rangle/\sqrt{\langle(\Delta n)^2\rangle} = \sqrt{\frac{n_\mathrm{th}}{1+n_\mathrm{th}}}\sqrt{l+1}$ increases monotonously. It means the energy advantageously increases faster than its fluctuations.

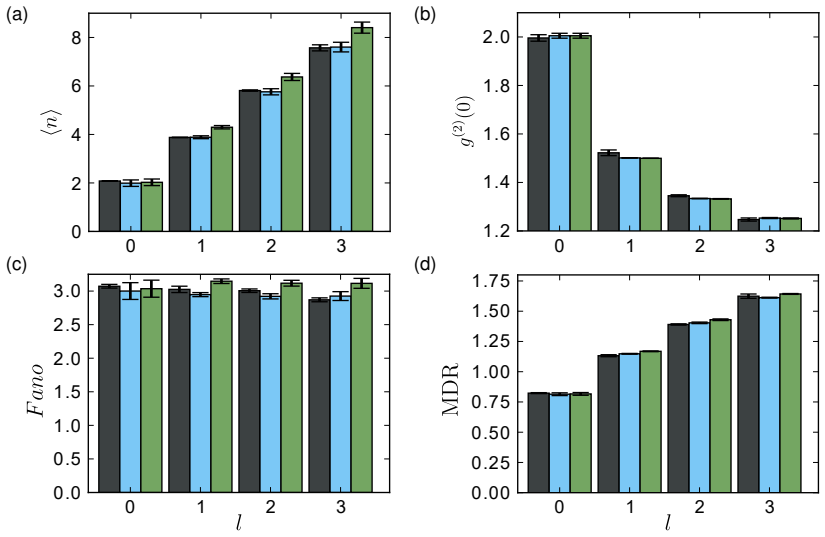

Figure 4.5: Mean number of photons (a), $g^{(2)}(0)$ function (b), Fano factor (c), and MDR (d) of the thermal ($l = 0$) and l-photon subtracted single-mode thermal ($l > 0$) states. l stands for the number of subtracted photons. Experimental results (black), full numerical model (blue), and the simplified model (2.29) (green). Data error bars show the standard deviation of the measurement, error bars of the models represent the uncertainty of input parameters, particularly of the mean number of photons determined from the measured initial thermal statistics.

Moreover, it is already sufficient to use $m = 1$ and $n_{\mathrm{th}} > 1$ to obtain MDR > 1 and the mean $\langle n \rangle$ increases even faster with l for larger n_{th}. Experimental evidence that $\langle n \rangle$ and MDR increase with l is shown in Figures. 4.5(a,d). Entropy slowly increases with the increasing number of subtracted quanta.

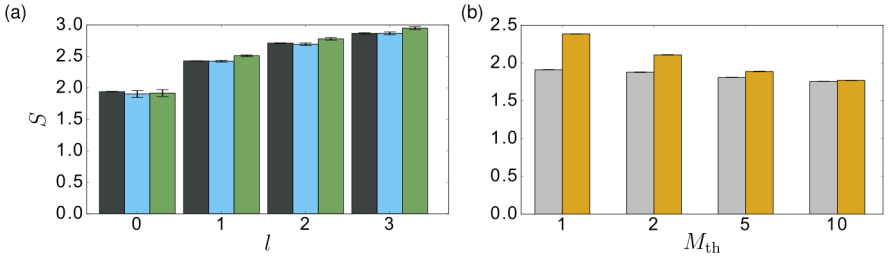

Figure 4.6: (a) Shannon entropy of the conditionally prepared states as a function of subtracted photon number l. Shown are experimental data (dark gray), full numerical model (blue), and the simplified model (green) based on Eq. (2.25). (b) Shannon entropy as a function of a number M_{th} of modes of the initial thermal state. Gray bars stand for the entropy of M_{th}-mode thermal states ($l = 0$) and yellow bars show the entropy of the same states after single-photon subtraction ($l = 1$).

4.2.3 Application

Quantum oscillators prepared out of thermal equilibrium can be used to produce work and transmit information. By intensive cooling of a single oscillator, its thermal energy deterministically

dissipates to a colder environment, and the oscillator substantially reduces its entropy. This out-of-equilibrium state allows us to obtain work and carry information. Although it conditionally subtracts the energy quanta from the oscillator, average energy grows, and the second-order correlation function approaches unity by coherent external driving. On the other hand, the Fano factor remains constant, and the entropy of the subtracted state increases, which raises doubts about a possible application of this approach. To resolve it, we predict and experimentally verify that both available work and transmitted information can be conditionally higher than by arbitrary cooling or adequate thermal heating up to the same average energy.

The generation starts from a single oscillator represented by a single mode of radiation prepared in the state $\rho_{\mathrm{th}} = \sum_{n=0}^{\infty} p_n^{\mathrm{th}} |n\rangle\langle n|$ with thermal Bose-Einstein statistics Eq.(2.23) determined only by the mean number n_{th} of energy quanta, where $|n\rangle$ are energy basis states. In our experiment, thermal light is generated by temporal intensity modulation of a pulsed laser by rotating ground glass (Section 2.3.2). The thermal state instantaneously dissipates a small part of its energy at the unbalanced beam splitter to a multimode reservoir *Res* in vacuum state $|0\rangle_{Res}$. The dissipation only negligibly cools down the thermal mode. Chiefly, it correlates states $|n\rangle$ of the oscillator's mode with a global photon number state $|k\rangle_{Res}$ of the reservoir. It is apparent from the transformation

$$|n\rangle\langle n| \otimes |0\rangle_{Res}\langle 0| \rightarrow \sum_{k=0}^{n} \binom{n}{k} p_s^k (1-p_s)^{n-k} |n-k\rangle\langle n-k| \otimes |k\rangle_{Res}\langle k|, \tag{4.1}$$

where p_s is a survival probability of single quantum in the oscillator. High single quantum survival probability p_s means weak coupling. Product $p_s^k(1-p_s)^{n-k}$ stands for the probability that k quanta will remain in the oscillator and $n-k$ quanta go to the reservoir *Res*.

This entirely classical correlation between the system and reservoir at a level of individual quanta is a useful resource. It arises from the classical (first-order) coherence of single-mode thermal light [B17]. For heavily multimode thermal oscillator (incoherent), the statistics of quanta over all weakly occupied modes approaches Poissonian, and the dissipative process does not produce this correlation. It means we cannot modify statistics by any measurement performed on the reservoir *Res*. The multimode thermal light establishes an incoherent (classical) limit. To realize the importance of first-order coherence for the formation of the out-of-equilibrium state, the subtraction experiment with multimode thermal states is also performed. M_{th} temporal thermal modes with the same overall mean photon number $\langle n\rangle = n_{\mathrm{th}}$ are selected to prepare a multimode state. The effective number of modes M_{th} preparation is described in Section 3.5.2. The partially coherent M_{th}-mode state would produce an interference visibility of $1/M_{\mathrm{th}}$ given by first-order coherence function $g^1(0)$.

Light dissipated to reservoir further scatters to many modes. To detect at least a small fraction of the dissipated light, we select l modes and detect them by single-photon avalanche diodes (SPADs). Only when l-fold coincidence is detected, the resulting optical output of the source is transmitted. The ideal version of this detection can be described by [274]

$$\Pi_l = \binom{N}{l} \sum_{s=l}^{\infty} \sum_{j=0}^{l} \frac{1}{N^s} \binom{l}{j} (-1)^j (l-j)^s |s\rangle_A\langle s|, \tag{4.2}$$

however, a real measurement collects only a small part of overall thermal energy dissipated into the reservoir *Res*. Therefore, we introduce an overall effective collection efficiency η by the transformation $|k\rangle\langle k| \rightarrow \sum_{r=0}^{k} \binom{k}{r} \eta^{k-r} (1-\eta)^r |k-r\rangle\langle k-r|$ of the energy states before the detection. Eqs. (4.1,4.2), together with the collection efficiency η, completely describe the instantaneous multiphoton subtraction process.

For a weak dissipative coupling with sufficiently high single-photon survival probability, $p_s \approx 1$, the out-of-equilibrium statistics approaches the Mandel-Rice statistics Eq.(2.26) by conditioning on l detection events. A potentially small $\eta \ll 1$ reduces the generation rate, but the prepared out-of-equilibrium states are very close to the theoretical limit. Importantly, Eq.(2.26) describes a single-mode light. Its statistics is purely mathematically analogical to the overall statistics of $l+1$-mode thermal light equally populated in all the modes by an average number n_{th} of quanta [B15]. In the case of multimode light, the different $l+1$ modes are principally distinguishable, and the light possesses lower first-order coherence quantified by $g^1(0) = 1/(l+1)$. Also, available energy, work, and information *per mode* are actually $l+1$ times lower, because the distinguishable modes are not used efficiently. Consequently, the single-mode state with the statistics Eq.(2.26) produced by a coherent light source thermodynamically outperforms multimode states with the same statistics and is better suited to our purpose.

The out-of-equilibrium statistics Eq.(2.25) is similar to the statistics of thermal oscillator coherently driven out of thermal equilibrium with mean $\langle n \rangle_c = n_{\mathrm{th}} + n_c$ and variance $\langle (\Delta n)^2 \rangle_c = 2n_c n_{\mathrm{th}} + n_c + n_{\mathrm{th}}^2 + n_{\mathrm{th}}$, where n_c is the mean number of coherent quanta caused by the driving. Considering $n_c = g n_{\mathrm{th}}$, where g is ratio between coherent and incoherent energy, we can see that both $\langle n \rangle_c$ and $\mathrm{MDR}_c = \frac{\langle n \rangle_c}{\sqrt{\langle (\Delta n)^2 \rangle_c}}$ monotonously increase with g for any n_{th}, similarly to $\langle n \rangle_{\mathrm{sub}}$ and $\mathrm{MDR}_{\mathrm{sub}}$ using the statistics Eq.(2.25) in the case of l-quanta subtraction. However, to reach $\mathrm{MDR}_c > 1$, $n_{\mathrm{th}} < (n_c - 1) n_c$ is necessary and, therefore, small coherent driving out of equilibrium is not sufficient for large n_{th}. For small $n_{\mathrm{th}} \ll 1$, achievable only by cooling, the mean-to-deviation ratio reaches $\mathrm{MDR}_c \approx \sqrt{n_{\mathrm{th}}(1+g)}$, similarly as for $\mathrm{MDR}_{\mathrm{sub}}$ with l substituted by g. Simultaneously, the second-order correlation function $g_c^{(2)}(0) = 1 + \frac{1}{1+\frac{g^2}{1+2g}}$ also does not depend on n_{th} similarly as for $g_{\mathrm{sub}}^{(2)}(0)$, although it has different dependency on g. Fano factor $F_c = 1 + n_{\mathrm{th}} + n_{\mathrm{th}} \frac{1+2g}{1+g}$ depends on g, whereas F_{sub} is principally independent on l. However, for large g, it also does not converge to $F_c = 1$ and Poissonian statistics. Both statistics converge to the Poissonian limit for small $n_{\mathrm{th}} \ll 1$. Despite (2.25) is not statistics of thermal state coherently driven out of equilibrium, it exhibits similar statistical features without any coherent drive.

Work available from out-of-equilibrium state

We predict and measure work available from the out-of-equilibrium state. Available average work $\langle W \rangle_{\mathrm{yield}}$, which is performed while the system equilibrates with the environment with temperature T, is expressed by relative entropy [511–515]

$$\langle W \rangle_{\mathrm{yield}} = k_B T S\left(, th || p_n^{eq}\right). \tag{4.3}$$

Here k_B is Boltzmann constant and $S(p_n|p_n^{eq}) = \sum_{n=0}^{\infty} p_n \ln p_n - \sum_{n=0}^{\infty} p_n \ln p_n^{eq}$ is relative Shannon entropy (Kullback-Leibler divergence) between the out-of-equilibrium statistics p_n and the distribution p_n^{eq} of a system in the equilibrium with an environment with temperature T [511]. Differently from the previous statistical analysis, which takes into account only the system, $\langle W \rangle_{\mathrm{yield}}$ depends on both the system state and the environment with constant temperature T. The bound (4.3) can be reached; some specific protocols are already developed [506].

The presented out-of-equilibrium state preparation method actually uses two reservoirs, hot one ($T > 0$) and cold auxiliary vacuum reservoir ($T = 0$), see Figure 4.7. However, the cold reservoir cannot be used to provide work Eq.(4.3), without heating some of its modes up using an external source. We can, therefore, consider the hot reservoir at temperature $T > 0$ and cool one mode to its ground state by a strong dissipation. The temperature $T > 0$ of the thermal source is always constant in the experiment; consequently, the available work can be normalized by $k_B T$. By cooling

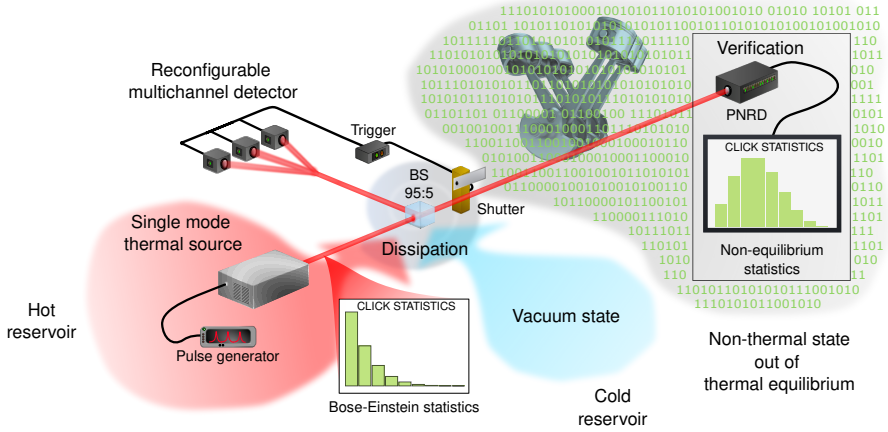

Figure 4.7: Preparation and characterization of out-of-equilibrium states conditionally generated via multiple-photon subtraction from single-mode thermal light. Thermal light governed by Bose-Einstein statistics dissipates at an unbalanced beam splitter (BS) to the vacuum reservoir modes. A small fraction of light in the reservoir modes is detected by a multichannel detector formed by M on-off detectors. Coincidence detection events, when all the M detectors fires, trigger the output and verification stage consisting of a photon-number-resolving detector. Subsequently, data are processed, and photon statistics of the conditionally prepared out-of-equilibrium state is analyzed. The statistics is evaluated for its capability to provide work and carry information.

the oscillator mode to the ground state, normalized work $\frac{\langle W\rangle_{\text{yield}}}{k_BT}|_0 = \ln\left[1+n_{\text{th}}\right]$ sets a benchmark for any useful conditional preparation of out-of-equilibrium state. If $\frac{\langle W\rangle_{\text{yield}}}{k_BT}| > \frac{\langle W\rangle_{\text{yield}}}{k_BT}|_0$, more work can be extracted from the state prepared conditionally by the measurement of a small part of dissipated energy (presented protocol) than by a complete cooling of one of the hot reservoir modes down. The cooling to ground state can be challenging for many systems such as mechanical oscillators and, therefore, the conditional procedure may be preferable to achieve more work.

For the statistics Eq.(2.25), we conditionally obtain the normalized available work

$$\frac{\langle W\rangle_{\text{yield}}}{k_BT} = \frac{1}{(1+n_{\text{th}})^{l+1}}\sum_{n=0}^{\infty}\left(\frac{n_{\text{th}}}{n_{\text{th}}+1}\right)^n \frac{(n+l)!}{n!l!}\ln\left[\frac{1}{(1+n_{\text{th}})^l}\frac{(n+l)!}{n!l!}\right], \tag{4.4}$$

which increases monotonously with l for any $n_{\text{th}} > 0$ without an offset or saturation. We experimentally verified that for $n_{\text{th}} = 2$, see Figure 4.8(a). The entropy also increases with l, as shown in Figure 4.6(a). The amount of extractable work decreases for increasing number M_{th} of modes of the initial thermal state, see Figure 4.8(b). It vanishes completely in the incoherent limit of large M_{th}. It clearly demonstrates that first-order coherence is a resource needed to extract available work using the instantaneous dissipation and photon measurement.

Despite the increase in entropy, the available work obtained by the subtraction procedure overcomes the threshold $\frac{\langle W\rangle_{\text{yield}}}{k_BT}|_0$ given by the complete cooling already for $l = 3$. The experimental results shown in Figure 4.8(a) demonstrate the violation by 5 standard deviations. Moreover, the available work also overcomes a threshold set by a thermal state heated to the same mean number of quanta as reached by the subtraction. The work available by the adequate thermal heating is illustrated by a light gray area of the bars. Heating or cooling to the ground state – heating/cooling strategy – represents a joint benchmark here. All experimental results in Figure 4.8(a) agree with

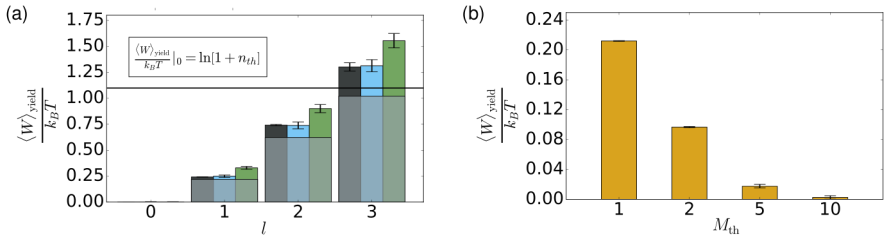

Figure 4.8: (a) The normalized available work as a function of subtracted photon number l. Shown are experimental data (dark gray), full numerical model (blue dots), and the simplified model (green tiles) based on Eq. (2.25). The horizontal threshold (solid black line) corresponds to the work available by a cooling of the oscillator mode to the ground state. Light gray areas represent lower bounds derived for thermal state heated with the same mean number of photons as the corresponding l-photon subtracted states. (b) The normalized available work plotted against a number of modes M_{th} for multimode thermal state after single-photon subtraction ($l = 1$).

the theory predictions. It opens the possibility to test other thermodynamical quantities and processes using the presented experimental photonic approach.

We evaluated the available work Eq.(4.3) that is performed while the oscillator in an initial thermal state $p^{(1)}_{n,\mathrm{th}}$ equilibrates with the environment in thermal state $p^{(2)}_{n,\mathrm{th}}$ with temperature T. The oscillator retains its thermal Bose-Einstein statistics but the mean number of quanta $n^{(1)}_{\mathrm{th}}$ decreases to $n^{(2)}_{\mathrm{th}} < n^{(1)}_{\mathrm{th}}$. For $n^{(2)}_{\mathrm{th}} > 0$, the normalized work reads

$$\frac{\langle W\rangle_{\mathrm{yield}}}{k_B T} = D(p^{(1)}_{n,\mathrm{th}} \| p^{(2)}_{n,\mathrm{th}}) = n^{(1)}_{\mathrm{th}} \ln \frac{n^{(1)}_{\mathrm{th}}}{n^{(2)}_{\mathrm{th}}} + (1 + n^{(1)}_{\mathrm{th}}) \ln \frac{1 + n^{(2)}_{\mathrm{th}}}{1 + n^{(1)}_{\mathrm{th}}}. \tag{4.5}$$

Expression Eq.(4.5) represents the lower bound (light gray areas) in Figure 4.8(a). The mean number difference $\delta n_{\mathrm{th}} = n^{(2)}_{\mathrm{th}} - n^{(1)}_{\mathrm{th}} < 0$ corresponds to cooling of the oscillator, where thermal energy is dissipated to another reservoir at a lower temperature. Positive $\delta n_{\mathrm{th}} > 0$ means that the system has been heated, which requires additional source of thermal energy and therefore this case is not considered here. The value of beam-splitter reflectivity represents a trade-off between the subtraction rate (and, consequently, the total measurement time) and the ability of the generated out-of-equilibrium state to perform work and transfer information. Both these quantities monotonously decrease with increasing reflectivity R (see Figure 4.10 for the three-photon-subtracted state). We can see that the chosen value of the reflectivity, $R = 5\%$, is close to the maximum possible one, which outperforms the tightest bound on the available work and information.

Information carried by out-of-equilibrium state

We complement the measurement of available work by verification that the out-of-equilibrium distribution Eq.(2.25), as a member of a binary alphabet, can carry information better than initial thermal distribution p_n^{th}. Average mutual information given in bits can be determined by the relative entropy

$$\langle I \rangle = D(p_{i,j}^{AB} \| p_i^A p_j^B) \tag{4.6}$$

where indices $i, j = 0, 1$ stand for a single bit at a sender side A and a single bit on a receiver side B, respectively. $p_{i,j}^{AB}$ is a joint (correlated) probability distribution and p_i^A, p_j^B are marginal probability distribution at the sender and receiver sides, respectively. In contrast to the average work Eq.(4.3), average information depends on joint statistics of both communicating parties. Also, it is optimal to use vacuum state of the cold reservoir for encoding of the symbol '0'. The '1' can be encoded using thermal distribution p_n^{th}, which sets a benchmark $\langle I \rangle_0$ for the mutual information, To overcome the thermal bound, we employ the conditional statistics Eq.(2.25) instead to encode the symbol '1'. In this case, the average mutual information reaches $\langle I \rangle = H\left((1-p_0^A)(1-p_E)\right) - (1-p_0^A)H(p_E)$, where $p_E = 1/(1+n_{\text{th}})^{l+1}$ is the probability of error (symbol '1' is identified as '0') and $H(p_E)$ is a binary entropy function. The maximum

$$\langle I \rangle_{\text{yield}} = \max_{p_0^A} \langle I \rangle_l = \log_2\left(1 + (1-p_E) p_E^{p_E/(1-p_E)}\right) \tag{4.7}$$

of mutual information $\langle I \rangle$ over the probability p_0^A at the sender side is monotonously increasing with l for any n_{th}. The experimental result for $n_{\text{th}} = 2$ is shown in Figure 4.9(a). It is not critically sensitive to a number of modes when a multimode thermal state is used instead of the single thermal mode. For the multimode states, the information gain has to be normalized per mode, because more modes can carry more information. It vanishes only gradually, as is presented in Figure 4.9(b). The first-order coherence is a key resource here, same as for the work extraction.

For arbitrary small n_{th} and any $l > 0$, average information $\langle I \rangle_{\text{yield}} \approx (1+l) n_{\text{th}}/(e \ln 2)$ overcomes the benchmark $\langle I \rangle_0$ for any n_{th}. The results of experimental verification for $n_{\text{th}} = 2$ are shown in Figure 4.9(a). Information gain $\langle I \rangle_{\text{yield}}$ approaches its maximum of 1 bit even faster than for a thermal state heated to the equivalent mean number of quanta. We reach more than 0.9 bit already for $l = 3$. Indeed, the conditionally generated state can carry maximum information despite its mixedness.

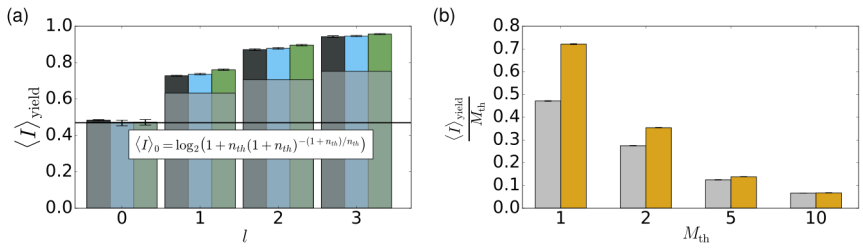

Figure 4.9: (a) The maximum mutual information per mode against a number of subtracted photons l. Dark gray bars stand for experimental results, blue dots stand for full numerical model, and green tiles represent the ideal model based on Eq. (2.25). Light gray areas represent lower bounds derived for thermal state heated with the same mean number of photons as the corresponding l-photon subtracted states. Solid black line represents a threshold of maximum mutual information available when encoding '1' using the initial thermal state. (b) The maximum mutual information per mode as a function of the number of modes M_{th} for multimode thermal state before and after l-photon subtraction. Colors refer to the value of l, gray: l=0, yellow: l=1.

For two thermal distributions $p_{n,\text{th}}^{(1)}$ with mean number of photons $n_{\text{th}}^{(1)}$ (representing bit 1) and

$p^{(0)}_{n,\mathrm{th}}$ with $n^{(0)}_{\mathrm{th}} < n^{(1)}_{\mathrm{th}}$ (representing bit 0), the optimal measurement strategy distinguishes between number of quanta less or equal to $n_{\max}$ (detection of bit 0) and higher than $n_{\max}$ (detection of bit 1). The maximum mutual information Eq.(4.6) over p^A_0 approaches

$$\max_{p^A_0} I = \log_2\left(1 + 2^{\frac{H(p_{01})-H(p_{10})}{1-p_{01}-p_{10}}}\right) - \frac{1-p_{10}}{1-p_{01}-p_{10}}H(p_{01}) + \frac{p_{10}}{1-p_{01}-p_{10}}H(p_{10}), \tag{4.8}$$

where and $H(x) = -x\log_2 x - (1-x)\log_2(1-x)$ is binary entropy function, $p_{01} = 1 - \left(n^{(1)}_{\mathrm{th}}/(1+n^{(1)}_{\mathrm{th}})\right)^{1+n_{\max}}$ is error probability of sending bit 1 and receiving it as bit 0, and $p_{10} = \left(n^{(0)}_{\mathrm{th}}/(1+n^{(0)}_{\mathrm{th}})\right)^{1+n_{\max}}$ is error probability of sending bit 0 and receiving it as bit 1. To minimize the total error probability it is necessary to use two states whose distributions have the smallest possible overlap. For thermal states we can assume $n^{(0)}_{\mathrm{th}} = 0$, which yields $p_{10} = 0$ and $n_{\max} = 0$. The optimal extraction of information is then simply the measurement of zero and non-zero energy. In this case, the maximum mutual information

$$\langle I\rangle_0 = \max_{p^A_0} I = \log_2\left(1 + n^{(1)}_{\mathrm{th}}(1+n^{(1)}_{\mathrm{th}})^{-(1+n^{(1)}_{\mathrm{th}})/n^{(1)}_{\mathrm{th}}}\right) \tag{4.9}$$

monotonously increases with $n^{(1)}_{\mathrm{th}}$, linearly as $n^{(1)}_{\mathrm{th}}/(e\ln 2)$ for small $n^{(1)}_{\mathrm{th}}$, and slowly saturates at 1 bit. The benchmark Eq.(4.9) sets a lower bound on mutual information available by using the vacuum state (bit 0) and a thermal state with the same mean photon number as the prepared l-photon subtracted state (bit 1). This bound is shown in Figure 4.9(a) by light gray areas for individual l. The dependence of the maximum mutual information on a beam splitter reflectivity R is depicted in Figure 4.10(a). Shown are also corresponding benchmarks.

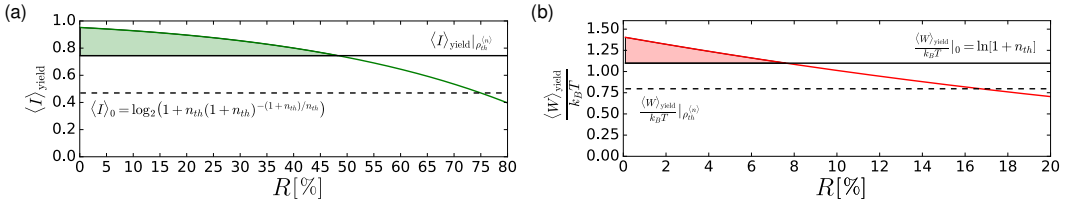

Figure 4.10: (a) The maximum mutual information (solid green curve) and (b) the available work (solid red curve) versus the beam-splitter reflectivity R for three-photon-subtracted thermal state ($l = 3$). Solid black lines and dashed black lines represent the corresponding benchmarks.

4.2.4 Discussion

We have experimentally produced the conditional out-of-equilibrium state Eq.(2.25) from single-mode thermal light by a weak dissipation to a reservoir and an inefficient detection of photons there. We have theoretically and experimentally verified that average work could be extracted from the conditional out-of-equilibrium state, which outperforms any cooling/heating strategy. Furthermore, this state can also be used to carry more average information (closer to one bit) than for any state produced by a cooling/heating strategy, despite entropy increase of the conditional state. The presented procedure does not require any external coherent drive or additional thermal energy. It only uses energy measurement to reach higher work and information rate conditionally. However, it conclusively requires the first-order (classical) coherence of the thermal source. Obtained results

complement the previous experiments demonstrating the applications of the subtraction procedure. The presented method can be translated to other experimental platforms and used for future experiments in currently merging fields of quantum information and quantum thermodynamics. It is also stimulating for current optomechanical experiments at single quanta level [516], where a mechanical oscillator is driven out-of-equilibrium by a weak optical cooling and incoherent photon detection more efficiently than by a complete cooling or adequate heating.

4.3 Deterministic preparation of the super-Poissonian statistics

In the Section 4.3, an experimental approach of deterministic modification of statistical properties of light by incoherent mixing of single-mode thermal state with the l-photon subtracted single-mode thermal state is presented. We combine weak single-photon measurements akin to photon subtraction techniques [A1, 28, 35, 159, 161, 298, 314, 384, 493, 494, 496, 517] on the first beam together with classical feedforward operation, that may swap the two light beams depending on the measurement outcome, to deterministically increase the mean energy of the beam. The success rate of photon subtraction determines the ratio of these states in the output state. We examine in detail the average extracted energy, the extracted energy fluctuations, and the corresponding mean-to-deviation ratio as well as the second-order photon autocorrelation function of the output mode [B19]. We show that the purely linear measurement-feedforward protocol effectively reduces photon correlations and energy fluctuations. At the same time, we find that it is able to enhance the mean energy as well as the mean-to-deviation ratio, that is, the stability [315, 518, 519], of the output mode above the thermal limit. Our measurement-feedforward protocol is advantageous from a thermodynamic point of view since it allows the implementation of the experimental realization and the thermodynamic analysis of a photonic quantum Maxwell demon.

4.3.1 Experimental setup

The experimental realization of deterministic preparation of the super-Poissonian statistics combines the generation of thermal states of light, photon subtraction, photonic switch, and photon-number-resolving detector. The scheme of the experimental setup is shown in Figure 4.11. A coherent nanosecond pulsed light is generated by a gain-switched semiconductor laser diode driven by a sub-nanosecond electronic pulse generator with a repetition rate of 2 MHz. The generated coherent light is split by a 50:50 beam splitter into two coherent states with the same photon number. The optical intensity of coherent pulses is temporally modulated by two independent rotating ground glasses (RGG) with a random spatial distribution of speckles. This method is frequently used to generate a quasi-thermal light with virtually perfect Bose-Einstein statistics (see Section 2.3.2). A single spatial mode is selected by collecting the scattered light into the single-mode optical fiber. As a result, we have two single-mode thermal states. One of the thermal states is modified by the subtraction of a single photon. When the single-photon detection is successful, the photon statistics of the initial thermal state are modified to create an out-of-equilibrium state with a higher mean photon number. The second thermal state is left unchanged.

These initial states are coupled into the input ports of the 2×2 photonic switch [34]. Fast switching is performed by a low-latency switchable coupler employing a high-visibility fiber Mach-Zehnder interferometer (MZI). The optical signals can be switched by changing an optical phase using an integrated waveguide electro-optic modulator (EOM) driven by optical feedback and feedforward circuits using output electronic signal from a single-photon detector. Active phase stabil-

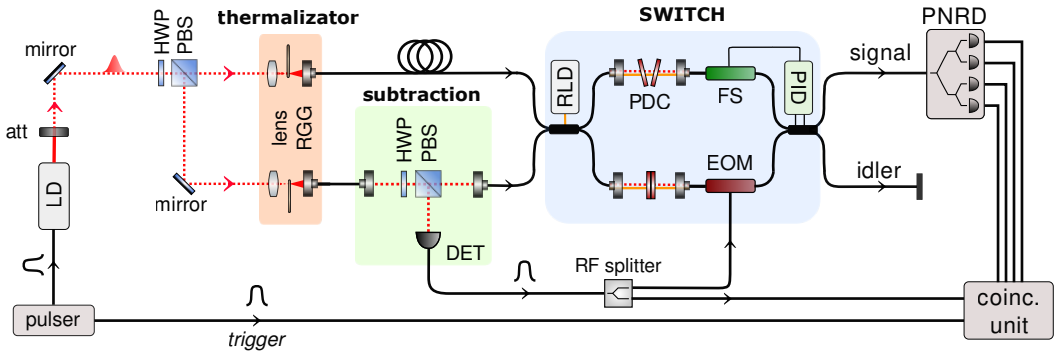

Figure 4.11: Simplified experimental scheme: Preparation of single-mode thermal states; detection of single-photon from the thermal state implemented using a beam splitter with a tunable transmitivity T; the photonic switch based on Mach-Zehnder interferometer (MZI) with phase dispersion compensator (PDC) and fiber stretcher (FS) used to lock the MZI phase and integrated electro-optic modulator (EOM) controlled by optical feedback for signal switching. The output signal is detected by PNRD. All detection events are processed by coincidence logic.

ization is necessary to keep the random phase fluctuation caused by temperature changes, airflow, and vibrations small enough for advanced long-term measurement. The real-time phase locking is performed by comparing the output signal to a fixed setpoint and adjusting the phase based on the error signal. The stabilization technique operating with the strong classical optical reference co-propagating with the initial signal through the MZI was employed to avoid photo-counting noise. More technical details about optical switch functionality are described in Švarc et al. [34]. The resulting output signal was analyzed by a photon-number-resolving detector (see Subsection 3.2). The probability distribution of the number of photons is evaluated from repeated multi-coincidence measurements (see Subsection 3.5).

4.3.2 Results

We have successfully implemented deterministic preparation of the super-Poissonian statistics employing single-photon subtraction. The controlled photon subtraction is treated in more detail in Section 1.3 and Section 2.3.3. According to the results presented in Section 4.2, we generate photon-subtracted thermal states by splitting the single-mode thermal state at a fully tunable beam splitter. We experimentally prepared input thermal states with different mean photon numbers per mode $n_{\mathrm{th}} = 3.94(2)$ and $7.97(3)$. The experimental data and theoretical prediction for mean photon number $\langle n \rangle$ at the output is shown in Figure 4.12(a) for these initial mean photon numbers, respectively, and for different scattering ratio R. For the presented experimental procedure, the optimal R was found far from $R \ll 1$, and the protocol is, therefore, different from the photon subtraction [A1]. As n_{th} increases, optimal R is smaller for the maximum output state mean photon number $\langle n \rangle$ (see Figure 4.12(a)). In general, continuous tunability of splitting ratios allows setting a sufficiently small reflectivity approximating the implementation of the annihilation operator. Alternatively, the reflectivity can be increased to achieve a higher probability of detecting subtracted photons. Figure 4.12 (b) shows the probability of subtracted photon detection as a function of reflectivity R. Furthermore, we investigated the effect of beam splitter reflectivity (ranging from 0.78(3)% up to 27.3(1)%) on the presented statistical modification process in terms of photon statistics characteristics.

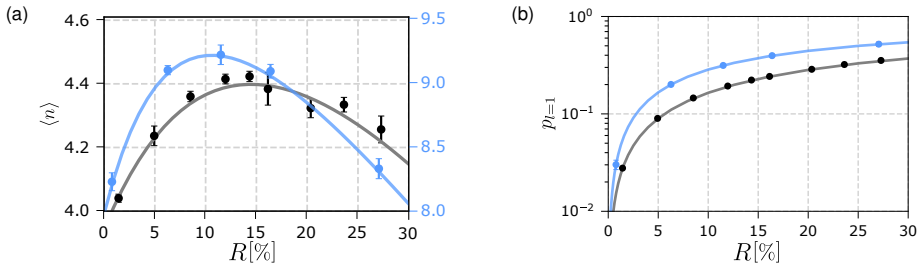

Figure 4.12: (a) Mean photon number of the output state and (b) probability of one photon detection as a function of scattering ratio R. Solid dots represent measured data and solid lines correspond to a theoretical model. Shown are instances of different input thermal states with mean photon number $n_{\mathrm{th}} = 3.94(2)$ (black), and $n_{\mathrm{th}} = 7.97(3)$ (blue).

We analyzed each optical state by its click and photon statistics. Figure 4.13 illustrates click statistics and photon statistics of the input single-mode thermal state, one-photon-subtracted single-mode thermal state, and deterministic prepared output state for different mean photon numbers. Depicted are only results for reflectivity $R = 14.33(3)\%$ for $n_{\mathrm{th}} = 3.94(2)$, respectively $R = 11.5(1)\%$ for $n_{\mathrm{th}} = 7.97(3)$. Retrieved photon statistics are in good agreement with the theoretical ones. We analyzed photon statistics retrieval accuracy evaluating the fidelities and total variation distances of all initial states (Figure 4.14). The average fidelity of all states is $\bar{F} = 0.997(4)$.

We also examine in detail other quantities such as the binomial parameter, the Mandel parameter, $g^2(0)$ function, and the Fano factor of the output beam (Figure 4.15). The values of the binomial (Figure 4.15(a)) and Mandel (Figure 4.15(b)) parameter declare the classical character of these non-equilibrium output states. As might be expected, $g^2(0)$ function decreases with increasing reflectivity R (Figure 4.15(c)). This effect is more significant for higher mean photon numbers of the input thermal state. The Fano factor depends on reflectivity R and is not constant anymore (Figure 4.15(d)). Notably, the output state is more super-Poissonian with an increasing mean photon number.

Several experimental imperfections cause a discrepancy between theoretical simulations and measured data. The generation of these states is conditioned by detecting photons on a multi-channel detector suffering from dark counts. These false detections contribute to the distortion of photon statistics, leading to an increase in the error of the evaluated parameters. Other possible causes are low transmittance of the SWAP [34] and the detectors' non-unity detection efficiency that are compensated using a retrieved photon statistics algorithm [A2]. Deviation of estimated system efficiency from the real one may increase the error within a few percentages.

Simulation of multimode scattering of N thermal modes and l-photon subtracted single-mode thermal states

In the experiment, we employed only single-photon subtraction to demonstrate the deterministic preparation of the output state, but in general, we can subtract an arbitrary number of photons. We utilized numerical simulations to predict the complementary strategy of l-photon subtracted photons for l from 1 up to 4. As aforementioned, the mean photon number of the output state is a function of the scattering ratio R. As we can see in Figure 4.16, the optimal value of R differs for the specific number of subtracted photons l. The higher number of l increases the mean photon number at the cost of decreasing l-photon detection probability $p_i(l)$. However, by increasing the number of selected thermal modes N we can reduce the effect of decreasing the probability of l-photon detection and thus gain the advantage of higher photon subtraction.

Figure 4.17 shows the mean photon number, the second-order autocorrelation function, Fano

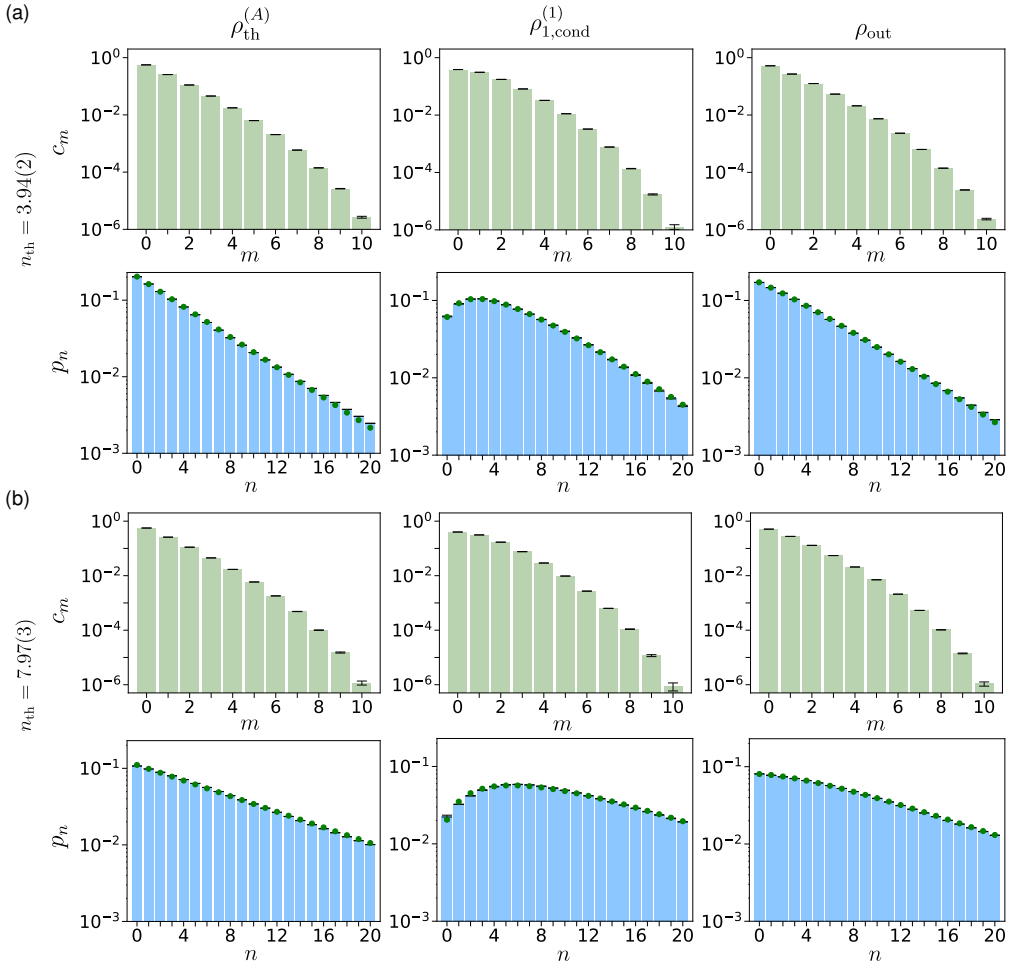

Figure 4.13: Experimental results of detection of photon statistics. Shown are the measured click statistics (green bars), retrieved (blue bars), and the corresponding theoretical photon statistics (green dots) of input thermal state $\rho_{\mathrm{th}}^{(A)}$, conditional state $\rho_{\mathrm{cond}}^{(1)}$, and ρ_{out} for several mean photon numbers: (a) $n_{\mathrm{th}} = 3.94(2)$ ($R = 14.33(3)\%$), and (b) $n_{\mathrm{th}} = 7.97(3)$ ($R = 11.5(1)\%$). All distributions are plotted on a logarithmic scale.

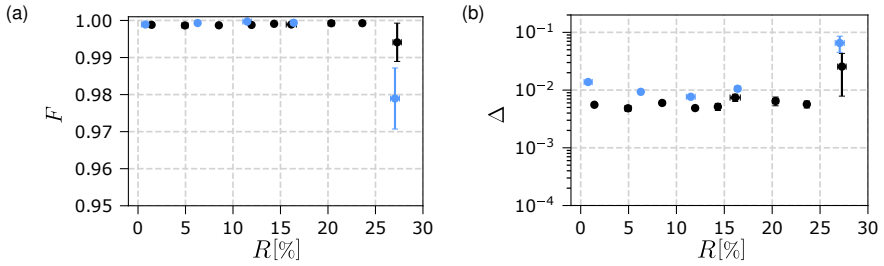

Figure 4.14: The discrepancy between the measured and the corresponding ideal photon statistics characterized by (a) fidelity F, and (b) the total variation distance Δ as a function of reflectivity R. Shown are instances of different input thermal states with mean photon number $n_{\mathrm{th}} = 3.94(2)$ (black), and $n_{\mathrm{th}} = 7.97(3)$ (blue).

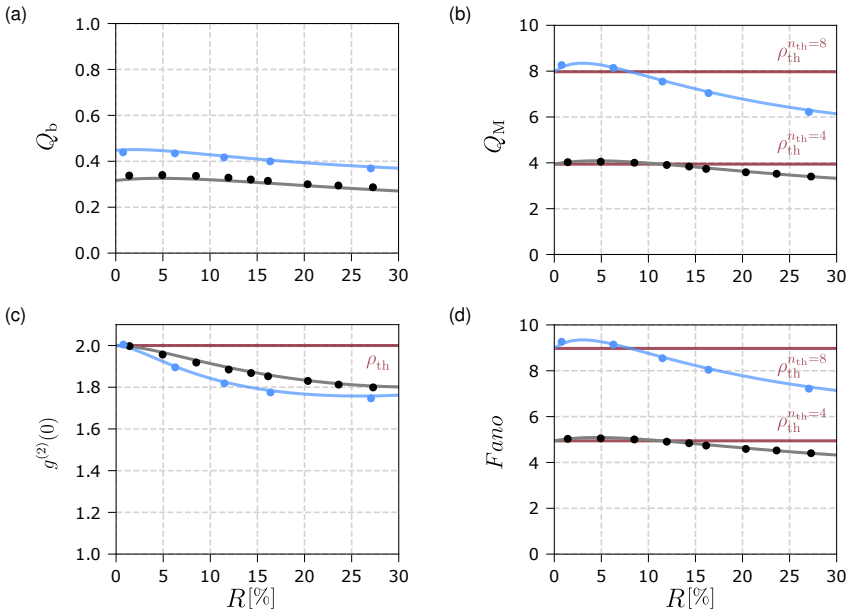

Figure 4.15: Characteristics of measured click and photon statistics: (a) the binomial parameter, (b) the Mandel parameter, (c) $g^2(0)$ function, and (d) Fano factor. Shown are instances of different input thermal states with mean photon number $n_{th} = 3.94(2)$ (black), and $n_{th} = 7.97(3)$ (blue).

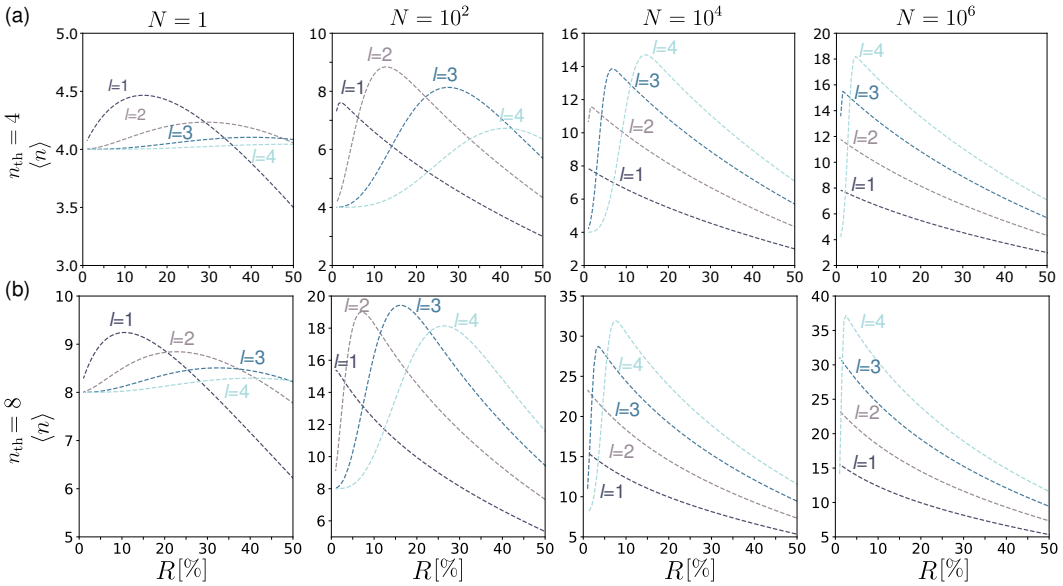

Figure 4.16: Numerical simulations of a higher number of subtracted photons. Shown is dependence of mean photon numbers on scattering ratio R for l-subtracted photons from 1 to 4. Subplots present results for a different mean photon number per mode: (a) $n_{th} = 4$, and (b) $n_{th} = 8$, and different number of thermal modes (slopes): $N = 1,\ 10^2,\ 10^4,$ and 10^6.

factor, and mean-to-deviation ratio of output state $\rho_{\text{out}}^{(l)}$ as a function of the number of thermal modes N. We compared the performed simulations with the results published in the work [A1]. On this basis, we can state that the simulation approaches the conditional l-photon subtraction in the limit of the large number of thermal modes N. Bounds of maximum capable energy correspond to the mean photon number increased by a factor $(l+1)$, which is the same factor as for the conditionally prepared l-photon subtracted thermal state (Figure 4.17(a)). The second-order correlation function converges to unity for the increasing number of subtracted photons and number of thermal modes (Figure 4.17(b)). Even with the increasing number of subtracted photons, the Fano factor of these output states remains a constant value close to $n_{\text{th}}+1$ (Figure 4.17(c)). Figure (4.17)(d) shows that the energy of output states advantageously increases faster than its fluctuations.

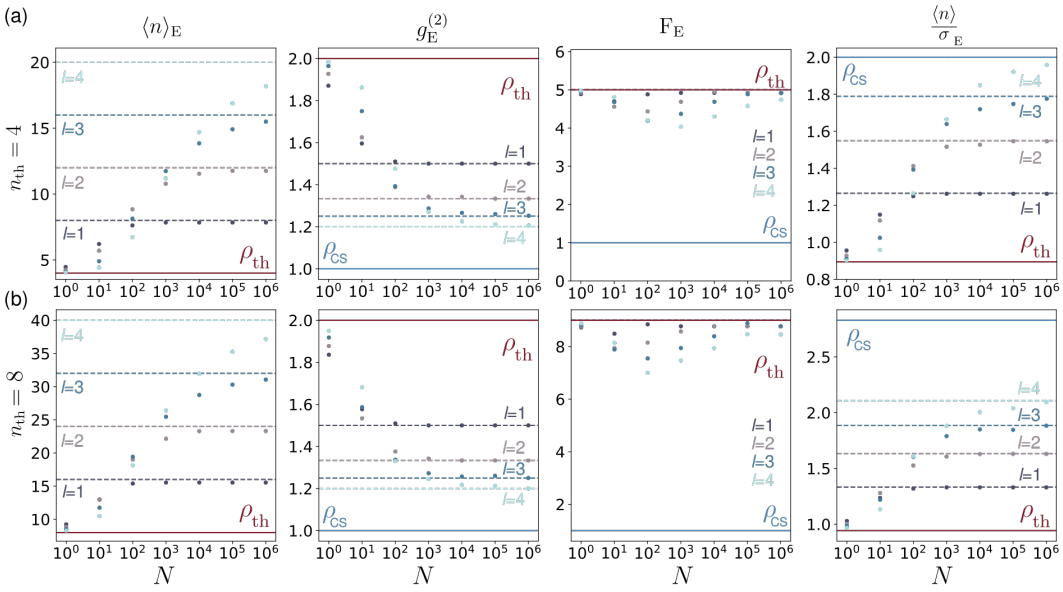

Figure 4.17: The strategy of energy maximization: scattering ration is set to maximize the energy (mean photon number) of the output state $\rho_{\text{out}}^{(l_{\text{th}})}$. Numerical simulations are done for different mean photon numbers per mode: (a) $n_{\text{th}} = 4$, and (b) $n_{\text{th}} = 8$, and number of subtracted photons from 1 up to 4. Several parameters as a function of thermal modes N from 1 up to 10^6 are shown: mean photon number $\langle n \rangle$, the second-order autocorrelation function $g^{(2)}$, fano factor F, and mean-to-deviation ratio $\langle n \rangle / \sigma$.

We mainly focus on the output states with the highest possible energy - mean photon number. However, another important alternative strategy to maximizing the energy of the output state is the mean-to-deviation ratio maximization. The parameters of output states prepared by the mean-to-deviation ratio maximization strategy are depicted in Figure 4.18. As one can see, this strategy leads to the faster convergence of the second-order autocorrelation function. However, the values of the fano factor are smaller and much closer to the value corresponding to the coherent state.

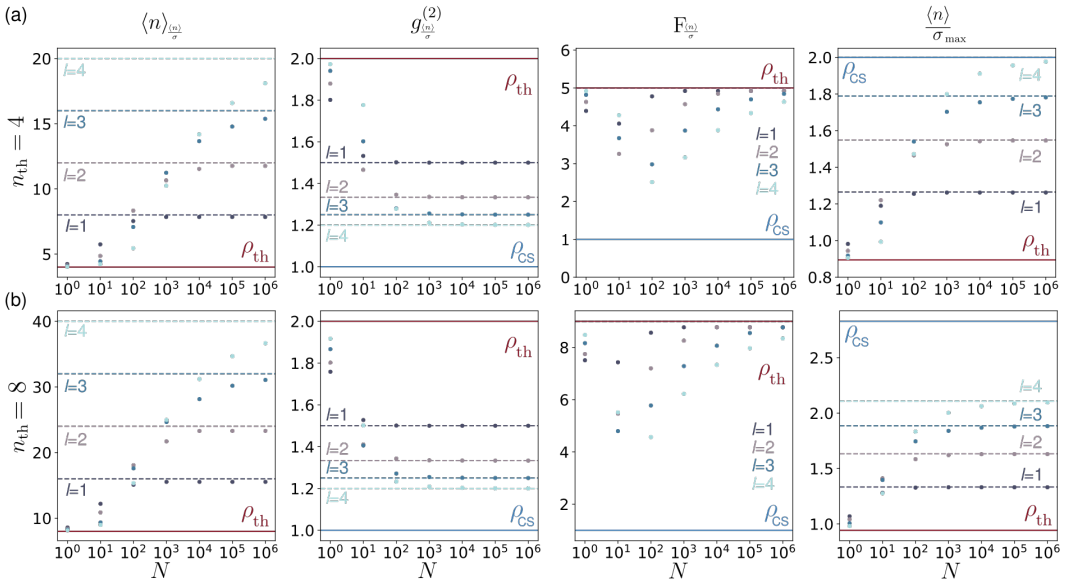

Figure 4.18: Strategy of mean-to-deviation ratio maximization: scattering ration is set to maximize the mean-to-deviation ratio of the output state $\rho_{\mathrm{out}}^{(l_{\mathrm{th}})}$. Numerical simulations are done for different mean photon number per mode: (a) $n_{\mathrm{th}} = 4$, (b) $n_{\mathrm{th}} = 8$, and number of subtracted photons from 1 up to 4. Several parameters as a function of thermal modes N from 1 up to 10^6 are shown: mean photon number $\langle n \rangle$, the second-order autocorrelation function $g^{(2)}$, fano factor F, and mean-to-deviation ratio $\langle n \rangle / \sigma$.

4.3.3 Application

Maxwell's demon thought experiment proposed several decades ago reveals a profound connection between quantum information processing and thermodynamics. By measuring positions and velocities of gas particles contained in two neighboring chambers connected by a small aperture, the demon exploits the acquired information to collect fast (hot) particles in one chamber and slow (cold) particles in the other [B22, 520, 521]. The resulting temperature difference may then be used to run a heat engine and perform work by lifting a weight—without the demon investing any work himself. In order to avoid any apparent violations, the second law has to be generalized to properly incorporate the information gained through the measurement [522, 523]. Originally a thought experiment, successful information-to-work conversion has been recently reported in a number of classical [361, 514, 524–534] and quantum [475, 515, 535–537] systems.

The idea of classical Maxwell's demon extracting force and work from measuring fluctuations in the system stimulates modern quantum physics. Quantum demon experiments have so far been realized with fermionic qubit systems, using nuclear magnetic resonance, superconducting and cavity QED setups [475, 515, 535–537]. On the other hand, quantum optics deals with bosonic systems, such as quantized modes of the electromagnetic field [B19]. Bosonic systems have been extensively studied in the context of quantum information processing [B18]. As a result, numerous theoretical methods, as well as experimental techniques, are available to analyze their quantum properties [538]. These systems are also advantageous from a thermodynamic point of view since their unbounded energy spectra allow them to accumulate large numbers of quanta per single mode, in contrast to systems with finite Hilbert spaces [475, 515, 535–537]. Moreover, surrounding empty modes naturally act as a zero-temperature quantum environment without the need of any external cooling [B19]. Thermal multimode light is a natural energy source in photonic Maxwell's

demon experiments instead of the thermal Maxwell-Boltzmann velocity distribution of particles. A classical photonic demon experiment has been implemented lately using intense thermal light (with a large mean photon number of the order of 10^8) and post-processing in Ref. [361]. In this macroscopic limit, the energy statistics of extracted work is practically continuous. After a weak scattering of such macroscopic light, sensitive microscopic measurements of individual photons made continuous conditional changes of work averaged in time at a classical battery represented by a macroscopic capacitor. Recently, the energy/work was extracted from two thermal baths at equilibrium by gaining information at single-photon-level measurement and applying classical feedforward control [497]. On a small microscopic scale in a cold environment and with only a few energy quanta in a mode, the measurement process manifests very differently than on a macroscopic scale. This photonic Maxwell's demon experiment was implemented at the low temperature of the thermal beams - low photon numbers $n_{\mathrm{th}} = 0.151(2)$. This study primarily focuses on the effects of correlations between the two input modes in a single-photon regime.

In a similar manner, the super-Poissonian statistics deterministic preparation technique mentioned above has enabled an experimental realization of a quantum photonic Maxwell's demon by employing two thermal light beams with a small mean photon number per mode ($n_{\mathrm{th}} = 3.94(2)$ and 7.97(3)). In contrast to the approaches of Maxwell's demon mentioned above, in this microscopic regime, discrete photon fluctuations dominate. We demonstrate successful information-to-energy conversion and examine in detail the average extracted energy, the extracted energy fluctuations, the corresponding mean-to-deviation ratio as well as the second-order photon autocorrelation function of the output mode [B19]. We show that the purely linear measurement-feedforward protocol effectively reduces photon correlations and energy fluctuations. At the same time, we find that it is able to enhance the mean energy as well as the mean-to-deviation ratio, that is, the stability [518, 519, 539], of the output mode above the thermal limit. We further theoretically analyze the charging of a quantum battery consisting of a two-level system resonantly coupled to the output mode. We show that the excitation probability of the qubit may surpass the thermal bound even though the photon statistics is super-Poissonian [B19]. We finally derive a quantum fluctuation relation, a generalization of the second law of thermodynamics that includes information gain [522, 523], and use it to obtain an upper bound on the stored work.

Experimental realization of a quantum photonic Maxwell's demon

Our system consists of two (input) thermal light modes at inverse temperature β with density operator $\rho_{L,R}$, mean photon number n_{th} and standard deviation $\bar{\sigma}$. These two modes play the role of the left (L) and right (R) chambers in Maxwell's thought experiment. Information about the system is gained by coherently scattering a fraction R of the photons of mode L into empty vacuum modes and weakly measuring l scattered photons with multiport single-photon detectors (mode R is not measured) (Figure 4.19). To that end, we employ a low-reflectivity beam splitter realized with a half-wave plate followed by a polarizing beam splitter. The reflected photons are detected via a reconfigurable multichannel detector with commercial on-off single-photon detectors. The measurement is optimized by varying the reflectivity R.

The probability of detecting l photons is $p(l) = \mathrm{Tr}[M(l)S(r)\rho_L S(r)^\dagger M^\dagger(l)]$, where $S(r)$ is a unitary beam splitter-like transformation that characterizes the scattering process and $M(l)$ is a positive operator-valued measure (POVM) that describes the photodetection process. The measurement affects the photon distribution, which becomes nonthermal [16, 28, 159]. When a photon is detected, the average energy of mode L is enhanced compared to that of mode R; it is otherwise reduced when no photon is detected. In the limit $R \ll 1$, such photon subtraction protocol is known to conditionally increase the mean photon number of thermal light up to $(l+1)n_{\mathrm{th}}$ [A1, 16, 28, 35, 159, 161, 298, 314, 493, 494, 496, 517]. We next implement feedforward control by swapping the two modes L and R, depending on the measurement outcome, to ensure that the output always has an

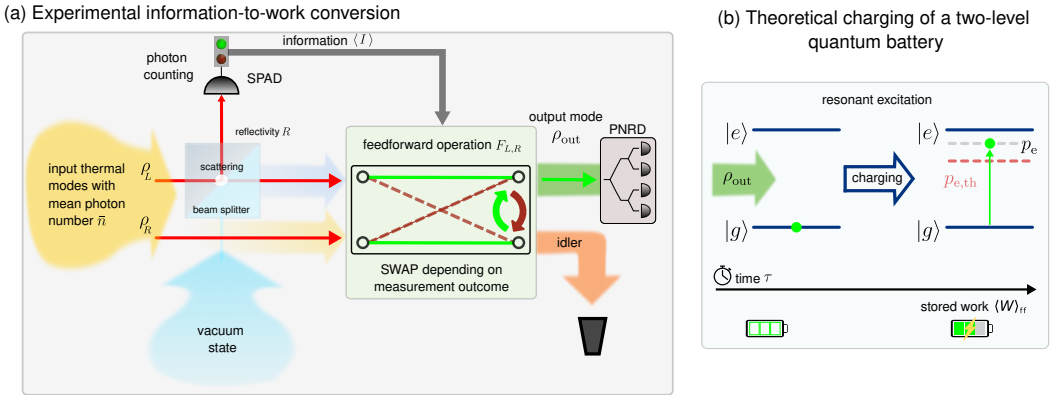

Figure 4.19: (a) The experimental setup contains two input thermal light modes L and R with mean photon number n_{th}. A low-reflectivity beam splitter, realized with a half-wave plate followed by a polarizing beam splitter, is employed to weakly measure the photons of mode L by coherently scattering a varying fraction R of them into vacuum modes. The scattered photons are detected using single-photon avalanche diodes (SPAD). The measurement may either increase or decrease the energy of the mode. The gained information $\langle I \rangle$ is then used to implement a feedforward operation in the form of an optical SWAP that flips either mode L or mode R to the output mode ρ_{out}, depending on the measurement outcome, so that the energy of the output mode is deterministically larger than that of the input mode. The click statistics of state ρ_{out} is measured with a photon-number-resolving detector (PNRD). b) This information-to-work conversion scheme may be theoretically utilized to resonantly charge a quantum two-level battery and store the amount of work $\langle W \rangle_{\text{ff}}$. The achievable excitation probability p_e from the ground state $|g\rangle$ may exceed the thermal bound $p_{e,\text{th}}$.

energy larger than the input mode L. We concretely use a tunable photon routing device [34] to realize the operation

$$F_{L,R}(l) = \begin{cases} \text{SWAP}_{L,\text{out}} & \text{if } l \geq 1 \\ \text{SWAP}_{R,\text{out}} & \text{if } l < 1, \end{cases} \tag{4.10}$$

where 'out' denotes the output mode ρ_{out}.

The experiment was performed with two single-mode ($N = 1$) thermal input states. In addition, we simulate the case of a multimode input state ρ_L. Maxwell's demon measures scattered photons simultaneously in N thermal modes and swap that mode, where the measurement counted a sufficient number of photons, to the output as depicted in Figure 4.20. If it does not happen, the demon fills the output with an unmeasured thermal mode A. It keeps the process deterministic with a maximal increase in the average energy. The remaining unsuccessfully measured modes can be discarded to a cold environment or thermalized again in the hot thermal bath for the next use.

First, we use N parallel modes of thermal light taken from the multimode hot bath to increase the probability p_{suc} of successful l-photon detection according to the formula $p_{\text{suc}} = 1-(1-p_i(l))^N$. If $l \geq l_{\text{th}}$ photons are detected at least in one i-th mode, the demon's measurement is successful, and the SWAP gate flips that mode to the output. The threshold l_{th} will be later optimized for a given R and initial n_{th} to achieve the best performance for the selected figure-of-merit. If no photon is detected instead, the demon's measurement is unsuccessful. In this case, we use the auxiliary mode R from the same bath with the mean n_{th} of thermal photons and swap it to the output mode. A classical SWAP does this feedforward routing for i-th mode

$$F_{i,R}(l) = \begin{cases} \text{SWAP}_{i,\text{out}} & \text{if } l \geq l_{\text{th}} \\ \text{SWAP}_{R,\text{out}} & \text{if } l < l_{\text{th}}, \end{cases} \tag{4.11}$$

where out denotes the output mode. So after applying it, the optical state for i-th mode and the second mode R may be written as

$$\rho_{i,R}^{(l)} = \sum_{l} F(l) \left(M(l) S \rho_L^{(i)} S^\dagger M(l)^\dagger \otimes \rho_R \right) F^\dagger(l), \tag{4.12}$$

The output state is obtained by taking the respective partial trace over the modes A

$$\rho_{\text{out}}^{(l_{\text{th}})} = \text{Tr}_R \left[\rho_{i,R}^{l_{\text{th}}} \right]. \tag{4.13}$$

After the whole procedure, we can discard all other unuseful modes and eventually mode R.

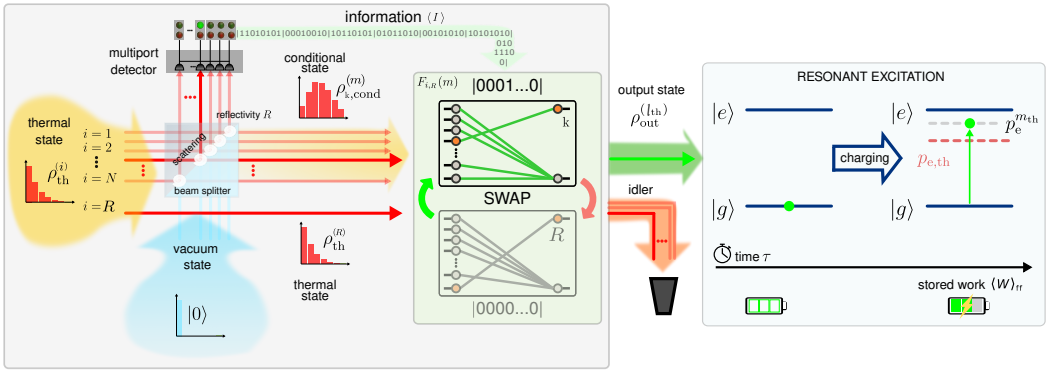

Figure 4.20: Experimental quantum photonic Maxwell's demon: A multimode scattering of $100 \times r[\%]$ of N modes of thermal light with photon number distribution p_n from a hot bath to a zero-temperature bath (environment) is measured by a multiport detector. Successful detection of at least $l > l_{\text{th}}$ photons in a k-th mode controls the SWAP fliping that mode to the output. Otherwise, the demon redirects an auxiliary thermal mode to the output. The remaining modes are discarded to a cold bath. Evaluation: The output light resonantly excites two-level atom by a Jaynes-Cummings interaction in a cavity. For an optimal time τ_{opt} the initial ground state deterministically turns an excited state with a probability larger than maximal $p_{\text{e,th}}$ for a thermal statistics p_n. The evaluation predicts the results for charging a microscopic battery.

Experimental results

We analyzed the energetics and quantum statistics of the output mode for two different input mean photon numbers, $n_{\text{th}} = 3.94(2)$ and $7.97(3)$. The energy extracted by the measurement-feedforward protocol is equal to $\langle \Delta E \rangle = \hbar\omega(\langle n \rangle - n_{\text{th}})$, where $\langle n \rangle$ is the average photon number of the output mode. The corresponding energy fluctuations are $\langle \Delta E^2 \rangle = (\hbar\omega)^2 \langle (n - n_{\text{th}})^2 \rangle = (\hbar\omega)^2 \sigma^2$; they are directly proportional to the photon-number variance $\sigma^2 = \langle \Delta n^2 \rangle$. Figure 4.21 presents the mean photon number $\langle n \rangle$, the photon autocorrelation function $g^{(2)}(0)$, the photon number fluctuations σ, and mean-to-deviation ratio, $\langle n \rangle / \sigma$ of the output state, as a function of the scattering ratio R. Already for $N = 1$ and $l_{\text{th}} = 1$, we observe a deterministic increase of the mean photon number (black dots) above the thermal value (red squares) for both input mean photon numbers (Figures 4.21(a,e)), indicating a successful information-to-energy conversion. A maximum energy increase of 8.42% is obtained for $R = 14.33\%$ and $n_{\text{th}} = 3.94$. For $R = 11.5\%$ and $n_{\text{th}} = 7.97$, an increase of 9.9% is achieved. A larger input mean photon number thus leads to a stronger energy enhancement at a smaller scattering ratio. We emphasize that the optimal values of the reflectivity (of more than 10% in both cases) lie outside the usual photon subtraction regime $R \ll 1$ [A1, 28, 35, 159, 161, 298, 314, 493, 494, 496, 517]. As n_{th} increases, optimal reflectivity is smaller for $\langle n \rangle$. For a

finite N, the optimal R to maximize $\langle n\rangle$ does not coincidence with the one for the smallest autocorrelation $g^{(2)}$ (also one for Fano factor and mean-to-deviation ratio). Meanwhile, the positive work extraction is accompanied by a pronounced suppression of photon correlations (Figures 4.21(b,f)), below the thermal limit $g^{(2)}(0)_{\rm th} = 2$ and towards uncorrelated photons (given by the shot-noise value $g^{(2)}(0)_{\rm sn} = 1$). This reduction is also amplified for larger input mean photon number $n_{\rm th}$.

The lowering of the photon correlations of the output mode has notable consequences as seen in Figures 4.21(c,g). It indeed increases the photon number fluctuations σ for moderate values of R but decreases it below that of a thermal state for bigger values of R (Figures 4.21(c,g)). This leads to a larger mean-to-deviation ratio, $\langle n\rangle/\sigma$, than for the input mode L, for all reflectivities R (Figures 4.21(d,h)). We may therefore conclude that the measurement-feedforward protocol enhances the thermodynamic stability of the output state, an important property of small devices subjected to fluctuations [518, 519, 539]. Whereas the output of macroscopic machines is deterministic and thus stable, it is stochastic, and hence unstable, for small engines owing to thermal and quantum fluctuations. While for thermal states, this ratio is given by $n_{\rm th}/\sigma = 1/(1 + n_{\rm th}^{-1})$ [B19] and is thus upper bounded by one, we find that this limit is exceeded for $n_{\rm th} = 7.97$ when $R > 6.28\%$. In this regime, the mean extracted energy is greater than its fluctuations.

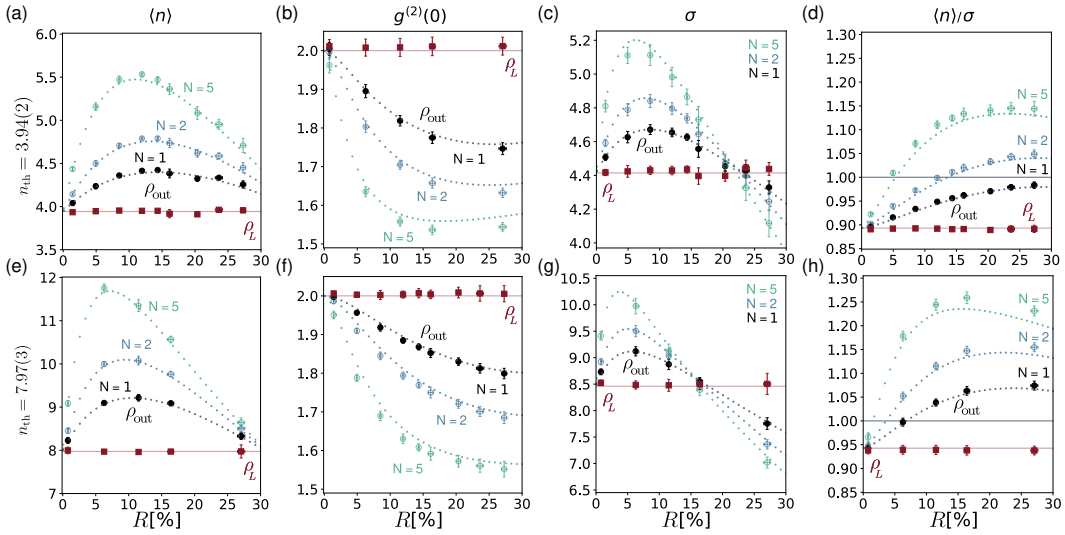

Figure 4.21: (a,e) Mean photon number $\langle n\rangle$, (b,f) second-order autocorrelation function $g^{(2)}(0)$, (c,g) photon number variance σ, and (d,h) mean-to-deviation ratio $\langle n\rangle/\sigma$ of the output mode $\rho_{\rm out}$ as a function of the scattering ratio R for input thermal states $\rho_{\rm L,R}$ with mean photon number $n_{\rm th} = 3.94(2)$ (upper) and $n_{\rm th} = 7.97(3)$ (lower). Full symbols represent measured data (red squares for the input thermal mode, black dots for the output mode). Error bars show three standard deviations of the measurements. Empty symbols indicate numerical simulations, based on measured data, for a multimode input state ρ_L with $N = 2$ and $N = 5$ modes. The measurement-feedforward protocol enhances the mean energy of the photons, reduces their correlations beyond the thermal limit, and amplifies photon fluctuations σ for moderate R and reduces them for larger R. The thermodynamic stability of the output mode, characterized by the mean-to-deviation ratio $\langle n\rangle/\sigma$, is always larger than the corresponding thermal value.

It is instructive to compare our quantum photonic information-to-energy conversion scheme with a laser. A laser is a device able to ideally enhance the energy of one mode to create a stream of uncorrelated (and Poissonian) photons that acts as a classical optical force high above the lasing threshold [B19]. This optical force may, for instance, be used to resonantly excite a two-level atom above the thermal excitation probability $p_{e,\rm th} \sim 0.64$, which is limited by the noise [540]. However,

this requires the saturation of atomic transitions, which is a strong nonlinear behavior [B19]. By contrast, our information machine only requires weak linear scattering, inefficient single-photon measurement, and classical feedforward swapping to increase the mean energy of one mode and reduce the correlations toward the uncorrelated photon regime. We will, moreover, show below that our measurement-feedforward protocol is able, by increasing the mean-to-deviation ratio in the output state, to excite a two-level system above the thermal limit $p_{e,\mathrm{th}}$. Numerical simulations with experimental parameters indicate that the discussed effects can be further amplified by using a multimode input thermal state L together with multiphoton subtraction [35], see empty symbols in Figure 4.21 for the concrete case of $N = 2$ and $N = 5$ modes. We mention that an experimental realization of the many modes scenario is still out of reach. It requires further development of multimode photon subtraction techniques [541, 542] and multimode classical lossless routers to swap fast between these modes.

The excitation probability of the two-level battery

As in all quantum Maxwell's demon experiments performed so far [475, 515, 535–537], we have analyzed the information-to-work conversion without an actual 'lifting' of a weight, which is still challenging to implement in free space optical experiments. In the following, we theoretically study the properties of the charging of a quantum battery [543–545] and evaluate them with our experimental data. The quantum battery consists of a two-level system coupled to the output mode via a resonant Jaynes-Cummings interaction [546] of the form $H = \omega a^\dagger a + \omega\sigma_z/2 + g(\sigma_+ a + \sigma_- a^\dagger)$, with interaction strength g [B19]. Here, a and $a^\dagger$ (σ_- and σ_+) denote the usual ladder operators of the output mode (two-level system), and σ_z the usual Pauli operator. The two-level atom may be seen as a microscopic quantum generalization of the macroscopic classical capacitor of Ref. [361]. We first compute the excitation probability p_e of the two-level atom as a function of the scattering ratio R using experimental data. The excitation probability is defined as

$$p_e = 1 - \sum_{n=0}^{\infty} \cos^2\left(\tau\sqrt{n}\right) \rho\,(n)\,. \tag{4.14}$$

We see that p_e grows with R before saturating (Figure 4.22(a)). Remarkably, the thermal bound $p_{e,\mathrm{th}}$ is surpassed for $n_{\mathrm{th}} = 7.97$ above $R > 13.41\%$, even though the photon statistics is still super-Poissonian. This may be explained by noting that, for photon distributions that are sufficiently peaked around a large $\langle n\rangle$, the optimal excitation time of the two-level atom is $\tau \approx \pi/(2\sqrt{\langle n\rangle})$[B19]. The probability of the excited state is then given by $p_e \approx 1 - \pi^2/(4\langle n\rangle/\sigma)^2$. As a consequence, the increase of the mean-to-deviation ratio $\langle n\rangle/\sigma$ displayed in Figures 4.21(d,h) is directly responsible for the increase of the excitation probability in this limit.

Theoretical results for a quantum load

We now move to the derivation of the maximal amount of work that may be stored in the two-level system with the help of the measurement-feedforward scheme. Our starting point is a quantum fluctuation theorem that relates the exponentiated average of the stored work W with (ff) and without (0) feedforward operation

$$\langle e^{\beta W - I}\rangle_{\mathrm{ff}} = \langle e^{\beta W}\rangle_0, \tag{4.15}$$

where $W = E_{b'} - E_b$ is the difference of eigenergies of the qubit (with corresponding eigenstates $|b\rangle$ and $|b'\rangle$) at the beginning and at the end of the charging process. The stochastic mutual information $I = \ln p(m|n) - \ln p(m)$, with the conditional probability $p(m|n)$ of measuring m photons given input eigenstate n, characterizes the information gained through the measurement. Equation (4.15) is a quantum extension of the nonequilibrium fluctuation relation presented in Ref. [361]. It is important to stress that the quantum fluctuation theorem of the Sagawa-Ueda type [547, 548],

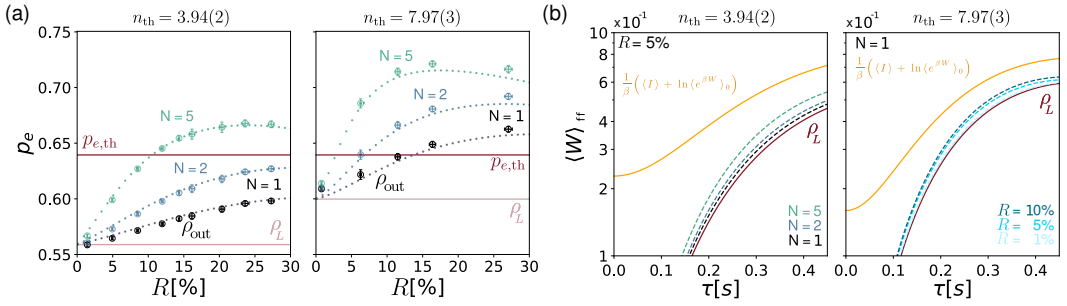

Figure 4.22: (a) Simulated excitation probability p_e of a resonantly coupled two-level battery as a function of the scattering ratio R for input thermal states $\rho_{\rm L,R}$ with mean photon number $n_{\rm th} = 3.94(2)$ (left) and $n_{\rm th} = 7.97(3)$ (right), for $N = 1, 2$ and 5. The thermal bound $p_{e,\rm th} \sim 0.64$ is exceeded when $R > 13.41\%$ for $n_{\rm th} = 7.97(3)$. (b) Simulated mean work $\langle W \rangle$ stored in the quantum battery as a function of the interaction time τ for $N = 1, 2$ and 5 for $R = 5\%$ and $n_{\rm th} = 3.94(2)$ (left), and for $R = 1, 5$ and 10% for $N = 1$ and $n_{\rm th} = 7.97(3)$ (right). The information-theoretic upper bound, Eq. (4.16), (yellow line) is shown for $N = 1$ (left) and $R = 1\%$ (right).

$\langle \exp(\beta W - I - \Delta F) \rangle = 1$, for mechanically driven systems with free energy difference ΔF, which has been been experimentally investigated in Refs. [535, 536], does not apply to the present photonic setup because of the absence of external driving. A different approach is thus required [361]. Using the concavity of the exponential, we obtain from Eq. (4.15) the inequality

$$\langle W \rangle_{\rm ff} \leq \frac{1}{\beta}\Big(\langle I \rangle + \ln\langle e^{\beta W} \rangle_0\Big). \tag{4.16}$$

The second term on the right-hand side can be evaluated explicitly for the Jaynes-Cummings model for an interaction (charging) time τ. We find

$$\langle e^{\beta W} \rangle_0 = \sum_n \frac{e^{-\beta n \omega}}{\sqrt{Z}} [\cos(g\tau\sqrt{n})^2 + \sin(g\tau\sqrt{n+1})^2], \tag{4.17}$$

where Z denotes the partition function on the thermal input states. On the other hand, the mutual information $\langle I \rangle = \sum_{m,n} p(m,n)[\ln p(m|n) + \ln p(m)]$ may be directly determined from measured data. Figure 4.22(b) shows the average work $\langle W \rangle_{\rm ff}$ stored in the quantum battery as a function of the charging time τ for varying mode numbers $N = 1, 2$ and 5 for $R = 5\%$ and $n_{\rm th} = 3.94(2)$ (left), and for varying reflectivities $R = 1, 5$ and 10% for $N = 1$ and $n_{\rm th} = 7.97(3)$ (right). The information-theoretic upper bound of Eq. (4.16) (yellow line) is indicated for $N = 1$ (left) and $R = 1\%$ (right). The amount of stored energy may be enhanced by increasing N or R. Moreover, the charging dynamics, and hence the time for maximum charging, can be controlled via the coupling constant g.

4.3.4 Discussion

We present an experimental approach of deterministic preparation of the super-Poissonian statistics employing single-photon measurements combined with feedforward operation. Single photon measurement provides information about the photon number in the beam. Based on this information, the feedforward operation may be applied to swap between input beams. We verify experimentally the scenario for single-photon subtraction $l_{\rm th} = 1$ and single-mode scattering $N = 1$. Also, based on available experimental data, we extrapolate theoretical predictions of multi-photon subtraction and multimode scattering for a future experiment. We predict that a multimode extension still produces the super-Poissonian statistics. Our experimental findings provide unique

insights into the thermodynamics of a quantum bosonic Maxwell's demon in a regime where discrete photon fluctuations play a central role. By combining weak single-photon measurement and feedforward swap operation, we have demonstrated successful deterministic information-to-work conversion. We have, in particular, showing that the mean energy and the mean-to-deviation ratio, that is, the stability, can be significantly enhanced and optimized by tuning the reflectivity. At the same time, the photon correlations can be suppressed without any nonlinear saturation effects. We theoretically investigated the use of these out-of-equilibrium states of light with super-Poissonian statistics as an input light for charging a microscopic two-level quantum system beyond the thermal bound. For $N = 1$, we can already overcome the limit of excitation by thermal light $p_{\mathrm{e,th}}$ for the measured output state $\rho_{\mathrm{out}}^{(1)}$ generated from a single thermal mode with mean photon number $n_{\mathrm{th}} = 7.97(3)$. It takes results even further from the previous photon subtraction regime [A1]. We have additionally derived an information-theoretic upper bound on the work that may be stored in the battery from a novel quantum fluctuation relation.

4.4 Summary and outlook

In Chapter 4, we applied the developed detection workflow (Chapter 3) to photon-number-resolving measurement, as required for conditional and deterministic state preparation and quantum simulations. We focus on the controlled modification of statistical properties of light, namely the single-mode thermal state of light, mainly by photon subtraction and fast optical switching.

First, we demonstrated the controlled multiple photon subtraction from a thermal state to conditional generate states with super-Poissonian statistics. Multiple-photon subtraction from the thermal state was implemented using a beam splitter with a 5% reflectivity. When a (multi)coincidence was detected by a multichannel single-photon detector in the reflected port, the heralded optical signal in the transmitted port was analyzed by the PNRD reported in Chapter 3. Increasing the number of subtracted photons results in a transition from super-Poissonian chaotic light to Poissonian signal. This procedure does not use any other source of energy; it is, therefore, energetically autonomous. It requires only reasonably good first-order coherence of thermal states, as is also proved experimentally.

These photon-subtracted thermal states perfectly simulate out-of-equilibrium states of light and can be employed in many applications in quantum information and thermodynamics. We provided numerical analysis, experiment, and operational measures proving the principal applicability of the subtracted thermal states to reach available work larger than can be obtained by any cooling of thermal state, even up to a ground state, and reach mutual information close to maximum of single bit per pulse in an ideal communication scenario, if the out-of-equilibrium state is used as a letter of a binary alphabet. Despite the increase of entropy by the subtraction of quanta, these noisy out-of-equilibrium states at a level of few quanta are therefore provably useful and their potential should not be underestimated. This source of valuable states will be applicable for merging quantum thermodynamics and information theory, and moreover, it can be directly translated to other experimental platforms like quantum optomechanics.

Furthermore, we presented a complex experimental realization of the fully controlled deterministic preparation of the states with super-Poissonian statistics by weak scattering of thermal light, sensitive photon-counting detection, and feedforward swap of the modes. A multimode scattering of two modes of thermal light is measured by a quantum detector. Successful detection of at least $l > l_{\mathrm{th}}$ photons in a mode controls the SWAP flipping that mode to the output. The remaining mode is discarded. As a result, the mean energy deterministically increases in a single-mode of light faster than energy fluctuations, and simultaneously, photon correlation decreases, keeping super-Poissonian statistics. Subsequently, we also numerically analyzed multimode scenario com-

bining subtraction of the arbitrary number of photons. The presented strategy of the increasing number of thermal modes N significantly increases the mean photon number of the output state and, for large N results, even approaches the single-photon subtraction. However, it is still challenging to find a suitable physical system or platform for this high number of modes scenario due to the need for simultaneous resolution of these modes and a multimode version of the classical lossless router.

A developed procedure was employed for the experimental implementation and the thermodynamic analysis of a photonic quantum Maxwell demon. Such bosonic systems are advantageous from a thermodynamic point of view since their unbounded energy spectra allow them to accumulate large numbers of quanta per single mode, in contrast to systems with finite Hilbert spaces. We specifically combine single-photons measurements and feedforward operation to deterministically increase the mean energy of a thermal light beam in a regime where photon fluctuations dominate. We show that a reduction of the photon correlations leads to a mean-to-deviation larger than that of a thermal state. We further discuss the charging of a two-level battery and find that excitation probabilities beyond the thermal limit may be achieved without nonlinear saturation. Finally, we predict that a multimode extension still producing super-Poissonian statistics can deterministically excite the atom as high and as fast as a classical driving force. Future extensions of this scheme to other bosonic systems would, for instance, allow the manipulation of phonon statistics in trapped ions [313] and quantum optomechanics [314].

Chapter 5

Characterization of quantum detectors

Chapter 5 presents a method for direct verification of quantum non-Gaussianity of a quantum measurement (Section 5.2) that is based on probing the measurement apparatus with two classical thermal states and a vacuum state. The same experimental procedure also enables to certify negativity of Wigner function (Section 5.3) representing the characterized POVM element Π. We have experimentally demonstrated the direct certification of quantum non-Gaussianity of a quantum measurement for a single-photon avalanche photodiode and the observed experimental data are in excellent agreement with theoretical model (Section 5.5). Our results extend the concept of quantum non-Gaussianity to quantum measurements and provide new simple and experimentally feasible tools to characterize highly non-classical features of quantum detectors with a few measurements. Our method can serve for fast and direct testing and benchmarking of various detectors including single-photon detectors, photon-number-resolving detectors, or even more complex detection schemes where the signal is preprocessed by some quantum operation such as squeezing or amplification before being detected. Since our method is wavelength-independent, it can be also utilized to characterize detectors of microwave photons employed in a cavity or circuit quantum electrodynamics [549–555].

Chapter 5 is based on the following publication:
[A3] J. Hloušek, M. Ježek, and Jaromír Fiurášek, '*Direct experimental certification of quantum non-Gaussian character and Wigner function negativity of single-photon detectors*', Physical Review Letters **126**, 043601 (2021).

5.1 Introduction

The concepts of nonclassicality and quantum non-Gaussianity are essential for the rapidly advancing development of novel techniques and technologies in quantum physics with interdisciplinary applications. Highly nonclassical character of optical quantum detectors, such as single-photon detectors, is essential for preparation of quantum states of light and a vast majority of applications in quantum metrology and quantum information processing. Therefore, it is both fundamentally interesting and practically relevant to investigate the nonclassical features of optical quantum measurements. Generally, the negativity of the Wigner function and quantum non-Gaussianity are targeted as the two highly nonclassical features. The state-of-the-art methods for characterizing photonic detectors and their nonclassicality level are indirect. They include 1. certification of nonclassicality of a state conditioned on a detection event of the detector, and 2. full detector tomography requiring a large number of probe states.

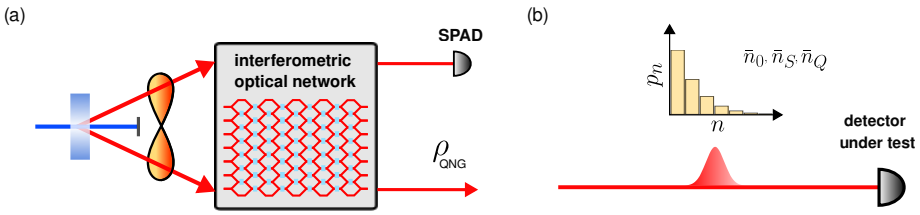

Figure 5.1: (a) Indirect certification of quantum non-Gaussian character of a single-photon detector, namely a single-photon avalanche diode (SPAD). A suitable multimode nonclassical Gaussian state is prepared using a parametric nonlinear process and an inteferometric network. A measurement with the single photon detector is performed on some of the output modes. Quantum non-Gaussianity of the heralded state certifies quantum non-Gaussianity of the detector. (b) Direct certification of quantum non-Gaussian character of a detector by probing it with two classical thermal states and a vacuum state. The same probing allows also for certifying negativity of the Wigner function of the detector.

Here we propose and experimentally demonstrate a procedure for direct certification of quantum non-Gaussianity and Wigner function negativity, two crucial nonclassicality levels, of photonic quantum detectors. Remarkably, we characterize the highly nonclassical properties of the detector by probing it with only two classical thermal states and a vacuum state. We experimentally demonstrate the quantum non-Gaussianity of single-photon avalanche diode even under the presence of background noise, and we also certify the negativity of the Wigner function of this detector. Our results open the way for direct benchmarking of photonic quantum detectors with a few measurements on classical states.

5.2 Quantum non-Gaussian character

Studying and exploiting nonclassical properties of light rely on precise measurement and manipulation of light at the single- and few-photon levels. Massive improvements in advanced detection technologies and techniques initiate the scientific community to develop novel certification methods to characterize their highly non-classical properties. In recent decade we have witnessed a big effort in the theoretical and experimental investigation of quantum non-Gaussianity in the form of non-Gaussian states, non-Gaussian operations, and non-Gaussian measurements. The effect of quantum non-Gaussianity already found its application potential in quantum computation,

quantum metrology, and quantum communication.

Quantum non-Gaussian (QNG) states [121] are defined as states whose density matrix cannot be expressed as a convex mixture of Gaussian states. Preparation of quantum non-Gaussian states thus requires nonlinear interaction or detection beyond the class of Gaussian operations that comprise interference in passive linear optical interferometers, quadrature squeezing, and homodyne detection. While every state with negative Wigner function is a quantum non-Gaussian state, the class of quantum non-Gaussian states is strictly larger and contains also states with positive Wigner function. During recent years, the quantum non-Gaussian states have been the subject of intensive research [C1, 158, 160, 304, 337, 386–401]. Several criteria and witnesses for detection of quantum non-Gaussian states have been established [304, 337, 386–392], and the quantum non-Gaussian character of various sources of nonclassical light has been demonstrated experimentally [C1, 158, 160, 393–396]. The most common way to generate a quantum non-Gaussian state of light is to first generate a suitable multimode nonclassical Gaussian state, perform measurements with single-photon detectors on some of its modes and condition on photon detection [27, 159, 383–385, 393, 394, 396, 402]. This is schematically illustrated in Figure 5.1 (a). The subsequent certification of quantum non-Gaussian character of the conditionally generated state can then be interpreted as an indirect certification of quantum non-Gaussian character of the measurement performed on the auxiliary modes.

Let us begin with a short recapitulation of the quantum non-Gaussianity criterion that will be utilized in this Thesis and adapted for direct characterization of quantum non-Gaussianity of quantum measurements. Consider a quantum state ρ and let $p_0 = \langle 0|\rho|0\rangle$ denote the probability of vacuum state in ρ. Let $\mathscr{L}$ denote a lossy channel with 50% transmittance, and define $q_0 = \langle 0|\mathscr{L}(\rho)|0\rangle$ as the probability of vacuum state at the output of the lossy channel. It holds that

$$q_0 = \sum_{n=0}^{\infty} \frac{p_n}{2^n}, \tag{5.1}$$

where $p_n = \langle n|\rho|n\rangle$ is the photon number distribution of state ρ. As shown in Ref. [387], a quantum non-Gaussianity criterion can be formulated in terms of q_0 and p_0. Specifically, the state is proved to be quantum non-Gaussian if q_0 exceeds certain threshold that depends on p_0. The dependence of maximum q_0 achievable for a given p_0 with Gaussian states and their mixtures can be expressed analytically in a parametric form [387],

$$\begin{aligned} p_0(V) &= \frac{2\sqrt{V}}{V+1} \exp\left[-\frac{(1-V)(3+V)}{2V(3V+1)}\right], \\ q_0(V) &= \frac{4\sqrt{V}}{\sqrt{(V+3)(3V+1)}} \exp\left[-\frac{1-V^2}{2V(3V+1)}\right], \end{aligned} \tag{5.2}$$

where $V \in (0, 1]$.

We focus on the certification of quantum non-Gaussianity of a quantum measurement. We specifically consider a particular measurement outcome associated with a POVM element Π. We can treat Π as a non-normalized density matrix. Assuming that $\mathrm{Tr}[\Pi]$ is finite, we could introduce normalized operator $\rho_\Pi = \Pi/\mathrm{Tr}[\Pi]$, treat it as an equivalent of a density matrix and define

$$P_0 = \frac{1}{\mathrm{Tr}[\Pi]}\langle 0|\Pi|0\rangle, \qquad Q_0 = \frac{1}{\mathrm{Tr}[\Pi]} \sum_{n=0}^{\infty} \frac{1}{2^n}\langle n|\Pi|n\rangle. \tag{5.3}$$

If we knew Q_0 and P_0 then we could apply the above described quantum non-Gaussianity criterion based on Eq. (5.2) to verify the quantum non-Gaussian character of the POVM element Π. However, $\mathrm{Tr}[\Pi]$ can be infinite, and even if finite, it could be difficult to measure.

We circumvent this obstacle by considering a regularized version of the POVM element

$$\tilde{\Pi} = W\Pi W^\dagger, \tag{5.4}$$

where

$$W = \sum_{n=0}^{\infty} \nu^n |n\rangle\langle n|. \tag{5.5}$$

The transformation (5.4) represents a noiseless quantum attenuation [556] with factor $0 < \nu < 1$. The noiseless quantum attenuation is a conditional Gaussian quantum operation that can be applied to a quantum state of an optical mode by sending the state through a beam splitter with amplitude transmittance ν, whose auxiliary input port is prepared in vacuum state and whose auxiliary output port is projected onto vacuum state. If ρ is a Gaussian state or a mixture of Gaussian states, then also $W\rho W^\dagger$ is a mixture of Gaussian states. Therefore, if we find that $W\rho W^\dagger$ is quantum non-Gaussian, then also ρ must have been quantum non-Gaussian state. This observation can be straightforwardly extended to quantum measurements. In particular, if we find that $\tilde{\Pi}$ is quantum non-Gaussian, then also the original POVM element Π must have been quantum non-Gaussian. We note that the quantum state $\rho_{\tilde{\Pi}} = \tilde{\Pi}^{\mathrm{T}}/\mathrm{Tr}[\tilde{\Pi}]$, where the transposition is performed in the Fock basis, can be conditionally generated by preparing a Gaussian two-mode squeezed vacuum state

$$|\Psi\rangle_{AB} = \sqrt{1-\nu^2} \sum_{n=0}^{\infty} \nu^n |n,n\rangle_{AB} \tag{5.6}$$

and performing the quantum measurement on mode B. Measurement outcome associated with the POVM element Π then heralds preparation of mode A in state $\rho_{\tilde{\Pi}}$. This shows that the regularization (5.4) of the POVM element Π has a direct experimental relevance and characterization of $\tilde{\Pi}$ specifies the ultimately achievable properties of the conditionally prepared state $\rho_{\tilde{\Pi}}$, when all other aspects of the state preparation are perfect.

Considering $\tilde{\Pi}$ instead of Π, we find that its trace is always well defined and finite,

$$S = \mathrm{Tr}[\tilde{\Pi}] = \sum_{n=0}^{\infty} \nu^{2n} \langle n|\Pi|n\rangle. \tag{5.7}$$

In fact, the quantity S can be experimentally determined by probing the detector with a thermal state. Recall that the density matrix of a thermal state with mean photon number $\rho_{\mathrm{th}}(\bar{n})$ reads

$$\rho_{\mathrm{th}}(\bar{n}) = \frac{1}{\bar{n}+1} \sum_{n=0}^{\infty} \left(\frac{\bar{n}}{\bar{n}+1}\right)^n |n\rangle\langle n|. \tag{5.8}$$

By choosing $\bar{n}_S = \nu^2/(1-\nu^2)$ we get $\nu^2 = \bar{n}_S/(\bar{n}_S+1)$ and

$$S = \frac{1}{1-\nu^2} \mathrm{Tr}[\rho_{\mathrm{th}}(\bar{n}_S)\Pi], \tag{5.9}$$

where $\mathrm{Tr}[\rho_{\mathrm{th}}(\bar{n}_S)\Pi]$ represents the probability of outcome Π when probing the detector with thermal state $\rho_{\mathrm{th}}(\bar{n}_S)$.

We can define the vacuum probabilities $\tilde{P}_0$ and $\tilde{Q}_0$ for the normalized operator $\rho_{\tilde{\Pi}} = \tilde{\Pi}/\mathrm{Tr}[\tilde{\Pi}]$ corresponding to the regularized POVM element $\tilde{\Pi}$ in full analogy to Eq. (5.3),

$$\begin{aligned} \tilde{P}_0 &= \frac{\langle 0|\tilde{\Pi}|0\rangle}{\mathrm{Tr}[\tilde{\Pi}]} = \frac{1}{S}\langle 0|\Pi|0\rangle, \\ \tilde{Q}_0 &= \frac{1}{\mathrm{Tr}[\tilde{\Pi}]} \sum_{n=0}^{\infty} \frac{1}{2^n} \langle n|\tilde{\Pi}|n\rangle = \frac{1}{S} \sum_{n=0}^{\infty} \frac{\nu^{2n}}{2^n} \langle n|\Pi|n\rangle. \end{aligned}$$

It follows that $\tilde{P}_0$ can be estimated by probing the detector with the vacuum state and $\tilde{Q}_0$ can be determined by probing the detector with thermal state with mean photon number $\bar{n}_Q = \nu^2/(2-\nu^2)$, which follows from $\frac{\nu^2}{2} = \bar{n}_Q/(\bar{n}_Q+1)$. In terms of the mean numbers of thermal photons, the probabilities $\tilde{P}_0$ and $\tilde{Q}_0$ can be expressed as

$$\tilde{P}_0 = \frac{1}{\bar{n}_S+1}\frac{\mathrm{Tr}[\Pi\,\rho_{\mathrm{th}}(0)]}{\mathrm{Tr}[\Pi\,\rho_{\mathrm{th}}(\bar{n}_S)]},\ \tilde{Q}_0 = \frac{\bar{n}_Q+1}{\bar{n}_S+1}\frac{\mathrm{Tr}[\Pi\,\rho_{\mathrm{th}}(\bar{n}_Q)]}{\mathrm{Tr}[\Pi\,\rho_{\mathrm{th}}(\bar{n}_S)]}, \tag{5.10}$$

where

$$\bar{n}_Q = \frac{\bar{n}_S}{\bar{n}_S+2}. \tag{5.11}$$

When conditioning on click of a single-photon avalanche diode, the POVM element whose quantum non-Gaussian character is effectively tested and certified reads $\Pi = I - |0\rangle\langle 0|$ for an ideal detector with unit efficiency. Let us now consider a more realistical SPAD with detection efficiency η and probability of dark counts R_D. Here R_D is the probability that the detector clicks when a vacuum state is injected into the detected signal mode. We can describe the click outcome of such detector with the POVM element (Eq. (2.37)). After some algebra, we obtain

$$\tilde{P}_0 = \frac{R_D(1-\nu^2)(1-\nu^2+\nu^2\eta)}{R_D(1-\nu^2)+\nu^2\eta} \tag{5.12}$$

and

$$\tilde{Q}_0 = 2\frac{R_D(2-\nu^2)+\nu^2\eta}{R_D(1-\nu^2)+\nu^2\eta}\times\frac{(1-\nu^2)(1-\nu^2+\nu^2\eta)}{(2-\nu^2)(2-\nu^2+\nu^2\eta)}. \tag{5.13}$$

In the experiment, the mean photon numbers of thermal states will be estimated and calibrated with some uncertainty specified by a confidence interval, $\bar{n}_j \in [\bar{n}_j^-, \bar{n}_j^+]$. We now show how to take this uncertainty into account and obtain suitable bounds on $\tilde{P}_0$ and $\tilde{Q}_0$ for which the quantum non-Gaussianity criterion remains applicable. First we exploit the convexity of the set $\mathscr{G}$ of probability pairs $[p_0, q_0]$ that can be obtained from Gaussian states and their mixtures. Since $[0,0]$ is an extremal point of $\mathscr{G}$, it holds that if $[p_0, q_0] \in \mathscr{G}$, then also $[xp_0, xq_0] \in \mathscr{G}$, where $0 \le x \le 1$. Conversely, if $[xp_0, xq_0] \notin \mathscr{G}$ then also $[p_0, q_0] \notin \mathscr{G}$. To account for the uncertainty in determination of $\bar{n}_S$ we can conservatively apply the quantum non-Gaussianity test to $[x\tilde{P}_0, x\tilde{Q}_0]$ instead of $[\tilde{P}_0, \tilde{Q}_0]$, where $x = \frac{\bar{n}_S+1}{\bar{n}_S^+ +1}$. Practically, this means that we replace $\bar{n}_S$ with the upper bound $\bar{n}_S^+$ in the denominators of prefactors in Eq. (5.10), and consider the probabilities

$$\tilde{P}_0' = \frac{1}{\bar{n}_S^+ +1}\frac{\mathrm{Tr}[\Pi\,\rho_{\mathrm{th}}(0)]}{\mathrm{Tr}[\Pi\,\rho_{\mathrm{th}}(\bar{n}_S)]},\ \tilde{Q}_0' = \frac{\bar{n}_Q+1}{\bar{n}_S^+ +1}\frac{\mathrm{Tr}[\Pi\,\rho_{\mathrm{th}}(\bar{n}_Q)]}{\mathrm{Tr}[\Pi\,\rho_{\mathrm{th}}(\bar{n}_S)]}. \tag{5.14}$$

The utilized quantum non-Gaussianity criterion certifies quantum non-Gaussianity when $\tilde{Q}_0'$ is larger than certain threshold that depends on $\tilde{P}_0'$. Since $\tilde{Q}_0'$ is an increasing function of $\bar{n}_Q$ we can avoid false positive certification of quantum non-Gaussianity due to uncertainty in $\bar{n}_Q$ calibration by utilizing a sufficiently low $\bar{n}_Q$ such that

$$\bar{n}_Q^+ \le \frac{\bar{n}_S^-}{\bar{n}_S^- + 2} \tag{5.15}$$

is satisfied. The condition (5.15) ensures that for any pair of true values of the mean photon numbers $\bar{n}_S$ and $\bar{n}_Q$ from the confidence intervals the estimated $\tilde{Q}_0'$ will not exceed the value of $\tilde{Q}_0'$ that would be obtained for $\bar{n}_Q = \bar{n}_S/(\bar{n}_S+2)$. To summarize, if one satisfies the condition (5.15) and utilizes the above defined $\tilde{P}_0'$ and $\tilde{Q}_0'$ then one can certify quantum non-Gaussianity of the POVM element Π even with uncertainty in calibration of the mean photon numbers $\bar{n}_S$ and $\bar{n}_Q$.

5.3 Wigner function negativity

An important subclass of nonclassical states is represented by states with negative Wigner function [27, 159, 336, 383–385]. In addition to certification of quantum non-Gaussianity, the probabilities $\tilde{P}_0$ and $\tilde{Q}_0$ can also be used to certify negativity of Wigner function that represents the characterized POVM element Π. Returning for a while back to q_0 and p_0, it follows from Eq. (5.1) that

$$q_0 - p_0 = \frac{p_1}{2} + \sum_{n=2}^{\infty} \frac{p_n}{2^n} \leq \frac{p_1}{2} + \frac{1}{4} \sum_{n=2}^{\infty} p_n. \tag{5.16}$$

Since $\sum_{n=2}^{\infty} p_n = 1 - p_0 - p_1$, we obtain from the inequality (5.16) a lower bound on p_1,

$$p_1 \geq 4q_0 - 3p_0 - 1. \tag{5.17}$$

If $p_1 > \frac{1}{2}$ then the Wigner function of state ρ with photon number distribution p_n is negative at the origin. Using inequality (5.17), the negativity of Wigner function of an optical quantum state can be certified from a simple measurement with a balanced beam splitter and a pair of detectors, that is commonly used for measurement of the anticorrelation factor [393, 557]. If we apply the condition (5.17) to the normalized operator $\rho_{\tilde{\Pi}} = \tilde{\Pi}/\mathrm{Tr}[\tilde{\Pi}]$, we find that the Wigner function of $\tilde{\Pi}$ must be negative at the origin of phase space if

$$4\tilde{Q}_0 - 3\tilde{P}_0 - 1 > \frac{1}{2}. \tag{5.18}$$

Since the noiseless attenuation (5.4) as a Gaussian operation preserves positivity of Wigner function of the POVM element, the inequality (5.18) implies also the negativity of Wigner function of the original POVM element Π.

5.4 Experimental setup

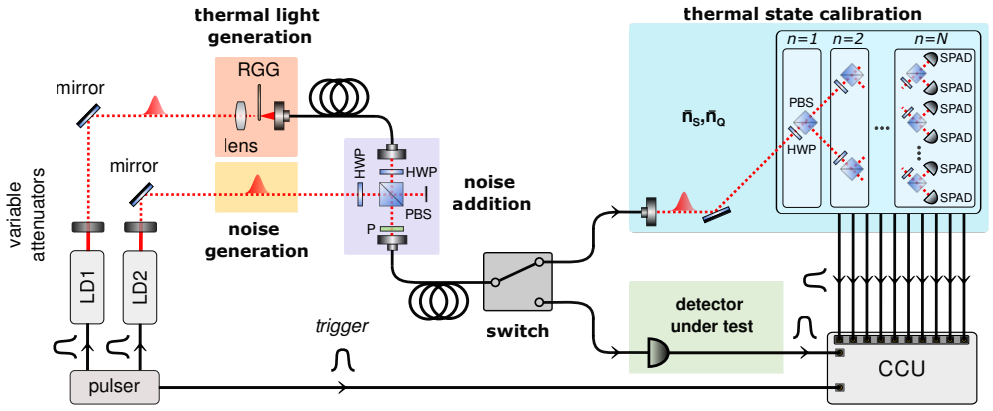

Figure 5.2: Experimental setup: the scheme includes preparation of pseudo-thermal state using a laser diode (LD1) and rotating ground glass (RGG); noise generation and addition using a laser diode (LD2), polarizing beam splitter (PBS), and polarizer (P); calibration of mean photon numbers of thermal states; detector under test; coincidence counting unit (CCU).

The experimental setup for direct certification of quantum non-Gaussianity of a single-photon detector is shown in Figure 5.2. Nanosecond optical pulses with the central wavelength of 0.8 μm are produced by a gain-switched semiconductor laser diode driven by an electronic pulser at a repetition rate of 1 MHz. The pulser drives also an auxiliary laser diode emulating noise of the detector under test, and provides an electronic trigger signal. To produce pseudo-thermal light with Bose-Einstein distribution, we used RGG technique discussed in Section 2.3.2. Let me stress that other single-mode thermal sources can be used here, see Section 2.3.2. The photodistribution of the generated thermal light and its mean photon number $\bar{n}$ per pulse is verified by PNRD detector presented in Section 3.2. The photon-number statistics of the optical signal is retrieved from the measured coincidence histogram using the expectation-maximization-entropy algorithm 2.6.3. The measured photon-number statistics matches very well to the ideal Bose-Einstein statistics with the typical fidelity of 0.999, and the mean photon number $\bar{n}$ is accurately determined.

Characterized thermal light is fed to the detector under test, which is, in our case, a SPAD module (SPCM-AQRH-14-FC manufactured by Excelitas) with the detection efficiency of 58% specified by the manufacturer and measured dark count probability of $R_{\mathrm{D}} = 1.44(8) \times 10^{-6}$. The output electronic signal is again processed by the CCU (Section 3.3) and the number of detection events is evaluated together with the total number of the triger events, i.e. the number of input optical pulses. The relative detection frequency is acquired for vacuum state and thermal states with the mean photon number of $\bar{n}_Q$ and $\bar{n}_S$, which sample the ideal probabilities $\mathrm{Tr}[\Pi\,\rho_{\mathrm{th}}(0)]$, $\mathrm{Tr}[\Pi\,\rho_{\mathrm{th}}(\bar{n}_Q)]$, $\mathrm{Tr}[\Pi\,\rho_{\mathrm{th}}(\bar{n}_S)]$.

5.5 Results

We have performed several measurements in order to check the robustness and reliability of the presented QNG certification method. Let me begin by overviewing the properties of the generated probe thermal states. We experimentally prepared thermal states with mean photon numbers $\bar{n}_S =$ ranging from from 0.0103 ± 0.0006 to 5.04 ± 0.02 and $\bar{n}_Q$ from 0.00475 ± 0.00004 to 0.6928 ± 0.0005 satisfying formula (5.15). In total, we generated and analyzed in details twenty thermal states of light. The precision of the thermal state preparation and calibration is influenced mainly by the uncertainty of the total detection efficiency η, which is $\pm 1\%$, and by possible long-term fluctuations of the source intensity.

In Figure 5.3 the click statistics and photon statistics of the one set of three probe states is shown. All photon statistics were retrieved from the measured click statistics by the expectation-maximization-entropy algorithm 2.6.3. We quantified the similarity of the reconstructed photon statistics with an exact Bose-Einstein distribution by evaluating the fidelity and the total variation distance (Figure 5.4). The experimental results are in excellent agreement with theory and the fidelities of the photon statistics exceed $F > 0.9996$ for all measured thermal states (Figure 5.4(a)). Additionally, we evaluated other characteristics associated with the statistical properties of light such as the Binomial parameter, the Mandel parameter, the Glauber correlation function, and the Fano factor (Figure 5.5). All parameters provide evidence of the almost ideal Bose-Einstein distribution.

Following the procedure described in Section 5.2, we have next tested the quantum non-Gaussianity of the single-photon avalanche diode. The quantities $\tilde{P}_0'$ and $\tilde{Q}_0'$ are evaluated as in Eq. (5.14) and the resulting diagram is shown in Figure 5.6. Ten pairs $[\tilde{P}_0', \tilde{Q}_0']$ are measured for the mean photon number $\bar{n}_S$ ranging from 0.0103 ± 0.0006 to 5.04 ± 0.02. The error bars represent one standard deviation. The measured data are compared to a theoretical plot based on the formulas (5.12,5.13). The results unequivocally certify quantum non-Gaussian character of the tested SPAD.

Similarly to quantum non-Gaussianity depth defined for single-photon states [160] we can ex-

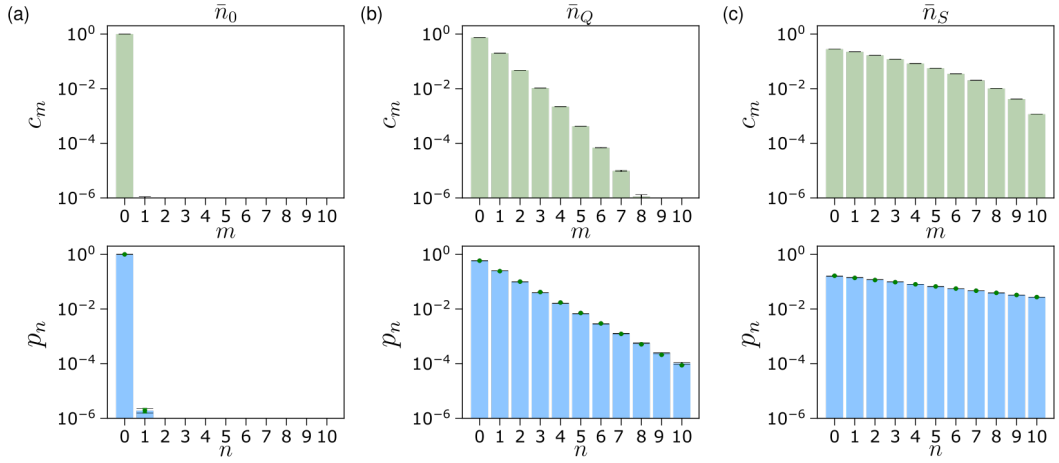

Figure 5.3: The experimentally generated optical thermal states and vacuum state with mean photon numbers: (a) $\bar{n}_0 = 1.9(4) \times 10^{-6}$, (b) $\bar{n}_Q = 0.6963 \pm 0.0005$, and (c) $\bar{n}_S = 5.043 \pm 0.001$.

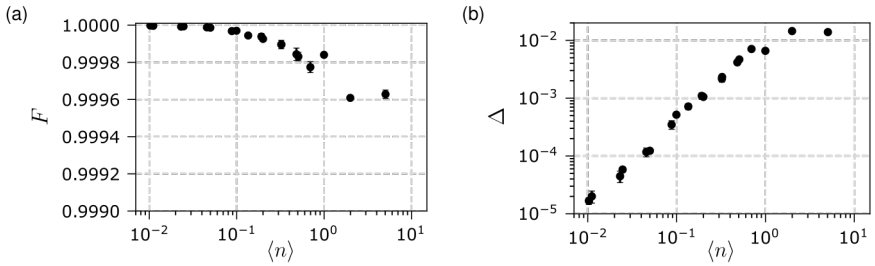

Figure 5.4: The discrepancy between the measured and the corresponding ideal photon statistics characterized by (a) fidelity F, and (b) the total variation distance Δ.

plore resilience of quantum non-Gausianity of the single-photon detector to its imperfections, such as loss and noise. Dark counts of the detector and background light are of main interest in many applications, such as quantum key distribution [558, 559] or mapping and counting single-photon emitters [C1, 96, 229]. The confirmation of quantum non-Gaussianity of the detector with injected background noise also certifies the quantum non-Gaussian character of the original detector without injected background light. The only assumption that we have to make is that the background light can be represented by a Gaussian state or a mixture of Gaussian states, which in the present case is ensured by the physical mechanism of background generation.

To emulate background noise, we drive an auxiliary laser diode, and superimpose incoherently the resulting Poisson signal with the probe thermal light. The background light and the probe thermal light propagate in different orthogonal spectral-temporal modes, because the two laser diodes emit at different central wavelengths 811 nm and 818 nm. Furthermore, while we adjust the time delays in the setup to ensure that the pulses from both diodes fit in the 20 ns coincidence window, we intentionally do not attempt to achieve precise temporal overlap of these two pulses. The background light effectively increases the probability of the dark counts of the detector R_D, and in our experiment we have probed the range of R_D from 0.005 to 0.58. Figure 5.7 shows the measured trajectory of the $[\tilde{P}_0', \tilde{Q}_0']$ pairs with increasing intensity of the noise for a fixed value of the probe mean photon number $\bar{n}_S = 1.0$. The data are compared to theoretical plots based on the formulas (5.12,5.13). As expected, the points move towards the boundary of the quantum

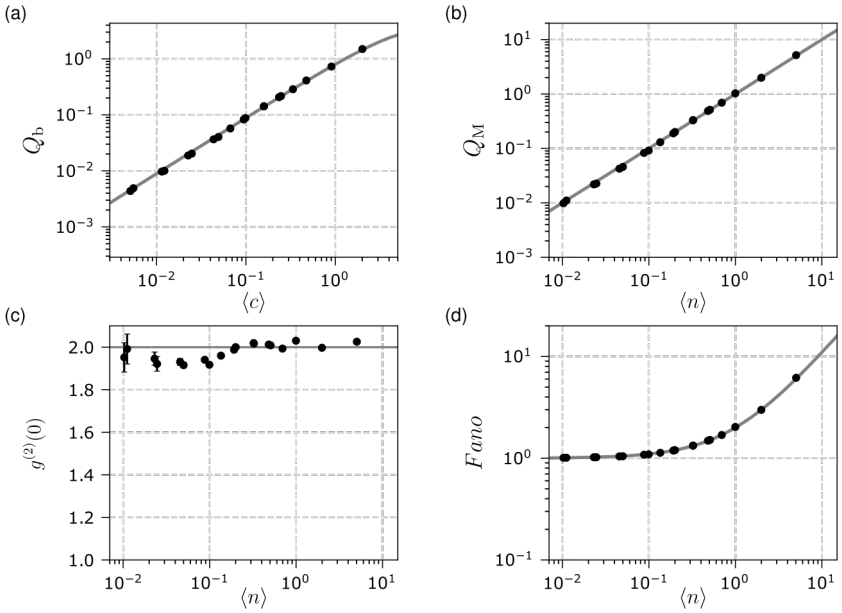

Figure 5.5: Characteristics of measured photon statistics: (a) the binomial parameter, (b) the Mandel parameter, (c) $g^2(0)$ function, and (d) *Fano* factor.

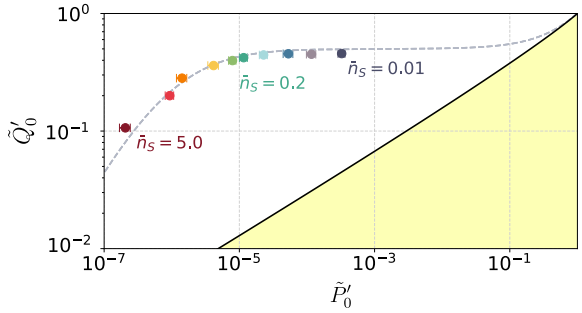

Figure 5.6: Quantum non-Gaussianity certification of single-photon avalanche diode for various mean photon numbers $\bar{n}_S$ of the probe thermal states. Measured data (markers) are compared to theoretical model (gray curve). Vertical error bars are smaller than data marker size. Quantum non-Gaussianity is certified for points lying outside the yellow area.

non-Gaussianity criterion and if the noise exceeds certain threshold, the quantum non-Gaussian character of the detector cannot be certified any more with the applied criterion.

Last but not least, we have unambiguously demonstrated Wigner function negativity of the characterized SPAD. The measured pairs $[\tilde{P}'_0, \tilde{Q}'_0]$ can be used also to certify negativity of Wigner function of the detector under test based on Eq. (5.18), see Figure 5.8. The negativity threshold is surpassed by 132 standard deviations for $\bar{n}_S = 0.0103 \pm 0.0006$, with $4\tilde{Q}'_0 - 3\tilde{P}'_0 - 1 = 0.824(7)$.

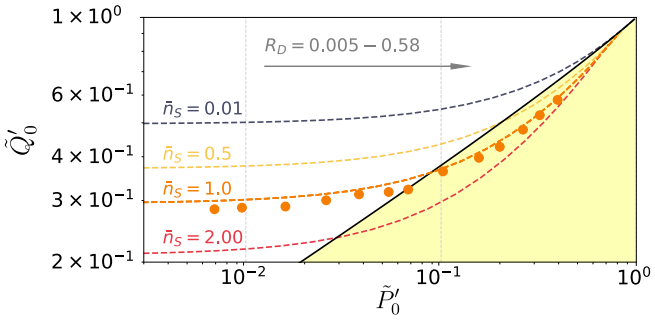

Figure 5.7: Quantum non-Gaussianity certification of single-photon avalanche diode for increased level of background noise and the particular value of the mean photon number $\bar{n}_S = 1.0$ of the probe thermal state. Background noise is emulated by injecting light to the detector during the certification and characterized by probability of false detection R_D. Measured data (markers) are compared to theoretical model (curve). For reference, the theoretical curves are plotted for 3 different values of $\bar{n}_S$. Error bars are smaller than data marker size. Quantum non-Gaussianity is certified for points lying outside the yellow area.

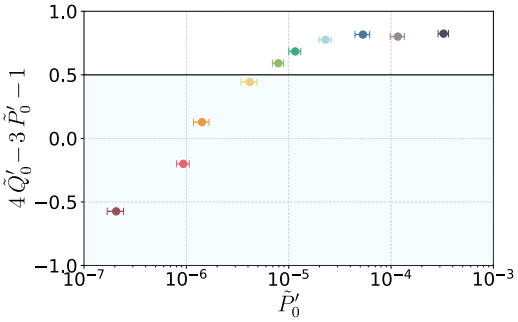

Figure 5.8: Certification of negativity of Wigner function of single-photon avalanche diode for various mean photon numbers $\bar{n}_S$ of the probe thermal states, color-coded similarly as in Figure 5.6. Vertical error bars are smaller than symbol size. Negativity of the Wigner function is certified when the threshold 0.5 is exceeded.

5.6 Summary and outlook

In Chapter 5 we have addressed the question whether the quantum non-Gaussian character of a quantum detector can be characterized more directly by performing measurements on suitably chosen probe states. We answer this question in affirmative and show that, interestingly, it may suffice to probe the detector with the vacuum state and two classical thermal states of different mean photon numbers, see Figure 5.1 (b).

Our procedure thus requires much less probe states than full quantum detector tomography [285, 449, 450, 452–456, 560, 561]. In our approach, the role of measurement and state is reversed with respect to the ordinary certification of quantum non-Gaussian character of quantum states. One specific feature of certification of quantum non-Gaussian character of some POVM element Π is that $\mathrm{Tr}[\Pi]$ need not be finite. We show that this obstacle can be circumvented by characterizing a suitably regularized POVM. Our method can serve for fast and direct testing and benchmarking of various detectors including single-photon detectors, photon-number-resolving detectors, or even more complex detection assemblies involving linear as well as nonlinear optical networks whose output is detected by several single-photon detectors.

We demonstrate the feasibility of the proposed certification method by verifying experimentally the quantum non-Gaussianity and the negativity of the Wigner function of single-photon avalanche diode for various mean photon numbers of the probe thermal states. We also explore the resilience of quantum non-Gaussianity of the single-photon detector to the presence of noise. Our procedure paves the way for direct benchmarking of photonic quantum detectors including single-photon detectors, photon-number-resolving detectors, or even more complex detection schemes where the signal is preprocessed by some quantum operation such as squeezing or amplification before being detected. Since our method is wavelength-independent, it can be also utilized to characterize detectors of microwave photons employed in cavity or circuit quantum electrodynamics [549–555]. One can try to follow the approach and adapt to quantum detectors other quantum non-Gaussianity or other non-classicality criteria, even those that are yet to be discovered in the future.

In this framework, we will aim to characterize our photon-number resolving detector based on spatially multiplexed binary detectors (Chapter 3.2). That would be the next logical step, therefore, in testing the robustness of the presented characterization method. We will also take considerable interest in attempts to modify the presented QNG certification protocol to avoid the vacuum probe state because of the significant required measurement time due to low probability of the measurement outcomes.

Chapter 6

Conclusions

Here, we will summarize the main contributions and significance of the presented results and findings. The goal of this Thesis was to design and develop a detection technique capable of photon-number resolution, a necessary condition for obtaining full information about of the photon statistics of unknown initial states of light. Subsequently, the presented photon-number-resolving detection technique was employed in various experiments to explore and modify the statistical properties of initial states of light, to simulate other physical systems for proof-of-principle tests in quantum information and thermodynamics, and to characterize quantum detectors. Above mentioned applications of photon-number-resolving detectors represent only a few examples of the wide range of interdisciplinary applicability of such advanced detection devices. The Thesis also covered a background in the research field of quantum state detection and generation, photon number distribution measurement, and quantum state characterization. Finally, here we will give a summary and reflection on the future extensions of the developed photon statistics measurement workflow.

6.1 Summary

In Chapter 3, a mesoscopic photon-number-resolving detector capable of detecting dozens of photons was designed and constructed. The developed photon-statistics sensor is based on spatial multiplexing in a reconfigurable optical network (Section 3.2). The tunability and balancing of the multiport network are performed by a tunable beam splitter cascade composed of a half-wave plate and a polarizing beam splitter allowing accurate adjustments of the splitting ratio. We use single-photon avalanche photodiodes to measure the multiplexed signal with the typical efficiency ranging from 55 to 70%, 250 ps timing jitter, and 25 ns recovery time. Different efficiencies of the SPADs are taken care of during balancing. The result is a balanced multiplex with optimized overall efficiency $\eta = 50(1)\%$. The dead time of the developed partially photon-number-resolving detector is given by the slowest single-photon detector, and the total jitter scales with the number of detection channels. Additionally, the multiport optical network of completely independent detection channels guarantees the absence of crosstalks.

The implemented detection device was completed with custom-built readout electronics to optimize its parameters and extend the functionality (Section 3.3). The electronic outputs of the SPADs need to be processed while keeping the individual channels synchronized. Two implementations of the coincidence circuit were designed and developed. First, the electronic outputs were summed by an analog coincidence circuit using linear fan-in/outs units or a passive RF summation

circuitry (Subsection 3.3.1). Each resulting $M + 1$ distinct voltage level corresponds to a particular number of m-fold coincidences. This output can be visualized and digitized using an oscilloscope operating in a memory-segmentation regime. Alternatively, a high-performance custom-built coincidence logic based on the emitter-coupled logic circuitry consisting of fast comparators, delay lines, and basic gates was developed (Subsection 3.3.2). The single-run output of a high-resolution coincidence system can be directly used for complex triggering or is counted and sorted in a coincidence histogram for repeated measurements by a microcontroller. The high performance and functionality of the developed coincidence counting unit is presented by a low propagation delay below 5 ns, the timing jitter of 10 ps, and virtually real-time classification of all possible detection events with full channel resolution.

As pointed out above, repeated measurements give rise to click statistics calculated from the stored coincidence histogram. In general, the developed photon-number-resolving detector can be adjusted to split the light equally to any number of detection channels, so there is no need to add or remove detectors physically. For example, the frequently used HBT type measurement could easily be configured using just two detector channels. For the presented experiments, the histogram was reduced to 11 elements corresponding to coincidence clicks of M detectors, with $0 \leq M \leq 10$. In the first instance, click statistics measurements were used to verify observable criteria characterizing the nature of the light directly. Namely, we investigated the behavior of the binomial Q_b parameter, which can serve as a witness of nonclassicality. Additionally, this parameter also quantified the quality of the preparation of all optical signals used in the Thesis. Achieved experimental results demonstrated that the click statistics measurements using a developed detector and coincidence unit are virtually free of systematic errors.

Furthermore, we employed the advanced quantum reconstruction algorithms to estimate the photon number distribution of the measured optical signal (Section 3.4). Theoretical analysis of the detector response allows numerically simulated click statistics of various states of light to be used for characterization of the reconstruction accuracy and convergence speed of the robust statistical reconstruction algorithms using Monte-Carlo simulations. Many efforts have been made to obtain the best possible faithful photon statistics retrieval coping with incomplete noisy data. Thus, the expectation-maximization-entropy algorithm using entropy regularization of the maximum-likelihood-based expectation-maximization technique was proposed to significantly improve the precision and stability of the reconstruction (Subsection 3.4.1). This efficient photon statistics retrieval algorithm overcomes the limitation of the finite number of detection channels. We demonstrated high-fidelity photon statistics measurement of dozens of photons of the various optical states such as coherent states, single and few-mode thermal states, and multi-photon quantum states (Section 3.5). The result opens new paths for optical technology by providing access to the photon-number information.

As one of many examples of the wide applicability of the photon-number-resolving detectors, we experimentally implemented two strategies of controlled modification of the statistical properties of light (Chapter 4). Both concepts involve thermal state generation, a photon-number-resolving detector, and both require a controlled multi-photon subtraction. First, the experimental procedure of subtraction of energy quanta from thermal light using a high-transmitivity beam splitter was implemented (Section 4.2). The subtraction of a given number of photons from a super-Poissonian light was analyzed. The l-photon subtracted single-mode thermal state was successfully generated for l up to 3. We provided the theoretical analysis and simulations of the multi-photon subtraction process under imperfect conditions such as beam-splitter reflectivity and non-unity detection efficiency. Notably, the effect of the beam-splitter reflectivity R on the resulting l-photon subtracted thermal state of light was investigated. Furthermore, in Section 4.2.3, we predicted and experimentally verified that a conditional subtraction of quanta from single-mode thermal state moves it sufficiently far from thermal equilibrium to reach available work larger than what can

be obtained by any cooling of thermal state, even up to a ground state. It also reaches mutual information close to a maximum of a single bit per pulse in an ideal communication scenario, if the out-of-equilibrium state is used as a letter of a binary alphabet. The procedure does not use any other source of energy. It is, therefore, energetically autonomous. Despite the increase of entropy by the subtraction of quanta, these noisy out-of-equilibrium states are, therefore applicable for merging quantum thermodynamics and information theory, and moreover, they can be directly translated to other experimental platforms like quantum optomechanics.

The achieved results motivated us to prepare a novel concept to prepare super-Poissonian states of light even deterministically (Section 4.3). We used the active optical feedforward control and swapping complemented by the complex triggering. We studied the theoretical multi-mode scenario of $N+1$ modes of single-mode thermal states and l-photon subtraction. This super-Poissonian light generator was analyzed in terms of mean photon number, $g^{(2)}$ function, *Fano*, and *MDR* as a function of the number of input modes N, subtracted photons l, and the beam-splitter reflectivity R. Unfortunately, manipulating a higher number of input modes is still experimentally challenging due to the complexity of the entire experimental apparatus and problematic mode discrimination. Thus, we experimentally verified the two-mode configuration with single-photon subtraction. To evaluate this out-of-equilibrium statistics of light, we consider a quantifier suitable for future experiments and thermodynamical evaluation. We assume that such light can deterministically excite a microscopic two-level quantum system from its ground state to the excited state beyond a thermal limit. The implemented advanced device allows us to experimentally investigate quantum photonic Maxwell's demon at a single-photon level. In this experiment, Maxwell's demon deterministically increases the energy in the single mode of light with decreasing photon correlation despite its super-Poissonian statistics. Broadly, our research stimulates the investigation of out-of-equilibrium statistics of bosons sufficient to fulfill the specific task and understand their thermodynamic characteristics.

The Thesis furthermore presented a direct experimental certification of the highly nonclassical character of the quantum optical detectors without the need for full quantum detector tomography (Section 5). The main principle of the presented approach is to reverse the role of state and measurement concerning the ordinary certification of quantum non-Gaussian character. An indisputable advantage of our method is that it allows direct benchmarking of photonic quantum detectors with a few measurements on classical probe states, namely two thermal states and vacuum state. Subsequently, a photon-number-resolving detector is a prerequisite for the precise calibration of the probe states. Our method is best suited for single-photon detectors, where the quantum non-Gaussianity (Subsection 5.2) or Wigner function negativity (Subsection 5.3) is implied by the lack of the vacuum term in the POVM element. First, we experimentally certified quantum non-Gaussianity of a single-photon avalanche diode for several different mean photon numbers of the probe thermal states without adding extra noise. In the second step, we investigated the robustness of our method under the presence of background noise. Additionally, our method can also be used to certify the negativity of the Wigner function of the detector under test. Also, instead of a simple single-photon detector such as an avalanche photodiode, one can characterize even a more complex detector such as a photon-number resolving detector or a detector where the signal is preprocessed by some quantum operation (such as squeezing or amplification, for example), before being detected.

6.2 Outlook and future prospects

We have presented measurement workflow which offers a practical solution for accurate photon-number detection of arbitrary optical signals. Furthermore, we will aim to substantially advance

photon statistics measurement by increasing the number of detection channels to a level where hundreds of photons can be detected. Nowadays, the generation, processing, and detection of quantum states of light are frequently realized by employing quantum photonic integrated circuits. In general, the technology of integrated quantum photonics enables to increase in the complexity of modern quantum experiments while maintaining the occupation of low-scale footprints. Since our method of arbitrary photon statistics measurement is multiplexed-detector-independent, it can be extended using versatile integrated platforms. Chip-based spatial multiplexed detector promises higher total efficiency boosted by superconducting nanowire detectors. Our photon statistics measurement approach can thus become a valid and practical alternative for advanced quantum state detection, multiple photon subtraction, and complex triggering in modern integrated quantum communications and simulations.

As a new spatial multiplexed detector will increase in complexity, the importance of precise coincidence counting techniques will also increase. We will aim to expand the developed electronic signal counting system to dozens of channels while keeping real-time operability. The key performances are fast and efficient multi-coincidence counting and storing, high counting rate, and time granularity. Ideally, these parameters should not be degraded at the expense of increasing the number of channels. Experience with some drawbacks of the coincidence unit designed and used in the Thesis triggered the evolution of the coincidence events processing concept. Subsequently, we will aim to increase the maximum speed of possible data rates in single-shot operation. Real-time analysis of multiple photon coincidence events can be employed in almost every modern quantum photonic application, such as quantum information processing, quantum computing, and simulating. Coincidence counters also represent enabling technology for many emerging biomedical imaging and particle-tracking techniques, such as positron emission tomography and fluorescence correlation spectroscopy.

Another subject of further research is the improvement of the reconstruction algorithm. Notably, we will study photon-statistics retrieval based on deep learning. Machine learning methods have previously proven to be a powerful tool in quantum state tomography. Our initial numerical analysis already shows an improvement in the accuracy of the reconstruction process. We will also aim to directly evaluate key quantities such as correlation functions and nonclassicality metrics rather than full tomography of the photon statistics. Such feature extraction can also cope with incomplete data and other experimental imperfections.

Following the scientific work dealing with the out-of-equilibrium states of light in thermodynamics, we will extend the presented concept of generating these states with more extraordinary super-Poisson statistics input states. It has been reported that thermal states of light with Bose-Einstein statistics are appropriate input states for statistical modification by photon subtraction to create out-of-equilibrium states of light. The benefits of their negative exponential statistics can be significantly overcome using heavy-tail distributions instead. Such particular types of states can be easily achieved by employing an arbitrary signal generator developed in Straka et al. [371].

In the near future, we will extend our investigation of the quantum non-Gaussian character to more complex POVM elements corresponding to an advanced class of detection devices such as photon-number-resolving detectors. One has to consider that the measurement with vacuum probe state on a coincidence basis is time-consuming. The challenge is to measure the output of the detector probing by a vacuum state to get a statistically significant number of m-fold coincidences. The higher element clicks of POVM for the vacuum state would be practically negligible, even on the measurement time scales of weeks. However, we can benefit from noise adding to overcome the achieved quantum non-Gaussianity certification limit of the POVM element. The noise is presented by the probability of dark counts well approximated by added coherent optical signal with photon number $\langle n \rangle$. We believe that we will verify the quantum non-Gaussian character of the highest POVM element up to date.

References

Books

B1 U. Leonhardt, *Measuring the quantum state of light*, (2003).

B2 C. Enss, ed., *Cryogenic particle detection*, (2005).

B3 M. Bellini, and A. Zavatta, *Manipulating light states by single-photon addition and subtraction*, (2010).

B4 A. Migdall, S. Polyakov, J. Fan, and J. Bienfang, *Single-photon generation and detection: physics and applications*, (2014).

B5 R. H. Hadfield, and G. Johansson, eds., *Superconducting devices in quantum optics*, (2016).

B6 K. Irwin, and G. Hilton, *Transition-edge sensors*, (2005).

B7 M. Paris, and Ř. Jaroslav, *Quantum state estimation*, (2004).

B8 J. Peřina, Z. Hradil, and B. Jurčo, *Quantum optics and fundamentals of physics*, (1994).

B9 A. N. Tikhonov, A. Goncharsky, V. V. Stepanov, and A. G. Yagola, *Numerical methods for the solution of ill-posed problems*, (1995).

B10 W. Feller, *On probability problems in the theory of counters*, (New York, 1948).

B11 C. R. Rao, and S. K. Mitra, *Generalized inverse of matrices and its applications*, (1971).

B12 C. R. Smith, and W. T. Grandy, eds., *Maximum-Entropy and Bayesian Methods in Inverse Problems*, (1985).

B13 G. F. Knoll, *Radiation detection and measurement*, (New York, 1989).

B14 R. L. Parker, *Geophysical Inverse Theory*, (1994).

B15 J. Peřina, *Coherence of light*, (1998).

B16 A. Ben-Israel, and T. N. E. Greville, *Generalized inverses – theory and applications*, (2003).

B17 R. J. Glauber, *Quantum theory of optical coherence*, (2006).

B18 M. A. Nielsen, and I. L. Chuang, *Quantum computation and quantum information*, (2009).

B19 R. Loudon, *The quantum theory of light*, (2010).

B20 R. D. Evans, *The atomic nucleus, applications of poisson statistics to some instruments used in nuclear physics*, (New York, 1955) Chap. 28.

B21 W. Greiner, L. Neise, and H. Stöcker, *Thermodynamics and statistical mechanics*, (1995).

B22 H. Leff, and A. F. Rex, eds., *Maxwell's demon 2 entropy, classical and quantum information, computing*, (2002).

Articles, proceedings and theses

1 H. Iams, and B. Salzberg, 'The secondary emission phototube', Proc. IRE **23** (1935).

2 V. Zworykin, G. Morton, and L. Malter, 'The secondary emission multiplier-a new electronic device', Proc. IRE **24** (1936).

3 L. Kubetsky, 'Multiple amplifier', Proc. IRE **25** (1937).

4 K. W. Ledingham, 'The development of detectors for use at low light levels', Contemp. Phys. **37** (1996).

5 C. Silberhorn, 'Detecting quantum light', Contemp. Phys. **48** (2007).

6 R. H. Hadfield, 'Single-photon detectors for optical quantum information applications', Nat. Photon. **3** (2009).

7 G. S. Buller, and R. J. Collins, 'Single-photon generation and detection', Meas. Sci. Technol. **21** (2009).

8 M. D. Eisaman, J. Fan, A. Migdall, and S. V. Polyakov, 'Invited review article: single-photon sources and detectors', Rev. Sci. Instrum. **82** (2011).

9 C. M. Natarajan, M. G. Tanner, and R. H. Hadfield, 'Superconducting nanowire single-photon detectors: physics and applications', Supercond. Sci. Technol. **25** (2012).

10 C. J. Chunnilall, I. P. Degiovanni, S. Kück, I. Müller, and A. G. Sinclair, 'Metrology of single-photon sources and detectors: a review', Opt. Eng. **53** (2014).

11 F. Ceccarelli, G. Acconcia, A. Gulinatti, M. Ghioni, I. Rech, and R. Osellame, 'Recent advances and future perspectives of single-photon avalanche diodes for quantum photonics applications', Adv. Quantum Technol. **4** (2020).

12 I. E. Zadeh, J. Chang, J. W. N. Los, S. Gyger, A. W. Elshaari, S. Steinhauer, S. N. Dorenbos, and V. Zwiller, 'Superconducting nanowire single-photon detectors: a perspective on evolution, state-of-the-art, future developments, and applications', Appl. Phys. Lett. **118** (2021).

13 C. Kurtsiefer, S. Mayer, P. Zarda, and H. Weinfurter, 'Stable solid-state source of single photons', Phys. Rev. Lett. **85** (2000).

14 A. Kuzmich, W. P. Bowen, A. D. Boozer, A. Boca, C. W. Chou, L.-M. Duan, and H. J. Kimble, 'Generation of nonclassical photon pairs for scalable quantum communication with atomic ensembles', Nature **423** (2003).

15 M. Hennrich, A. Kuhn, and G. Rempe, 'Transition from antibunching to bunching in cavity QED', Phys. Rev. Lett. **94** (2005).

16 J. S. Neergaard-Nielsen, B. M. Nielsen, C. Hettich, K. Mølmer, and E. S. Polzik, 'Generation of a superposition of odd photon number states for quantum information networks', Phys. Rev. Lett. **97** (2006).

17 E. A. Goldschmidt, M. D. Eisaman, J. Fan, S. V. Polyakov, and A. Migdall, 'Spectrally bright and broad fiber-based heralded single-photon source', Phys. Rev. A **78** (2008).

18 M. Assmann, F. Veit, M. Bayer, M. van der Poel, and J. M. Hvam, 'Higher-order photon bunching in a semiconductor microcavity', Science **325** (2009).

19 D. Elvira et al., 'Higher-order photon correlations in pulsed photonic crystal nanolasers', Phys. Rev. A **84** (2011).

20 G. Harder, T. J. Bartley, A. E. Lita, S. W. Nam, T. Gerrits, and C. Silberhorn, 'Single-mode parametric-down-conversion states with 50 photons as a source for mesoscopic quantum optics', Phys. Rev. Lett. **116** (2016).

21 G. Digeronimo, M. Petruzzella, S. Birindelli, R. Gaudio, S. F. Poor, F. van Otten, and A. Fiore, 'Integration of single-photon sources and detectors on GaAs', Photonics **3** (2016).

22 S. Khasminskaya et al., 'Fully integrated quantum photonic circuit with an electrically driven light source', Nat. Photon. **10** (2016).

23 T. Kiyohara, R. Okamoto, and S. Takeuchi, 'Realization of multiplexing of heralded single photon sources using photon number resolving detectors', Opt. Express **24** (2016).

24 F. Bodog, M. Mechler, M. Koniorczyk, and P. Adam, 'Optimization of multiplexed single-photon sources operated with photon-number-resolving detectors', Phys. Rev. A **102** (2020).

25 M. Engelkemeier, J. Sperling, J. Tiedau, S. Barkhofen, I. Dhand, M. B. Plenio, B. Brecht, and C. Silberhorn, 'Climbing the fock ladder: advancing multiphoton state generation', (2021).

26 M. Dakna, L. Knöll, and D.-G. Welsch, 'Quantum state engineering using conditional measurement on a beam splitter', Eur. Phys. J. D **3** (1998).

27 A. Zavatta, S. Viciani, and M. Bellini, 'Quantum-to-classical transition with single-photon-added coherent states of light', Science **306** (2004).

28 V. Parigi, A. Zavatta, M. Kim, and M. Bellini, 'Probing quantum commutation rules by addition and subtraction of single photons to/from a light field', Science **317** (2007).

29 V. Parigi, A. Zavatta, and M. Bellini, 'Manipulating thermal light states by the controlled addition and subtraction of single photons', Laser Phys. Lett. **5** (2008).

30 A. Zavatta, V. Parigi, M. Kim, and M. Bellini, 'The weird math of photon subtraction', Opt. Photonics News **20** (2009).

31 A. Allevi, A. Andreoni, M. Bondani, M. G. Genoni, and S. Olivares, 'Reliable source of conditional states from single-mode pulsed thermal fields by multiple-photon subtraction', Phys. Rev. A **82** (2010).

32 S. Wang, H.-y. Fan, and L.-y. Hu, 'Photon-number distributions of non-gaussian states generated by photon subtraction and addition', J. Opt. Soc. Am. B **29** (2012).

33 F. E. Becerra, J. Fan, and A. Migdall, 'Photon number resolution enables quantum receiver for realistic coherent optical communications', Nat. Photon. **9** (2014).

34 V. Švarc, M. Nováková, G. Mazin, and M. Ježek, 'Fully tunable and switchable coupler for photonic routing in quantum detection and modulation', Opt. Lett. **44** (2019).

35 K. G. Katamadze, G. V. Avosopiants, N. A. Bogdanova, Y. I. Bogdanov, and S. P. Kulik, 'Multimode thermal states with multiphoton subtraction: study of the photon-number distribution in the selected subsystem', Phys. Rev. A **101** (2020).

36 G. L. Zanin, M. J. Jacquet, M. Spagnolo, P. Schiansky, I. A. Calafell, L. A. Rozema, and P. Walther, 'Fiber-compatible photonic feed-forward with 99% fidelity', Opt. Express **29** (2021).

37 Z. BAY, 'Electron multiplier as an electron counting device', Nature **141** (1938).

38 D. H. Andrews, R. M. Milton, and W. DeSorbo, 'A fast superconducting bolometer', J. Opt. Soc. Am. **36** (1946).

39 R. J. McIntyre, 'Theory of microplasma instability in silicon', J. Appl. Phys. **32** (1961).

40 D. E. Groom, 'Silicon photodiode detection of bismuth germanate scintillation light', Nucl. Instrum. Methods Phys. Res. **219** (1984).

41 A. Peacock et al., 'Single optical photon detection with a superconducting tunnel junction', Nature **381** (1996).

42 S. Cova, M. Ghioni, A. Lacaita, C. Samori, and F. Zappa, 'Avalanche photodiodes and quenching circuits for single-photon detection', Appl. Opt. **35** (1996).

43 A. D. Semenov, G. N. Gol'tsman, and A. A. Korneev, 'Quantum detection by current carrying superconducting film', Physica C: Superconductivity **351** (2001).

44 S. Somani, S. Kasapi, K. Wilsher, W. Lo, R. Sobolewski, and G. Gol'tsman, 'New photon detector for device analysis: superconducting single-photon detector based on a hot electron effect', J. Vac. Sci. Technol. B: Nanotechnol. Microelectron. **19** (2001).

45 O. Haderka, M. Hamar, and J. P. Jr, 'Experimental multi-photon-resolving detector using a single avalanche photodiode', Eur. Phys. J. D **28**, 149–154 (2004).

46 S. Pellegrini et al., 'Design and performance of an InGaAs–InP single-photon avalanche diode detector', IEEE J. Quantum Electron. **42** (2006).

47 S. N. Dorenbos, E. M. Reiger, N. Akopian, U. Perinetti, V. Zwiller, T. Zijlstra, and T. M. Klapwijk, 'Superconducting single photon detectors with minimized polarization dependence', Appl. Phys. Lett. **93** (2008).

48 B. E. Kardynał, Z. L. Yuan, and A. J. Shields, 'An avalanche-photodiode-based photon-number-resolving detector', Nat. Photon. **2** (2008).

49 A. Divochiy et al., 'Superconducting nanowire photon-number-resolving detector at telecommunication wavelengths', Nat. Photon. **2** (2008).

50 E. A. Dauler, A. J. Kerman, B. S. Robinson, J. K. Yang, B. Voronov, G. Goltsman, S. A. Hamilton, and K. K. Berggren, 'Photon-number-resolution with sub-30-ps timing using multi-element superconducting nanowire single photon detectors', J. Mod. Opt. **56** (2009).

51 F. Marsili et al., 'Superconducting parallel nanowire detector with photon number resolving functionality', J. Mod. Opt. **56** (2009).

52 J. P. Sprengers et al., 'Waveguide superconducting single-photon detectors for integrated quantum photonic circuits', Appl. Phys. Lett. **99** (2011).

53 T. Gerrits, B. Calkins, N. Tomlin, A. E. Lita, A. Migdall, R. Mirin, and S. W. Nam, 'Extending single-photon optimized superconducting transition edge sensors beyond the single-photon counting regime', Opt. Express **20** (2012).

54 V. B. Verma, F. Marsili, S. Harrington, A. E. Lita, R. P. Mirin, and S. W. Nam, 'A three-dimensional, polarization-insensitive superconducting nanowire avalanche photodetector', Appl. Phys. Lett. **101** (2012).

55 D. Rosenberg, A. J. Kerman, R. J. Molnar, and E. A. Dauler, 'High-speed and high-efficiency superconducting nanowire single photon detector array', Opt. Express **21** (2013).

56 Z. Zhou, S. Jahanmirinejad, F. Mattioli, D. Sahin, G. Frucci, A. Gaggero, R. Leoni, and A. Fiore, 'Superconducting series nanowire detector counting up to twelve photons', Opt. Express **22** (2014).

57 H.-Y. Yin, H. Cai, R.-S. Cheng, Z. Xu, Z.-N. Jiang, J.-S. Liu, T.-F. Li, and W. Chen, 'Polarization independent superconducting nanowire detector with high-detection efficiency', Rare Metals **34** (2014).

58 P. Rath et al., 'Superconducting single-photon detectors integrated with diamond nanophotonic circuits', Light: Sci. Appl. **4** (2015).

59 M. K. Akhlaghi, E. Schelew, and J. F. Young, 'Waveguide integrated superconducting single-photon detectors implemented as near-perfect absorbers of coherent radiation', Nat. Commun. **6** (2015).

60 T. Gerrits, A. Lita, B. Calkins, and S. W. Nam, 'Superconducting transition edge sensors for quantum optics', in *Quantum science and technology* (2016).

61 J. Liu, Y. Li, L. Ding, Y. Wang, T. Zhang, Q. Wang, and J. Fang, 'Fast active-quenching circuit for free-running InGaAs(p)/InP single-photon avalanche diodes', IEEE J. Quantum Electron. **52** (2016).

62 A. Vetter et al., 'Cavity-enhanced and ultrafast superconducting single-photon detectors', Nano Lett. **16** (2016).

63 F. Mattioli, Z. Zhou, A. Gaggero, R. Gaudio, R. Leoni, and A. Fiore, 'Photon-counting and analog operation of a 24-pixel photon number resolving detector based on superconducting nanowires', Opt. Express **24** (2016).

64 X. Chen, C. Ding, H. Pan, K. Huang, J. Laurat, G. Wu, and E. Wu, 'Temporal and spatial multiplexed infrared single-photon counter based on high-speed avalanche photodiode', Sci. Rep. **7** (2017).

65 N. J. D. Martinez, M. Gehl, C. T. Derose, A. L. Starbuck, A. T. Pomerene, A. L. Lentine, D. C. Trotter, and P. S. Davids, 'Single photon detection in a waveguide-coupled ge-on-si lateral avalanche photodiode', Opt. Express **25** (2017).

66 E. E. Wollman et al., 'UV superconducting nanowire single-photon detectors with high efficiency, low noise, and 4 k operating temperature', Opt. Express **25** (2017).

67 R. Xu et al., 'Demonstration of polarization-insensitive superconducting nanowire single-photon detector with si compensation layer', J. Lightwave Technol. **35** (2017).

68 C. Cahall, K. L. Nicolich, N. T. Islam, G. P. Lafyatis, A. J. Miller, D. J. Gauthier, and J. Kim, 'Multi-photon detection using a conventional superconducting nanowire single-photon detector', Optica **4** (2017).

69 D. Zhu, Q.-Y. Zhao, H. Choi, T.-J. Lu, A. E. Dane, D. Englund, and K. K. Berggren, 'A scalable multi-photon coincidence detector based on superconducting nanowires', Nat. Nanotechnol. **13** (2018).

70 K. Zou, Y. Meng, Z. Wang, and X. Hu, 'Superconducting nanowire multi-photon detectors enabled by current reservoirs', Photon. Res. **8** (2020).

71 M. A. Wolff, S. Vogel, L. Splitthoff, and C. Schuck, 'Superconducting nanowire single-photon detectors integrated with tantalum pentoxide waveguides', Sci. Rep. **10** (2020).

72 M. Renna, A. Ruggeri, M. Sanzaro, F. Villa, F. Zappa, and A. Tosi, 'High detection rate fast-gated CMOS single-photon avalanche diode module', IEEE Photonics J. **12** (2020).

73 Y. Meng et al., 'Fractal superconducting nanowires detect infrared single photons with 84% system detection efficiency, 1.02 polarization sensitivity, and 20.8 ps timing resolution', ACS Photonics (2022).

74 M. Eaton, A. Hossameldin, R. J. Birrittella, P. M. Alsing, C. C. Gerry, C. Cuevas, H. Dong, and O. Pfister, 'Resolving 100 photons and quantum generation of unbiased random numbers', (2022).

75 J. Wu, Y. Liu, B. Zhang, X. Jin, Y. Wang, H. Wang, and X. Yang, 'A benchmark test of boson sampling on tianhe-2 supercomputer', Natl. Sci. Rev. **5** (2018).

76 H. Wang et al., 'Boson sampling with 20 input photons and a 60-mode interferometer in a 10^{14}-dimensional hilbert space', Phys. Rev. Lett. **123** (2019).

77 D. J. Brod, E. F. Galvão, A. Crespi, R. Osellame, N. Spagnolo, and F. Sciarrino, 'Photonic implementation of boson sampling: a review', Adv. Photonics **1** (2019).

78 H. Wang et al., 'Boson sampling with 20 input photons and a 60-mode interferometer in a 1014–dimensional hilbert space', Phys. Rev. Lett. **123** (2019).

79 H.-S. Zhong et al., 'Quantum computational advantage using photons', Science **370** (2020).

80 J. C. F. Matthews, A. Politi, A. Stefanov, and J. L. O'Brien, 'Manipulation of multiphoton entanglement in waveguide quantum circuits', Nature Photon. **3** (2009).

81 X.-C. Yao et al., 'Observation of eight-photon entanglement', Nat. Photon. **6** (2012).

82 X.-L. Wang et al., 'Experimental ten-photon entanglement', Phys. Rev. Lett. **117** (2016).

83 N. Zhou et al., 'Sine wave gating silicon single-photon detectors for multiphoton entanglement experiments', Rev. Sci. Instrum. **88** (2017).

84 J. Wang et al., 'Multidimensional quantum entanglement with large-scale integrated optics', Science **360** (2018).

85 D. Llewellyn et al., 'Chip-to-chip quantum teleportation and multi-photon entanglement in silicon', Nat. Phys. **16** (2019).

86 F. Flamini, N. Spagnolo, and F. Sciarrino, 'Photonic quantum information processing: a review', Rep. Prog. Phys. **82** (2018).

87 S. Slussarenko, and G. J. Pryde, 'Photonic quantum information processing: a concise review', Appl. Phys. Rev. **6** (2019).

88 E. Lavie, I. W. Primaatmaja, W. Y. Kon, C. Wang, and C. C. W. Lim, 'Estimating the photon-number distribution of photonic channels for realistic devices and applications in photonic quantum information processing', Phys. Rev. Appl. **16** (2021).

89 K. J. Gordon, V. Fernandez, G. S. Buller, I. Rech, S. D. Cova, and P. D. Townsend, 'Quantum key distribution system clocked at 2 GHz', Opt. Express **13** (2005).

90 X. Michalet, O. H. W. Siegmund, J. V. Vallerga, P. Jelinsky, J. E. Millaud, and S. Weiss, 'Detectors for single-molecule fluorescence imaging and spectroscopy', J. Mod. Opt. **54** (2007).

91 A. Pifferi et al., 'Time-resolved diffuse reflectance using small source-detector separation and fast single-photon gating', Phys. Rev. Lett. **100** (2008).

92 L. Lydersen, C. Wiechers, C. Wittmann, D. Elser, J. Skaar, and V. Makarov, 'Hacking commercial quantum cryptography systems by tailored bright illumination', Nat. Photon. **4** (2010).

93 P. Eraerds, M. Legre, J. Zhang, H. Zbinden, and N. Gisin, 'Photon counting OTDR: advantages and limitations', J. Lightwave Technol. **28** (2010).

94 V. Giovannetti, S. Lloyd, and L. Maccone, 'Advances in quantum metrology', Nat. Photon. **5** (2011).

95 K. R. Motes, J. P. Olson, E. J. Rabeaux, J. P. Dowling, S. J. Olson, and P. P. Rohde, 'Linear optical quantum metrology with single photons: exploiting spontaneously generated entanglement to beat the shot-noise limit', Phys. Rev. Lett. **114** (2015).

96 H. Ta et al., 'Mapping molecules in scanning far-field fluorescence nanoscopy', Nat. Commun. **6** (2015).

97 J. Sabines-Chesterking et al., 'Sub-shot-noise transmission measurement enabled by active feed-forward of heralded single photons', Phys. Rev. Appl. **8** (2017).

98 R. Whittaker, C. Erven, A. Neville, M. Berry, J. L. O'Brien, H. Cable, and J. C. F. Matthews, 'Absorption spectroscopy at the ultimate quantum limit from single-photon states', New J. Phys. **19** (2017).

99 A. Boaron et al., 'Secure quantum key distribution over 421 km of optical fiber', Phys. Rev. Lett. **121** (2018).

100 J. Sabines-Chesterking, A. R. McMillan, P. A. Moreau, S. K. Joshi, S. Knauer, E. Johnston, J. G. Rarity, and J. C. F. Matthews, 'Twin-beam sub-shot-noise raster-scanning microscope', Opt. Express **27** (2019).

101 A. Stanco, D. G. Marangon, G. Vallone, S. Burri, E. Charbon, and P. Villoresi, 'Efficient random number generation techniques for CMOS single-photon avalanche diode array exploiting fast time tagging units', Phys. Rev. Research **2** (2020).

102 E. M. Fisher, 'Principles and early historical development of silicon avalanche and geiger-mode photodiodes', in *Photon counting - fundamentals and applications* (2018).

103 H. Paul, P. Törmä, T. Kiss, and I. Jex, 'Photon chopping: new way to measure the quantum state of light', Phys. Rev. Lett. **76** (1996).

104 K. Banaszek, and I. A. Walmsley, 'Photon counting with a loop detector', Opt. Lett. **28** (2003).

105 P. Eraerds, M. Legré, A. Rochas, H. Zbinden, and N. Gisin, 'SiPM for fast photon-counting and multiphoton detection', Opt. Express **15** (2007).

106 E. Grigoriev, A. Akindinov, M. Breitenmoser, S. Buono, E. Charbon, C. Niclass, I. Desforges, and R. Rocca, 'Silicon photomultipliers and their bio-medical applications', Nucl. Instrum. Methods Phys. Res. Section A: Accelerators, Spectrometers, Detectors and Associated Equipment **571** (2007).

107 M. Ramilli, A. Allevi, V. Chmill, M. Bondani, M. Caccia, and A. Andreoni, 'Photon-number statistics with silicon photomultipliers', J. Opt. Soc. Am. B **27** (2010).

108 A. Allevi, and M. Bondani, 'Direct detection of super-thermal photon-number statistics in second-harmonic generation', Opt. Lett. **40** (2015).

109 J. Tiedau, E. Meyer-Scott, T. Nitsche, S. Barkhofen, T. J. Bartley, and C. Silberhorn, 'A high dynamic range optical detector for measuring single photons and bright light', Opt. Express **27** (2019).

110 J. C. Matthews, X.-Q. Zhou, H. Cable, P. J. Shadbolt, D. J. Saunders, G. A. Durkin, G. J. Pryde, and J. L. O'Brien, 'Towards practical quantum metrology with photon counting', npj Quantum Inf. **2** (2016).

111 S. Slussarenko, M. M. Weston, H. M. Chrzanowski, L. K. Shalm, V. B. Verma, S. W. Nam, and G. J. Pryde, 'Unconditional violation of the shot-noise limit in photonic quantum metrology', Nat. Photon. **11** (2017).

112 J. Wang, F. Sciarrino, A. Laing, and M. G. Thompson, 'Int. phot. quantum technol.', **14** (2019).

113 C. Bruschini, H. Homulle, I. M. Antolovic, S. Burri, and E. Charbon, 'Single-photon avalanche diode imagers in biophotonics: review and outlook', Light: Sci. Appl. **8** (2019).

114 M. Cattaneo, M. G. A. Paris, and S. Olivares, 'Hybrid quantum key distribution using coherent states and photon-number-resolving detectors', Phys. Rev. A **98** (2018).

115 D. Sahin et al., 'Waveguide photon-number-resolving detectors for quantum photonic integrated circuits', Appl. Phys. Lett. **103** (2013).

116 F. Najafi et al., 'On-chip detection of non-classical light by scalable integration of single-photon detectors', Nat. Commun. **6** (2015).

117 C. Schuck, X. Guo, L. Fan, X. Ma, M. Poot, and H. X. Tang, 'Quantum interference in heterogeneous superconducting-photonic circuits on a silicon chip', Nat. Commun. **7** (2016).

118 R. Heilmann, J. Sperling, A. Perez-Leija, M. Gräfe, M. Heinrich, S. Nolte, W. Vogel, and A. Szameit, 'Harnessing click detectors for the genuine characterization of light states', Sci. Rep. **6** (2016).

119 P. Vines, K. Kuzmenko, J. Kirdoda, D. C. S. Dumas, M. M. Mirza, R. W. Millar, D. J. Paul, and G. S. Buller, 'High performance planar germanium-on-silicon single-photon avalanche diode detectors', Nat. Commun. **10** (2019).

120 S. Buckley, A. Tait, J. Chiles, A. McCaughan, S. Khan, R. Mirin, S. Nam, and J. Shainline, 'Integrated-photonic characterization of single-photon detectors for use in neuromorphic synapses', Phys. Rev. Appl. **14** (2020).

121 L. Lachman, and R. Filip, 'Quantum non-gaussianity of light and atoms', Prog. Quantum Electron. (2022).

122 U. Chabaud, P.-E. Emeriau, and F. Grosshans, 'Witnessing wigner negativity', Quantum **5** (2021).

123 M. Walschaers, V. Parigi, and N. Treps, 'Practical framework for conditional non-gaussian quantum state preparation', PRX Quantum **1** (2020).

124 E. Knill, R. Laflamme, and G. J. Milburn, 'A scheme for efficient quantum computation with linear optics', Nature **409** (2001).

125 C. Simon, H. de Riedmatten, M. Afzelius, N. Sangouard, H. Zbinden, and N. Gisin, 'Quantum repeaters with photon pair sources and multimode memories', Phys. Rev. Lett. **98** (2007).

126 D. T. Smithey, M. Beck, M. G. Raymer, and A. Faridani, 'Measurement of the wigner distribution and the density matrix of a light mode using optical homodyne tomography: application to squeezed states and the vacuum', Phys. Rev. Lett. **70** (1993).

127 M. Munroe, D. Boggavarapu, M. E. Anderson, and M. G. Raymer, 'Photon-number statistics from the phase-averaged quadrature-field distribution: theory and ultrafast measurement', Phys. Rev. A **52** (1995).

128 M. G. Raymer, J. Cooper, H. J. Carmichael, M. Beck, and D. T. Smithey, 'Ultrafast measurement of optical-field statistics by dc-balanced homodyne detection', J. Opt. Soc. Am. B **12** (1995).

129 H. Hansen, T. Aichele, C. Hettich, P. Lodahl, A. I. Lvovsky, J. Mlynek, and S. Schiller, 'Ultrasensitive pulsed, balanced homodyne detector: application to time-domain quantum measurements', Opt. Lett. **26** (2001).

130 A. Zavatta, F. Marin, and G. Giacomelli, 'Quantum-state reconstruction of a squeezed laser field by self-homodyne tomography', Phys. Rev. A **66** (2002).

131 J. Wenger, R. Tualle-Brouri, and P. Grangier, 'Pulsed homodyne measurements of femtosecond squeezed pulses generated by single-pass parametric deamplification', Opt. Lett. **29** (2004).

132 A. I. Lvovsky, and M. G. Raymer, 'Continuous-variable optical quantum-state tomography', Rev. Mod. Phys. **81** (2009).

133 G. M. D'Ariano, and M. G. A. Paris, 'Adaptive quantum homodyne tomography', Phys. Rev. A **60** (1999).

134 K. Banaszek, G. M. D'Ariano, M. G. A. Paris, and M. F. Sacchi, 'Maximum-likelihood estimation of the density matrix', Phys. Rev. A **61** (1999).

135 A. I. Lvovsky, 'Iterative maximum-likelihood reconstruction in quantum homodyne tomography', J. Opt. B: Quantum Semiclass. Opt. **6** (2004).

136 J. Řeháček, Z. Hradil, and M. Ježek, 'Iterative algorithm for reconstruction of entangled states', Phys. Rev. A **63** (2001).

137 D. Gross, Y.-K. Liu, S. T. Flammia, S. Becker, and J. Eisert, 'Quantum state tomography via compressed sensing', Phys. Rev. Lett. **105** (2010).

138 L. Mandel, 'Sub-poissonian photon statistics in resonance fluorescence', Opt. Lett. **4** (1979).

139 R. Short, and L. Mandel, 'Observation of sub-poissonian photon statistics', Phys. Rev. Lett. **51** (1983).

140 R. S. Bondurant, P. Kumar, J. H. Shapiro, and M. M. Salour, 'Photon-counting statistics of pulsed light sources', **7** (1982).

141 H. Lee, U. Yurtsever, P. Kok, G. M. Hockney, C. Adami, S. L. Braunstein, and J. P. Dowling, 'Towards photostatistics from photon-number discriminating detectors', J. Mod. Opt. **51** (2004).

142 E. Waks, E. Diamanti, B. C. Sanders, S. D. Bartlett, and Y. Yamamoto, 'Direct observation of nonclassical photon statistics in parametric down-conversion', Phys. Rev. Lett. **92** (2004).

143 D. Achilles, C. Silberhorn, and I. A. Walmsley, 'Direct, loss-tolerant characterization of nonclassical photon statistics', Phys. Rev. Lett. **97** (2006).

144 G. Brida, M. Genovese, F. Piacentini, and M. G. A. Paris, 'Joint multipartite photon statistics by on/off detection', Opt. Lett. **31** (2006).

145 K. Laiho, M. Avenhaus, K. N. Cassemiro, and C. Silberhorn, 'Direct probing of the wigner function by time-multiplexed detection of photon statistics', New J. Phys. **11** (2009).

146 A. Kurz, J. J. Schmied, K. S. Grußmayer, P. Holzmeister, P. Tinnefeld, and D.-P. Herten, 'Counting fluorescent dye molecules on DNA origami by means of photon statistics', Small **9** (2013).

147 K. Wakui et al., 'Ultrabroadband direct detection of nonclassical photon statistics at telecom wavelength', Sci. Rep. **4** (2014).

148 G. Harder, D. Mogilevtsev, N. Korolkova, and C. Silberhorn, 'Tomography by noise', Phys. Rev. Lett. **113** (2014).

149 J. L. Habif, A. Jagannathan, S. Gartenstein, P. Amory, and S. Guha, 'Quantum-limited discrimination of laser light and thermal light', Opt. Express **29** (2021).

150 G. S. Thekkadath, S. Sempere-Llagostera, B. A. Bell, R. B. Patel, M. S. Kim, and I. A. Walmsley, 'Single-shot discrimination of coherent states beyond the standard quantum limit', Opt. Lett. **46** (2021).

151 V. N. Starkov, A. A. Semenov, and H. V. Gomonay, 'Numerical reconstruction of photon-number statistics from photocounting statistics: regularization of an ill-posed problem', Phys. Rev. A **80** (2009).

152 S. Wallentowitz, and W. Vogel, 'Unbalanced homodyning for quantum state measurements', Phys. Rev. A **53** (1996).

153 K. Banaszek, C. Radzewicz, K. Wódkiewicz, and J. S. Krasiński, 'Direct measurement of the wigner function by photon counting', Phys. Rev. A **60** (1999).

154 M. Bondani, A. Allevi, and A. Andreoni, 'Wigner function of pulsed fields by direct detection', Opt. Lett. **34** (2009).

155 A. Allevi, S. Olivares, and M. Bondani, 'Manipulating the non-gaussianity of phase-randomized coherent states', Opt. Express **20** (2012).

156 M. Bina, A. Allevi, M. Bondani, and S. Olivares, 'Homodyne-like detection for coherent state-discrimination in the presence of phase noise', Opt. Express **25** (2017).

157 E. Losero, I. Ruo-Berchera, A. Meda, A. Avella, and M. Genovese, 'Unbiased estimation of an optical loss at the ultimate quantum limit with twin-beams', Sci. Rep. **8** (2018).

158 L. Lachman, I. Straka, J. Hloušek, and R. F. Miroslav Ježek and, 'Faithful hierarchy of genuine n-photon quantum non-gaussian light', Phys. Rev. Lett. **123** (2019).

159 A. Ourjoumtsev, R. Tualle-Brouri, J. Laurat, and P. Grangier, 'Generating optical schrödinger kittens for quantum information processing', Science **312** (2006).

160 I. Straka et al., 'Quantum non-gaussian depth of single-photon states', Phys. Rev. Lett. **113** (2014).

161 A. Zavatta, V. Parigi, M. S. Kim, and M. Bellini, 'Subtracting photons from arbitrary light fields: experimental test of coherent state invariance by single-photon annihilation', New J. Phys. **10** (2008).

162 Y. Zhai et al., 'Photon-number-resolved detection of photon-subtracted thermal light', Opt. Lett. **38** (2013).

163 M. A. Wayne, and P. G. Kwiat, 'Low-bias high-speed quantum random number generator via shaped optical pulses', Opt. Express **18** (2010).

164 M. Fürst, H. Weier, S. Nauerth, D. G. Marangon, C. Kurtsiefer, and H. Weinfurter, 'High speed optical quantum random number generation', Opt. Express **18** (2010).

165 G. Vallone et al., 'Adaptive real time selection for quantum key distribution in lossy and turbulent free-space channels', Phys. Rev. A **91** (2015).

166 M. Stipčević, and R. Ursin, 'An on-demand optical quantum random number generator with in-future action and ultra-fast response', Sci. Rep. **5** (2015).

167 X. Ma, X. Yuan, Z. Cao, B. Qi, and Z. Zhang, 'Quantum random number generation', npj Quantum Inf. **2** (2016).

168 V. C. Spanoudaki, A. B. Mann, A. N. Otte, I. Konorov, I. Torres-Espallardo, S. Paul, and S. I. Ziegler, 'Use of single photon counting detector arrays in combined PET/MR: characterization of LYSO-SiPM detector modules and comparison with a LSO-APD detector', J. Instrum. **2** (2007).

169 U. Lieberwirth et al., 'Multiplex dye DNA sequencing in capillary gel electrophoresis by diode laser-based time-resolved fluorescence detection', Anal. Chem. **70** (1998).

170 J.-P. Knemeyer, N. Marmé, and M. Sauer, 'Probes for detection of specific DNA sequences at the single-molecule level', Anal. Chem. **72** (2000).

171 D. N. Gavrilov et al., 'Dynamic range of fluorescence detection and base-calling accuracy in DNA sequencer based on single-photon counting', Electrophoresis **24** (2003).

172 I. Rech, A. Restelli, S. Cova, M. Ghioni, M. Chiari, and M. Cretich, 'Microelectronic photosensors for genetic diagnostic microsystems', Sens. Actuator. B: Chem. **100** (2004).

173 T. Isoshima, Y. Isojima, K. Hakomori, K. Kikuchi, K. Nagai, and H. Nakagawa, 'Ultrahigh sensitivity single-photon detector using a si avalanche photodiode for the measurement of ultraweak biochemiluminescence', Rev. Sci. Instrum. **66** (1995).

174 S. Weiss, 'Fluorescence spectroscopy of single biomolecules', Science **283** (1999).

175 I. Rech, G. Luo, M. Ghioni, H. Yang, X. Xie, and S. Cova, 'Photon-timing detector module for single-molecule spectroscopy with 60-ps resolution', IEEE J. Sel. Top. Quantum Electron. **10** (2004).

176 M. Wahl, F. Koberling, M. Patting, and E. H. Rahn, 'Time-resolved confocal fluorescence imaging and spectrocopy system with single molecule sensitivity and sub-micrometer resolution', Curr. Pharm. Biotechnol. **5** (2004).

177 M. Gösch et al., 'Parallel single molecule detection with a fully integrated single-photon 2x2 CMOS detector array', J. Biomed. Opt. **9** (2004).

178 J. R. Lakowicz, 'Single-molecule detection', in *Principles of fluorescence spectroscopy* (2006).

179 A. J. Berglund, A. C. Doherty, and H. Mabuchi, 'Photon statistics and dynamics of fluorescence resonance energy transfer', Phys. Rev. Lett. **89** (2002).

180 K. Suhling, P. M. W. French, and D. Phillips, 'Time-resolved fluorescence microscopy', Photochem. Photobiol. Sci. **4** (2005).

181 S. Felekyan, R. Kühnemuth, V. Kudryavtsev, C. Sandhagen, W. Becker, and C. A. M. Seidel, 'Full correlation from picoseconds to seconds by time-resolved and time-correlated single photon detection', Rev. Sci. Instrum. **76** (2005).

182 G. Brida, M. Genovese, and I. R. Berchera, 'Experimental realization of sub-shot-noise quantum imaging', Nat. Photon. **4** (2010).

183 P.-A. Moreau, E. Toninelli, T. Gregory, and M. J. Padgett, 'Imaging with quantum states of light', Nat. Rev. Phys. **1** (2019).

184 M. A. Taylor, J. Janousek, V. Daria, J. Knittel, B. Hage, H.-A. Bachor, and W. P. Bowen, 'Biological measurement beyond the quantum limit', Nat. Photon. **7** (2013).

185 A. L. Lacaita, G. Riparmonti, P. A. Francese, and S. D. Cova, 'Single-photon optical-time-domain reflectometer at 13 μm with 5-cm resolution and high sensitivity', Opt. Lett. **18** (1993).

186 F. Scholder, J.-D. Gautier, M. Wegmüller, and N. Gisin, 'Long-distance OTDR using photon counting and large detection gates at telecom wavelength', Opt. Commun. **213** (2002).

187 M. Wegmuller, F. Scholder, and N. Gisin, 'Photon-counting OTDR for local birefringence and fault analysis in the metro environment', J. Lightwave Technol. **22** (2004).

188 C. Schuck, W. H. P. Pernice, X. Ma, and H. X. Tang, 'Optical time domain reflectometry with low noise waveguide-coupled superconducting nanowire single-photon detectors', Appl. Phys. Lett. **102** (2013).

189 D. A. Kalashnikov, A. V. Paterova, S. P. Kulik, and L. A. Krivitsky, 'Infrared spectroscopy with visible light', Nat. Photon. **10** (2016).

190 M. K. Akhlaghi, A. H. Majedi, and J. S. Lundeen, 'Nonlinearity in single photon detection: modeling and quantum tomography', Opt. Express **19** (2011).

191 J. Hlousek, I. Straka, and M. Jezek, *Experimental observation of anomalous supralinear response of single-photon detectors*, 2021.

192 Z. Cheng, X. Zheng, D. Palubiak, M. J. Deen, and H. Peng, 'A comprehensive and accurate analytical SPAD model for circuit simulation', IEEE T. Electron Dev. **63** (2016).

193 S. Cova, A. Lacaita, and G. Ripamonti, 'Trapping phenomena in avalanche photodiodes on nanosecond scale', IEEE Electron Dev. Lett. **12** (1991).

194 K. E. Jensen et al., 'Afterpulsing in geiger-mode avalanche photodiodes for 1.06μm wavelength', Appl. Phys. Lett. **88** (2006).

195 M. Fujiwara et al., 'Afterpulse-like phenomenon of superconducting single photon detector in high speed quantum key distribution system', Opt. Express **19** (2011).

196 V. Burenkov, H. Xu, B. Qi, R. H. Hadfield, and H.-K. Lo, 'Investigations of afterpulsing and detection efficiency recovery in superconducting nanowire single-photon detectors', J. Appl. Phys. **113** (2013).

197 J. Münzberg, A. Vetter, F. Beutel, W. Hartmann, S. Ferrari, W. H. P. Pernice, and C. Rockstuhl, 'Superconducting nanowire single-photon detector implemented in a 2d photonic crystal cavity', Optica **5** (2018).

198 G. Humer, M. Peev, C. Schaeff, S. Ramelow, M. Stipcevic, and R. Ursin, 'A simple and robust method for estimating afterpulsing in single photon detectors', J. Lightwave Technol. **33** (2015).

199 A. W. Ziarkash, S. K. Joshi, M. Stipčević, and R. Ursin, 'Comparative study of afterpulsing behavior and models in single photon counting avalanche photo diode detectors', Sci. Rep. **8** (2018).

200 S. V. Polyakov, and A. L. Migdall, 'High accuracy verification of a correlated-photon- based method for determining photoncounting detection efficiency', Opt. Express **15** (2007).

201 M. Ware, A. Migdall, J. C. Bienfang, and S. V. Polyakov, 'Calibrating photon-counting detectors to high accuracy: background and deadtime issues', J. Mod. Opt. **54** (2007).

202 I. Straka, J. Grygar, J. Hlousek, and M. Jezek, 'Counting statistics of actively quenched SPADs under continuous illumination', J. Lightwave Technol. **38** (2020).

203 B. Cabrera, R. M. Clarke, P. Colling, A. J. Miller, S. Nam, and R. W. Romani, 'Detection of single infrared, optical, and ultraviolet photons using superconducting transition edge sensors', Appl. Phys. Lett. **73** (1998).

204 J. Kim, S. Takeuchi, Y. Yamamoto, and H. H. Hogue, 'Multiphoton detection using visible light photon counter', Appl. Phys. Lett. **74** (1999).

205 D. Rosenberg, A. Lita, A. Miller, and S. Nam, 'Noise-free high-efficiency photon-number-resolving detectors', Phys. Rev. A **71** (2005).

206 M. Fujiwara, and M. Sasaki, 'Photon-number-resolving detection at a telecommunications wavelength with a charge-integration photon detector', Opt. Lett. **31** (2006).

207 M. Huber et al., 'DC SQUID series array amplifiers with 120 MHz bandwidth', IEEE Trans. Appl. Supercond. **11** (2001).

208 D. V. Reddy, R. R. Nerem, S. W. Nam, R. P. Mirin, and V. B. Verma, 'Superconducting nanowire single-photon detectors with 98% system detection efficiency at 1550 nm', Optica **7** (2020).

209 J. Chang et al., 'Detecting telecom single photons with 99.5-2.07+0.5% system detection efficiency and high time resolution', APL Photonics **6** (2021).

210 F. Marsili, F. Najafi, E. Dauler, F. Bellei, X. Hu, M. Csete, R. J. Molnar, and K. K. Berggren, 'Single-photon detectors based on ultranarrow superconducting nanowires', Nano Lett. **11** (2011).

211 C. Gu, Y. Cheng, X. Zhu, and X. Hu, 'Fractal-inspired, polarization-insensitive superconducting nanowire single-photon detectors', in Adv. photonics 2015 (2015).

212 A. Mukhtarova et al., 'Polarization-insensitive fiber-coupled superconducting-nanowire single photon detector using a high-index dielectric capping layer', Opt. Express **26** (2018).

213 T. Gerrits et al., 'On-chip, photon-number-resolving, telecommunication-band detectors for scalable photonic information processing', Phys. Rev. A **84** (2011).

214 W. Pernice, C. Schuck, O. Minaeva, M. Li, G. Goltsman, A. Sergienko, and H. Tang, 'High-speed and high-efficiency travelling wave single-photon detectors embedded in nanophotonic circuits', Nat. Commun. **3** (2012).

215 B. Calkins et al., 'High quantum-efficiency photon-number-resolving detector for photonic on-chip information processing', Opt. Express **21** (2013).

216 G. Zambra, A. Andreoni, M. Bondani, M. Gramegna, M. Genovese, G. Brida, A. Rossi, and M. G. A. Paris, 'Experimental reconstruction of photon statistics without photon counting', Phys. Rev. Lett. **95** (2005).

217 G. Zambra, and M. G. A. Paris, 'Reconstruction of photon-number distribution using low-performance photon counters', Phys. Rev. A **74** (2006).

218 M. Genovese, M. Gramegna, G. Brida, M. Bondani, G. Zambra, A. Andreoni, A. R. Rossi, and M. G. A. Paris, 'Measuring the photon distribution with ON/OFF photodetectors', Laser Phys. **16** (2006).

219 L. Dovrat, M. Bakstein, D. Istrati, A. Shaham, and H. S. Eisenberg, 'Measurements of the dependence of the photon-number distribution on the number of modes in parametric down-conversion', Opt. Express **20** (2012).

220 W. Schmunk et al., 'Photon number statistics of NV centre emission', Metrologia **49** (2012).

221 N. Sridhar, R. Shahrokhshahi, A. J. Miller, B. Calkins, T. Gerrits, A. Lita, S. W. Nam, and O. Pfister, 'Direct measurement of the wigner function by photon-number-resolving detection', J. Opt. Soc. Am. B **31** (2014).

222 S. Olivares, A. Allevi, G. Caiazzo, M. G. A. Paris, and M. Bondani, 'Quantum tomography of light states by photon-number-resolving detectors', New J. Phys. **21** (2019).

223 T. Kiesel, and W. Vogel, 'Complete nonclassicality test with a photon-number-resolving detector', Phys. Rev. A **86** (2012).

224 J. Sperling et al., 'Identification of nonclassical properties of light with multiplexing layouts', Phys. Rev. A **96** (2017).

225 M. Bohmann, L. Qi, W. Vogel, and M. Chekhova, 'Detection-device-independent verification of nonclassical light', Phys. Rev. Research **1** (2019).

226 J. Peřina, O. Haderka, and V. Michálek, 'Simultaneous observation of higher-order non-classicalities based on experimental photocount moments and probabilities', Sci. Rep. **9** (2019).

227 R. Pestotnik et al., 'Silicon photomultiplier as a detector of cherenkov photons', in 2007 IEEE nuclear science symposium conference record (2007).

228 S. Takeshita et al., 'Development of positron detector for μSR based on multi-pixel photon counter', Nucl. Instrum. Methods Phys. Res. Section A: Accelerators, Spectrometers, Detectors and Associated Equipment **600** (2009).

229 L. Qi et al., 'Multiphoton nonclassical light from clusters of single-photon emitters', New J. Phys. **20** (2018).

230 E. Waks, E. Diamanti, and Y. Yamamoto, 'Generation of photon number states', New J. Phys. **8** (2006).

231 M. Cooper, L. J. Wright, C. Söller, and B. J. Smith, 'Experimental generation of multi-photon fock states', Opt. Express **21** (2013).

232 M. Yukawa, K. Miyata, T. Mizuta, H. Yonezawa, P. Marek, R. Filip, and A. Furusawa, 'Generating superposition of up-to three photons for continuous variable quantum information processing', Opt. Express **21** (2013).

233 M. Bouillard, G. Boucher, J. F. Ortas, B. Kanseri, and R. Tualle-Brouri, 'High production rate of single-photon and two-photon fock states for quantum state engineering', Opt. Express **27** (2019).

234 J. Tiedau, T. J. Bartley, G. Harder, A. E. Lita, S. W. Nam, T. Gerrits, and C. Silberhorn, 'Scalability of parametric down-conversion for generating higher-order fock states', Phys. Rev. A **100** (2019).

235 D. Su, C. R. Myers, and K. K. Sabapathy, 'Conversion of gaussian states to non-gaussian states using photon-number-resolving detectors', Phys. Rev. A **100** (2019).

236 M. W. Mitchell, J. S. Lundeen, and A. M. Steinberg, 'Super-resolving phase measurements with a multiphoton entangled state', Nature **429** (2004).

237 I. Afek, O. Ambar, and Y. Silberberg, 'High-NOON states by mixing quantum and classical light', Science **328** (2010).

238 P. Kok, W. J. Munro, K. Nemoto, T. C. Ralph, J. P. Dowling, and G. J. Milburn, 'Linear optical quantum computing with photonic qubits', Rev. Mod. Phys. **79** (2007).

239 J. L. O'Brien, 'Optical quantum computing', Science **318** (2007).

240 J. Shapiro, 'The quantum theory of optical communications', IEEE J. Sel. Top. Quantum Electron. **15** (2009).

241 M. Ren, E. Wu, Y. Liang, Y. Jian, G. Wu, and H. Zeng, 'Quantum random-number generator based on a photon-number-resolving detector', Phys. Rev. A **83** (2011).

242 P. C. Humphreys, B. J. Metcalf, J. B. Spring, M. Moore, X.-M. Jin, M. Barbieri, W. S. Kolthammer, and I. A. Walmsley, 'Linear optical quantum computing in a single spatial mode', Phys. Rev. Lett. **111** (2013).

243 B. Haylock, D. Peace, F. Lenzini, C. Weedbrook, and M. Lobino, 'Multiplexed quantum random number generation', Quantum **3** (2019).

244 Y. Zhai, F. E. Becerra, J. Fan, and A. Migdall, 'Direct measurement of sub-wavelength interference using thermal light and photon-number-resolved detection', Appl. Phys. Lett. **105** (2014).

245 G. Y. Xiang, B. L. Higgins, D. W. Berry, H. M. Wiseman, and G. J. Pryde, 'Entanglement-enhanced measurement of a completely unknown optical phase', Nat. Photon. **5** (2010).

246 P. Liu, and G. R. Jin, 'Ultimate phase estimation in a squeezed-state interferometer using photon counters with a finite number resolution', J. Phys. A Math. Theor. **50** (2017).

247 J.-D. Zhang, Z.-J. Zhang, L.-Z. Cen, J.-Y. Hu, and Y. Zhao, 'Nonlinear phase estimation: parity measurement approaches the quantum cramér-rao bound for coherent states', Phys. Rev. A **99** (2019).

248 L. A. Howard, G. G. Gillett, M. E. Pearce, R. A. Abrahao, T. J. Weinhold, P. Kok, and A. G. White, 'Optimal imaging of remote bodies using quantum detectors', Phys. Rev. Lett. **123** (2019).

249 S. Moehrs, A. D. Guerra, D. J. Herbert, and M. A. Mandelkern, 'A detector head design for small-animal PET with silicon photomultipliers (SiPM)', Phys. Med. Biol. **51** (2006).

250 S. J. Sahl, S. W. Hell, and S. Jakobs, 'Fluorescence nanoscopy in cell biology', Nat. Rev. Mol. Cell Biol. **18** (2017).

251 H. Eisenberg, Y. Sher, L. Cohen, and D. Istrati, 'Low intensity LiDAR using compressed sensing and a photon number resolving detector', in Emerging digital micromirror device based systems and applications x, edited by M. R. Douglass, and B. L. Lee (2018).

252 L. Cohen, E. S. Matekole, Y. Sher, D. Istrati, H. S. Eisenberg, and J. P. Dowling, 'Thresholded quantum LIDAR: exploiting photon-number-resolving detection', Phys. Rev. Lett. **123** (2019).

253 K. S. McKay, J. Kim, and H. H. Hogue, 'Enhanced quantum efficiency of the visible light photon counter in the ultraviolet wavelengths', Opt. Express **17** (2009).

254 E. Waks, K. Inoue, W. Oliver, E. Diamanti, and Y. Yamamoto, 'High-efficiency photon-number detection for quantum information processing', IEEE J. Sel. Top. Quantum Electron. **9**, 10.1109/jstqe.2003.820917 (2003).

255 A. E. Lita, A. J. Miller, and S. W. Nam, 'Counting near-infrared single-photons with 95% efficiency', Opt. Express **16** (2008).

256 D. Fukuda, G. Fujii, A. Yoshizawa, H. Tsuchida, R. M. T. Damayanthi, H. Takahashi, S. Inoue, and M. Ohkubo, 'High speed photon number resolving detector with titanium transition edge sensor', J. Low Temp. Phys. **151** (2008).

257 D. Fukuda et al., 'Photon number resolving detection with high speed and high quantum efficiency', Metrologia **46** (2009).

258 D. Fukuda et al., 'Titanium-based transition-edge photon number resolving detector with 98% detection efficiency with index-matched small-gap fiber coupling', Opt. Express **19** (2011).

259 G. Wu, Y. Jian, E. Wu, and H. Zeng, 'Photon-number-resolving detection based on InGaAs/InP avalanche photodiode in the sub-saturated mode', Opt. Express **17** (2009).

260 O. Thomas, Z. L. Yuan, J. F. Dynes, A. W. Sharpe, and A. J. Shields, 'Efficient photon number detection with silicon avalanche photodiodes', Appl. Phys. Lett. **97** (2010).

261 Z. L. Yuan, B. E. Kardynal, A. W. Sharpe, and A. J. Shields, 'High speed single photon detection in the near infrared', Appl. Phys. Lett. **91** (2007).

262 E. Pomarico, B. Sanguinetti, R. Thew, and H. Zbinden, 'Room temperature photon number resolving detector for infared wavelengths', Opt. Express **18** (2010).

263 A. Allevi, M. Bondani, and A. Andreoni, 'Photon-number correlations by photon-number resolving detectors', Opt. Lett. **35** (2010).

264 M. J. Fitch, B. C. Jacobs, T. B. Pittman, and J. D. Franson, 'Photon-number resolution using time-multiplexed single-photon detectors', Phys. Rev. A **68** (2003).

265 D. Achilles, C. Silberhorn, C. Śliwa, K. Banaszek, and I. A. Walmsley, 'Fiber-assisted detection with photon number resolution', Opt. Lett. **28** (2003).

266 J. Řeháček, Z. Hradil, O. Haderka, J. Peřina, and M. Hamar, 'Multiple-photon resolving fiber-loop detector', Phys. Rev. A **67** (2003).

267 M. Mičuda, O. Haderka, and M. Ježek, 'High-efficiency photon-number-resolving multichannel detector', Phys. Rev. A **78** (2008).

268 P. Kok, and S. L. Braunstein, 'Detection devices in entanglement-based optical state preparation', Phys. Rev. A **63** (2001).

269 I. Afek, A. Natan, O. Ambar, and Y. Silberberg, 'Quantum state measurements using multipixel photon detectors', Phys. Rev. A **79** (2009).

270 D. A. Kalashnikov, S. H. Tan, M. V. Chekhova, and L. A. Krivitsky, 'Accessing photon bunching with a photon number resolving multi-pixel detector', Opt. Express **19** (2011).

271 O. Thomas, Z. Yuan, and A. Shields, 'Practical photon number detection with electric field-modulated silicon avalanche photodiodes', Nat. Commun. **3** (2012).

272 J. Kröger, T. Ahrens, J. Sperling, W. Vogel, H. Stolz, and B. Hage, 'High intensity click statistics from a 10 × 10 avalanche photodiode array', J. Phys. B: At. Mol. Opt. **50** (2017).

273 R. Chrapkiewicz, 'Photon counts statistics of squeezed and multimode thermal states of light on multiplexed on–off detectors', J. Opt. Soc. Am. B **31** (2014).

274 J. Sperling, W. Vogel, and G. S. Agarwal, 'True photocounting statistics of multiple on-off detectors', Phys. Rev. A **85** (2012).

275 L. Cohen, Y. Pilnyak, D. Istrati, N. M. Studer, J. P. Dowling, and H. S. Eisenberg, 'Absolute calibration of single-photon and multiplexed photon-number-resolving detectors', Phys. Rev. A **98** (2018).

276 G. A. P. Thé, and R. V. Ramos, 'Multiple-photon number resolving detector using fibre ring and single-photon detector', J. Mod. Opt. **54** (2007).

277 A. P. Worsley, H. B. Coldenstrodt-Ronge, J. S. Lundeen, P. J. Mosley, B. J. Smith, G. Puentes, N. Thomas-Peter, and I. A. Walmsley, 'Absolute efficiency estimation of photon-number-resolving detectors using twin beams', Opt. Express **17** (2009).

278 P. Eraerds, E. Pomarico, J. Zhang, B. Sanguinetti, R. Thew, and H. Zbinden, '32 bin near-infrared time-multiplexing detector with attojoule single-shot energy resolution', Rev. Sci. Instrum. **81** (2010).

279 J. Tiedau, E. Meyer-Scott, T. Nitsche, S. Barkhofen, T. J. Bartley, and C. Silberhorn, 'A high dynamic range optical detector for measuring single photons and bright light', Opt. Express **27** (2019).

280 L. A. Jiang, E. A. Dauler, and J. T. Chang, 'Photon-number-resolving detector with10bitsof resolution', Phys. Rev. A **75** (2007).

281 I. M. Antolovic, C. Bruschini, and E. Charbon, 'Dynamic range extension for photon counting arrays', Opt. Express **26** (2018).

282 Y. Du, and F. Retière, 'After-pulsing and cross-talk in multi-pixel photon counters', Nucl. Instrum. Methods Phys. Res. A **596** (2008).

283 I. Rech, A. Ingargiola, R. Spinelli, I. Labanca, S. Marangoni, M. Ghioni, and S. Cova, 'Optical crosstalk in single photon avalanche diode arrays: a new complete model', Opt. Express **16** (2008).

284 D. A. Kalashnikov, S.-H. Tan, and L. A. Krivitsky, 'Crosstalk calibration of multi-pixel photon counters using coherent states', Opt. Express **20** (2012).

285 J. S. Lundeen et al., 'Tomography of quantum detectors', Nat. Phys. **5** (2008).

286 L. Bonolis, 'Walther bothe and bruno rossi: the birth and development of coincidence methods in cosmic-ray physics', Am. J. Phys. **79** (2011).

287 L. collaboration, 'Observation of structure in the j/ψ-pair mass spectrum', Sci. Bull. **65** (2020).

288 S. Gong, I. Labanca, I. Rech, and M. Ghioni, 'A 32-channel photon counting module with embedded auto/cross-correlators for real-time parallel fluorescence correlation spectroscopy', Rev. Sci. Instrum. **85** (2014).

289 R. Salomon, and R. Joost, 'PCDA – a massively parallel, scalable, precise, FPGA-based coincidence detector array', in 2016 12th IEEE international conference on control and automation (ICCA) (2016).

290 Y. Israel, R. Tenne, D. Oron, and Y. Silberberg, 'Quantum correlation enhanced super-resolution localization microscopy enabled by a fibre bundle camera', Nat. Commun. **8** (2017).

291 S. Paesani et al., 'Generation and sampling of quantum states of light in a silicon chip', Nat. Phys. **15** (2019).

292 S. Aaronson, and A. Arkhipov, 'The computational complexity of linear optics', in Research in optical sciences (2014).

293 S. Pirandola et al., 'Advances in quantum cryptography', Adv. Opt. Photonics **12** (2020).

294 A. Aspuru-Guzik, and P. Walther, 'Photonic quantum simulators', Nat. Phys. **8** (2012).

295 H. J. Kimble, M. Dagenais, and L. Mandel, 'Photon antibunching in resonance fluorescence', Phys. Rev. Lett. **39** (1977).

296 H. E. Kondakci, A. Szameit, A. F. Abouraddy, D. N. Christodoulides, and B. E. A. Saleh, 'Sub-thermal to super-thermal light statistics from a disordered lattice via deterministic control of excitation symmetry', Optica **3** (2016).

297 J. Sperling et al., 'Identification of nonclassical properties of light with multiplexing layouts', Phys. Rev. A **96** (2017).

298 Y. I. Bogdanov, K. G. Katamadze, G. V. Avosopiants, L. V. Belinsky, N. A. Bogdanova, A. A. Kalinkin, and S. P. Kulik, 'Multiphoton subtracted thermal states: description, preparation, and reconstruction', Phys. Rev. A **96** (2017).

299 M. Beck, 'Comparing measurements of $g^{(2)}(0)$ performed with different coincidence detection techniques', J. Opt. Soc. Am. B **24** (2007).

300 D. Branning, S. Bhandari, and M. Beck, 'Low-cost coincidence-counting electronics for undergraduate quantum optics', Am. J. Phys. **77** (2009).

301 M. Wahl et al., 'Integrated multichannel photon timing instrument with very short dead time and high throughput', Rev. Sci. Instrum. **84** (2013).

302 S. Gaertner, H. Weinfurter, and C. Kurtsiefer, 'Fast and compact multichannel photon coincidence unit for quantum information processing', Rev. Sci. Instrum. **76** (2005).

303 D. Branning, S. Khanal, Y. H. Shin, B. Clary, and M. Beck, 'Note: scalable multiphoton coincidence-counting electronics', Rev. Sci. Instrum. **82** (2011).

304 B. K. Park, Y.-S. Kim, O. Kwon, S.-W. Han, and S. Moon, 'High-performance reconfigurable coincidence counting unit based on a field programmable gate array', Appl. Opt. **54** (2015).

305 C. Zhang, W. Li, Y. Hu, T. Yang, G. Jin, and X. Jiang, '48-channel coincidence counting system for multiphoton experiment', Rev. Sci. Instrum. **87** (2016).

306 A. K. Gupta, R. S. Prasad, L. Srivani, D. T. Murthy, B. K. Panigrahi, and G. Raghavan, 'Design and development of flexible and low-cost coincidence counting unit', in 2018 IEEE international conference on electronics, computing and communication technologies (CONECCT) (2018).

307 W. Li, Y. Hu, H.-s. Zhong, Y.-f. Wang, X.-l. Wang, C.-z. Peng, and X. Jiang, 'Time-tagged coincidence counting unit for large-scale photonic quantum computing', Rev. Sci. Instrum. **89** (2018).

308 E. Arabul, S. Paesani, S. Tancock, J. Rarity, and N. Dahnoun, 'A precise high count-rate FPGA based multi-channel coincidence counting system for quantum photonics applications', IEEE Photonics J. **12** (2020).

309 M. G. Genoni, M. G. A. Paris, and K. Banaszek, 'Quantifying the non-gaussian character of a quantum state by quantum relative entropy', Phys. Rev. A **78** (2008).

310 T. S. Iskhakov, V. C. Usenko, R. Filip, M. V. Chekhova, and G. Leuchs, 'Low-noise macroscopic twin beams', Phys. Rev. A **93** (2016).

311 Y. I. Bogdanov, K. G. Katamadze, G. V. Avosopyants, L. V. Belinsky, N. A. Bogdanova, S. P. Kulik, and V. F. Lukichev, 'Study of higher order correlation functions and photon statistics using multiphoton-subtracted states and quadrature measurements', in International conference on micro- and nano-electronics 2016, edited by V. F. Lukichev, and K. V. Rudenko (2016).

312 G. S. Agarwal, and K. Tara, 'Nonclassical character of states exhibiting no squeezing or sub-poissonian statistics', Phys. Rev. A **46** (1992).

313 M. Um et al., 'Phonon arithmetic in a trapped ion system', Nat. Commun. **7** (2016).

314 G. Enzian et al., 'Non-gaussian mechanical motion via single and multiphonon subtraction from a thermal state', Phys. Rev. Lett. **127** (2021).

315 G. Enzian, J. J. Price, L. Freisem, J. Nunn, J. Janousek, B. C. Buchler, P. K. Lam, and M. R. Vanner, 'Single-phonon addition and subtraction to a mechanical thermal state', Phys. Rev. Lett. **126** (2021).

316 Y. Yang, and F.-L. Li, 'Nonclassicality of photon-subtracted and photon-added-then-subtracted gaussian states', J. Opt. Soc. Am. B **26** (2009).

317 S. Rosenblum, O. Bechler, I. Shomroni, Y. Lovsky, G. Guendelman, and B. Dayan, 'Extraction of a single photon from an optical pulse', Nat. Photon. **10** (2015).

318 S. M. Barnett, G. Ferenczi, C. R. Gilson, and F. C. Speirits, 'Statistics of photon-subtracted and photon-added states', Phys. Rev. A **98** (2018).

319 V. Parigi, A. Zavatta, and M. Bellini, 'Implementation of single-photon creation and annihilation operators: experimental issues in their application to thermal states of light', J. Phys. B: At. Mol. Opt. **42** (2009).

320 G. N. Jones, J. Haight, and C. T. Lee, 'Nonclassical effects in the photon-added thermal state', J. Eur. Opt. Soc. B: Quantum semiclass. opt. **9** (1997).

321 A. R. U. Devi, R. Prabhu, and M. S. Uma, 'Non-classicality of photon added coherent and thermal radiations', Eur. Phys. J. D **40** (2006).

322 A. Zavatta, V. Parigi, and M. Bellini, 'Experimental nonclassicality of single-photon-added thermal light states', Phys. Rev. A **75** (2007).

323 A. Zavatta, S. Viciani, and M. Bellini, 'Single-photon excitation of a coherent state: catching the elementary step of stimulated light emission', Phys. Rev. A **72** (2005).

324 M. S. Kim, E. Park, P. L. Knight, and H. Jeong, 'Nonclassicality of a photon-subtracted gaussian field', Phys. Rev. A **71** (2005).

325 A. Ourjoumtsev, A. Dantan, R. Tualle-Brouri, and P. Grangier, 'Increasing entanglement between gaussian states by coherent photon subtraction', Phys. Rev. Lett. **98** (2007).

326 H. Takahashi, J. S. Neergaard-Nielsen, M. Takeuchi, M. Takeoka, K. Hayasaka, A. Furusawa, and M. Sasaki, 'Entanglement distillation from gaussian input states', Nat. Photon. **4** (2010).

327 K. Zhang, J. Jing, N. Treps, and M. Walschaers, 'Maximal entanglement increase with single-photon subtraction', Quantum **6** (2022).

328 C. Wittmann, D. Elser, U. L. Andersen, R. Filip, P. Marek, and G. Leuchs, 'Quantum filtering of optical coherent states', Phys. Rev. A **78** (2008).

329 M. A. Usuga, C. R. Müller, C. Wittmann, P. Marek, R. Filip, C. Marquardt, G. Leuchs, and U. L. Andersen, 'Noise-powered probabilistic concentration of phase information', Nat. Phys. **6** (2010).

330 F. Ferreyrol, M. Barbieri, R. Blandino, S. Fossier, R. Tualle-Brouri, and P. Grangier, 'Implementation of a nondeterministic optical noiseless amplifier', Phys. Rev. Lett. **104** (2010).

331 A. Zavatta, J. Fiurášek, and M. Bellini, 'A high-fidelity noiseless amplifier for quantum light states', Nat. Photon. **5** (2010).

332 C. R. Müller, C. Wittmann, P. Marek, R. Filip, C. Marquardt, G. Leuchs, and U. L. Andersen, 'Probabilistic cloning of coherent states without a phase reference', Phys. Rev. A **86** (2012).

333 S. M. H. Rafsanjani et al., 'Quantum-enhanced interferometry with weak thermal light', Optica **4** (2017).

334 The LIGO Scientific Collaboration, 'Enhanced sensitivity of the LIGO gravitational wave detector by using squeezed states of light', Nat. Photon. **7** (2013).

335 M. Barbieri, 'Optical quantum metrology', PRX Quantum **3** (2022).

336 P. Bertet, A. Auffeves, P. Maioli, S. Osnaghi, T. Meunier, M. Brune, J. M. Raimond, and S. Haroche, 'Direct measurement of the wigner function of a one-photon fock state in a cavity', Phys. Rev. Lett. **89** (2002).

337 M. G. Genoni, M. L. Palma, T. Tufarelli, S. Olivares, M. S. Kim, and M. G. A. Paris, 'Detecting quantum non-gaussianity via the wigner function', Phys. Rev. A **87** (2013).

338 E. Wigner, 'On the quantum correction for thermodynamic equilibrium', Phys. Rev. **40** (1932).

339 U. Fano, 'Ionization yield of radiations. II. the fluctuations of the number of ions', Phys. Rev. **72** (1947).

340 F. Pennini, and A. Plastino, 'Diverging fano factors', J. Phys. Conf. Ser. **246** (2010).

341 E. J. O'Reilly, and A. Olaya-Castro, 'Non-classicality of the molecular vibrations assisting exciton energy transfer at room temperature', Nat. Commun. **5** (2014).

342 J. Sperling, W. Vogel, and G. S. Agarwal, 'Sub-binomial light', Phys. Rev. Lett. **109** (2012).

343 P. Grangier, G. Roger, and A. Aspect, 'Experimental evidence for a photon anticorrelation effect on a beam splitter: a new light on single-photon interferences', Europhys. Lett. **1** (1986).

344 K. Stensson, and G. Björk, 'Measurement of the two-time intensity-correlation function of arbitrary states', Phys. Rev. A **98** (2018).

345 F. Grosshans, and P. Grangier, 'Continuous variable quantum cryptography using coherent states', Phys. Rev. Lett. **88** (2002).

346 A. M. Lance, T. Symul, V. Sharma, C. Weedbrook, T. C. Ralph, and P. K. Lam, 'No-switching quantum key distribution using broadband modulated coherent light', Phys. Rev. Lett. **95** (2005).

347 S. Pirandola et al., 'Advances in quantum cryptography', Adv. Opt. Photonics **12** (2020).

348 Y. Qu, and S. Singh, 'Photon correlation effects in second harmonic generation', Opt. Commun. **90** (1992).

349 K. Y. Spasibko, D. A. Kopylov, V. L. Krutyanskiy, T. V. Murzina, G. Leuchs, and M. V. Chekhova, 'Multiphoton effects enhanced due to ultrafast photon-number fluctuations', Phys. Rev. Lett. **119** (2017).

350 A. Jechow, M. Seefeldt, H. Kurzke, A. Heuer, and R. Menzel, 'Enhanced two-photon excited fluorescence from imaging agents using true thermal light', Nat. Photon. **7** (2013).

351 D. Zhang, Y.-H. Zhai, L.-A. Wu, and X.-H. Chen, 'Correlated two-photon imaging with true thermal light', Opt. Lett. **30** (2005).

352 A. Valencia, G. Scarcelli, M. D'Angelo, and Y. Shih, 'Two-photon imaging with thermal light', Phys. Rev. Lett. **94** (2005).

353 J. Sprigg, T. Peng, and Y. Shih, 'Super-resolution imaging using the spatial-frequency filtered intensity fluctuation correlation', Sci. Rep. **6** (2016).

354 C. Weedbrook, S. Pirandola, and T. C. Ralph, 'Continuous-variable quantum key distribution using thermal states', Phys. Rev. A **86** (2012).

355 R. S. Bennink, S. J. Bentley, and R. W. Boyd, '"two-photon" coincidence imaging with a classical source', Phys. Rev. Lett. **89** (2002).

356 A. Gatti, E. Brambilla, M. Bache, and L. A. Lugiato, 'Ghost imaging with thermal light: comparing entanglement and ClassicalCorrelation', Phys. Rev. Lett. **93** (2004).

357 F. Ferri, D. Magatti, A. Gatti, M. Bache, E. Brambilla, and L. A. Lugiato, 'High-resolution ghost image and ghost diffraction experiments with thermal light', Phys. Rev. Lett. **94** (2005).

358 L. Basano, and P. Ottonello, 'Experiment in lensless ghost imaging with thermal light', Appl. Phys. Lett. **89** (2006).

359 Y. Zhou, J. Simon, J. Liu, and Y. Shih, 'Third-order correlation function and ghost imaging of chaotic thermal light in the photon counting regime', Phys. Rev. A **81** (2010).

360 X.-F. Liu, X.-H. Chen, X.-R. Yao, W.-K. Yu, G.-J. Zhai, and L.-A. Wu, 'Lensless ghost imaging with sunlight', Opt. Lett. **39** (2014).

361 M. D. Vidrighin, O. Dahlsten, M. Barbieri, M. S. Kim, V. Vedral, and I. A. Walmsley, 'Photonic maxwell's demon', Phys. Rev. Lett. **116** (2016).

362 W. Martienssen, and E. Spiller, 'Coherence and fluctuations in light beams', Am. J. Phys. **32** (1964).

363 F. T. Arecchi, 'Measurement of the statistical distribution of gaussian and laser sources', Phys. Rev. Lett. **15** (1965).

364 L. E. Estes, L. M. Narducci, and R. A. Tuft, 'Scattering of light from a rotating ground glass*', J. Opt. Soc. Am. **61** (1971).

365 M. Rousseau, 'Statistical properties of optical fields scattered by random media application to rotating ground glass', J. Opt. Soc. Am. **61** (1971).

366 T. A. Kuusela, 'Measurement of the second-order coherence of pseudothermal light', Am. J. Phys. **85** (2017).

367 H. E. Kondakci, A. F. Abouraddy, and B. E. A. Saleh, 'A photonic thermalization gap in disordered lattices', Nat. Phys. **11** (2015).

368 O. S. Magaña-Loaiza, M. Mirhosseini, R. M. Cross, S. M. H. Rafsanjani, and R. W. Boyd, 'Hanbury brown and twiss interferometry with twisted light', Sci. Adv. **2** (2016).

369 P. R. Prucnal, and M. C. Teich, 'Statistical properties of counting distributions for intensity-modulated sources', J. Opt. Soc. Am. **69** (1979).

370 D. Pandey, N. Satapathy, B. Suryabrahmam, J. S. Ivan, and H. Ramachandran, 'Classical light sources with tunable temporal coherence and tailored photon number distributions', Eur. Phys. J. Plus **129** (2014).

371 I. Straka, J. Mika, and M. Ježek, 'Generator of arbitrary classical photon statistics', Opt. Express **26** (2018).

372 I. Straka, and M. Ježek, 'Shaping the g(2) autocorrelation and photon statistics', Phys. Rev. A **103** (2021).

373 M. Nazarathy, S. Newton, R. Giffard, D. Moberly, F. Sischka, W. Trutna, and S. Foster, 'Real-time long range complementary correlation optical time domain reflectometer', J. Lightwave Technol. **7** (1989).

374 T. Mehringer, S. Oppel, and J. von Zanthier, 'An optical multimode fiber as pseudothermal light source', Appl. Phys. B **123** (2017).

375 F. Boitier, A. Godard, E. Rosencher, and C. Fabre, 'Measuring photon bunching at ultrashort timescale by two-photon absorption in semiconductors', Nat. Phys. **5** (2009).

376 J. Schmitt, T. Damm, D. Dung, F. Vewinger, J. Klaers, and M. Weitz, 'Observation of grand-canonical number statistics in a photon bose-einstein condensate', Phys. Rev. Lett. **112** (2014).

377 J. Schmitt, T. Damm, D. Dung, C. Wahl, F. Vewinger, J. Klaers, and M. Weitz, 'Spontaneous symmetry breaking and phase coherence of a photon bose-einstein condensate coupled to a reservoir', Phys. Rev. Lett. **116** (2016).

378 M. Ueda, 'Nonequilibrium open-system theory for continuous photodetection processes: a probability-density-functional description', Phys. Rev. A **41** (1990).

379 M. Ueda, N. Imoto, and T. Ogawa, 'Quantum theory for continuous photodetection processes', Phys. Rev. A **41** (1990).

380 E. Bimbard, N. Jain, A. MacRae, and A. I. Lvovsky, 'Quantum-optical state engineering up to the two-photon level', Nat. Photon. **4** (2010).

381 R. J. Glauber, 'Coherent and incoherent states of the radiation field', Phys. Rev. **131** (1963).

382 E. C. G. Sudarshan, 'Equivalence of semiclassical and quantum mechanical descriptions of statistical light beams', Phys. Rev. Lett. **10** (1963).

383 A. I. Lvovsky, H. Hansen, T. Aichele, O. Benson, J. Mlynek, and S. Schiller, 'Quantum state reconstruction of the single-photon fock state', Phys. Rev. Lett. **87** (2001).

384 J. S. Neergaard-Nielsen, B. M. Nielsen, C. Hettich, K. Mølmer, and E. S. Polzik, 'Generation of a superposition of odd photon number states for quantum information networks', Phys. Rev. Lett. **97** (2006).

385 K. Wakui, H. Takahashi, A. Furusawa, and M. Sasaki, 'Photon subtracted squeezed states generated with periodically poled KTiOPO_4', Opt. Express **15** (2007).

386 R. Filip, and L. Mišta, 'Detecting quantum states with a positive wigner function beyond mixtures of gaussian states', Phys. Rev. Lett. **106** (2011).

387 L. Lachman, and R. Filip, 'Robustness of quantum nonclassicality and non-Gaussianity of single-photon states in attenuating channels', Phys. Rev. A **88** (2013).

388 C. Hughes, M. G. Genoni, T. Tufarelli, M. G. A. Paris, and M. S. Kim, 'Quantum non-gaussianity witnesses in phase space', Phys. Rev. A **90** (2014).

389 L. Lachman, and R. Filip, 'Quantum non-gaussianity from a large ensemble of single photon emitters', Opt. Express **24** (2016).

390 J. Park et al., 'Revealing nonclassicality beyond gaussian states via a single marginal distribution', Proc. Natl. Acad. Sci. U.S.A. **114** (2017).

391 L. Happ, M. A. Efremov, H. Nha, and W. P. Schleich, 'Sufficient condition for a quantum state to be genuinely quantum non-gaussian', New J. Phys. **20** (2018).

392 B. Kühn, and W. Vogel, 'Quantum non-gaussianity and quantification of nonclassicality', Phys. Rev. A **97** (2018).

393 M. Ježek, I. Straka, M. Mičuda, M. Dušek, J. Fiurášek, and R. Filip, 'Experimental test of the quantum non-gaussian character of a heralded single-photon state', Phys. Rev. Lett. **107** (2011).

394 M. Ježek, A. Tipsmark, R. Dong, J. Fiurášek, L. Mišta, R. Filip, and U. L. Andersen, 'Experimental test of the strongly nonclassical character of a noisy squeezed single-photon state', Phys. Rev. A **86** (2012).

395 A. Predojević, M. Ježek, T. Huber, H. Jayakumar, T. Kauten, G. S. Solomon, R. Filip, and G. Weihs, 'Efficiency vs multi-photon contribution test for quantum dots', Opt. Express **22** (2014).

396 Y.-S. Ra, A. Dufour, M. Walschaers, C. Jacquard, T. Michel, C. Fabre, and N. Treps, 'Non-gaussian quantum states of a multimode light field', Nat. Phys. **16** (2019).

397 H. Song, K. B. Kuntz, and E. H. Huntington, 'Limitations on the quantum non-gaussian characteristic of schrödinger kitten state generation', New J. Phys. **15** (2013).

398 F. Albarelli, M. G. Genoni, M. G. A. Paris, and A. Ferraro, 'Resource theory of quantum non-gaussianity and wigner negativity', Phys. Rev. A **98** (2018).

399 R. Takagi, and Q. Zhuang, 'Convex resource theory of non-gaussianity', Phys. Rev. A **97** (2018).

400 J. Lee, J. Park, and H. Nha, 'Quantum non-gaussianity and secure quantum communication', npj Quantum Inf. **5** (2019).

401 J. Park, J. Lee, K. Baek, S.-W. Ji, and H. Nha, 'Faithful measure of quantum non-gaussianity via quantum relative entropy', Phys. Rev. A **100** (2019).

402 A. I. Lvovsky, P. Grangier, A. Ourjoumtsev, V. Parigi, M. Sasaki, and R. Tualle-Brouri, *Production and applications of non-gaussian quantum states of light*, 2020.

403 K. S. Champlin, 'Microplasma fluctuations in silicon', J. Appl. Phys. **30** (1959).

404 J. Zhang, M. A. Itzler, H. Zbinden, and J.-W. Pan, 'Advances in InGaAs/InP single-photon detector systems for quantum communication', Light: Sci. Appl. **4** (2015).

405 M. Legré, R. Thew, H. Zbinden, and N. Gisin, 'High resolution optical time domain reflectometer based on 1.55μm up-conversion photon-counting module', Opt. Express **15** (2007).

406 L.-Q. Li, and L. M. Davis, 'Single photon avalanche diode for single molecule detection', Rev. Sci. Instrum. **64** (1993).

407 G. Ribordy, J.-D. Gautier, H. Zbinden, and N. Gisin, 'Performance of InGaAs/InP avalanche photodiodes as gated-mode photon counters', Appl. Opt. **37** (1998).

408 G. Wu, C. Zhou, X. Chen, and H. Zeng, 'High performance of gated-mode single-photon detector at 1.55μm', Opt. Commun. **265** (2006).

409 N. Namekata, S. Sasamori, and S. Inoue, '800 MHz single-photon detection at 1550-nm using an InGaAs/InP avalanche photodiode operated with a sine wave gating', Opt. Express **14** (2006).

410 X.-L. Liang et al., 'Fully integrated InGaAs/InP single-photon detector module with gigahertz sine wave gating', Rev. Sci. Instrum. **83** (2012).

411 A. Tosi, A. D. Frera, A. B. Shehata, and C. Scarcella, 'Fully programmable single-photon detection module for InGaAs/InP single-photon avalanche diodes with clean and sub-nanosecond gating transitions', Rev. Sci. Instrum. **83** (2012).

412 Y. Zhang, X. Zhang, and S. Wang, 'Gaussian pulse gated InGaAs/InP avalanche photodiode for single photon detection', Opt. Lett. **38** (2013).

413 G. Boso, A. D. Mora, A. D. Frera, and A. Tosi, 'Fast-gating of single-photon avalanche diodes with 200ps transitions and 30ps timing jitter', Sens. Actuator. A: Phys. **191** (2013).

414 J. Huang et al., 'Photon-counting laser ranging with InGaAs/InP avalanche photodiode in the passively quenched and 1-GHz sinusoidally gated', Optik **125** (2014).

415 S. Suzuki, N. Namekata, K. Tsujino, and S. Inoue, 'Highly enhanced avalanche probability using sinusoidally-gated silicon avalanche photodiode', Appl. Phys. Lett. **104** (2014).

416 C. Hu, T.-H. Ju, and Y. Yao, 'Advantages and demonstration of gated-mode passive quenching with active reset circuit', in 2014 IEEE workshop on advanced research and technology in industry applications (WARTIA) (2014).

417 W.-H. Jiang et al., 'Miniaturized high-frequency sine wave gating InGaAs/InP single-photon detector', Rev. Sci. Instrum. **89** (2018).

418 R. G. W. Brown, K. D. Ridley, and J. G. Rarity, 'Characterization of silicon avalanche photodiodes for photon correlation measurements 1: passive quenching', Appl. Opt. **25** (1986).

419 R. G. W. Brown, R. Jones, J. G. Rarity, and K. D. Ridley, 'Characterization of silicon avalanche photodiodes for photon correlation measurements 2: active quenching', Appl. Opt. **26** (1987).

420 M. Ghioni, S. Cova, F. Zappa, and C. Samori, 'Compact active quenching circuit for fast photon counting with avalanche photodiodes', Rev. Sci. Instrum. **67** (1996).

421 F. Zappa, M. Ghioni, S. Cova, C. Samori, and A. Giudice, 'An integrated active-quenching circuit for single-photon avalanche diodes', IEEE T. Instrum. Meas. **49** (2000).

422 R. Mita, G. Palumbo, and P. G. Fallica, 'A fast driver circuit for single-photon sensors', Microelectron. J. **37** (2006).

423 M. Stipčević, 'Active quenching circuit for single-photon detection with geiger mode avalanche photodiodes', Appl. Opt. **48** (2009).

424 F. Acerbi, A. D. Frera, A. Tosi, and F. Zappa, 'Fast active quenching circuit for reducing avalanche charge and afterpulsing in InGaAs/InP single-photon avalanche diode', IEEE J. Quantum Electron. **49** (2013).

425 M. Stipčević, B. G. Christensen, P. G. Kwiat, and D. J. Gauthier, 'Advanced active quenching circuit for ultra-fast quantum cryptography', Opt. Express **25** (2017).

426 J. Liu, Y. Xu, Z. Wang, Y. Li, Y. Gu, Z. Liu, and X. Zhao, 'Reducing afterpulsing in InGaAs(p) single-photon detectors with hybrid quenching', Sensors **20** (2020).

427 M. Liu, C. Hu, J. C. Campbell, Z. Pan, and M. M. Tashima, 'Reduce afterpulsing of single photon avalanche diodes using passive quenching with active reset', IEEE J. Quantum Electron. **44** (2008).

428 I. Berdalovic, Z. Osrecki, F. Segmanovic, D. Grubisic, T. Knezevic, and T. Suligoj, 'Design of passive-quenching active-reset circuit with adjustable hold-off time for single-photon avalanche diodes', in 2016 39th international convention on information and communication technology, electronics and microelectronics (MIPRO) (2016).

429 A. Gallivanoni, I. Rech, and M. Ghioni, 'Progress in quenching circuits for single photon avalanche diodes', IEEE T. Nucl. Sci. (2010).

430 G. Vincent, A. Chantre, and D. Bois, 'Electric field effect on the thermal emission of traps in semiconductor junctions', J. Appl. Phys. **50** (1979).

431 P. A. Martin, B. G. Streetman, and K. Hess, 'Electric field enhanced emission from non-coulombic traps in semiconductors', J. Appl. Phys. **52** (1981).

432 J. W. Müller, 'Dead-time problems', Nucl. Instrum. Methods. Phys. Res. B **112** (1973).

433 L. Neri, S. Tudisco, F. Musumeci, A. Scordino, G. Fallica, M. Mazzillo, and M. Zimbone, 'Dead time of single photon avalanche diodes', Nucl. Phys. B Proc. Suppl. **215** (2011).

434 M. Stipcevic, D. Wang, and R. Ursin, 'Characterization of a commercially available large area, high detection efficiency single-photon avalanche diode', J. Lightwave Technol. **31** (2013).

435 V. Kornilov, 'Effects of dead time and afterpulses in photon detector on measured statistics of stochastic radiation', J. Opt. Soc. Am. A **31** (2013).

436 F.-X. Wang et al., 'Non-markovian property of afterpulsing effect in single-photon avalanche detector', J. Light. Technol. **34** (2016).

437 T. F. da Silva, G. B. Xavier, and J. P. von der Weid, 'Real-time characterization of gated-mode single-photon detectors', IEEE J. Quantum Electron. **47** (2011).

438 A. Restelli, J. C. Bienfang, and A. L. Migdall, 'Time-domain measurements of afterpulsing in InGaAs/InP SPAD gated with sub-nanosecond pulses', J. Mod. Opt. **59** (2012).

439 M. A. Wayne, J. C. Bienfang, and S. V. Polyakov, 'Simple autocorrelation method for thoroughly characterizing single-photon detectors', Opt. Express **25** (2017).

440 M. A. Karami, L. Carrara, C. Niclass, M. Fishburn, and E. Charbon, 'RTS noise characterization in single-photon avalanche diodes', IEEE Electron Dev. Lett. **31** (2010).

441 C. Levert, and W. Scheen, 'Probability fluctuations of discharges in a geiger-müller counter produced by cosmic radiation', Physica **10** (1943).

442 G. E. Albert, and L. Nelson, 'Contributions to the statistical theory of counter data', Ann. Math. Stat. **24** (1953).

443 L. Takacs, 'On a probability problem in the theory of counters', Ann. Math. Stat. **29** (1958).

444 J. W. Muller, 'A simple derivation of the takacs formula', in A simple derivation of the takacs formula, Rapport BIPM-88/3 (1988).

445 J. W. Müller, 'Generalized dead times', Nucl. Instrum. Methods. Phys. Res. B **301** (1991).

446 R. P. Gardner, and L. Liu, 'On extending the accurate and useful counting rate range of GM counter detector systems', Appl. Radiat. Isot. **48** (1997).

447 S. H. Lee, and R. P. Gardner, 'A new g–m counter dead time model', Appl. Radiat. Isot. **53** (2000).

448 J. Lee, I. Kim, and H. Choi, 'On the dead time problem of a GM counter', Appl. Radiat. Isot. **67** (2009).

449 A. Luis, and L. L. Sánchez-Soto, 'Complete characterization of arbitrary quantum measurement processes', Phys. Rev. Lett. **83** (1999).

450 J. Fiurášek, 'Maximum-likelihood estimation of quantum measurement', Phys. Rev. A **64** (2001).

451 B. J. Smith, D. Kundys, N. Thomas-Peter, P. G. R. Smith, and I. A. Walmsley, 'Phase-controlled integrated photonic quantum circuits', Opt. Express **17** (2009).

452 G. Brida et al., 'Quantum characterization of superconducting photon counters', New J. Phys. **14** (2012).

453 C. M. Natarajan, L. Zhang, H. Coldenstrodt-Ronge, G. Donati, S. N. Dorenbos, V. Zwiller, I. A. Walmsley, and R. H. Hadfield, 'Quantum detector tomography of a time-multiplexed superconducting nanowire single-photon detector at telecom wavelengths', Opt. Express **21** (2013).

454 M. Cooper, M. Karpiński, and B. J. Smith, 'Local mapping of detector response for reliable quantum state estimation', Nat. Commun. **5** (2014).

455 S. Grandi, A. Zavatta, M. Bellini, and M. G. A. Paris, 'Experimental quantum tomography of a homodyne detector', New J. Phys. **19** (2017).

456 S. Izumi, J. S. Neergaard-Nielsen, and U. L. Andersen, 'Tomography of a feedback measurement with photon detection', Phys. Rev. Lett. **124** (2020).

457 S. Ferrari, V. Kovalyuk, A. Vetter, C. Lee, C. Rockstuhl, A. Semenov, G. Gol'tsman, and W. Pernice, 'Analysis of the detection response of waveguide-integrated superconducting nanowire single-photon detectors at high count rate', Appl. Phys. Lett. **115** (2019).

458 J. Řeháček, D. Mogilevtsev, and Z. Hradil, 'Operational tomography: fitting of data patterns', Phys. Rev. Lett. **105** (2010).

459 M. Altorio, M. G. Genoni, F. Somma, and M. Barbieri, 'Metrology with unknown detectors', Phys. Rev. Lett. **116** (2016).

460 A. N. Tikhonov, 'On the stability of inverse problems', Doklady Akademii Nauk SSSR **39** (1943).

461 A. E. Hoerl, 'Application of ridge analysis to regression problems', Chem. Eng. Prog. **58** (1962).

462 A. P. Dempster, N. M. Laird, and D. B. Rubin, 'Maximum likelihood from incomplete data via the em algorithm', J. Royal Stat. Soc. B **39** (1977).

463 Y. Vardi, and D. Lee, 'From image deblurring to optimal investments: maximum likelihood solutions for positive linear inverse problems', J. Royal Stat. Soc. B **55** (1993).

464 K. Banaszek, 'Maximum-likelihood estimation of photon-number distribution from homodyne statistics', Phys. Rev. A **57** (1998).

465 F. Marsili, D. Bitauld, A. Gaggero, S. Jahanmirinejad, R. Leoni, F. Mattioli, and A. Fiore, 'Physics and application of photon number resolving detectors based on superconducting parallel nanowires', New J. Phys. **11** (2009).

466 K. Banaszek, 'Reconstruction of photon distribution with positivity constraints', Acta Phys. Slov. **48** (1998).

467 Y. Grandvalet, and Y. Bengio, 'Semi-supervised learning by entropy minimization', in *Advances in neural information processing systems 17*, edited by L. K. Saul, Y. Weiss, and L. Bottou (2005).

468 Y. S. Teo, H. Zhu, B.-G. Englert, J. Řeháček, and Z. Hradil, 'Quantum-state reconstruction by maximizing likelihood and entropy', Phys. Rev. Lett. **107** (2011).

469 J. Hloušek, I. Straka, and M. Ježek, `https://https://github.com/PepaHlousek/eme`, Expectation-Maximization-Entropy method – GitHub repository, 2019.

470 R. H. Btown, and R. Q. Twiss, 'Correlation between photons in two coherent beams of light', Nature **177** (1956).

471 R. H. Brown, and R. Q. Twiss, 'A test of a new type of stellar interferometer on sirius', Nature **178** (1956).

472 Y. Zhang, K. Kasai, and M. Watanabe, 'Investigation of the photon-number statistics of twin beams by direct detection', Opt. Lett. **27** (2002).

473 J. L. O'Brien, A. Furusawa, and J. Vučković, 'Photonic quantum technologies', Nat. Photon. **3** (2009).

474 J. F. Dynes, M. Lucamarini, K. A. Patel, A. W. Sharpe, M. B. Ward, Z. L. Yuan, and A. J. Shields, 'Testing the photon-number statistics of a quantum key distribution light source', Opt. Express **26** (2018).

475 N. Cottet et al., 'Observing a quantum maxwell demon at work', Proc. Natl. Acad. Sci. U.S.A. **114** (2017).

476 D. Press, S. Götzinger, S. Reitzenstein, C. Hofmann, A. Löffler, M. Kamp, A. Forchel, and Y. Yamamoto, 'Photon antibunching from a single quantum-dot-microcavity system in the strong coupling regime', Phys. Rev. Lett. **98** (2007).

477 M. Scholz, L. Koch, and O. Benson, 'Statistics of narrow-band single photons for quantum memories generated by ultrabright cavity-enhanced parametric down-conversion', Phys. Rev. Lett. **102** (2009).

478 M. Aßmann et al., 'Ultrafast tracking of second-order photon correlations in the emission of quantum-dot microresonator lasers', Physical Review B **81** (2010).

479 B. K. Park, Y.-S. Kim, Y.-W. Cho, S. Moon, and S.-W. Han, 'Arbitrary configurable 20-channel coincidence counting unit for multi-qubit quantum experiment', Electronics **10** (2021).

480 T. J. Bartley, G. Donati, X.-M. Jin, A. Datta, M. Barbieri, and I. A. Walmsley, 'Direct observation of sub-binomial light', Phys. Rev. Lett. **110**, `10.1103/physrevlett.110.173602` (2013).

481 A. Mandarino, M. Bina, C. Porto, S. Cialdi, S. Olivares, and M. G. A. Paris, 'Assessing the significance of fidelity as a figure of merit in quantum state reconstruction of discrete and continuous-variable systems', Phys. Rev. A **93** (2016).

482 M. A. Golub, 'Laser beam splitting by diffractive optics', Opt. & Photon. News **15** (2004).

483 A. Hermerschmidt, S. Krüger, and G. Wernicke, 'Binary diffractive beam splitters with arbitrary diffraction angles', Opt. Lett. **32** (2007).

484 M. M. Rajadhyaksha, and R. H. Webb, 'Plate beamsplitter to produce multiple equal-intensity beams', Appl. Opt. **34** (1995).

485 F. Flamini et al., 'Thermally reconfigurable quantum photonic circuits at telecom wavelength by femtosecond laser micromachining', Light Sci. Appl. **4** (2015).

486 J. Carolan et al., 'Universal linear optics', Science **349** (2015).

487 G. Torlai, G. Mazzola, J. Carrasquilla, M. Troyer, R. Melko, and G. Carleo, 'Neural-network quantum state tomography', Nat. Phys. **14** (2018).

488 G. Torlai et al., 'Integrating neural networks with a quantum simulator for state reconstruction', Phys. Rev. Lett. **123** (2019).

489 E. S. Tiunov, V. V. T. (Vyborova), A. E. Ulanov, A. I. Lvovsky, and A. K. Fedorov, 'Experimental quantum homodyne tomography via machine learning', Optica **7** (2020).

490 A. M. Palmieri, E. Kovlakov, F. Bianchi, D. Yudin, S. Straupe, J. D. Biamonte, and S. Kulik, 'Experimental neural network enhanced quantum tomography', npj Quantum Inf. **6** (2020).

491 M. Yang et al., 'Experimental simultaneous learning of multiple nonclassical correlations', Phys. Rev. Lett. **123** (2019).

492 C. You et al., 'Identification of light sources using machine learning', Appl. Phys. Rev. **7** (2020).

493 I. A. Fedorov, A. E. Ulanov, Y. V. Kurochkin, and A. I. Lvovsky, 'Quantum vampire: collapse-free action at a distance by the photon annihilation operator', Optica **2** (2015).

494 K. G. Katamadze, G. V. Avosopiants, Y. I. Bogdanov, and S. P. Kulik, 'How quantum is the "quantum vampire" effect?: testing with thermal light', Optica **5** (2018).

495 C. G. Parazzoli, B. A. Capron, B. Koltenbah, D. Gerwe, P. Idell, J. Dowling, C. Gerry, and R. W. Boyd, 'Enhanced thermal images of faint objects via photon addition / subtraction', in Conference on lasers and electro-optics (2016).

496 S. M. H. Rafsanjani et al., 'Quantum-enhanced interferometry with weak thermal light', Optica **4** (2017).

497 G. L. Zanin, M. Antesberger, M. J. Jacquet, P. H. S. Ribeiro, L. A. Rozema, and P. Walther, 'Enhanced photonic maxwell's demon with correlated baths', Quantum **6** (2022).

498 M. Ueda, N. Imoto, and T. Ogawa, 'Continuous state reduction of correlated photon fields in photodetection processes', Phys. Rev. A **41** (1990).

499 N. Imoto, M. Ueda, and T. Ogawa, 'Microscopic theory of the continuous measurement of photon number', Phys. Rev. A **41** (1990).

500 C. Guerlin et al., 'Progressive field-state collapse and quantum non-demolition photon counting', Nature **448** (2007).

501 C. Sayrin et al., 'Real-time quantum feedback prepares and stabilizes photon number states', Nature **477** (2011).

502 C. W. Helstrom, 'Quantum detection and estimation theory', J. Stat. Phys. **1** (1969).

503 D. Gelbwaser-Klimovsky, and G. Kurizki, 'Heat-machine control by quantum-state preparation: from quantum engines to refrigerators', Phys. Rev. E **90** (2014).

504 A. Dechant, N. Kiesel, and E. Lutz, 'All-optical nanomechanical heat engine', Phys. Rev. Lett. **114** (2015).

505 M. Brunelli, A. Xuereb, A. Ferraro, G. D. Chiara, N. Kiesel, and M. Paternostro, 'Out-of-equilibrium thermodynamics of quantum optomechanical systems', New J. Phys. **17** (2015).

506 A. Mari, A. Farace, and V. Giovannetti, 'Quantum optomechanical piston engines powered by heat', J. Phys. B: At. Mol. Opt. **48** (2015).

507 M. Kolář, A. Ryabov, and R. Filip, 'Extracting work from quantum states of radiation', Phys. Rev. A **93** (2016).

508 G. Francica, J. Goold, F. Plastina, and M. Paternostro, 'Daemonic ergotropy: enhanced work extraction from quantum correlations', Npj Quantum Inf. **3** (2017).

509 P. Strasberg, G. Schaller, T. Brandes, and M. Esposito, 'Quantum and information thermodynamics: a unifying framework based on repeated interactions', Phys. Rev. X **7** (2017).

510 S. Vinjanampathy, and J. Anders, 'Quantum thermodynamics', Contemp. Phys. **57** (2016).

511 M. Esposito, and C. V. den Broeck, 'Second law and landauer principle far from equilibrium', Europhys. Lett. **95** (2011).

512 J. Åberg, 'Truly work-like work extraction via a single-shot analysis', Nat. Commun. **4** (2013).

513 J. Åberg, 'Catalytic coherence', Phys. Rev. Lett. **113** (2014).

514 É. Roldán, I. A. Martínez, J. M. R. Parrondo, and D. Petrov, 'Universal features in the energetics of symmetry breaking', Nat. Phys. **10** (2014).

515 P. A. Camati, J. P. S. Peterson, T. B. Batalhão, K. Micadei, A. M. Souza, R. S. Sarthour, I. S. Oliveira, and R. M. Serra, 'Experimental rectification of entropy production by maxwell's demon in a quantum system', Phys. Rev. Lett. **117** (2016).

516 R. Riedinger et al., 'Non-classical correlations between single photons and phonons from a mechanical oscillator', Nature **530** (2016).

517 K. G. Katamadze, E. V. Kovlakov, G. V. Avosopiants, and S. P. Kulik, 'Direct test of the "quantum vampire's" shadow absence with use of thermal light', Opt. Lett. **44**, 10.1364/ol.44.003286 (2019).

518 V. Holubec, and A. Ryabov, 'Cycling tames power fluctuations near optimum efficiency', Phys. Rev. Lett. **121** (2018).

519 T. Denzler, and E. Lutz, 'Power fluctuations in a finite-time quantum carnot engine', Phys. Rev. Research **3** (2021).

520 M. B. Plenio, and V. Vitelli, 'The physics of forgetting: landauer's erasure principle and information theory', Contemp. Phys. **42** (2001).

521 K. Maruyama, F. Nori, and V. Vedral, 'Colloquium: the physics of maxwell's demon and information', Rev. Mod. Phys. **81** (2009).

522 J. M. R. Parrondo, J. M. Horowitz, and T. Sagawa, 'Thermodynamics of information', Nat. Phys. **11** (2015).

523 E. Lutz, and S. Ciliberto, 'Information: from maxwell's demon to landauer's eraser', Phys. Today **68** (2015).

524 M. G. Raizen, 'Comprehensive control of atomic motion', Science **324** (2009).

525 S. Toyabe, T. Sagawa, M. Ueda, E. Muneyuki, and M. Sano, 'Experimental demonstration of information-to-energy conversion and validation of the generalized jarzynski equality', Nat. Phys. **6** (2010).

526 J. V. Koski, V. F. Maisi, J. P. Pekola, and D. V. Averin, 'Experimental realization of a szilard engine with a single electron', Proc. Natl. Acad. Sci. U.S.A **111** (2014).

527 J. V. Koski, V. F. Maisi, T. Sagawa, and J. P. Pekola, 'Experimental observation of the role of mutual information in the nonequilibrium dynamics of a maxwell demon', Phys. Rev. Lett. **113** (2014).

528 J. V. Koski, A. Kutvonen, I. M. Khaymovich, T. Ala-Nissila, and J. P. Pekola, 'On-chip maxwell's demon as an information-powered refrigerator', Phys. Rev. Lett. **115** (2015).

529 K. Chida, S. Desai, K. Nishiguchi, and A. Fujiwara, 'Power generator driven by maxwell's demon', Nat. Commun. **8** (2017).

530 A. Kumar, T.-Y. Wu, F. Giraldo, and D. S. Weiss, 'Sorting ultracold atoms in a three-dimensional optical lattice in a realization of maxwell's demon', Nature **561** (2018).

531 G. Paneru, D. Y. Lee, T. Tlusty, and H. K. Pak, 'Lossless brownian information engine', Phys. Rev. Lett. **120** (2018).

532 T. Admon, S. Rahav, and Y. Roichman, 'Experimental realization of an information machine with tunable temporal correlations', Phys. Rev. Lett. **121** (2018).

533 M. Ribezzi-Crivellari, and F. Ritort, 'Large work extraction and the landauer limit in a continuous maxwell demon', Nat. Phys. **15** (2019).

534 M. Debiossac, D. Grass, J. J. Alonso, E. Lutz, and N. Kiesel, 'Thermodynamics of continuous non-markovian feedback control', Nat. Commun. **11** (2020).

535 Y. Masuyama et al., 'Information-to-work conversion by maxwell's demon in a superconducting circuit quantum electrodynamical system', Nat. Commun. **9** (2018).

536 M. Naghiloo, J. J. Alonso, A. Romito, E. Lutz, and K. W. Murch, 'Information gain and loss for a quantum maxwell's demon', Phys. Rev. Lett. **121** (2018).

537 B.-L. Najera-Santos, P. A. Camati, V. Métillon, M. Brune, J.-M. Raimond, A. Auffèves, and I. Dotsenko, 'Autonomous maxwell's demon in a cavity QED system', Phys. Rev. Research **2** (2020).

538 S. L. Braunstein, and P. van Loock, 'Quantum information with continuous variables', Rev. Mod. Phys. **77** (2005).

539 P. Pietzonka, and U. Seifert, 'Universal trade-off between power, efficiency, and constancy in steady-state heat engines', Phys. Rev. Lett. **120** (2018).

540 J. I. Cirac, R. Blatt, A. S. Parkins, and P. Zoller, 'Quantum collapse and revival in the motion of a single trapped ion', Phys. Rev. A **49** (1994).

541 Y.-S. Ra, C. Jacquard, A. Dufour, C. Fabre, and N. Treps, 'Tomography of a mode-tunable coherent single-photon subtractor', Phys. Rev. X **7** (2017).

542 Y.-S. Ra, A. Dufour, M. Walschaers, C. Jacquard, T. Michel, C. Fabre, and N. Treps, 'Non-gaussian quantum states of a multimode light field', Nat. Phys. **16** (2019).

543 F. Campaioli, F. A. Pollock, F. C. Binder, L. Céleri, J. Goold, S. Vinjanampathy, and K. Modi, 'Enhancing the charging power of quantum batteries', Phys. Rev. Lett. **118** (2017).

544 D. Ferraro, M. Campisi, G. M. Andolina, V. Pellegrini, and M. Polini, 'High-power collective charging of a solid-state quantum battery', Phys. Rev. Lett. **120** (2018).

545 F. Barra, 'Dissipative charging of a quantum battery', Phys. Rev. Lett. **122** (2019).

546 E. Jaynes, and F. Cummings, 'Comparison of quantum and semiclassical radiation theories with application to the beam maser', Proc. IEEE **51**, 89–109 (1963).

547 T. Sagawa, and M. Ueda, 'Generalized jarzynski equality under nonequilibrium feedback control', Phys. Rev. Lett. **104** (2010).

548 Y. Morikuni, and H. Tasaki, 'Quantum jarzynski-sagawa-ueda relations', J. Stat. Phys. **143** (2011).

549 S. Gleyzes et al., 'Quantum jumps of light recording the birth and death of a photon in a cavity', Nature **446** (2007).

550 D. I. Schuster et al., 'Resolving photon number states in a superconducting circuit', Nature **445** (2007).

551 B. R. Johnson et al., 'Quantum non-demolition detection of single microwave photons in a circuit', Nat. Phys. **6** (2010).

552 B. Royer, A. L. Grimsmo, A. Choquette-Poitevin, and A. Blais, 'Itinerant microwave photon detector', Phys. Rev. Lett. **120** (2018).

553 S. Kono, K. Koshino, Y. Tabuchi, A. Noguchi, and Y. Nakamura, 'Quantum non-demolition detection of an itinerant microwave photon', Nat. Phys. **14** (2018).

554 A. Opremcak et al., 'Measurement of a superconducting qubit with a microwave photon counter', Science **361** (2018).

555 J.-C. Besse, S. Gasparinetti, M. C. Collodo, T. Walter, A. Remm, J. Krause, C. Eichler, and A. Wallraff, 'Parity detection of propagating microwave fields', Phys. Rev. X **10** (2020).

556 M. Mičuda, I. Straka, M. Miková, M. Dušek, N. J. Cerf, J. Fiurášek, and M. Ježek, 'Noiseless loss suppression in quantum optical communication', Phys. Rev. Lett. **109** (2012).

557 P. Grangier, G. Roger, and A. Aspect, 'Experimental evidence for a photon anticorrelation effect on a beam splitter: a new light on single-photon interferences', Europhys. Lett. **1** (1986).

558 E. Diamanti, H.-K. Lo, B. Qi, and Z. Yuan, 'Practical challenges in quantum key distribution', npj Quantum Inf. **2** (2016).

559 R. Bedington, J. M. Arrazola, and A. Ling, 'Progress in satellite quantum key distribution', npj Quantum Inf. **3** (2017).

560 V. D'Auria, N. Lee, T. Amri, C. Fabre, and J. Laurat, 'Quantum decoherence of single-photon counters', Phys. Rev. Lett. **107** (2011).

561 J. Ma, X. Chen, H. Hu, H. Pan, E. Wu, and H. Zeng, 'Quantum detector tomography of a single-photon frequency upconversion detection system', Opt. Express **24** (2016).

Detektory počtu fotonů a jejich aplikace v kvantových technologiích

autoreferát k disertační práci

Josef Hloušek

Přírodovědecká fakulta
Univerzita Palackého

Olomouc
2022

Uchazeč:	Mgr. Josef Hloušek
Studijní obor:	Optika a optoelektronika
Instituce:	Katedra optiky, Přírodovědecká fakulta, Univerzita Palackého
ORCID:	0000-0003-2923-3492
ResearcherID:	D-2890-2018
Školitel:	prof. Mgr. Radim Filip, PhD.
Konzultant:	RNDr. Miroslav Ježek, PhD.
Oponenti:	

Termín obhajoby:	
Místo obhajoby:	
Místo pro seznámení se s DP a posudky:	

Anotace

Hlavním objektem zájmu v kvantové optice jsou jednotlivá energetická kvanta elektromagnetického záření, fotony. Moderní kvantová fotonika stojí na experimentálních technikách generace, detekce a manipulace se stavy světla na úrovni jednotlivých fotonů. Jednou z nejvýznamnějších charakterizačních metod je zkoumání světla z hlediska jeho statistických vlastností. Měření fotonové statistiky libovolného stavu světla se opírá o schopnost rozlišovat mezi jednotlivými fotony a určovat jejich počet. Vědecká komunita věnovala mnoho úsilí, aby dosáhla rozlišení počtu fotonů pomocí rozličných detekčních přístupů. Detektory s rozlišením počtu fotonů posouvají hranice v oblasti pokročilé detekce světla a se svým velkým mezioborovým aplikačním potenciálem se staly technologickou špičkou.

Cílém disertační práce je návrh a experimentální realizace ultrapřesné detekční techniky měření statistiky počtu fotonů neznámého optického signálu a jeho korelačních vlastností. Vyvinutá detekční technika je nezkreslená systematickými chybami, což je revoluční vlastnost, jíž nedosahují ani kryogenické detektory na bázi supravodivého přechodu. Detekční technika byla ověřena experimentálně pro desítky různých statistik světla včetně neklasických zdrojů a výpočetně pro desetitisíce numericky simulovaných optických signálů. Metoda je škálovatelná a nevyžaduje náročnou charakterizaci detektoru nebo korekce nedokonalostí detektoru, což řeší dlouhodobě existující problém detekce statistiky světla nezávislé na detekčním zařízení.

Precizní měření statistiky počtu fotonů se v předložené práci využívá k charakterizaci typu procesu generace světla, k cílené modifikace statistických vlastností kvantových stavů světla a k charakterizaci jednofotonových detektorů. Podařilo se úspěšně kvantifikovat světelné zdroje chaotického, klasického, neklasického a negaussovského světla. Modifikace statistických vlastností světla bylo docíleno subtrakcí jednotlivých fotonů z termálních stavů světla. Práce uvádí metody podmíněné a deterministické přípravy klasických stavů světla mimo termodynamickou rovnováhu za účelem demonstrace kvantových termodynamických jevů. Dále je prezentována metoda certifikace dvou vysoce neklasických vlastností jednofotonových detektorů - kvantové negaussovosti a negativity Wignerovi funkce. V diskutovaném přístupu je role měření a stavu obrácená s ohledem na běžné testování negaussovského charakteru kvantových stavů.

Abstract

In quantum optics, the main object of interest is the individual energy quanta of light, photons. Every modern quantum photonics experiment hinges on the ability to generate, detect, and manipulate the states of light at the single-photon level. One of the most essential questions is unveiling the nature of light from the perspective of its statistical properties. Photon statistics characterization relies on the capability to distinguish, detect, and count individual photons. As a consequence, the scientific community has devoted significant effort to accomplishing photon-number resolution by various detection approaches employing different physical phenomena. Nowadays, photon-number-resolving detectors represent the rapid advancement of the field of light detection with tremendous interdisciplinary application potential.

The aim of this dissertation is to design and experimentally develop an ultra-precise detection technique for measuring the photon statistics of an unknown optical signal and its statistical correlations. Developed measurement workflow free of systematic errors consists of a reconfigurable photon-number-resolving detector, custom electronic circuitry, and a novel data processing algorithm. The result opens new paths for optical technologies by providing access to the photon-number information without the necessity of full detector tomography. It also aims to directly evaluate key quantities such as correlation functions and non-classicality metrics rather than full tomography of the photon statistics.

Furthermore, the Thesis presents the application of the precise measurement of photon statistics to characterize the physical processes that generate the optical signal, modify the statistical properties of quantum states of light, and characterize single-photon detectors. It was possible to successfully detect chaotic, classical, nonclassical, non-Gaussian, and negative-Wigner-function light. Modifying the statistical properties of light was achieved by subtracting individual photons from the thermal states of light. The thesis also presents methods of conditional and deterministic preparation of classical states of light out of thermal equilibrium, which can be employed as useful sources for future experiments in the field of quantum thermodynamics. Finally, a method for certifying two highly non-classical properties of quantum detectors - quantum non-Gaussianity and negativity of the Wigner function - is presented. In this approach, the role of measurement and state is reversed with respect to the standard certification of

the quantum non-Gaussian character of quantum states.

Klíčová slova: foton, statistické vlastnosti světla, detekční statistika, jednofotonový detektor, jednofotonový detektor s částečným rozlišením počtu fotonů, subtrakce fotonů, kvantová negaussovost

Keywords: Photon; statistics of light; counting statistics; single-photon detector; photon-number-resolving detector; photon subtraction; quantum non-Gaussianity.

List of publications

The following page contains lists of selected articles covering the results presented in this Thesis.

First-author publications

A1 J. Hloušek, M. Ježek, and R. Filip, 'Work and information from thermal states after subtraction of energy quanta', Sci. Rep. **7** (2017).

A2 J. Hloušek, M. Dudka, I. Straka, and M. Ježek, 'Accurate detection of arbitrary photon statistics', Phys. Rev. Lett. **123** (2019).

A3 J. Hloušek, M. Ježek, and J. Fiurášek, 'Direct experimental certification of quantum non-Gaussian character and wigner function negativity of single-photon detectors', Phys. Rev. Lett. **126** (2021).

Other co-author publications

C1 I. Straka, L. Lachman, J. Hloušek, M. Miková, M. Mičuda, M. Ježek, and R. Filip, 'Quantum non-gaussian multiphoton light', Npj Quantum Inf. **4** (2018).

C2 J. Mika, L. Podhora, L. Lachman, P. Obšil, J. Hloušek, R. F. M. Ježek, and L. Slodička, 'Generation of ideal thermal light in warm atomic vapor', New J. Phys. **20** (2018).

Articles in preparation

P1 J. Hloušek, J. Grygar, M. Dudka, and M. Ježek, 'High-resolution multi-channel coincidence counting system for large-scale photonic quantum technology', in preparation (2022).

P2 J. Hloušek, T. Denzler, V. Švarc, M. Ježek, E. Lutz, and R. Filip, 'Experimental quantum photonic Maxwell's demon', Submitted (2022).

Author contributions

The projects presented in this Thesis are the product of the close scientific colaboration. Here I give a detailed account of my speciffic involvements and contributions to each presented project and also appropriate credit to co-authors is ascribed.

[A1] J. Hloušek, M. Ježek, and R. Filip, *'Work and information from thermal states after subtraction of energy quanta'*, Scientific Reports **7**, 13046 (2017).
I constructed experimental setup, performed measurements and numerical simulations, and analyzed data. Miroslav Ježek helped supervise the project. Radim Filip suggested the theoretical idea, performed calculations, and supervised the project. All authors participated in writing the manuscript.

[C1] I. Straka, L. Lachman, J. Hloušek, M. Miková, M. Ježek, and R. Filip, *'Quantum non-Gaussian multiphoton light'*, Nature Partner Journals Quantum Information **4**, 4 (2018).
Lukáš Lachman and Radim Filip are responsible for the theoretical part. Ivo Straka constructed the source, performed the measurement, and process the data. I constructed the PNRD and helped with the alignment and setting the detector. All authors provided critical feedback and helped shape the research, analysis and manuscript.

[C2] J. Mika, L. Podhora, L. Lachmann, P. Obšil, J. Hloušek, M. Ježek, R. Filip, and L. Slodička, *'Generation of ideal thermal light in warm atomic vapor'*, New Journal of Physics **20**, 093002 (2018).
Jaromír Mika measured and proccesed the data. Lukáš Podhora built the experimental setup. The theoretical analysis was performed by Lukáš Lachman and Radim Filip. Petr Obšil prepared the pumping laser. I and Miroslav Ježek analyzed data, retrieved photon statistics and characterized the quality of observed Bose–Einstein statistics by evaluation of the Shannon entropy and relative entropy. Radim Filip and Lukáš Slodička initiated and coordinated project. All authors contributed to the manuscript preparation.

[A2] J. Hloušek, M. Dudka, I. Straka, and M. Ježek, *'Accurate detection of arbitrary photon statistics'*, Physical Review Letters **123**, 153604 (2019).
I worked out almost all of the technical details, and performed the numerical calculations for the suggested measurement workflow. I also built the experimental

setup and performed the measurements and data analysis. Miroslav Ježek initiated and coordinated the project and supervised the experiment. Ivo Straka construct the a down-conversion source and participated in data analysis. I prepared the manuscript and all authors were involved in creating and revising the manuscript. All authors contributed to the discussion of the results.

[A3] J. Hloušek, M. Ježek, and Jaromír Fiurášek, *'Direct experimental certification of quantum non-Gaussian character and Wigner function negativity of single-photon detectors'*, Physical Review Letters **126**, 043601 (2021).
Jaromír Fiurášek initiated and coordinated the project. He was the lead investigator, responsible for all major areas of concept formation. I built the experimental setup for the direct certification of non-classical features of quantum detectors and performed the measurement and data analysis. Miroslav Ježek supervised the experiment and participated in analysis and interpretation of data. I and Miroslav Fiurášek provided the theoretical analysis and simulations of the detector response to explore the non-Gaussian character and Wigner function negativity of SPAD. Jaromír Fiurášek prepared the manuscript and all authors were involved in creating and revising the manuscript. All authors contributed to the discussion of the results.

[P1] J. Hloušek, M. Dudka, J. Grygar, and M. Ježek, *'High-resolution multi-channel coincidence counting system for large-scale photonic quantum technology'*.
I built the experimental setup for the multi-coincidence measurement and performed the measurement and data analysis. Michal Dudka designed and built presented high-resolution multi-channel coincidence counting system (CCU). Jan Grygar and Michal Dudka analyzed the performance and capabilities of the CCU, and developed the software library. Miroslav Ježek initiated and coordinated the project. I wrote the manuscript with input from all authors.

[P2] J. Hloušek, T. Denzler, V. Švarc, M. Ježek, Eric Lutz, and R. Filip, *'Experimental Quantum Photonic Maxwell Demon'*.
Radim Filip conceived the idea and were in charge of overall direction and planning. Eric Lutz coordinated and supervised the theoretical statements of quantum thermodynamics. Tobias Denzler performed the analytic thermodynamical calculations and helped carry out the simulations. Vojtěch Švarc built a fully tunable and switchable coupler and assisted with the data collection. I built experimental setup, measured and analyzed the data. Miroslav Ježek helped carry out the experiment and contributed to the interpretation of the results. All authors contributed

to the manuscript preparation.

Funding

The research presented in this Thesis was primarily supported by the Czech Science Foundation under the projects 17-26143S and 21-18545S. We have also received national funding from the MEYS and the funding from European Union's Horizon 2020 (2014-2020) research and innovation framework program under grant agreement No 731473 (project 8C18002). Project HYPER-U-P-S has received funding from the QuantERA ERA-NET Cofund in Quantum Technologies implemented within the European Union's Horizon 2020 Programme. Finally, Palacky University supported presented research by IGA projects: IGA-PrF-2016-009, IGA-PrF-2017-008, IGA-PrF-2018-010, IGA-PrF-2019-010, and IGA-PrF-2020-009.

Preface

My interest in optics goes back to my high school years. In the early stage of my bachelor's studies, I have joined the research group Quantum Optics Lab Olomouc, especially the photonic sources & detectors team. Under the co-supervision of Miroslav Ježek, I have actively participated in research projects of the lab. I started working on experimental research in the field of detection of single photons, photon-number-resolving techniques, and characterization of sources of light at the single-photon level. Our scientific efforts resulted in the development of an efficient workflow for photon-number detection of arbitrary optical signals with unprecedented accuracy (fidelity > 0.999) and a dynamic range of photon-number resolution (photon numbers up to 50). We also developed a method for direct verification of the highly nonclassical features of optical quantum measurements, such as quantum non-Gaussianity and the negativity of the Wigner function. Simultaneously, this experimental direction has been supported by my collaborations in quantum optics theory with supervisor Radim Filip and Jaromír Fiurášek.

This Thesis comprehensively presents mostly experimental outcomes based on the results achieved during my post-graduate studies at the Department of Optics, Faculty of Science, Palacký University, Olomouc. All of the results presented henceforth was conducted in the Quantum Optics Lab Olomouc. The presented

Thesis is based on five published publications denoted in List of publications under [A1–A3, C1, C2]. The Thesis also uses other results achieved in ongoing projects whose manuscripts [P1, P2] are in preparation at the time of writing.

To bring the reader closer to the contribution of the presented experimental work, I aim to give a review of the experimental implementations and applications of single-photon detection and resolving the number of photons. I believe this Thesis will be of broad interest primarily to scientists working in the fields of quantum foundations, quantum information processing and quantum communication. Presented detection workflow can also be directly translated to other experimental platforms like emerging biomedical imaging and particle-tracking techniques. Moreover, the community dealing with a conditioned modification in photon statistics to achieve the required properties of measured light should appreciate the contribution of the presented results.

Olomouc
December 2022

Josef Hloušek
hlousek@optics.upol.cz
@PepaHlousek

Introduction and brief summary

In recent decades, a large part of the quantum optics community has focused on developing and characterizing single-photon light sources and detectors. It has been almost 90 years since the demonstration of the devices exhibiting single-photon sensitivity [1–3]. This major breakthrough initiated a multitude of new developments and technical improvements in single-photon technologies [B1–B5, 4–12]. Specifically, it includes quantum photonics technologies for single-photon generation [13–25], manipulation [26–36], and detection [37–74]. Appropriate detection techniques are necessary to determine the quality of the methods for generating quantum states of light. The generation of single photons goes hand in hand with their accurate detection, and technological progress in one of these disciplines will inevitably contribute to innovation in the other.

In general, single-photon detector (SPD) approaches are based on a proportional conversion of absorbed photons to current or voltage pulses, which are amplified and measured. These well-defined detector output signals "clicks" are collected and processed by electronic counting devices whose functionality solely depends on the used application. The growth of the optical network complexity in photon-consuming applications, such as multi-photon boson sampling [75–79], high-dimensional entanglement [80–85], and multi-photon qubits quantum information processing [86–88], motivates the research for detection technology improvements to process a high number of photons in the explored signal. Nowadays, highly efficient low-noise single-photon detectors are still merging as important devices for realizing many photonic applications [33, 89–101], both classical and quantum. However, studying and exploiting quantum properties of light rely on precise measurement and manipulation of light at the single-photon level. One of the critical requirements allowing this research area is the capability to detect and count individual photons. Of particular interest are the advanced detection techniques that make possible to distinguish the exact number of photons arriving at the detector. As indicated, the growing demand in modern quantum physics experiments for this type of information about the statistical properties of light drives the current effort to improve these advanced detection technologies.

Conventional single-photon detection concepts are primarily sensitive to the presence of light without any information about the number of input photons

[B2, B4, B5, 5, 6, 8–12, 102]. Nevertheless, even these detection devices can be employed in a temporal or spatial configuration to obtain photon-number resolution [50, 64, 103–109]. In addition, the development of a new class of detectors based on superconducting materials has demonstrated inherent sensitivity to individual numbers of photons [B2, 38, B6]. These devices significantly outperform all existing single-photon detectors in detection efficiency and timing jitter. Advanced photon-number-resolving detectors (PNRDs) found their broadwise applicability in modern optical experiments benefits from the counting individual photons of the optical signal. The knowledge of photon-number statistics allows for exploring the statistical properties of an unknown state of light required for the complete classification of optical sources. Photon-number resolution is a pivotal problem of quantum technology, impacting quantum metrology [110, 111], information processing [86–88, 112], and imaging [113]. The measurement of the statistical properties of light is a condition of secure communication [114] and quantum simulation. Furthermore, novel super-resolving emitter counting techniques will incorporate quantum statistics and correlations into classical super-resolving imaging. The recent progress in integrated photonics transforms SPDs and PNRDs into feasible technology for integrated quantum photonic systems [21, 22, 52, 58, 59, 62, 63, 65, 69, 71, 112, 115–120]

Outline

This Thesis covers most of the experiments and results of scientific research, which were realized during my Ph.D. study. My research is primarily focused on the precise measurement and conditional and deterministic modulation of quantum statistics of light using a photon-number resolving detector. Additionally, this type of detection device is employed in a novel direct experimental certification of the non-Gaussianity of the quantum optical detectors, namely single-photon avalanche diodes.The Thesis has in total five chapters organized as follows.

First, I start with the key goals and objectives of the presented research (Section 1.2), its challenges, further improvements, and its applicability in modern quantum experiments. Special emphasis is given to provide adequate information

about the study area for the readers to analyze and evaluate proposed research in the context of the state-of-the-art methods in the field of photonic detection techniques and requisite complex signal processing (Section 1.3). I give details about basic properties and measurement metrics that are generally accepted for the characterization of the quantum state. Notably, key insights into different aspects of modern approaches of photon-number-resolving detectors are reviewed.

In Chapter 2 I give a brief account of experimental methods that are used in disertation. The key theoretical and experimental terminology is introduced and explained. The subject of Section 2.1 is the statistical properties of light, namely: definition in Fock basis and phase space, and how it can be obtained. Section 2.2 introduces several parameters associated with photon statistics which are commonly used to characterize quantum states of light. Furthemore, the various techniques to generate different quantum states of light are described (Section 2.3). Section 2.4 reviews one of today's most used single-photon detectors in optical laboratories: single-photon avalanche diode. In Section 2.5, the spatial multiplexed detection technique is fully discussed. In addition, the methods to reconstruct the photon statistics from the measured click statistics such as direct inversion and maximum-likelihood strategies are analyzed (Section 2.6).

In Chapter 3, an accurate detection technique is proposed that can distinguish between number of photons to achieve photon statistics and statistical correlations of the unknown state of light. Section 3.2 provides the description of the experimental implementation of the developed detection method based on a complex detector capable of partial photon-number resolution composed of several multiplexed single-photon avalanche photodiodes. Section 3.3 treats the problem of the electronic signal processing. Section 3.4 focuses on numerical simulations of the photon statistics retrieval processes in order to compare several algorithms in terms of accuracy and convergence speed. Experimental demonstration of the detection approach to access photon statistics is presented in Section 3.5. Various light sources were used to test the response of the detector: stabilized laser, quasi-thermal light, and heralded single-photon source based on spontaneous parametric down conversion. Finally, I discuss the future challenges of technological development and photon-statistics retrieval required to bring the presented PNRD configuration even further (Section 3.6).

Chapter 4 extends the arbitrary photon statistics detection concept to modify the statistical properties of light. Single-shot photon counting is used for condi-

tional subtraction of the exact number of photons from the pseudo-thermal light to increase the mean photon number of the output state of light (Section 4.2). Furthermore, it is shown that these out-of-equilibrium states of light are useful for many applications in quantum information and thermodynamics. In Section 4.3 I discuss results of a custom-built source of arbitrary super-Poissonian statistics based on l-photon subtraction and active feedforward control and swapping. This experimental approach allows for deterministic generation of light states with super-Poissonian statistics created by mixing thermal state with the l-photon subtracted thermal state. Subsequently, the thermodynamics analysis of a quantum bosonic Maxwell's demon is presented.

Chapter 5 introduces a novel method to experimentally certify the quantum non-Gaussian character (Section 5.2) and Wigner-function negativity (Section 5.3) of the quantum photonic detectors. The presented technique builds on previous works focused on certification of quantum non-Gaussian character of quantum states and extends it to the detectors. Regularization of the detector POVM elements is done by using noiseless attenuation, which can be experimentally implemented by specific probe states: a vacuum state and two thermal states with different mean photon numbers.

Finally, the main results of the Thesis are reviewed in Chapter 6. I summarize our particular results and findings (Section 6.1). In Section 6.2 I also give the overview of problems and possible extensions of the developed methods.

Goals of the Thesis

The quantum properties of light are determined by its statistical properties. The knowledge of photon statistics can facilitate many applications not only in photonic quantum technology [86–88, 112] but also in quantum imaging [113], quantum metrology [110, 111], and many other fields. However, accurate detection of arbitrary photon statistics is still challenging mainly due to finite dynamic range of existing photon-number-resolving detectors. The chief goal of this Thesis is to advance scalable detection method of ultra weak photonic signals and remove some drawbacks of current analyzers of quantum statistics to achieve unprecedented accuracy of photon-number resolution without the necessity of detector

tomography. We dealt with experimental development and characterization of a measurement workflow free of systematic errors consisting of a complex reconfigurable partial photon-number-resolving detector, custom electronic circuitry, and novel data processing algorithm.

Particularly, we have developed a complex single-photon detector capable of photon-number resolution with a fully tunable number of input channels, optimized efficiency, and time response. Presented detector is based on multiplexing of binary single-photon detectors. The tunability of the developed detector enables us to easily change the number of constituent single-photon detectors. Optical signal under test can be analyzed by one detector, two detectors (Hanbury-Brown and Twiss measurement), three detectors, and so on. This reconfigurability is useful for direct tests of nonclassical features of various physical systems, as it was later demonstrated.

The large number of output channels represents a challenge to subsequent data processing. Coincidence counters need to register single-detection events in all the output channels as well as all the possible coincidence events between the channels. The real-time processing of coincidence events becomes essential in the large-scale modern quantum photonics experiments, where the total number of events is too large to be stored and post-processed. Taking these requirements into account, we developed an ultra-fast multi-channel coincidence system with ten picosecond jitter allowing sub-nanosecond coincidence windows and dead time smaller than recovery time of the used single-photon detectors. The coincidence unit was designed for counting coincidence events from singles to 16-fold coincidences with the full channel-number resolution.

Employing the advanced quantum reconstruction algorithms we have compensated for imperfections of detection process to estimate the photon statistics from the measured counting distribution. In addition, the photon statistics retrieval method has to cope with incomplete data which is the a typical problem of the channel-limited photon counting measurement. We have solved the inverse task of photon statistics retrieval by developing efficient algorithm based on the maximization-expectation method weakly-regularized by maximum-entropy principle which significantly improved the precision of the photon statistics measurement proposed so far. It breaks the finite-multiplexing limit and achieves unprecedented accuracy of photon-number resolution demonstrated for various photonic signals, including highly non-classical states, which surpasses even bleeding-

edge cryogenic detectors.

Afterwards, employing a developed detector we have performed the measurement of quantum statistics of light from various sources. We also aim for direct evaluation of key statistical quantities, such as moments, Fano factor, entropy, $g^2(\tau)$ and other correlation parameters. Additionally, the non-classicality of multi-photon states of light was discerned. Experimental data confirmed the numerical simulations and quantified the developed method as a plausible characterization of the statistical properties of unknown states of light.

Furthermore, the developed detector enabled the realization of projects investigating conditional and deterministic modification of quantum statistics of light. Knowledge of the statistical properties of light allowed us to prepare states of light with super-Poissonian statistics. First, the conditional subtraction of l single photons from the thermal states of light results in a l-photon subtracted thermal states exhibiting super-Poissonian statistics with a l-times larger mean photon number than of the original thermal state. However, the photon correlation decreases closer to Poissonian light, and the mean photon number grows faster than its standard deviation. We performed this experiment to simulate thermodynamic processes, namely the dissipation of the energy of a quantum oscillator into a cold reservoir to produce energy that can be used to do work or transfer information. Afterwards, we used experimental experience with the generation of out-of-equilibrium states to design and implement a more advanced method to deterministically modify the statistical properties of light. By exploiting this technique, a complex triggering, controlling, and fast optical switching between states of light employing the novel fast photonic switch based on Mach-Zehnder interferometer, we have experimentally generated and characterized deterministic out-of-equilibrium states. As a result, other thermodynamic simulations were performed to analyze bosonic Maxwell's demon in the quantum regime.

The final goal of the work was to develop a new characterization method for photonic detectors. The presented approach requires only three probe states without any need for complex tomographic data processing. Accurate detection of photon statistics has application potential in the precise preparation of these probe states of the light, namely vacuum state and two thermal states with different mean photon numbers. Our efficient scheme allows the direct certification of quantum non-Gaussianity [121] or Wigner function negativity [122] of the optical

quantum detector while avoiding all potential complications of quantum detector tomography. The results shown that this detector benchmarking technique can lead to further insight on the capabilities and limitations of quantum detectors.

In the future, our results could pave the way for precise verification and benchmarking of various photonic sources, a key requirement for their applications in diverse fields. It includes the characterization of statistics of single-photon and entangled sources with imminent applications in quantum communications. Future development of the presented detector will tackle the problem of super-resolution and counting of emitters with different brightness, blurred due to diffraction, and buried in excess noise. Also, the developed detection workflow allows for a single shot measurement, as required for conditional state preparation [123], linear-optics quantum computing [124], quantum repeaters [125] and etc.

References

Books

B1 U. Leonhardt, *Measuring the quantum state of light*, (2003).

B2 C. Enss, ed., *Cryogenic particle detection*, (2005).

B3 M. Bellini, and A. Zavatta, *Manipulating light states by single-photon addition and subtraction*, (2010).

B4 A. Migdall, S. Polyakov, J. Fan, and J. Bienfang, *Single-photon generation and detection: physics and applications*, (2014).

B5 R. H. Hadfield, and G. Johansson, eds., *Superconducting devices in quantum optics*, (2016).

B6 K. Irwin, and G. Hilton, *Transition-edge sensors*, (2005).

Articles, proceedings and theses

1 H. Iams, and B. Salzberg, 'The secondary emission phototube', Proc. IRE **23** (1935).

2 V. Zworykin, G. Morton, and L. Malter, 'The secondary emission multiplier-a new electronic device', Proc. IRE **24** (1936).

3 L. Kubetsky, 'Multiple amplifier', Proc. IRE **25** (1937).

4 K. W. Ledingham, 'The development of detectors for use at low light levels', Contemp. Phys. **37** (1996).

5 C. Silberhorn, 'Detecting quantum light', Contemp. Phys. **48** (2007).

6 R. H. Hadfield, 'Single-photon detectors for optical quantum information applications', Nat. Photon. **3** (2009).

7 G. S. Buller, and R. J. Collins, 'Single-photon generation and detection', Meas. Sci. Technol. **21** (2009).

8 M. D. Eisaman, J. Fan, A. Migdall, and S. V. Polyakov, 'Invited review article: single-photon sources and detectors', Rev. Sci. Instrum. **82** (2011).

9 C. M. Natarajan, M. G. Tanner, and R. H. Hadfield, 'Superconducting nanowire single-photon detectors: physics and applications', Supercond. Sci. Technol. **25** (2012).

10 C. J. Chunnilall, I. P. Degiovanni, S. Kück, I. Müller, and A. G. Sinclair, 'Metrology of single-photon sources and detectors: a review', Opt. Eng. **53** (2014).

11 F. Ceccarelli, G. Acconcia, A. Gulinatti, M. Ghioni, I. Rech, and R. Osellame, 'Recent advances and future perspectives of single-photon avalanche diodes for quantum photonics applications', Adv. Quantum Technol. **4** (2020).

12 I. E. Zadeh, J. Chang, J. W. N. Los, S. Gyger, A. W. Elshaari, S. Steinhauer, S. N. Dorenbos, and V. Zwiller, 'Superconducting nanowire single-photon detectors: a perspective on evolution, state-of-the-art, future developments, and applications', Appl. Phys. Lett. **118** (2021).

13 C. Kurtsiefer, S. Mayer, P. Zarda, and H. Weinfurter, 'Stable solid-state source of single photons', Phys. Rev. Lett. **85** (2000).

14 A. Kuzmich, W. P. Bowen, A. D. Boozer, A. Boca, C. W. Chou, L.-M. Duan, and H. J. Kimble, 'Generation of nonclassical photon pairs for scalable quantum communication with atomic ensembles', Nature **423** (2003).

15 M. Hennrich, A. Kuhn, and G. Rempe, 'Transition from antibunching to bunching in cavity QED', Phys. Rev. Lett. **94** (2005).

16 J. S. Neergaard-Nielsen, B. M. Nielsen, C. Hettich, K. Mølmer, and E. S. Polzik, 'Generation of a superposition of odd photon number states for quantum information networks', Phys. Rev. Lett. **97** (2006).

17 E. A. Goldschmidt, M. D. Eisaman, J. Fan, S. V. Polyakov, and A. Migdall, 'Spectrally bright and broad fiber-based heralded single-photon source', Phys. Rev. A **78** (2008).

18 M. Assmann, F. Veit, M. Bayer, M. van der Poel, and J. M. Hvam, 'Higher-order photon bunching in a semiconductor microcavity', Science **325** (2009).

19 D. Elvira et al., 'Higher-order photon correlations in pulsed photonic crystal nanolasers', Phys. Rev. A **84** (2011).

20 G. Harder, T. J. Bartley, A. E. Lita, S. W. Nam, T. Gerrits, and C. Silberhorn, 'Single-mode parametric-down-conversion states with 50 photons as a source for mesoscopic quantum optics', Phys. Rev. Lett. **116** (2016).

21 G. Digeronimo, M. Petruzzella, S. Birindelli, R. Gaudio, S. F. Poor, F. van Otten, and A. Fiore, 'Integration of single-photon sources and detectors on GaAs', Photonics **3** (2016).

22 S. Khasminskaya et al., 'Fully integrated quantum photonic circuit with an electrically driven light source', Nat. Photon. **10** (2016).

23 T. Kiyohara, R. Okamoto, and S. Takeuchi, 'Realization of multiplexing of heralded single photon sources using photon number resolving detectors', Opt. Express **24** (2016).

24 F. Bodog, M. Mechler, M. Koniorczyk, and P. Adam, 'Optimization of multiplexed single-photon sources operated with photon-number-resolving detectors', Phys. Rev. A **102** (2020).

25 M. Engelkemeier, J. Sperling, J. Tiedau, S. Barkhofen, I. Dhand, M. B. Plenio, B. Brecht, and C. Silberhorn, 'Climbing the fock ladder: advancing multiphoton state generation', (2021).

26 M. Dakna, L. Knöll, and D.-G. Welsch, 'Quantum state engineering using conditional measurement on a beam splitter', Eur. Phys. J. D **3** (1998).

27 A. Zavatta, S. Viciani, and M. Bellini, 'Quantum-to-classical transition with single-photon-added coherent states of light', Science **306** (2004).

28 V. Parigi, A. Zavatta, M. Kim, and M. Bellini, 'Probing quantum commutation rules by addition and subtraction of single photons to/from a light field', Science **317** (2007).

29 V. Parigi, A. Zavatta, and M. Bellini, 'Manipulating thermal light states by the controlled addition and subtraction of single photons', Laser Phys. Lett. **5** (2008).

30 A. Zavatta, V. Parigi, M. Kim, and M. Bellini, 'The weird math of photon subtraction', Opt. Photonics News **20** (2009).

31 A. Allevi, A. Andreoni, M. Bondani, M. G. Genoni, and S. Olivares, 'Reliable source of conditional states from single-mode pulsed thermal fields by multiple-photon subtraction', Phys. Rev. A **82** (2010).

32 S. Wang, H.-y. Fan, and L.-y. Hu, 'Photon-number distributions of non-gaussian states generated by photon subtraction and addition', J. Opt. Soc. Am. B **29** (2012).

33 F. E. Becerra, J. Fan, and A. Migdall, 'Photon number resolution enables quantum receiver for realistic coherent optical communications', Nat. Photon. **9** (2014).

34 V. Švarc, M. Nováková, G. Mazin, and M. Ježek, 'Fully tunable and switchable coupler for photonic routing in quantum detection and modulation', Opt. Lett. **44** (2019).

35 K. G. Katamadze, G. V. Avosopiants, N. A. Bogdanova, Y. I. Bogdanov, and S. P. Kulik, 'Multimode thermal states with multiphoton subtraction: study of the photon-number distribution in the selected subsystem', Phys. Rev. A **101** (2020).

36 G. L. Zanin, M. J. Jacquet, M. Spagnolo, P. Schiansky, I. A. Calafell, L. A. Rozema, and P. Walther, 'Fiber-compatible photonic feed-forward with 99% fidelity', Opt. Express **29** (2021).

37 Z. BAY, 'Electron multiplier as an electron counting device', Nature **141** (1938).

38 D. H. Andrews, R. M. Milton, and W. DeSorbo, 'A fast superconducting bolometer', J. Opt. Soc. Am. **36** (1946).

39 R. J. McIntyre, 'Theory of microplasma instability in silicon', J. Appl. Phys. **32** (1961).

40 D. E. Groom, 'Silicon photodiode detection of bismuth germanate scintillation light', Nucl. Instrum. Methods Phys. Res. **219** (1984).

41 A. Peacock et al., 'Single optical photon detection with a superconducting tunnel junction', Nature **381** (1996).

42 S. Cova, M. Ghioni, A. Lacaita, C. Samori, and F. Zappa, 'Avalanche photodiodes and quenching circuits for single-photon detection', Appl. Opt. **35** (1996).

43 A. D. Semenov, G. N. Gol'tsman, and A. A. Korneev, 'Quantum detection by current carrying superconducting film', Physica C: Superconductivity **351** (2001).

44 S. Somani, S. Kasapi, K. Wilsher, W. Lo, R. Sobolewski, and G. Gol'tsman, 'New photon detector for device analysis: superconducting single-photon detector based on a hot electron effect', J. Vac. Sci. Technol. B: Nanotechnol. Microelectron. **19** (2001).

45 O. Haderka, M. Hamar, and J. P. Jr, 'Experimental multi-photon-resolving detector using a single avalanche photodiode', Eur. Phys. J. D **28**, 149–154 (2004).

46 S. Pellegrini, R. Warburton, L. Tan, J. Ng, A. Krysa, K. Groom, J. David, S. Cova, M. Robertson, and G. Buller, 'Design and performance of an InGaAs–InP single-photon avalanche diode detector', IEEE J. Quantum Electron. **42** (2006).

47 S. N. Dorenbos, E. M. Reiger, N. Akopian, U. Perinetti, V. Zwiller, T. Zijlstra, and T. M. Klapwijk, 'Superconducting single photon detectors with minimized polarization dependence', Appl. Phys. Lett. **93** (2008).

48 B. E. Kardynał, Z. L. Yuan, and A. J. Shields, 'An avalanche-photodiode-based photon-number-resolving detector', Nat. Photon. **2** (2008).

49 A. Divochiy et al., 'Superconducting nanowire photon-number-resolving detector at telecommunication wavelengths', Nat. Photon. **2** (2008).

50 E. A. Dauler, A. J. Kerman, B. S. Robinson, J. K. Yang, B. Voronov, G. Goltsman, S. A. Hamilton, and K. K. Berggren, 'Photon-number-resolution with sub-30-ps timing using multi-element superconducting nanowire single photon detectors', J. Mod. Opt. **56** (2009).

51 F. Marsili et al., 'Superconducting parallel nanowire detector with photon number resolving functionality', J. Mod. Opt. **56** (2009).

52 J. P. Sprengers et al., 'Waveguide superconducting single-photon detectors for integrated quantum photonic circuits', Appl. Phys. Lett. **99** (2011).

53 T. Gerrits, B. Calkins, N. Tomlin, A. E. Lita, A. Migdall, R. Mirin, and S. W. Nam, 'Extending single-photon optimized superconducting transition edge sensors beyond the single-photon counting regime', Opt. Express **20** (2012).

54 V. B. Verma, F. Marsili, S. Harrington, A. E. Lita, R. P. Mirin, and S. W. Nam, 'A three-dimensional, polarization-insensitive superconducting nanowire avalanche photodetector', Appl. Phys. Lett. **101** (2012).

55 D. Rosenberg, A. J. Kerman, R. J. Molnar, and E. A. Dauler, 'High-speed and high-efficiency superconducting nanowire single photon detector array', Opt. Express **21** (2013).

56 Z. Zhou, S. Jahanmirinejad, F. Mattioli, D. Sahin, G. Frucci, A. Gaggero, R. Leoni, and A. Fiore, 'Superconducting series nanowire detector counting up to twelve photons', Opt. Express **22** (2014).

57 H.-Y. Yin, H. Cai, R.-S. Cheng, Z. Xu, Z.-N. Jiang, J.-S. Liu, T.-F. Li, and W. Chen, 'Polarization independent superconducting nanowire detector with high-detection efficiency', Rare Metals **34** (2014).

58 P. Rath, O. Kahl, S. Ferrari, F. Sproll, G. Lewes-Malandrakis, D. Brink, K. Ilin, M. Siegel, C. Nebel, and W. Pernice, 'Superconducting single-photon detectors integrated with diamond nanophotonic circuits', Light: Sci. Appl. **4** (2015).

59 M. K. Akhlaghi, E. Schelew, and J. F. Young, 'Waveguide integrated superconducting single-photon detectors implemented as near-perfect absorbers of coherent radiation', Nat. Commun. **6** (2015).

60 T. Gerrits, A. Lita, B. Calkins, and S. W. Nam, 'Superconducting transition edge sensors for quantum optics', in *Quantum science and technology* (2016).

61 J. Liu, Y. Li, L. Ding, Y. Wang, T. Zhang, Q. Wang, and J. Fang, 'Fast active-quenching circuit for free-running InGaAs(p)/InP single-photon avalanche diodes', IEEE J. Quantum Electron. **52** (2016).

62 A. Vetter et al., 'Cavity-enhanced and ultrafast superconducting single-photon detectors', Nano Lett. **16** (2016).

63 F. Mattioli, Z. Zhou, A. Gaggero, R. Gaudio, R. Leoni, and A. Fiore, 'Photon-counting and analog operation of a 24-pixel photon number resolving detector based on superconducting nanowires', Opt. Express **24** (2016).

64 X. Chen, C. Ding, H. Pan, K. Huang, J. Laurat, G. Wu, and E. Wu, 'Temporal and spatial multiplexed infrared single-photon counter based on high-speed avalanche photodiode', Sci. Rep. **7** (2017).

65 N. J. D. Martinez, M. Gehl, C. T. Derose, A. L. Starbuck, A. T. Pomerene, A. L. Lentine, D. C. Trotter, and P. S. Davids, 'Single photon detection in a waveguide-coupled ge-on-si lateral avalanche photodiode', Opt. Express **25** (2017).

66 E. E. Wollman et al., 'UV superconducting nanowire single-photon detectors with high efficiency, low noise, and 4 k operating temperature', Opt. Express **25** (2017).

67 R. Xu et al., 'Demonstration of polarization-insensitive superconducting nanowire single-photon detector with si compensation layer', J. Lightwave Technol. **35** (2017).

68 C. Cahall, K. L. Nicolich, N. T. Islam, G. P. Lafyatis, A. J. Miller, D. J. Gauthier, and J. Kim, 'Multi-photon detection using a conventional superconducting nanowire single-photon detector', Optica **4** (2017).

69 D. Zhu, Q.-Y. Zhao, H. Choi, T.-J. Lu, A. E. Dane, D. Englund, and K. K. Berggren, 'A scalable multi-photon coincidence detector based on superconducting nanowires', Nat. Nanotechnol. **13** (2018).

70 K. Zou, Y. Meng, Z. Wang, and X. Hu, 'Superconducting nanowire multi-photon detectors enabled by current reservoirs', Photon. Res. **8** (2020).

71 M. A. Wolff, S. Vogel, L. Splitthoff, and C. Schuck, 'Superconducting nanowire single-photon detectors integrated with tantalum pentoxide waveguides', Sci. Rep. **10** (2020).

72 M. Renna, A. Ruggeri, M. Sanzaro, F. Villa, F. Zappa, and A. Tosi, 'High detection rate fast-gated CMOS single-photon avalanche diode module', IEEE Photonics J. **12** (2020).

73 Y. Meng, K. Zou, N. Hu, L. Xu, X. Lan, S. Steinhauer, S. Gyger, V. Zwiller, and X. Hu, 'Fractal superconducting nanowires detect infrared single photons with 84% system detection efficiency, 1.02 polarization sensitivity, and 20.8 ps timing resolution', ACS Photonics (2022).

74 M. Eaton, A. Hossameldin, R. J. Birrittella, P. M. Alsing, C. C. Gerry, C. Cuevas, H. Dong, and O. Pfister, 'Resolving 100 photons and quantum generation of unbiased random numbers', (2022).

75 J. Wu, Y. Liu, B. Zhang, X. Jin, Y. Wang, H. Wang, and X. Yang, 'A benchmark test of boson sampling on tianhe-2 supercomputer', Natl. Sci. Rev. **5** (2018).

76 H. Wang et al., 'Boson sampling with 20 input photons and a 60-mode interferometer in a<mml:math xmlns:mml="http://www.w3.org/1998/math/MathML" display="inline"><mml:mn>1</mml:mn dimensional hilbert space', Phys. Rev. Lett. **123** (2019).

77 'Photonic implementation of boson sampling: a review', Adv. Photonics **1** (2019).

78 H. Wang et al., 'Boson sampling with 20 input photons and a 60-mode interferometer in a 1014-dimensional hilbert space', Phys. Rev. Lett. **123** (2019).

79 H.-S. Zhong et al., 'Quantum computational advantage using photons', Science **370** (2020).

80 J. C. F. Matthews, A. Politi, A. Stefanov, and J. L. O'Brien, 'Manipulation of multiphoton entanglement in waveguide quantum circuits', Nature Photon. **3** (2009).

81 X.-C. Yao, T.-X. Wang, P. Xu, H. Lu, G.-S. Pan, X.-H. Bao, C.-Z. Peng, C.-Y. Lu, Y.-A. Chen, and J.-W. Pan, 'Observation of eight-photon entanglement', Nat. Photon. **6** (2012).

82 X.-L. Wang et al., 'Experimental ten-photon entanglement', Phys. Rev. Lett. **117** (2016).

83 N. Zhou, W.-H. Jiang, L.-K. Chen, Y.-Q. Fang, Z.-D. Li, H. Liang, Y.-A. Chen, J. Zhang, and J.-W. Pan, 'Sine wave gating silicon single-photon detectors for multiphoton entanglement experiments', Rev. Sci. Instrum. **88** (2017).

84 J. Wang et al., 'Multidimensional quantum entanglement with large-scale integrated optics', Science **360** (2018).

85 D. Llewellyn et al., 'Chip-to-chip quantum teleportation and multi-photon entanglement in silicon', Nat. Phys. **16** (2019).

86 F. Flamini, N. Spagnolo, and F. Sciarrino, 'Photonic quantum information processing: a review', Rep. Prog. Phys. **82** (2018).

87 S. Slussarenko, and G. J. Pryde, 'Photonic quantum information processing: a concise review', Appl. Phys. Rev. **6** (2019).

88 E. Lavie, I. W. Primaatmaja, W. Y. Kon, C. Wang, and C. C. W. Lim, 'Estimating the photon-number distribution of photonic channels for realistic devices and applications in photonic quantum information processing', Phys. Rev. Appl. **16** (2021).

89 K. J. Gordon, V. Fernandez, G. S. Buller, I. Rech, S. D. Cova, and P. D. Townsend, 'Quantum key distribution system clocked at 2 GHz', Opt. Express **13** (2005).

90 X. Michalet, O. H. W. Siegmund, J. V. Vallerga, P. Jelinsky, J. E. Millaud, and S. Weiss, 'Detectors for single-molecule fluorescence imaging and spectroscopy', J. Mod. Opt. **54** (2007).

91 A. Pifferi et al., 'Time-resolved diffuse reflectance using small source-detector separation and fast single-photon gating', Phys. Rev. Lett. **100** (2008).

92 L. Lydersen, C. Wiechers, C. Wittmann, D. Elser, J. Skaar, and V. Makarov, 'Hacking commercial quantum cryptography systems by tailored bright illumination', Nat. Photon. **4** (2010).

93 P. Eraerds, M. Legre, J. Zhang, H. Zbinden, and N. Gisin, 'Photon counting OTDR: advantages and limitations', J. Lightwave Technol. **28** (2010).

94 V. Giovannetti, S. Lloyd, and L. Maccone, 'Advances in quantum metrology', Nat. Photon. **5** (2011).

95 K. R. Motes, J. P. Olson, E. J. Rabeaux, J. P. Dowling, S. J. Olson, and P. P. Rohde, 'Linear optical quantum metrology with single photons: exploiting spontaneously generated entanglement to beat the shot-noise limit', Phys. Rev. Lett. **114** (2015).

96 H. Ta, J. Keller, M. Haltmeier, S. K. Saka, J. Schmied, F. Opazo, P. Tinnefeld, A. Munk, and S. W. Hell, 'Mapping molecules in scanning far-field fluorescence nanoscopy', Nat. Commun. **6** (2015).

97 J. Sabines-Chesterking, R. Whittaker, S. K. Joshi, P. M. Birchall, P. A. Moreau, A. McMillan, H. V. Cable, J. L. O'Brien, J. G. Rarity, and J. C. F. Matthews, 'Sub-shot-noise transmission measurement enabled by active feed-forward of heralded single photons', Phys. Rev. Appl. **8** (2017).

98 R. Whittaker, C. Erven, A. Neville, M. Berry, J. L. O'Brien, H. Cable, and J. C. F. Matthews, 'Absorption spectroscopy at the ultimate quantum limit from single-photon states', New J. Phys. **19** (2017).

99 A. Boaron et al., 'Secure quantum key distribution over 421 km of optical fiber', Phys. Rev. Lett. **121** (2018).

100 J. Sabines-Chesterking, A. R. McMillan, P. A. Moreau, S. K. Joshi, S. Knauer, E. Johnston, J. G. Rarity, and J. C. F. Matthews, 'Twin-beam sub-shot-noise raster-scanning microscope', Opt. Express **27** (2019).

101 A. Stanco, D. G. Marangon, G. Vallone, S. Burri, E. Charbon, and P. Villoresi, 'Efficient random number generation techniques for CMOS single-photon avalanche diode array exploiting fast time tagging units', Phys. Rev. Research **2** (2020).

102 E. M. Fisher, 'Principles and early historical development of silicon avalanche and geiger-mode photodiodes', in *Photon counting - fundamentals and applications* (2018).

103 H. Paul, P. Törmä, T. Kiss, and I. Jex, 'Photon chopping: new way to measure the quantum state of light', Phys. Rev. Lett. **76** (1996).

104 K. Banaszek, and I. A. Walmsley, 'Photon counting with a loop detector', Opt. Lett. **28** (2003).

105 P. Eraerds, M. Legré, A. Rochas, H. Zbinden, and N. Gisin, 'SiPM for fast photon-counting and multiphoton detection', Opt. Express **15** (2007).

106 E. Grigoriev, A. Akindinov, M. Breitenmoser, S. Buono, E. Charbon, C. Niclass, I. Desforges, and R. Rocca, 'Silicon photomultipliers and their bio-medical applications', Nucl. Instrum. Methods Phys. Res. Section A: Accelerators, Spectrometers, Detectors and Associated Equipment **571** (2007).

107 M. Ramilli, A. Allevi, V. Chmill, M. Bondani, M. Caccia, and A. Andreoni, 'Photon-number statistics with silicon photomultipliers', J. Opt. Soc. Am. B **27** (2010).

108 A. Allevi, and M. Bondani, 'Direct detection of super-thermal photon-number statistics in second-harmonic generation', Opt. Lett. **40** (2015).

109 J. Tiedau, E. Meyer-Scott, T. Nitsche, S. Barkhofen, T. J. Bartley, and C. Silberhorn, 'A high dynamic range optical detector for measuring single photons and bright light', Opt. Express **27** (2019).

110 J. C. Matthews, X.-Q. Zhou, H. Cable, P. J. Shadbolt, D. J. Saunders, G. A. Durkin, G. J. Pryde, and J. L. O'Brien, 'Towards practical quantum metrology with photon counting', npj Quantum Inf. **2** (2016).

111 S. Slussarenko, M. M. Weston, H. M. Chrzanowski, L. K. Shalm, V. B. Verma, S. W. Nam, and G. J. Pryde, 'Unconditional violation of the shot-noise limit in photonic quantum metrology', Nat. Photon. **11** (2017).

112 J. Wang, F. Sciarrino, A. Laing, and M. G. Thompson, 'Int. phot. quantum technol.', **14** (2019).

113 C. Bruschini, H. Homulle, I. M. Antolovic, S. Burri, and E. Charbon, 'Single-photon avalanche diode imagers in biophotonics: review and outlook', Light: Sci. Appl. **8** (2019).

114 M. Cattaneo, M. G. A. Paris, and S. Olivares, 'Hybrid quantum key distribution using coherent states and photon-number-resolving detectors', Phys. Rev. A **98** (2018).

115 D. Sahin et al., 'Waveguide photon-number-resolving detectors for quantum photonic integrated circuits', Appl. Phys. Lett. **103** (2013).

116 F. Najafi et al., 'On-chip detection of non-classical light by scalable integration of single-photon detectors', Nat. Commun. **6** (2015).

117 C. Schuck, X. Guo, L. Fan, X. Ma, M. Poot, and H. X. Tang, 'Quantum interference in heterogeneous superconducting-photonic circuits on a silicon chip', Nat. Commun. **7** (2016).

118 R. Heilmann, J. Sperling, A. Perez-Leija, M. Gräfe, M. Heinrich, S. Nolte, W. Vogel, and A. Szameit, 'Harnessing click detectors for the genuine characterization of light states', Sci. Rep. **6** (2016).

119 P. Vines, K. Kuzmenko, J. Kirdoda, D. C. S. Dumas, M. M. Mirza, R. W. Millar, D. J. Paul, and G. S. Buller, 'High performance planar germanium-on-silicon single-photon avalanche diode detectors', Nat. Commun. **10** (2019).

120 S. Buckley, A. Tait, J. Chiles, A. McCaughan, S. Khan, R. Mirin, S. Nam, and J. Shainline, 'Integrated-photonic characterization of single-photon detectors for use in neuromorphic synapses', Phys. Rev. Appl. **14** (2020).

121 L. Lachman, and R. Filip, 'Quantum non-gaussianity of light and atoms', Prog. Quantum Electron. (2022).

122 U. Chabaud, P.-E. Emeriau, and F. Grosshans, 'Witnessing wigner negativity', Quantum **5** (2021).

123 M. Walschaers, V. Parigi, and N. Treps, 'Practical framework for conditional non-gaussian quantum state preparation', PRX Quantum **1** (2020).

124 E. Knill, R. Laflamme, and G. J. Milburn, 'A scheme for efficient quantum computation with linear optics', Nature **409** (2001).

125 C. Simon, H. de Riedmatten, M. Afzelius, N. Sangouard, H. Zbinden, and N. Gisin, 'Quantum repeaters with photon pair sources and multimode memories', Phys. Rev. Lett. **98** (2007).